



The University of Sheffield

Department of Civil & Structural Engineering

# **Robustness of Steel Connections Loaded at High Rates**

By

**Rahi Rahbari**

A thesis submitted in partial fulfilment of the requirements for the  
Degree of Doctor of Philosophy

November, 2014

We are not now that strength which in old days  
Moved earth and heaven, that which we are, we are,  
One equal temper of heroic hearts,  
Made weak by time and fate, but strong in will  
To strive, to seek, to find, and not to yield.

Lord Alfred Tennyson

# Abstract

Robustness of structures to prevent progressive collapse has been considered by different building codes since the Ronan Point accident in the UK in 1968 and research on this type of collapse was brought to the fore after the building collapses at the World Trade Center on 9/11 2001. In the case of losing a column, to maintain the integrity of the building large end rotation of the beams is likely to be required in order to transfer the vertical loads from the floor above by redistribution of loads through the remaining structure. For this reason connections are important in enabling the structure to bridge over the lost column. Connections also need to be capable of resisting high strain rates arising from the dynamic redistribution of moments and tension loads which means they require high ductility to dissipate energy and undergo deformation without failure.

This thesis presents results from both experimental tests conducted on connections under quasi-static and rapidly applied loading (performed as part of an EPSRC funded research project [1] Prior to the PhD research), and a series of ANSYS LS-DYNA finite element analyses which have been developed to model the connection response. Web-cleat and End-plate connection models, with their complex geometry, has been produced and validated against experimental data. The effect of rate of applied loading on connection response has been investigated both experimentally and by numerical modelling. It is important to understand the effect of loading rate on the response of connections in dynamic frame response to column loss. The results indicate that web angle cleat connections are relatively insensitive to the rate of loading within the range considered here. This suggests that static characterisation of web angle cleat connections may yield suitable data for use in dynamic analysis of frame response in column loss scenarios. End-plate connections behaved differently and this type of connection was sensitive to loading rates and this showed that static characterisation of this connection is not enough for dynamic analysis. This study highlight a gap in knowledge of welded material properties, and provided the results of parametric studies (different loading types, rates and connection geometry) on these two types of connections.

## Acknowledgements

I want to express my gratitude and appreciation to my supervisors **Dr. Andrew Tyas** and **Professor Buick Davison** for all their guidance and encouragement on doing this research for past four years. Your invaluable advice helped me to grow as a research scientist and will be with me through my future career. I also would like thank the **Department of Civil and Structural Engineering** of University of Sheffield for funding my PhD as a part of EPSRC Doctoral Training Grant scheme.

My sincere gratitude goes to my dad, **Mr. Mehrdad Rahbari** who is my mentor and introduced me to the field of structural engineering from an early age. My sincere appreciation goes to **my mom** and **my sister** whom always supported me and their good thoughts helped me to strive towards my aims in life.

I would like especially to thank all my **dear friends** who supported me in the journey of research and writing, also my **fellow researchers in room D120a** in which we all spent four years of our life together and last but not least, I want to say thank you to all the **staff in the department** who always supported me through these years.

Rahi Rahbari  
November 2014

## **Declaration**

Except where specific reference has been made to the work of others, this thesis is the result of my own work. No part of it has been submitted to any university or other educational establishment for a degree, diploma, or other qualification.

Rahi Rahbari  
November 2014



# Table of Contents

Abstract .....	I
Acknowledgements .....	II
Declaration .....	III
Table of Contents .....	V
List of Figures .....	XI
List of Tables.....	XX
1 Introduction.....	1
2 Literature Review .....	7
2.1 Progressive collapse .....	7
2.1.1 Defining progressive collapse .....	8
2.1.2 Notable progressive collapses .....	9
2.2 Standards and codes .....	13
2.2.1 Europe .....	13
2.2.2 United States .....	14
2.2.3 Canada.....	15
2.3 Different methods for preventing progressive collapse.....	15
2.3.1 Redundancy or alternate load paths .....	15
2.3.2 Interconnection or continuity (Tie strength) .....	16
2.3.3 Local resistance .....	16
2.4 The importance of steel connections .....	16
2.4.1 International reports and their recommendations on progressive collapse	17
2.4.2 Previous Projects & Researches on steel connection behaviour .....	19
2.4.3 Different failure modes of bolt bearing connection .....	26

2.5	Conclusion.....	28
3	Methodology .....	29
3.1	Experimental study.....	29
3.1.1	Web-cleat connection.....	31
3.1.2	End-plate connection.....	34
3.2	Numerical study .....	38
3.2.1	Material models.....	39
3.2.2	Explicit and implicit solvers .....	41
3.2.3	Force and moment calculation method .....	43
3.3	Conclusion.....	44
4	Development of steel connection model using finite element method .....	45
4.1	Universal column H-section with stiffener plates .....	46
4.1.1	Building the geometry of the column.....	46
4.1.2	Material properties and mesh generation of the column.....	50
4.2	Universal beam I-sections and the splice connection.....	51
4.2.1	Building the geometry of the beams .....	52
4.2.2	Material properties and mesh generation of the beam .....	56
4.3	Modelling bolts, nuts and washers .....	59
4.3.1	Building the geometry of the bolt .....	59
4.3.2	Building the bolt model by nodes and elements .....	60
4.4	Angle sections (for Web-cleat connections) .....	63
4.4.1	Building the geometry of the angles .....	63
4.4.2	Material properties and mesh generation of the beam .....	64
4.5	End-plate and welding (for end- plate connections).....	66
4.5.1	Building the geometry of the plate and welding.....	66

4.5.2	Material properties and mesh generation of the plate .....	67
4.6	Rigid plate or load application .....	70
4.7	Parts and Components .....	72
4.8	Contacts .....	74
4.9	Boundary conditions.....	76
4.10	Conclusion .....	77
5	Finite element model of connections .....	78
5.1	Free column validation .....	78
5.2	Instabilities problems in dynamic analysis.....	80
5.3	Web-cleat connection .....	82
5.3.1	Quantitative validation against dynamic tests 4, 5 and 7 .....	83
5.3.2	Qualitative validation against dynamic tests 4, 5 and 7 .....	92
5.3.3	Quantitative validation against static tests 6 and 9 .....	96
5.3.4	Qualitative validation against static tests 6 and 9 .....	101
5.3.5	Simplified model of Web-cleat connection.....	103
5.4	End-plate connections .....	104
5.4.1	Complications regarding connection failure .....	104
5.4.2	Quantitative validation against dynamic tests 4, 6 and 11 .....	105
5.4.3	Qualitative validation against dynamic tests 4 and 11 .....	114
5.4.4	Quantitative validation against static tests 1, 5 and 15 .....	117
5.4.5	Qualitative validation against static tests 1, 5 and 15 .....	124
5.4.6	Simplified model of End-plate connection .....	128
5.5	Conclusion.....	128
6	Parametric study of Web-cleat connection behaviour .....	129
6.1	Influence of different loading types and rates .....	132

6.1.1	Column displacement in time .....	132
6.1.2	Column response due to connection reaction.....	135
6.1.3	Deformation of the Angle-cleats.....	137
6.1.4	Connection force resistance .....	139
6.1.5	Connection moment resistance .....	143
6.1.6	Median and mean values of force and moment resisted in the connection 145	
6.2	Influence of bolt strength on connection behaviour.....	148
6.3	Effect of washer size on connection behaviour.....	150
6.4	Effect of bolt size on connection behaviour.....	152
6.4.1	Column displacement in time .....	152
6.4.2	Connection force resistance .....	153
6.4.3	Connection moment resistance .....	154
6.5	Influence of bolt gauge on connection behaviour .....	155
6.5.1	Column displacement in time .....	156
6.5.2	Deformation of the Angle-cleats.....	157
6.5.3	Connection force resistance .....	158
6.5.4	Connection moment resistance .....	159
6.6	Influence of bolt pitch on connection behaviour.....	161
6.6.1	Column displacement in time .....	161
6.6.2	Deformation of the Angle-cleats.....	162
6.6.3	Connection force resistance .....	164
6.6.4	Connection moment resistance .....	165
6.7	Summary .....	167
6.8	Conclusion.....	171

7	Parametric study of End-plate connection behaviour .....	173
7.1	Influence of different loading types and rates .....	174
7.1.1	Column displacement in time .....	174
7.1.2	Column response due to connection reaction.....	177
7.1.3	Deformation of the End-plate.....	180
7.1.4	Connection force resistance .....	182
7.1.5	Connection moment resistance .....	186
7.1.6	Median and mean values of force and moment resisted in the connection 187	
7.2	Influence of bolt strength on connection behaviour .....	189
7.3	Effect of washer size on connection behaviour .....	191
7.4	Effect of Bolt Size on Connection Behaviour .....	192
7.4.1	Column displacement in time .....	192
7.4.2	Deformation of the End-plate.....	194
7.4.3	Connection force resistance .....	194
7.4.4	Connection moment resistance .....	195
7.5	Influence of bolt gauge on connection behaviour .....	197
7.5.1	Column displacement in time .....	198
7.5.2	Deformation of the End-plate.....	199
7.5.3	Connection force resistance .....	200
7.5.4	Connection moment resistance .....	202
7.6	Influence of bolt pitch on connection behaviour .....	203
7.6.1	Column displacement in time .....	205
7.6.2	Deformation of the End-plate.....	206
7.6.3	Connection force resistance .....	207

7.6.4	Connection moment resistance .....	208
7.7	Summary .....	210
7.8	Conclusion.....	214
8	Discussion.....	215
8.1	Overview of model results .....	215
8.2	Web-cleat connection.....	217
8.2.1	Column displacement.....	218
8.2.2	Deformation of the Angle-cleat .....	220
8.2.3	Connection moment resistance .....	223
8.2.4	Connection force resistance .....	225
8.3	End-plate connection.....	227
8.3.1	Column displacement.....	229
8.3.2	Connection force resistance .....	230
8.3.3	Connection moment resistance .....	232
8.3.4	Plate strain.....	233
8.4	Comparing two connections.....	238
8.5	Conclusion.....	240
9	Conclusion .....	241
	References.....	245
	Appendix A Model geometry and drawings .....	252
	Appendix B Dimensions .....	254

## List of Figures

Figure 1-1 Tying forces (a) design assumption (b) prying action as a result of connection rotation[after [2]].....	2
Figure 2-1 Ronan Point building after the May 1968 collapse [22] .....	10
Figure 2-2 Status of Construction at Time of Collapse [36].....	11
Figure 2-3 Ruins of L'Ambiance Plaza [36] .....	11
Figure 2-4 (a) Building Prior to Attack (b) Federal Building after collapse [38] .....	12
Figure 2-5 WTC in the time of collapse [40].....	13
Figure 2-6 Experiment arrangements before and after [47].....	20
Figure 2-7 A picture of these experiments [47] .....	20
Figure 2-8 experimental setup [16] [17] .....	21
Figure 2-9 ANSYS model made for analysing the connection [49] .....	22
Figure 2-10 LS-DYNA model made of the connection [50] .....	23
Figure 2-11 Finite element model made to study the experiments [51] .....	24
Figure 2-12 An image of the experiment after the connection failure [51] .....	24
Figure 2-13 Experiments arrangement before and after [2].....	25
Figure 2-14 (a) Shear failure (b) Splitting failure (c) Net-cross section failure [53].....	26
Figure 2-15 (a) Simple finite element model (b) Plate stress distribution [53] .....	27
Figure 3-1 Schematic diagram of the test arrangement .....	30
Figure 3-2 Photograph of test specimen assembled in the test rig.....	31
Figure 3-3 Geometric details of the web cleat test specimens.....	32
Figure 3-4 Geometric details of the end plate test specimens.....	34
Figure 3-5 LS-DYNA uniaxial tension test .....	41
Figure 3-6 Stress strain curve for 275 steel for two different strain rates with J-C material model.....	41
Figure 3-7 (a) Free-body force/moment diagram for flying column (b) Displacement/rotation diagram for flying column [14] .....	44
Figure 4-1 Final model of the connection, beam and column.....	46
Figure 4-2 Drawing of column section dimensions .....	47
Figure 4-3 Drawing of the column's flange.....	47
Figure 4-4 Drawing of the column web and stiffener plates.....	48
Figure 4-5 Dividing the column to different sections .....	48
Figure 4-6 Column first section's key-points (the rest of these sections and their key-points are provided in Appendix A).....	48
Figure 4-7 Column geometry made by volumes.....	49
Figure 4-8 Column volumes with square holes .....	49
Figure 4-9 Four bolt holes attached to the column .....	50
Figure 4-10 Example of different Components on the column.....	50
Figure 4-11 Pictures of column after meshing.....	51

Figure 4-12 Drawing of beam section dimensions .....	52
Figure 4-13 Side drawing of beams and splice dimensions.....	53
Figure 4-14 Flange plate of splice.....	53
Figure 4-15 Beam splice plates.....	54
Figure 4-16 Beam section divisions.....	55
Figure 4-17 Section A- A, example of key points numbering (the rest of these sections and their key-points are provided in Appendix A).....	55
Figure 4-18 Beam & splice geometry in ANSYS.....	56
Figure 4-19 (a) Beam with square holes (b) Bolt holes attached to the beams and plates .....	56
Figure 4-20 Sample of different Components on the beams.....	57
Figure 4-21 Finer meshing at the end of the beam which was connected to the Web-cleat connection .....	58
Figure 4-22 Beam mesh and splice mesh.....	58
Figure 4-23 Bolt drawing and its dimensions .....	59
Figure 4-24 Bolt Head (R), Nut (M), Washer (R).....	59
Figure 4-25 Bolt different parts.....	60
Figure 4-26 (a) Helix line (b) Element section .....	61
Figure 4-27 (a) Bolt grip and head (b) Bolt nut .....	62
Figure 4-28 Complete bolt model .....	62
Figure 4-29 Angle parameters.....	63
Figure 4-30 Angle sections .....	63
Figure 4-31 (a) Angle section key points (b) Angle geometry .....	64
Figure 4-32 (a) Angles with square holes (b) Angles with the bolt holes.....	64
Figure 4-33 Sample of different Components on the angles.....	65
Figure 4-34 Angles after meshing.....	65
Figure 4-35 End plate connected to the beam.....	66
Figure 4-36 (a) End-Plate sections (b) End plate key points for section A- A .....	66
Figure 4-37 End plate Components .....	67
Figure 4-38 (a) Welded T-Stub, (b) Closer look to heat affected zones [83] .....	67
Figure 4-39 Drawing to show different zones in the end-plate.....	68
Figure 4-40 End plate mesh .....	70
Figure 4-41 Loading Ram and load cell (a) Experiment (b) Model .....	71
Figure 4-42 Force plate & load cell (a) Experiment (b) Model .....	71
Figure 4-43 Example of column Parts .....	72
Figure 4-44 Example of beam Parts & Component .....	73
Figure 4-45 Example of angles Parts & Components.....	73
Figure 4-46 Example of Five different Parts of the bolt.....	74
Figure 4-47 Example of (a) Force plate (b) Loading ram and load cell .....	74
Figure 4-48 Example of (a) ESTS contacts between the bolt parts .....	75

Figure 4-49 Example of ASTS contacts between the angle and column flange .....	75
Figure 4-50 Boundary condition around the model .....	76
Figure 5-1 (a) Initial position of the column (b) Column at 40ms.....	78
Figure 5-2 Applied load to the free column against time .....	79
Figure 5-3 Displacement time history of the free column .....	79
Figure 5-4 (a) Washer with instability problem (b) Washer with no instability problem	81
Figure 5-5 Washer deformation (a) Front view (b) Side view .....	81
Figure 5-6 Bolt and beam web .....	82
Figure 5-7 Applied force time history (a) Test WC5 (b) Test WC4 (c) Test WC7 .....	84
Figure 5-8 Displacement time history (a) Test WC5 (b) Test WC4 (c) Test WC7 .....	85
Figure 5-9 WC7 – Column rotation vs time: comparison of results from experimental connection test, model connection test and model with same applied load but no connection .....	85
Figure 5-10 Rotation time history (a) Test WC5 (b) Test WC4 (c) Test WC7 .....	87
Figure 5-11 Moment rotation diagrams (a) Test WC5 (b) Test WC4 (c) Test WC7.....	88
Figure 5-12: Moment rotation diagrams (a) Test WC5 (b) Test WC4 (c) Test WC7.....	89
Figure 5-13 Force rotation (a) Test WC5 (b) Test WC4 (c) Test WC7.....	90
Figure 5-14 Force rotation (a) Test WC5 (b) Test WC4 (c) Test WC7 .....	91
Figure 5-15 Post-test web failure .....	93
Figure 5-16 Post-test angle deformation for test WC4 (a) Experiments (b) Ls-Dyna ....	93
Figure 5-17 – Test WC5 deformation of connection at key points.....	94
Figure 5-18 – Test WC7 deformation of connection at key points.....	95
Figure 5-19 Applied force time history (a) Test WC6 (b) Test WC9.....	96
Figure 5-20 Displacement time history (a) Test WC6 (b) Test WC9.....	98
Figure 5-21 Rotation time history (a) Test WC6 (b) Test WC9 .....	99
Figure 5-22 Moment rotation diagram (a) Test WC6 (b) Test WC9 .....	100
Figure 5-23 Final deformation of beam web (a) Experiments (b) Ls-Dyna .....	101
Figure 5-24: Post-test angle deformation (a) Experiments (b) Ls-Dyna.....	101
Figure 5-25– Test WC6 deformation of connection at key points.....	102
Figure 5-26 Simplified model after removing the splice .....	103
Figure 5-27 Applied force time history (a) Test EP4 (b) Test EP6 (c) Test EP11 .....	106
Figure 5-28 Displacement time history (a) Test EP4 (b) Test EP6 (c) Test EP11.....	107
Figure 5-29 Rotation time history (a) Test EP4 (b) Test EP6 (c) Test EP11 .....	108
Figure 5-30 Moment rotation (a) Test EP4 (b) Test EP6 (c) Test EP11.....	109
Figure 5-31 Moment rotation (a) Test EP4 (b) Test EP6 (c) Test EP11.....	111
Figure 5-32 Force rotation (a) Test EP4 (b) Test EP6 (c) Test EP11 .....	112
Figure 5-33 Force rotation (a) Test EP4 (b) Test EP6 (c) Test EP11 .....	113
Figure 5-34 Deformed shape of plate and beam web in test EP6 after the failure (a) Exp. beam web front view (b) Model beam web front view (c) Exp. End-plate (d) Model end-plate (e) Exp. Beam web (f) Model beam web .....	114

Figure 5-35 End- plate deformation after the failure in test EP6 (a) Model (b) Experiment .....	114
Figure 5-36 Test EP6 deformation of connection at key points. ....	115
Figure 5-37 Test EP11 deformation of connection at key points.....	116
Figure 5-38 Applied force time history (a) Test EP1 (b) Test EP5 (C) Test EP15 .....	118
Figure 5-39 Displacement time history (a) Test EP1 (b) Test EP5 (C) Test EP15.....	119
Figure 5-40 Rotation time history (a) Test EP1 (b) Test EP5 (c) Test EP15.....	120
Figure 5-41 Moment rotation (a) Test EP1 (b) Test EP5 (C) Test EP15.....	122
Figure 5-42 Force rotation (a) Test EP1 (b) Test EP5 (C) Test EP15 .....	123
Figure 5-43 Test EP5 End plate deformation (a) Experiment (b) Meshed model (c) Unmeshed model.....	124
Figure 5-44 Test 5 End plate deformation side view (a) Experiment (b) Meshed model (c) Unmeshed model.....	125
Figure 5-45 Test EP5 welding deformation (a) Experiment (b) Finite element model	125
Figure 5-46 Test EP1 deformation of connection at key points. ....	126
Figure 5-47 Test EP15 deformation of connection at key points.....	127
Figure 5-48 Simplified model after removing the splice .....	128
Figure 6-1 Different types of loading, red arrows are the forces and blue lines shows the direction of the column displacement (a) Type1, one applied force (b) Type 2, two applied forces equal in same direction (c) Type 3, two equal forces but opposite in direction (d) Type 4, two applied forces in the same direction but one force half the magnitude of the other.....	130
Figure 6-2 Example of different loading rates .....	130
Figure 6-3 Column displacement time history LT1 10mm angle .....	133
Figure 6-4 Column displacement time history LT2 10mm angle .....	133
Figure 6-5 Column displacement time history LT3 10mm angle .....	134
Figure 6-6 Column displacement time history LT4 10mm angle .....	134
Figure 6-7 Mid bolt and column displacement LT1-4 10mm angle. Green points show the total connection failure.....	135
Figure 6-8 Median and mean value of column rotation and translation (a,b) 10mm thick angle, (c,d) 8mm thick angle and (e,f) 6mm thick angle .....	137
Figure 6-9 Mid bolt and column displacement LT2 8mm angle .....	138
Figure 6-10 Mid bolt and column displacement LT1 10 & 8 & 6mm angle .....	139
Figure 6-11 Force and column displacement LT1 10mm angle .....	140
Figure 6-12 Force and column displacement LT2 10 & 8 & 6mm angle .....	141
Figure 6-13 Force and column displacement LT3 6mm angle .....	142
Figure 6-14 Force and column displacement LT4 10mm angle .....	143
Figure 6-15 Moment and column rotation LT1 10mm angle, rates were in kN/s .....	144
Figure 6-16 Moment and column rotation LT3 8mm angle .....	145

Figure 6-17 Median and mean value of the force and moment resistance for LT1 (a,b) 10mm thick angle (c,d) 8mm thick angle.....	146
Figure 6-18 Median and mean value of the force and moment resistance for LT2 (a,b) 10mm thick angle (c,d) 8mm thick angle.....	147
Figure 6-19 Median and mean value of the force and moment resistance for LT3 (a,b) 10mm thick angle (c,d) 8mm thick angle.....	148
Figure 6-20 Column displacement time history for strong bolt LT2 10mm angle, OB is original bolt and SB is stronger bolt simulations.....	149
Figure 6-21 Moment & column disp for strong bolt LT3 6mm angle, OB is original bolt and SB is stronger bolt simulations.....	149
Figure 6-22 (a) Angles and washers deformation (b) Washers deformation .....	150
Figure 6-23 Column displacement time history for washer size 24 LT3 10mm angle; W20 is original washer size 20 and W24 is the washer size 24 simulations.....	151
Figure 6-24 Moment & column displacement for washer size 24 LT3 6mm angle; W20 is original washer size 20 and W24 is the washer size 24 simulations.....	151
Figure 6-25 Column displacement time history for bolt M24 LT2 10mm angle, B20 is original bolt size 20 and B24 is the bolt size 24 simulations.....	152
Figure 6-26 Column displacement time history for bolt M24 LT3 10mm angle, B20 is original bolt size 20 and B24 is the bolt size 24 simulations.....	153
Figure 6-27 Force and column displacement for bolt M24 LT2 10mm angle, B20 is original bolt size 20 and B24 is the bolt size 24 simulations.....	154
Figure 6-28 Moment and column Rotation for bolt M24 LT3 10mm angle, B20 is original bolt size 20 and B24 is the bolt size 24 simulations.....	155
Figure 6-29 Drawing of the bolt gauge.....	155
Figure 6-30 Column displacement time history for BG less LT2 8mm angle, OBG is original bolt gauge (90mm) and LBG is the lower bolt gauge (80mm) simulation.....	156
Figure 6-31 Column displacement time history for BG more LT2 8mm angle, OBG is original bolt gauge and MBG is the maximum bolt gauge simulation.....	157
Figure 6-32 Bolt and column displacement for BG more & less LT2 8mm angle, OBG is original bolt gauge and LBG is the less bolt gauge simulations.....	158
Figure 6-33 Force and column displacement for BG more & less LT2 8mm angle, OBG is original bolt gauge and LBG is the least bolt gauge simulation.....	159
Figure 6-34 Moment and column rotation for BG less LT3 8mm angle, OBG is original bolt gauge and LBG is the least bolt gauge simulation.....	160
Figure 6-35 Moment and column rotation for BG more LT3 8mm angle, OBG is original bolt gauge and MBG is the maximum bolt gauge simulation.....	160
Figure 6-36 Drawing of the bolt locations .....	161
Figure 6-37 Column displacement time history for BP less LT2 8mm angle, OBP is original bolt pitch and LBP is the less bolt pitch simulations.....	162

Figure 6-38 Column displacement time history for BP more LT2 8mm angle, OBP is original bolt pitch and MBP is the more bolt pitch simulations. ....	162
Figure 6-39 Bolt and column displacement for BP less LT3 8mm angle, rates were in kN/s. OBP is original bolt pitch and LBP is the less bolt pitch simulations.....	163
Figure 6-40 Bolt and column displacement for BP more LT3 8mm angle, rates were in kN/s. OBP is original bolt pitch and MBP is the more bolt pitch simulations. ....	163
Figure 6-41 Force and column displacement for BP less LT2 8mm angle, OBP is original bolt pitch and LBP is the least bolt pitch simulations. ....	164
Figure 6-42 Force and column displacement for BP more LT2 8mm angle, OBP is original bolt pitch and MBP is the maximum bolt pitch simulations.....	165
Figure 6-43 Moment and column displacement for BP less LT3 8mm angle, OBP is original bolt pitch and LBP is the least bolt pitch simulation. ....	166
Figure 6-44 Moment and column displacement for BP more LT3 8mm angle, OBP is original bolt pitch and MBP is the maximum bolt pitch simulation. ....	166
Figure 7-1 Column displacement time history LT1 10mm.....	174
Figure 7-2 Column displacement time history LT2 10mm.....	175
Figure 7-3 Column displacement time history LT3 10mm.....	176
Figure 7-4 Column displacement time history LT4 10mm.....	176
Figure 7-5 Column rotation against displacement LT1-4 10mm.....	177
Figure 7-6 Column rotation against displacement LT1 10-8mm.....	178
Figure 7-7 Median and mean value of column rotation and translation for LT1 (a,b) 10mm thick plate (c, d) 8mm thick plate.....	179
Figure 7-8 Median and mean value of column rotation and translation for LT2 (a,b) 10mm thick plate (c, d) 8mm thick plate.....	179
Figure 7-9 two measured points on the end-plate .....	180
Figure 7-10 Displacement of the two corner LT1 8mm .....	181
Figure 7-11 Displacement of the two corner LT3 8mm .....	181
Figure 7-12 Force and column displacement LT1 10mm.....	183
Figure 7-13 Force and column displacement LT2 10mm.....	184
Figure 7-14 Force and column displacement LT3 10mm.....	185
Figure 7-15 Force and column displacement LT4 10mm.....	186
Figure 7-16 Moment and column rotation LT1 10mm .....	187
Figure 7-17 Median and mean value of the force and moment resistance for LT1 (a,b) 10mm thick plate (c,d) 8mm thick plate .....	188
Figure 7-18 Median and mean value of the force and moment resistance for LT2 (a,b) 10mm thick plate (c,d) 8mm thick plate .....	189
Figure 7-19 Column displacement time history for strong bolt LT3 8mm, OB is original bolt and SB is stronger bolt simulations. ....	190
Figure 7-20 Moment and column rotation by strong bolt LT3 10mm, OB is original bolt and SB is stronger bolt simulations.....	190

Figure 7-21 Column displacement time history by washer size 24 LT3 8mm; W20 is original washer size 20 and W24 is the washer size 24 simulations..... 191

Figure 7-22 Moment and column rotation by washer size 24 LT3 8mm; W20 is original washer size 20 and W24 is the washer size 24 simulations. .... 192

Figure 7-23 Column displacement time history by bolt M24 LT2 8mm, B20 is original bolt size 20 and B24 is the bolt size 24 simulations. .... 193

Figure 7-24 Column displacement time history by bolt M24 LT4 8mm, B20 is original bolt size 20 and B24 is the bolt size 24 simulations. .... 193

Figure 7-25 Displacement of the two corner by bolt M24 LT4 8mm, B20 is original bolt size 20 and B24 is the bolt size 24 simulations..... 194

Figure 7-26 Force and column displacement by bolt M24 LT2 8mm, B20 is original bolt size 20 and B24 is the bolt size 24 simulations..... 195

Figure 7-27 Moment and column rotation by bolt M24 LT4 8mm, B20 is original bolt size 20 and B24 is the bolt size 24 simulations. .... 196

Figure 7-28 Shear stress generated in the connection ..... 197

Figure 7-29 End plate deformation contour plot..... 198

Figure 7-30 Column displacement time history by BG less LT2 8mm, OBG is original bolt gauge (90mm) and LBG is the lower bolt gauge (80mm) simulation. .... 198

Figure 7-31 Column displacement time history by BG more LT2 8mm, OBG is original bolt gauge and MBG is the maximum bolt gauge simulation..... 199

Figure 7-32 Displacement of the two corner by BG less and more LT2 8mm, OBG is original bolt gauge (90mm), MBG is the maximum bolt gauge simulation and LBG is the lower bolt gauge (80mm) simulation. .... 200

Figure 7-33 Force and column displacement by BG less LT2 8mm, OBG is original bolt gauge (90mm) and LBG is the lower bolt gauge (80mm) simulation. .... 201

Figure 7-34 Force and column displacement by BG more LT2 8mm, OBG is original bolt gauge and MBG is the maximum bolt gauge simulation..... 201

Figure 7-35 Moment and column rotation by BG less LT3 8mm, OBG is original bolt gauge (90mm) and LBG is the lower bolt gauge (80mm) simulation. .... 202

Figure 7-36 Moment and column rotation by BG more LT3 8mm, OBG is original bolt gauge and MBG is the maximum bolt gauge simulation..... 203

Figure 7-37 Shear stress generated in the connection ..... 204

Figure 7-38 End plate deformation counter plot ..... 204

Figure 7-39 Column displacement time history by BD less LT2 8mm, OBP is original bolt pitch and LBP is the less bolt pitch simulations. .... 205

Figure 7-40 Column displacement time history by BD more LT2 8mm, OBP is original bolt pitch and MBP is the more bolt pitch simulations. .... 206

Figure 7-41 Displacement of the two corner by BD more and less LT3 8mm, OBP is original bolt pitch, MBP is the more bolt pitch simulations and LBP is the less bolt pitch simulations. .... 207

Figure 7-42 Force and column displacement by BD less LT2 8mm, OBP is original bolt pitch and LBP is the less bolt pitch simulations. ....	208
Figure 7-43 Force and column displacement by BD more LT2 8mm, OBP is original bolt pitch and MBP is the more bolt pitch simulations. ....	208
Figure 7-44 Moment and column rotation by BD less LT3 8mm, OBP is original bolt pitch and LBP is the less bolt pitch simulations. ....	209
Figure 7-45 Moment and column rotation by BD more LT3 8mm, OBP is original bolt pitch and MBP is the more bolt pitch simulations. ....	209
Figure 8-1 Different type of beam and column impact (a) the original gap (OG) (b) no gap (NG) (c) (NC) no contact .....	217
Figure 8-2 Column rotation and displacement LT1 10mm angle, .....	218
Figure 8-3 Column displacement time history LT1 8mm angle with and without a gap .....	219
Figure 8-4 Column displacement time history LT1 8mm angle, no contact .....	220
Figure 8-5 Mid bolt and column displacement LT1 10mm angle, no gap.....	221
Figure 8-6 Mid bolt and column displacement LT1 8mm angle, no gap.....	222
Figure 8-7 Mid bolt and column displacement LT1 8mm angle, no contact.....	223
Figure 8-8 Moment and column rotation LT1 10mm angle, no gap.....	224
Figure 8-9 Moment and column rotation LT1 8mm angle, no gap.....	224
Figure 8-10 Moment and column rotation LT1 8mm angle, no contact.....	225
Figure 8-11 Force and column displacement LT1 8mm angle, no gap .....	226
Figure 8-12 Force and column displacement LT1 8mm angle, no contact.....	226
Figure 8-13 Example of end-plate connection failure.....	227
Figure 8-14 Column rotation against displacement LT1 10mm .....	228
Figure 8-15 Column rotation against displacement LT1 8mm .....	228
Figure 8-16 Column displacement time history LT1 8mm, no gap.....	229
Figure 8-17 Column displacement time history LT1 10mm, no contact .....	230
Figure 8-18 Force and column displacement LT1 10mm no gap .....	231
Figure 8-19 Force and column displacement LT1 8mm no contact .....	231
Figure 8-20 Moment and column rotation LT1 8mm no gap .....	232
Figure 8-21 Moment and column rotation LT1 8mm no contact .....	233
Figure 8-22 The location of the element on the plate which strain was measured .....	233
Figure 8-23 Strain against column rotation of the single element, with different loading rates .....	235
Figure 8-24 Strain against time unit of the single element, with different loading rates .....	235
Figure 8-25 The location of three element on the plate which strain was measured ....	236
Figure 8-26 Strain against time of the three elements for 10mm thick plate, with different loading rates .....	237

Figure 8-27 Strain against time of the three elements for 8mm thick plate, with different loading rates ..... 237

Figure A- 1, Main drawing of the model ..... 253

Figure A- 2, Column drawings ..... 254

Figure A- 3, Column sections and key-points..... 255

Figure A- 4, Beam drawings and dimensions ..... 256

Figure A- 5, Beam sections and key-points ..... 257

Figure A- 6, Angle and End-plate sections and key-points ..... 258

# List of Tables

Table 3-1 Results from 10 experimental web-cleat tests ..... 33

Table 3-2 Results from 17 experimental end-plate tests..... 37

Table 4-1 Material properties for the column ..... 51

Table 4-2 Simplified Johnson Cook material model for the beam ..... 57

Table 4-3 Plastic Kinematic parameters for the splice plates ..... 57

Table 4-4 Johnson cook material for bolt 8.8 ..... 61

Table 4-5 Angle material properties ..... 65

Table 4-6 End plate and welding material properties ..... 69

Table 6-1 Summarize the parametric conclusions ..... 169

Table 6-2 Web-cleat connection results from parametric studies ..... 170

Table 7-1 Summary of parametric study results for end-plate..... 211

Table 7-2 End-plate connection results from parametric studies..... 213

Table 8-1 Comparison between two different connection types..... 239

Table B- 1, Model dimensions ..... 256

# 1 Introduction

A considerable amount of research effort has been expended over the last 15-20 years on investigations of the response of framed structures to the sudden loss of vertical load-bearing members due to accidental or malicious loading. Whilst the concept of progressive collapse of structures following failure of load bearing elements had been well known since at least the time of the Ronan Point disaster in 1968 [2], the more recent work was motivated by events such as the collapse of the Alfred P. Murrah building following a terrorist attack in 1995 [3] and the collapse of the WTC towers in 2001 [4].

Numerous computational analyses of frame response to column loss have been reported, utilising dynamic analysis or static analysis with dynamic load factors (e.g. Yang and Kim [5], Izzuddin et al. [6]). Whilst the actual time over which a column may lose its load carrying capacity following damage will vary depending on the causal action, Gudmundsson and Izzuddin [7] have recently suggested using an instantaneous column loss scenario as an upper bound design scenario. This potentially leads to a rapid dynamic redistribution of loads around the surviving frame members as the damaged frame deforms.

In the case of steel framed structures, particularly where the connections are not of a very stiff moment-resisting design and hence are likely to be much weaker and more flexible than the beams and columns, the most vulnerable part of the frame is likely to be the connections. Izzuddin et. al. [6] note that “...*the initiation of progressive collapse is largely determined by the deformation demands on the connections at the maximum dynamic response in relation to their ductility.*”

In the UK almost 25 years ago design rules for steel connections to meet axial tying capacity requirements were developed based on the experimental work of Owens and Moore [8] on static direct (axial) tension loading of typical nominally pinned or semi-rigid connections. But, as Paramasivam and Byfield [2] and Stoddart et al. [9] have noted, in the case of column loss, the resulting frame deformation is likely to produce a combination of axial extension and rotation, with prying action developed as a consequence of the rotation (Figure 1-1). Hamburger [10] similarly noted that “...*demands*

*applied on members and connections when resisting the initiation of a collapse may produce somewhat higher strain rates, may be of larger magnitude and will occur simultaneously with large axial tension demands.”*

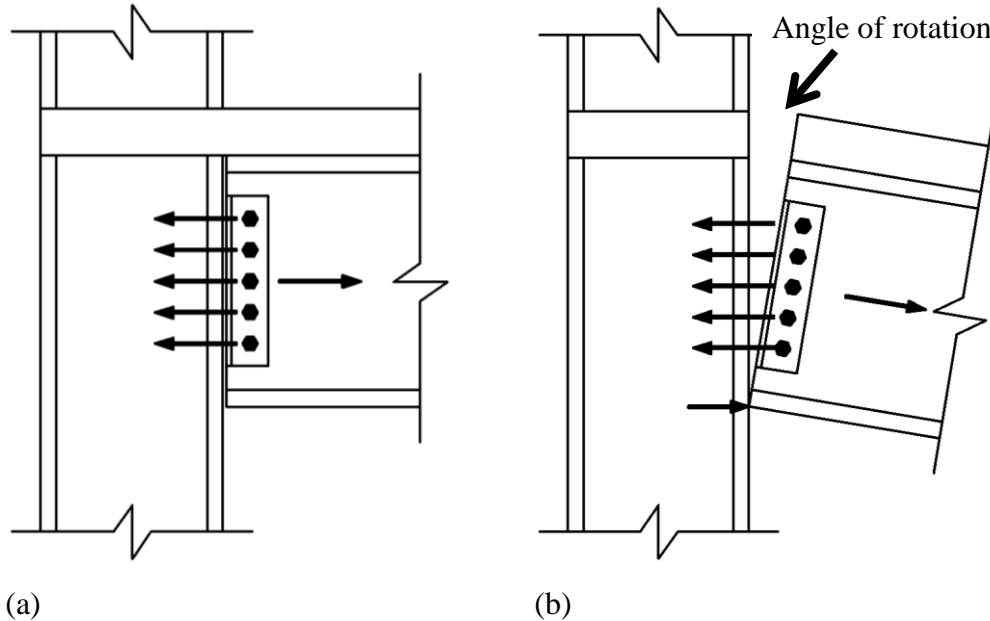


Figure 1-1 Tying forces (a) design assumption (b) prying action as a result of connection rotation[after [2]]

Reports compiled after the WTC collapses [11][12] state that there was a lack of knowledge on the dynamic behaviour of connections when loaded monotonically to failure. Thus, utilising the static axial tying capacity of the connections as a means of assessing their response in a progressive collapse scenario risks missing two important mechanisms: (i) the effect of applying load dynamically and (ii) the combination of axial and rotational deformation. Furthermore, this lack of knowledge raises questions over the validity of frame analyses which do not incorporate realistic connection models, since both the stiffness of the frame and the eventual failure criteria are likely to be affected by the connection response during dynamic loading.

Recent work has been published by Liu et al. [13] on experimental and numerical studies of the response of two-span beams, joined to a central column by web-cleat connections, when the column support is suddenly removed. This work shows good correlation between the experimental tests and the numerical model, but on a level related to the entire system rather than specifically concentrating on the connection performance.

As a response to the lack of knowledge on the dynamic capacities of connections and the mechanisms influencing failure at different loading rates, a programme of experimental work on quasi-static and dynamic monotonic loading to failure of steel connections was conducted at the University of Sheffield in 2010-11, with the underlying experimental approach outlined in Tyas et. al. [14]. This led to work at the University of Southampton [9][15] on component-based models of connection response to dynamically combined axial extension and rotation, which appears to offer a promising approach to the development of simplified connection models that could be incorporated in a dynamic frame progressive collapse analysis.

Dynamic finite element analysis has been used extensively to model the response of steel connections to cyclical loading, predominantly in seismic analysis. However, other than the work conducted at NTU Singapore [13], relatively little has been reported on modelling of rapid, monotonically increasing deformation of steel connections to failure. Sabuwala et. al. [16] present a study of the response of beam-column connections to blast loading using the ABAQUS FE code. Their model was well validated against static experimental tests conducted by Englehardt et al. [17] but no validation of the dynamic response was conducted. Crawford [18] and Morrill et. al. [19] present modelling and full-scale experimental results of steel frames subjected to blast loading, which show excellent qualitative correlation, but little detailed discussion of the quantitative response of the connections is provided. Jahromi et al. [20] present proposals for experimental tests of steel frame response to blast loading together with detailed modelling of the event using component-based mechanical models to represent the moment-axial force interaction of the connections although no details or results from the connection finite element models are presented or reported.

The main aim of the research presented in this thesis concerned the possibility of developing a detailed FE models of the connection response, validated against experimental data, which could be used to investigate the mechanisms of connection response and failure, and subsequently conduct parametric studies of connection performance and propose alterations to connections to improve their resistance and ductility.

This thesis consist of two parts. A finite element model is first constructed and validated and is then used in the next part for connection behaviour studies. The first part consists of Chapter 4 and 5, where development and validation of the model are presented and explained. The second is presented in chapter 6, 7 and 8, where different parametric studies have been done on both types of connection (web-cleat and end-plate) to find the effect of different loading rates, type and connection geometry. This thesis divided into 9 chapters; the main contents of each one are presented as follows:

Chapter 2: **Literature** review, this chapter explains the definition of progressive collapse by reviewing different codes of practice and providing some examples of historical events. This chapter emphasis is on importance of the study of dynamic behaviour of connections to prevent progressive collapse and provides some examples of previous research in this area.

Chapter 3: **Methodology**, gives a brief explanation on how the experimental studies on both types of connections (web-cleat and end-plate) were conducted prior to the start of this PhD research. This chapter also provides a brief insight on material models, different solvers and how the connection resistance was measured in numerical studies.

Chapter 4: **Development of steel connection model using finite element method**, describes how these finite element models were developed, including the building of different parts geometry, meshing and applying the boundary conditions using ANSYS and LS-DYNA software.

Chapter 5: **Finite element model of connections**, provides the details of different stages of validation and how numerical instability were solved. Firstly, validation of the inertia of the main parts of the model was provided. Then each connection model (web-cleat or end-plate) was validated against experimental results both quantitatively and qualitatively

Chapters 6 and 7: **parametric studies of web-cleat and end-plate connections behaviour**, these two chapters provide the results of different studies on loading rate, type and connection geometry. These two chapters answer the main question about connection sensitivity to different changes and provide comparison between these two types of connection (web-cleat and end-plate).

Chapter 8: **Discussion**, describes the key findings of the modelling from previous chapters and some suggestions on how to improve the connection behaviour, also include two extra different analysis on both connections (web-cleat and end-plate) and a short comparison between web-cleat and end-plate connections.



## 2 Literature Review

For the past 20 years an extensive amount of work has been done on structural integrity and progressive collapse, which was the result of tragic events happened all around the world and caused the international community to become aware of the importance of structural collapse. An exhaustive search in literature showed that as there are many different connection types and dynamic experiments are very expensive there is a lack of research and explanation on dynamic behaviour of connections and most structural analysis were just based on static performance of the connection. As there is a gap in knowledge, research on performance of steel connections under the fast dynamic loading became the main objective of this thesis.

### 2.1 Progressive collapse

The General Services Administration [21] offers a specific description of the phenomenon of progressive collapse: “*Progressive collapse is a situation where local failure of a primary structural component leads to the collapse of adjoining members which, in turn, leads to additional collapse. Hence, the total collapse is disproportionate to the original collapsed area*”. Also it has been suggested that the ratio between the total collapsed volume of the structure over the volume which directly damaged by the triggering event be called the degree of “progressivity” [22] [23].

Almost all structural collapses start from local as opposed to system-wide damage (earthquakes being a possible exception) but the point that distinguishes progressive collapse is that the total damage is disproportionate to the local damage caused by the initiating event. Such collapses can be caused by many different reasons, including abnormal loads not normally considered in design (e.g., gas explosions, vehicular collisions, and sabotage), severe fires, human errors in design and construction and mismanagement ([24][25]).

Highly redundant structures with ductility are likely to absorb local damage better than the non-redundant structures. Structures which are well tied yet lack ductility are more

vulnerable, such as large panel or bearing wall systems, pre-cast concrete slabs or steel joist floors supported on masonry walls [26].

The Tie Force technique is a design method to resist progressive collapse and is adopted by different a number of codes [27], [28], and [29]. In the Tie Force method, the building is mechanically tied together, improving continuity, ductility and permitting the development of alternate load paths [29]. Tie forces are generally provided by the structural elements and connections, which are designed using conventional techniques to carry the standard loads applied upon the structure [29] but are also required to be capable of resisting tensile forces in the event of damage to the structure. Most standards recognize the desirability for continuity between structural elements, and several specify minimum tie forces to achieve continuity. [30]

Depending on the function and location of these ties, they can be categorised as: internal, external, horizontal and vertical and the required tie strength for each must be satisfied [31].

### **2.1.1 Defining progressive collapse**

The word ‘progressive collapse’ can have different meanings and related terms often appear in the literature. The word ‘disproportionate’ is sometimes used as a synonym for ‘progressive’ as almost all structural failures involve to some degree an element of some progression [32]. A number of different definitions can be found in the literature and standards in relation to progressive collapse mitigation, for example:

- **ASCE/SEI 7-05 Minimum Design Loads for Buildings and Other Structures** defines term progressive collapse as *“the spread of an initial local failure from element to element resulting, eventually, in the collapse of an entire structure or a disproportionately large part of it.”*
- **NIST Best Practices for Reducing the Potential for Progressive Collapse in Buildings** states: *“Progressive collapse – The spread of local damage, from an initiating event, from element to element, resulting, eventually, in the collapse of*

*an entire structure or a disproportionately large part of it; also known as disproportionate collapse” [30].*

- **Eurocode 1 – Actions on structures – Part 1-7: General Actions – Accidental actions** does not provide a specific definition for the term progressive collapse. A related term, robustness, is defined as *“the ability of a structure to withstand events like fire, explosions, impacts or the consequence of human error, without being damaged to an extent disproportionate to the original cause”*. Thus a robust structure is one capable of resisting progressive collapse.
- **United States General Services Administration (GSA)** released the Progressive Collapse Analysis and Design Guidelines in 2003 [21] and explained progressive collapse as *“a situation where local failure of a primary structural component leads to the collapse of adjoining members which, in turn, leads to additional collapse. Hence, the total damage is disproportionate to the original cause.”*

Eurocodes [28], United States Departments of Defence [29], GSA [21] and British Standards define an acceptable limit on the extent of floor area that can collapse as result of an initial local failure [33]. These standards thus assume any damage spreading beyond a defined acceptable collapse area as a result of a local failure to be disproportionate [34]

### **2.1.2 Notable progressive collapses**

Unfortunately there are many examples of progressive collapse around the world, some of which resulted in a large loss of life. In modern times the importance of this type of failure came into attention in the late 1960s with the Ronan Point building failure in UK but the collapse of World Trade Center buildings in New York in 2001 was the catalyst for intense research in this area. Four examples of serious collapses are discussed here:

- **Ronan Point, London, 16 May 1968**

A gas explosion in the kitchen on the 18<sup>th</sup> floor of a 22 storey tower block at Ronan Point caused a progressive collapse of the corner of the building due to the lack of horizontal ties between the precast panels and explosion caused the removal of precast walls of that

floor, this event initiated a domino reaction and caused the collapses completely to the ground [35] [22]. The main lesson learnt from this incident was to keep the continuity in the structures, by making the joints more capable to resist the loading caused by the collapse.



Figure 2-1 Ronan Point building after the May 1968 collapse [22]

- **L’Ambiance Plaza, 23 April 1987**

L’Ambiance Plaza had 16 floors, it collapsed while under construction, in Bridgeport, Connecticut, USA. The building had two wings of post-tensioned concrete slabs supported on steel columns. The structure collapsed during construction, but unfortunately the exact reason was never discovered. Two theories exist for initiation of the collapse; the inadequate strength of one of the lifting jacks or failing of a wedge support caused the local collapse happened at the upper of the west wing was followed by the east wing collapse, which meant the complete collapse of the structure system [34].

A possible reason of the east wing collapse was that the slabs had post-tensioning tendons, therefore when the tendons were damaged in one bay of the west wing during the course of collapse, all the bays through which the tendons were transmitted, including the east wing, and so no longer had suitable strength to resist the gravity loads [34]. This collapse

showed the importance of tie strength and continuity in structures even at the time of their construction.

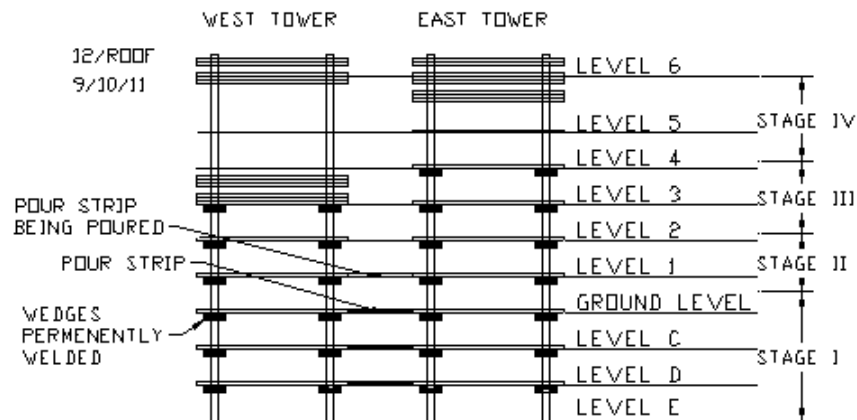


Figure 2-2 Status of Construction at Time of Collapse [36]

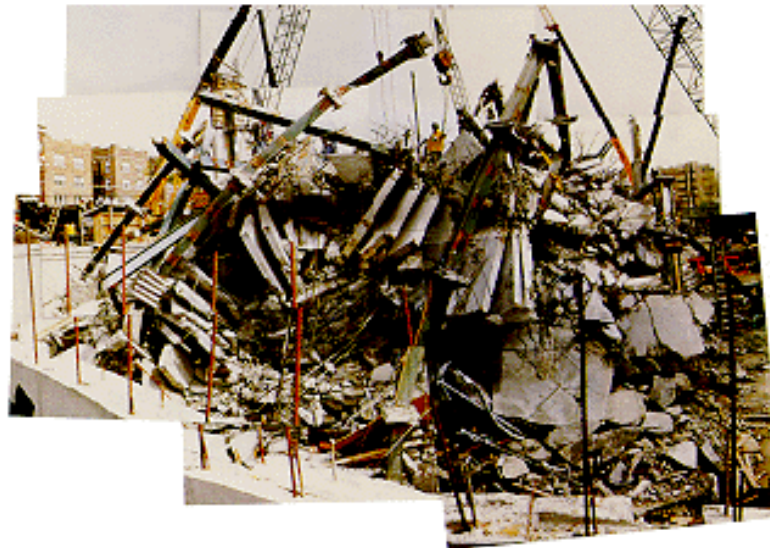
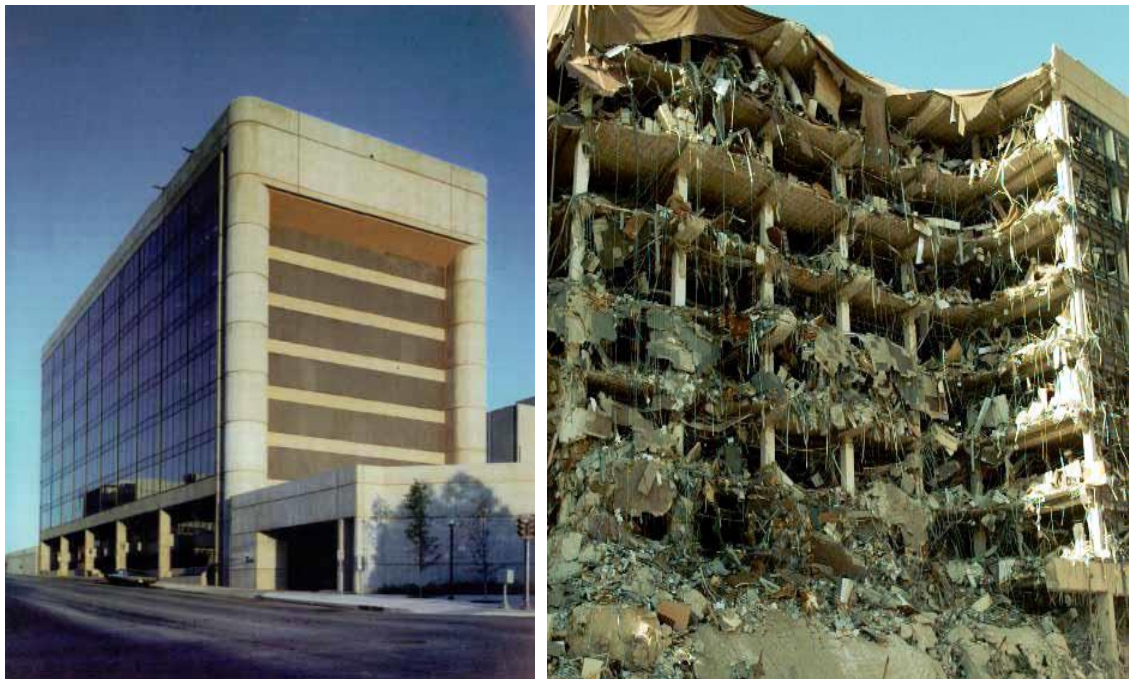


Figure 2-3 Ruins of L'Ambiance Plaza [36]

- **Alfred P. Murrah Federal Building Bombing, April 19, 1995**

A truck bomb was exploded in front of the Alfred P. Murrah Federal Building. The magnitude of the explosion was such that one-third of the structure was destroyed. The north face of the structure was destroyed totally and the rest of the structure suffered extensive damage [37]. The truck was located at the base of the building and destroyed

three columns which led to failure of a transfer girder. Failure of the transfer girder caused the breakdown of columns supported by the girder and floor areas supported by those columns. The Murrah Building disaster was clearly a progressive collapse involving a clear order or progression of events: column demolition; transfer girder failure; failure of structure above [22].



(a)

(b)

Figure 2-4 (a) Building Prior to Attack (b) Federal Building after collapse [38]

- **World Trade Centre, New York USA, 2001**

On the morning of Tuesday, September 11, 2001, terrorists flew two hijacked commercial jets into the WTC towers. Both towers collapsed within two hours of impact, killing almost 2,800 people. In addition to the devastating loss of life, the dust and debris emanating from the collapse and the ensuing fires created environmental concerns for the public that persisted more than a year after the disaster [39].

A combination of impact and fire damage caused the structure at the impact zone to lose its ability to support the load above it, and when the support was destroyed the structure above collapsed. The mass and impact of the collapsing upper part of the tower caused a progression of failures extending downward all the way to the ground [40].

Although the World Trade Tower collapses were “progressive collapse” it is arguable whether they could be classified as “disproportionate collapse.” The initial damage to the upper parts of the buildings was extensive but the towers did not collapse immediately. The resulting fires were extreme and resulted in weakening of the damaged structure to such an extent that the top part collapsed and progressively destroyed each floor as the debris fell [40].



Figure 2-5 WTC in the time of collapse [40]

## **2.2 Standards and codes**

### **2.2.1 Europe**

In the United Kingdom important changes were made in regulations to prevent progressive collapse from unintentional loading events following the Ronan Point collapse. Building Regulations (1976) required that: “The building shall be constructed so that in the event of an accident the building will not suffer collapse to an extent disproportionate to the cause” [26].

These requirements were for buildings with five or more floors, and provided three approaches in order of complexity: (i) Tying (mainly used to provide the continuity), (ii) Bridging over (theoretical removal of components with a limitation on damage to 15% of the floor zone) and (iii) Key element resistance design in which elements are designed to resist a pressure of  $34 \text{ kN/m}^2$  [26]. It is unclear to what extent these requirements have

added to the robustness of buildings against progressive or disproportionate collapse. On one hand, it is clear that provisions which require additional robustness against direct damage, and some consideration of load paths and adequacy of structural strength in case of primary damage, must provide some inherent additional robustness. But on the other hand, the arbitrary value of  $34\text{kN/m}^2$  applied as a *static* load, can in no way precisely mimic the loading from a real explosion. And there is no detailed evaluation of the ability of the prescribed *static* tying capacities to produce an adequate reserve of strength for the *dynamic* loading which will be produced as a structure re-distributes loads following a sudden column loss.

Eurocode 1, section 2 [28] provides requirements which form the basis of structural design and indicate that a structure should be designed in such a manner that the system will not collapse as a result of events such as blast, fire and human faults to a degree of disproportionate to the initial cause. Engineers are able to choose the best method to design the structural system to resist the progressive collapse event e.g. using tie forces in the structure or having a redundant structure which can endure unintentional elimination of a key component [26].

### **2.2.2 United States**

After the 1968 Ronan Point collapse [26] ASCE 7/ANSI A58 [41], was edited and for the first time provided a requirement for progressive collapse as a result of “local failure caused by severe overloads” (Unit 1.3.1 of ANSI Code A58.1-1972. ANSI Code A58.1-1982, Unit 1.3) renamed General Structural Integrity, included an additional comprehensive procedure, and for guidance refers to a significantly extended comment part and citations.

ASCE 7 suggested many structural designs which would contribute to alternative load paths design i.e. the transfer of load from a location with local damage to the rest of the structure with no damage [18]. Beam to column connections should have the important role of transferring the load from damaged parts to the rest of structure, as for this reason they have to be improved in the capacity and also accommodate the resistance for seismic design and different loading conditions like the load reversals. And at the time of design

it is necessary to consider some damage transfer to the top and bottom floors, and also the horizontal damage must be limited [26].

### **2.2.3 Canada**

National Building code of Canada (Published in 1995)[42] suggested that structures should be designed in a way to keep their unity and endure all damages could happen throughout the construction and service life of structure [18].

Commentary C in part 4 describes structural integrity as “the ability of the structure to absorb local failure without widespread collapse,” and suggests designers consider the structures’ behaviour under extreme loading. Different methods of design were introduced in this guideline e.g. providing alternative loading paths, local resistance of each key-elements and minimum tie forces in the structure. These recommendations are provided in Commentary to the code and they are not mandatory to the designers for solving the general problem of structural collapse [26].

## **2.3 Different methods for preventing progressive collapse**

Three different methods of design are available to provide structures with resistance against progressive collapse.

### **2.3.1 Redundancy or alternate load paths**

In this method, the structure is designed having redundancy which makes it possible for loads to be transferred via alternative paths in the event of a local failure to a component. This method has a benefit of being direct and simple, and the most common application is when a building loses one of its columns but does not collapse as result of its redundancy [22]. However, there is a danger with this method if the vulnerability of different components in the structure is not considered. Codes and standards incorporating the alternative load path approach do not consider the ease with which relatively lightly loaded columns might be removed compared with more massive ones. Thus designers might consider it preferable to use more small (and vulnerable) columns rather than fewer larger (but more robust) columns. For resistance against malicious attacks (as opposed to random accidents), this could be the wrong strategy in design [22].

As a general rule, it is beneficial to have redundancy in lateral and vertical load resistance of the structures against progressive collapse. This method promotes more robustness in structures and helps to ensure that alternate load paths are available in the case of individual member failure [43].

### **2.3.2 Interconnection or continuity (Tie strength)**

The alternative load path method is one of the main methods to prevent the progressive collapse, and to make sure structure is capable of bridging over the damaged area, all the structural components should have to meet the tie force criteria [29].

It is important to maintain the continuity of the load path around the plan geometry to be able to develop alternative load path in the structure, for that reason connecting elements that are used to tie different structural components (like beam and column) together must have sufficient resistance to undergo the extra load generated after missing a key-element in the structure [29]. Majority of the standards identify the continuity between structural components, and provide a number of specification to develop least possible tie forces to reach continuity. [30]

### **2.3.3 Local resistance**

In this method, critical elements which can be subjected to attack or damage should be provided with sufficient resistance to prevent their removal and thus avoid progressive collapse. However this design approach requires assessment of the magnitude and location of accidental or malicious loadings which is impossible to define in a simple and objective way [22].

## **2.4 The importance of steel connections**

When analysing buildings under accidental dynamic loading conditions, structural properties which are not typically considered by the designer, such as rate-dependent material properties and inertial effects, must be considered. For example, the optimal structural response to blast occurs when elements deform and use up or absorb energy prior to fracture or failure [38]. Effect of strain rate on the mechanical properties of steel structural joints is a significant factor in assessing the safety of structures against high

speed loadings [44] to maintain the structural integrity after the local loss of key structural members, thus preventing a disproportionate or progressive collapse of the structure, it may be necessary to consider the rate dependent effects.

Early work by Owens and Moore [8] investigated the ultimate axial capacity of steel connections subject to direct tension loading and formed the basis for calculating the tying (or tensile) capacity used in UK design today [45]. However these calculations did not account for joint rotation, which must inevitably occur if the primary alternative load-carrying mechanism involves axial forces in the frame members, as envisaged by the tying force approach. This rotation will inevitably induce moments in the connections, in addition to the envisaged axial tensile forces. If rotations are high, prying action can develop when the lower beam flange contacts the supporting column, even in a nominally pinned connection such as a web-cleat connection. This moment action on the connection will inevitably reduce the axial capacity. This is extremely important when considering the loss of a primary column element and the frame is required to support a double bay span with large connection rotations [9].

The effect of strain rate on the mechanical properties of steel structural joints is a significant factor when assessing the safety of structures subject to high speed loadings [6].

#### **2.4.1 International reports and their recommendations on progressive collapse**

Many institutes have conducted research and investigations to produce reports on progressive collapse; in these reports they tried to address and explain how damage can be initiated, propagate through the structures and gave some recommendations on how to prevent or reduce the effects of this type of collapse. Two of these reports and some of their recommendations which are about the connection's influence are introduced here:

- **Arup (UK):**

Arup were commissioned to conduct a state of the art international literature review into robustness and disproportionate collapse in structures on behalf of Communities & Local Governments (CLG) and the Centre for the Protection of National Infrastructures (CPNI) [46]. The report aimed to ascertain both the state of knowledge in the subject and, perhaps more importantly, identify the gaps in knowledge against which future research initiatives should be targeted. The report contained a number of recommendations related to steel connections.

*Recommendation 15: Develop guidance on the rotational and combined rotational/axial capacity of steel, steel-concrete composite and reinforced concrete connections.*

“Because of insufficient data, a designer cannot undertake an alternate load path analysis and based on the results show that there is adequate rotational ductility capacity in the connections. No comprehensive and systematic data exists on the rotational capacities of the main connection types in either steel or reinforced concrete construction, although significant advances have been made in particular areas by various researchers.”

*Recommendation 25: Assess the influence of strain rate sensitivity.*

“Materials are known to experience increased yield strength at high strain rates, an effect which is typically taken into account in the analysis of structural elements under blast and impact loading. The total response of the structure undergoing the loss of a column occurs over a longer period than the immediate response of the structural element exposed to blast or impact load. Studies show that strain rate increase plays an important role on the response of the connections. As mentioned, little data is available to examine the importance of strain rate enhancement in an alternate load path analysis and research would be useful in this area.”

- **AISC (Blast and Impact Progressive Collapse, US)**

The American Institute of Steel Construction (AISC), has published guidance for commercial and industrial buildings subjected to extraordinary loads and responses [38].

Two recommendations from this document relevant to steel connections are:

- i. Investigations needed to find out how to maintain reserve axial tension capacity of steel beam to column connections (i.e., simple and moment resisting) after reaching significant inelastic rotations.
- ii. The important key issue of finding the effect of blast loads on beam to column connection performance including severe beam and column twist, lateral bending and strain rate effects on weld and base material ductility needs to be investigated and the solution needs to be found.

#### **2.4.2 Previous Projects & Researches on steel connection behaviour**

Lack of prior data, especially on connection behaviour, was the motivation for an extensive program of dynamic connection tests recently conducted at the University of Sheffield, UK. A bespoke test rig was developed, which facilitates testing of connections to failure at varying loading rates, from (effectively) static to very fast dynamic range. Loading is imposed either in axial tension or a combination of axial tension and moment [14].

A number of projects have been conducted on the robustness of steel connections but none have studied connection behaviour for fast dynamic behaviour experimentally. The most relevant studies are presented below.

- Kuhlmann et al. [47]

The aim of this project was to carry out experimental and theoretical investigations on the behaviour of steel and composite joints in framed structures to derive robustness requirements in order to develop good practice recommendations. Figure 2-6 shows the experimental set up before and after the tests, and Figure 2-7 provides a picture of a test after the experiment has been performed. The results from numerical simulations showed the difficulty to model the real behaviour of

structural joints exposed to bending moments and axial loads with the elements in the existing finite element software. And as they suggested to be able to simulate the behaviour of these joints in a more accurate way the development of a new FE model for future research is necessary.

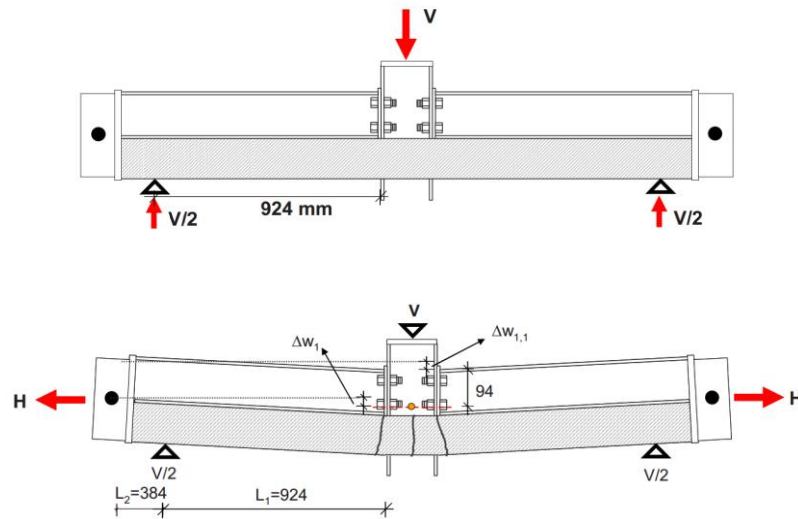


Figure 2-6 Experiment arrangements before and after [47]



Figure 2-7 A picture of these experiments [47]

- Sabuwala, Linzell & Krauthammer, 2005 [16]

In this study the efficiency of three different connections designed to withstand seismic and blast loads was evaluated. To develop various connection models ABAQUS software was employed. Finite element models were calibrated using test data; verified models were then subjected to simulated blast loads and the

efficiency and behaviour of the connections evaluated. The experimental arrangement is provided in Figure 2-8.

The conclusions from this study appear to indicate that criteria provided in the US armed forces design manual for the munitions stores UFC [48] which is used to measure the capability of a steel frame based on rotations of the structural elements is not suitable and it is better to be revised. The connection details satisfied the criteria provided in the code but results showed high localized stresses which indicated the failure in the connection. It could be beneficial to have strength based criterion in the code document to expand the existing serviceability criteria to evaluate the steel frame performance under blast and impact loadings.

Also in this study it was recommended that unreinforced connections should not to be used under blast conditions as they showed undesirable failures within the connection zone near the column face.

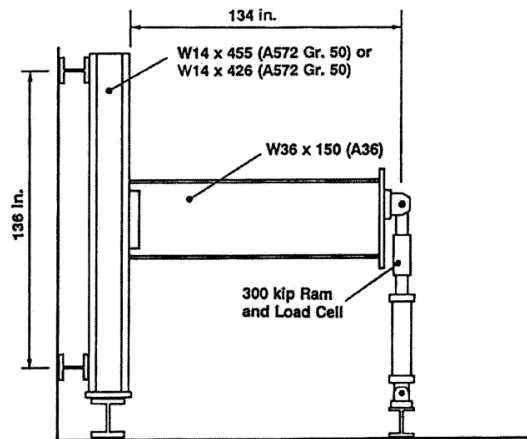


Figure 2-8 experimental setup [16] [17]

- Hauran, 2009 [49]

Ascertaining how much moment can be transferred by the connection and its relevant rotation during progressive collapse was the aim of this project. 3D non-linear finite element analysis was conducted and compared with the test results for different types of semi-rigid connections. Additional comparisons were made with

mathematical models developed by other researchers. An example finite element model example is illustrated in Figure 2-9.

The research review in this study observed that generally previous experiments used strong beams in order to ensure that the connection fails prior to the connecting beam, and also columns were selected that would not experience plastic deformations. Both of these behaviours were well captured by the finite element analysis.

This study showed the importance of knowing the connection behaviour and having more realistic dynamic experiments. Also having a well-validated finite element model of these connection helped to develop good mathematical models to predict the connection resistance in different loading conditions.

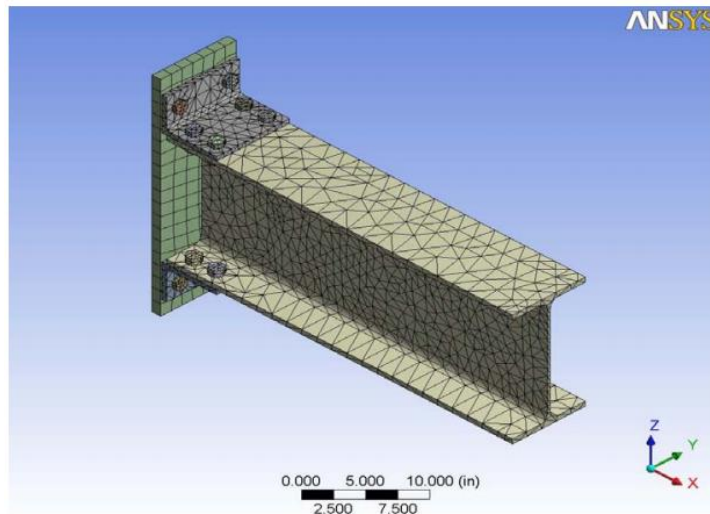


Figure 2-9 ANSYS model made for analysing the connection [49]

- Muñoz-Garcia, 2005 [50]  
A series of analyses was conducted on some of the most common types of connections like simple and semi rigid steel which are used in UK such as flexible end plates, web cleats, flush and extended endplates. LS-DYNA software was used to develop an explicit finite element analysis code and to assess the connections ability to resist rapidly applied tensile loads; the model is shown in Figure 2-10.

Cowper Symonds material properties were used to capture the effects of strain rate as these analyses were conducted for fast dynamic analysis. Results from these analyses on steel connections showed that static methods of analysis are not suitable to predict the structural performance during progressive collapse. These analyses also showed that steel connection response was affected by the load rate and, in general, tended to make connection failure more brittle thus negating the benefits associated with steel strength enhancement arising from the increased rate of loading.

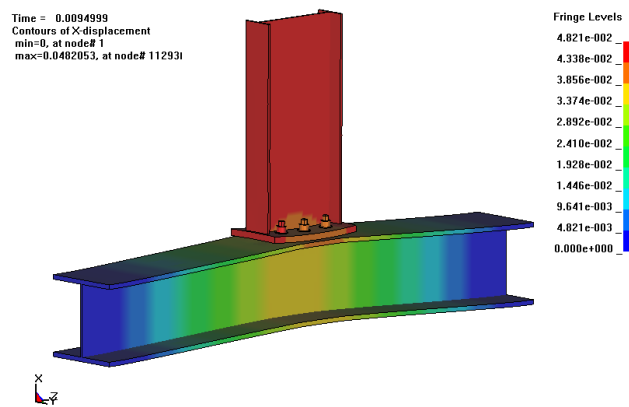


Figure 2-10 LS-DYNA model made of the connection [50]

- Sadek, Main, & Lew, 2010 [51]

Tests were conducted both experimentally and computationally on steel beam to column cruciform assemblies, with three different column sections and two beam sizes. The assembly represented a portion of a steel frame building designed as part of the National Institute of Standard and Technology research programme to prevent progressive collapse.

Each assembly was analysed using two levels of modelling resolution. First, large number of elements with solid and shell elements were used to develop a complex model, and second, a model was developed with less elements but using beam and spring elements. An example of the complex model is shown in Figure 2-11 and the connection after failure is provided in Figure 2-12. Results from these studies showed an insight into connection behaviour and failure modes, including their capacity for tensile load developed in the beams.

Conclusions from these studies showed that the model with less elements and beam and springs could capture the behaviour as well as the complicated model. This model could then be used in frame analysis for steel structures to assessing the capacity and robustness of the building structures.

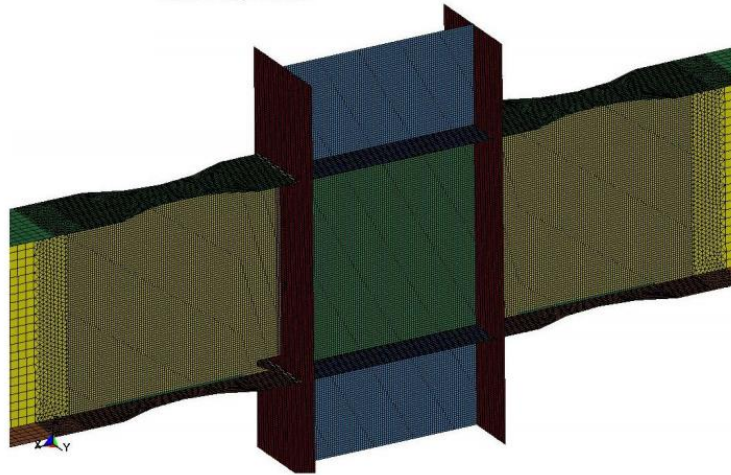


Figure 2-11 Finite element model made to study the experiments [51]

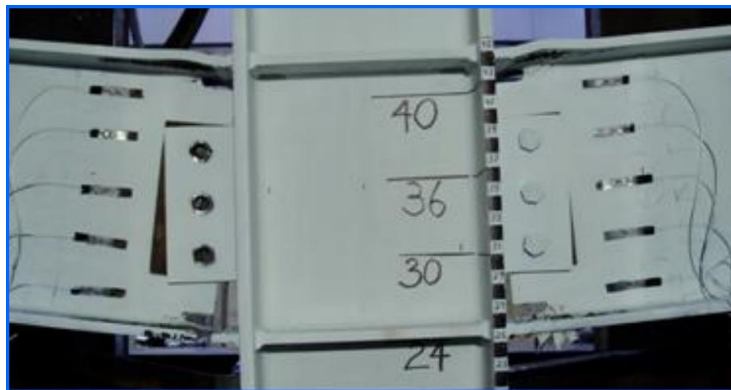


Figure 2-12 An image of the experiment after the connection failure [51]

- Paramasivam & Byfield, 2007 [2]

This research was conducted to investigate the tying force by using a case study on a steel frame building in which support to a perimeter column is removed. Results from this study showed that standard beam-to-column connections have insufficient ductility to endure the large deflection that occurs during catenary

action and the factor of safety against collapse was less than 0.2. An example of this connection failure is provided in Figure 2-13.

The tying resistance of the connections are generally measured with no rotations and just tension in the connection. By having rotation applied to the connection as a result of catenary action, prying action develops in the connection and leads to rapid failure. The conclusion from this study was that multi-storey buildings would resist the malicious actions by providing an emergency bracing over the localised damaged location in the structure, rather than just using catenary actions as the only option to provide robustness. However in both cases the connection resistance has an important role in structural resistance.

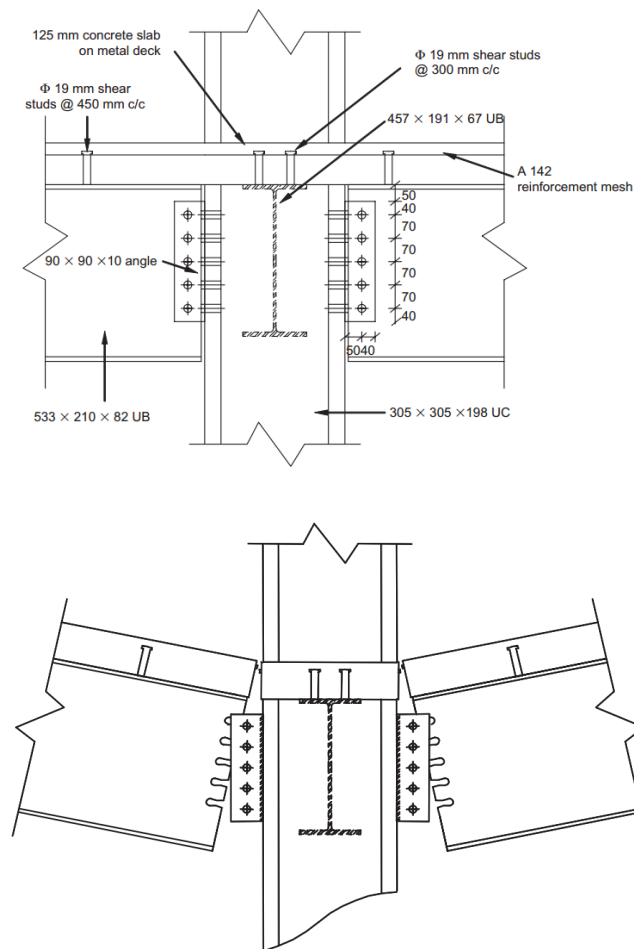


Figure 2-13 Experiments arrangement before and after [2]

### 2.4.3 Different failure modes of bolt bearing connection

Connected plates in bearing joints are in contact with bolts shank which then transfer the load by developing shear force in the bolt and bearing stress around the bolt holes. The behaviour of this type of joint was widely studied over the past half a century [52][53].

By applying load to the joint, failure can occur at a critical location if the this load exceed the bearing strength of the material, the bolt hole net cross-section tensile capacity, splitting failure at the plate edge, the bolt's shear capacity. Of all of these the tensile failure of the net cross-section is the most well defined. Material properties and geometrical factors are the two most important parameters on which the failure mode depends. Some research also exists on curling failure [52] which reduces the bearing strength [53]. Figure 2-14 shows an example of each plate failure.

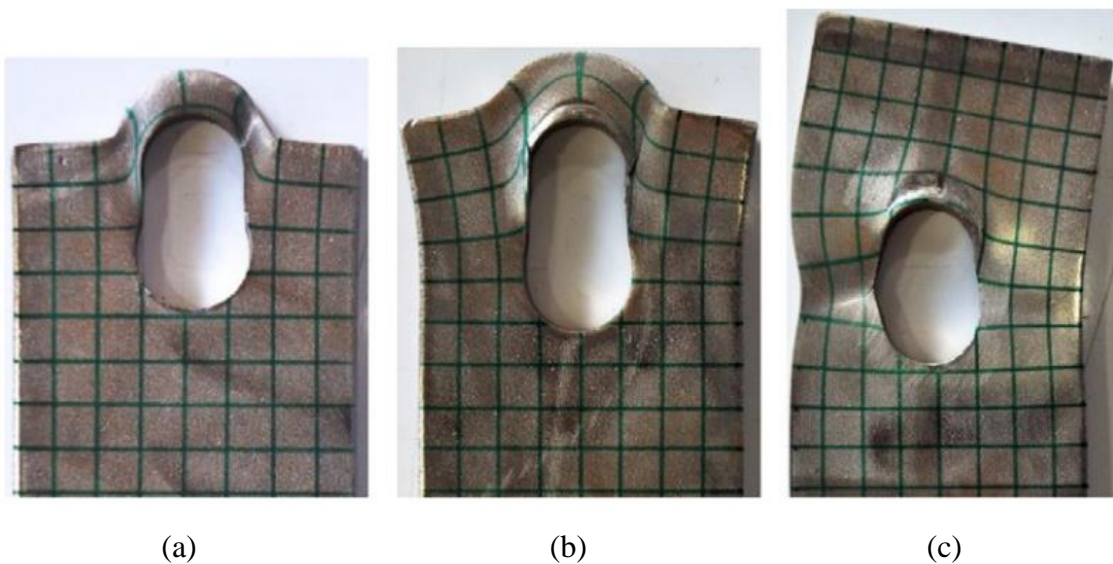


Figure 2-14 (a) Shear failure (b) Splitting failure (c) Net-cross section failure [53]

The failure mechanism becomes increasingly non-linear as the material plasticity spreads around the connection with the effect of strain hardening until the failure happens at one of the critical locations mentioned above. Unless preloaded bolts are used, the resistance to movement caused by inter plate friction is relatively small and connection resistance increases greatly, after initial slip and the bolts move into bearing [54].

The contact pressure develops a bearing stress between the bolt and plate. Initially the area of the contact is small and can build a very high concentration of stress and yield the

material at a very low level of loading. The embedment caused by yielding allows the bolt to have a larger contact area, this kind of behaviour is nominally interpreted as elastic behaviour, as in early stages of loading the connection stress concentrations effects are removed by material yielding [53].

To understand the correct mechanism of failure in the connection and help to achieve a ductile response it is necessary to study the bearing force distribution [55][56]. Detailed finite element analysis has made it possible to investigate the stress-strain effect in the bolt and plate at different stages from elastic up to plastic and failure deformations [53][57]. Figure 2-15 shows a simple plate and the results of a bolt/plate simulation.

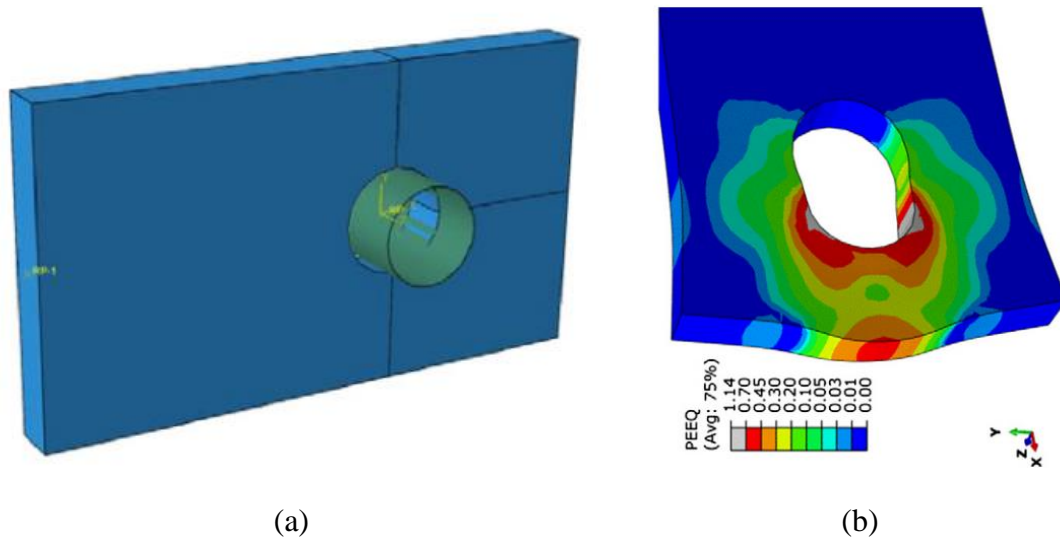


Figure 2-15 (a) Simple finite element model (b) Plate stress distribution [53]

## **2.5 Conclusion**

Initiation of progressive collapse begins by losing a key-element, and continues throughout the structure by over-loading adjacent structural members as the load is re-distributed. The proportion of the collapse can be controlled if the rest of the structure can successfully transfer the load to the undamaged part in the absence of a key-element (alternative path). Tie strength and continuity are the important parameters in order that structure can resist this condition and be able to establish this new alternative load path. This can't be done without having a reliable connection between vertical and horizontal elements of the structure. As progressive collapse is a dynamic event, it is necessary to know the connection response under dynamic conditions. There is still considerable uncertainty on this topic and consequently this research been conducted to help in understanding and filling the gap in knowledge on the behaviour of two different connections (web-cleat and end-plate) under different loading rates, types and geometries.

### **3 Methodology**

This chapter explains how studies on web-cleat and end-plate connections subjected to rapid rates of loading were conducted. Prior to the start of the author's PhD study, a series of experiments were performed as part of an EPSRC funded research project [1]. The research detailed herein concerns the development of numerical models validated with the experimental results and parametric studies to investigate connection behaviour across a wider range of loading rates and test configurations than was possible in the physical tests. In this chapter a brief description is given of the experiments before a detailed explanation is presented of the numerical modelling approach adopted.

#### **3.1 Experimental study**

Experimental work was conducted at the University of Sheffield Blast & Impact Laboratory, Buxton, UK, using a purpose built pneumatic loading rig. Full details of the rig and the experimental methodology are presented in Tyas et. al. [14] but a brief overview is given here.

The approach to testing these non-preloaded connections (Figure 3-1) was to fix one end of a beam stub to a stiff reaction frame, and connect the other end to a stiff column using the connection under investigation. The column is mounted on roller bearings such that it is free to move ("fly") both translationally and rotationally. Loading is applied to the "flying" column through loading rams, forced by pneumatic pressure, either statically (by attaching a compressor to the rear of the piston bores) or dynamically (by retaining the

pressure in a reservoir prior to the bursting of a brass retaining diaphragm). The system has the capability to produce dynamic loads of up to ~200kN per ram, with rise times from 5ms but controllable to slower rates by constricting the airflow. In the absence of definitive data on the actual loading rates which a connection might experience in the progressive collapse of a structure, the loading rates for this study were chosen to represent quasi-static conditions (>100s to failure) and an upper bound on what might be expected in sudden load and geometry redistribution in a column-out scenario (<100ms to failure).

The loading rams were used to push the “flying” column away from the test connection. For direct axial tension tests, two rams equally spaced about the test connection were used. A single ram used eccentrically gave combined axial and moment loading. In all tests conducted in the work presented here a single ram was used parallel to the axis of the test beam and offset by 660mm. A schematic diagram of the rig is shown in Figure 3-1 and a photograph in Figure 3-2.

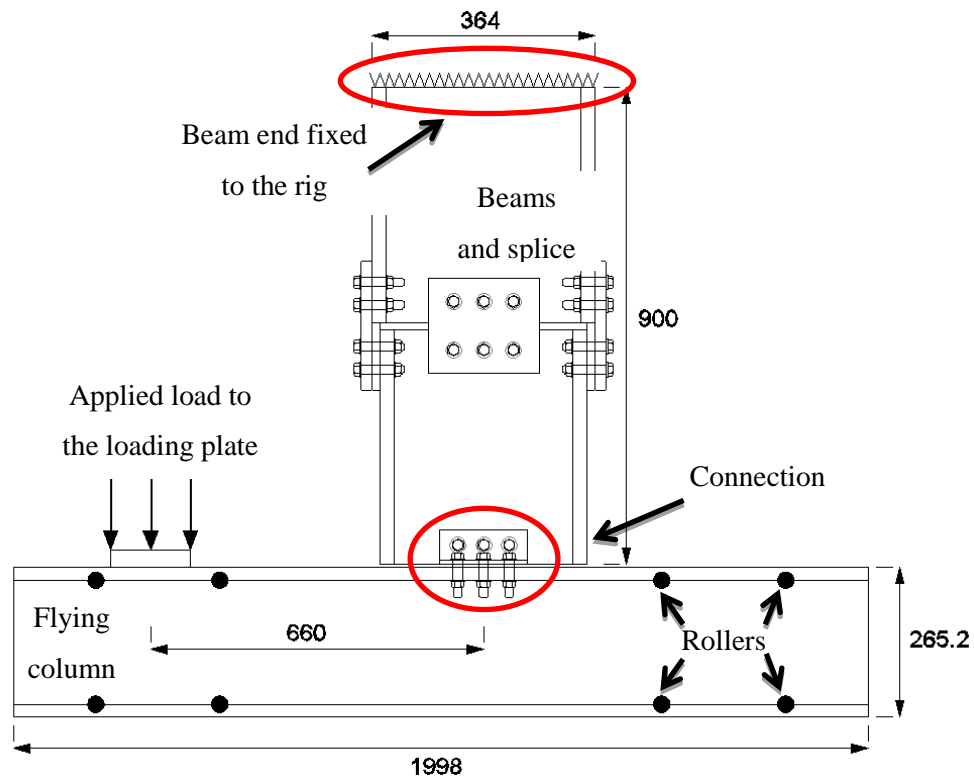


Figure 3-1 Schematic diagram of the test arrangement

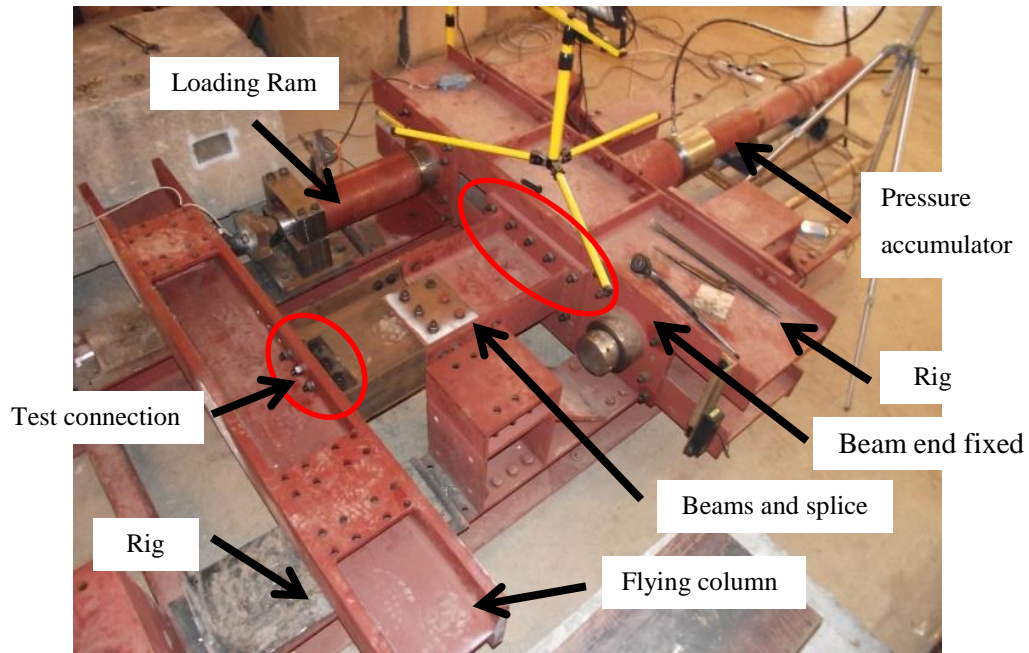


Figure 3-2 Photograph of test specimen assembled in the test rig

Applied loads were recorded using a purpose built and calibrated load cell placed between the loading ram and column. Column displacements were recorded at two points using M7 laser distance sensors and with a bandwidth of 10 kHz and resolution accuracy of  $\pm 0.6$  mm, manufactured by MEL Microelektronik GMBH. All data were recorded using HS4 Handyscope USB 16-bit digital oscilloscopes, operating at up to 20 kHz in the dynamic tests. High speed video footage of the connection deformation was obtained at up to 1,000fps using a Phantom v4.2 recorder with a digital video camera. Rotation and translation of the connection, together with the connection moment and axial tension forces, were calculated using the approach set out in Tyas et al. [14].

### 3.1.1 Web-cleat connection

Web-cleat test connections comprised double angle web cleats, with three property class 8.8 M20 bolts connecting the angles through the beam web and a total of six property class 8.8 M20 bolts connecting the angles to the column flange, all in 2mm tolerance holes. Web angles were fabricated from S275 steel 90mm equal leg angles in 8 or 10mm thickness. The 356x171UKB45 test beam stub was S355 steel. Geometric details are shown in Figure 3-3.

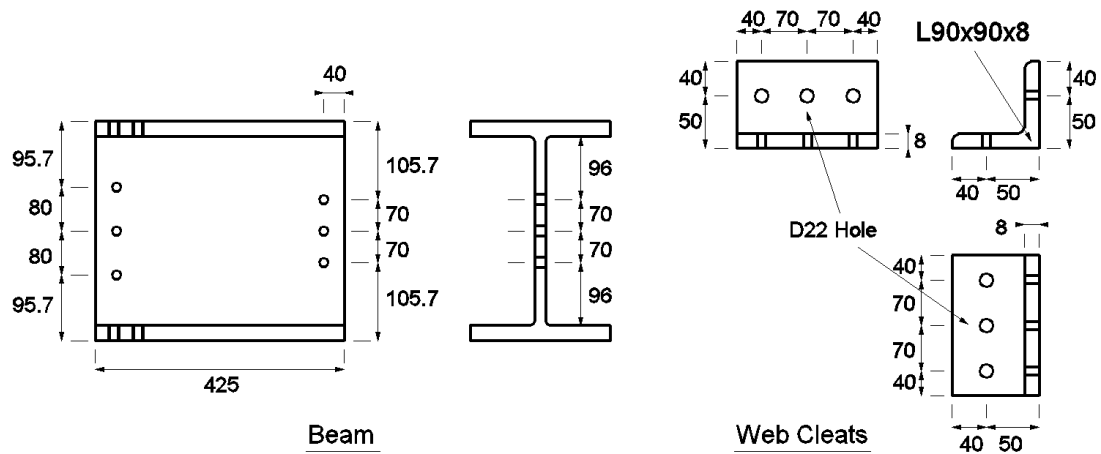


Figure 3-3 Geometric details of the web cleat test specimens

A total of ten tests were conducted, from which useful quantitative data was obtained from seven tests, (failure of the data recording system resulted in no useful loading data in tests WC1, WC2 and WC3) as shown in Table 3-1. Tests WC4, WC5, EC6, WC7 and WC9 were used to validate the web cleat model; these comparisons are provided in chapter 5.

Test	Peak connection resistance		Time to reach 6 degree rotation (s)	Failure mode	Post test beam web	Post-test angle deformation (from load ram end of connection)
	Tensile (kN)	Moment (kNm)				
WC1 8mm cleat static	NA*	NA*	240	Beam web block shear	 NB: Beam not stopped by end-stop, hence failure at all three holes	
WC2 8mm cleat dynamic	NA*	NA*	0.03	Beam web block shear		
WC3 8mm cleat dynamic	NA*	NA*	0.038	Beam web block shear		

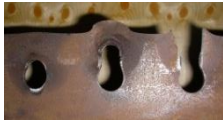
WC4 8mm cleat dynamic	60	47.5	0.033	Beam web block shear		
WC5 8mm cleat dynamic	63	47	0.050	Beam web block shear		
WC6 10mm cleat static	72	48	185	Beam web block shear		
WC7 10mm cleat dynamic	65	43	0.035	Beam web block shear		
WC8 10mm cleat dynamic	63	50	0.053	No failure – peak rotation 10.0 degrees		
WC9 10mm cleat static	73	48	190	No failure – peak rotation 10.2 degrees		
WC10 10mm cleat dynamic	73	49	0.038	Beam web block shear		

Table 3-1 Results from 10 experimental web-cleat tests

(\* NA, indicates that no quantitative data was recorded for these tests due to instrumentation failure)

### 3.1.2 End-plate connection

End-plate test connections included a plate connected to the beam web by an 8mm leg length weld and bolted to the column flange by six property class 8.8 M20 bolts. The plate was fabricated from 150mm wide S275 steel with thicknesses of 8 and 10mm. The beam was a 356x171UKB45 in S355 steel, the same as used in the web cleat tests. Geometric details are shown in Figure 3-4.

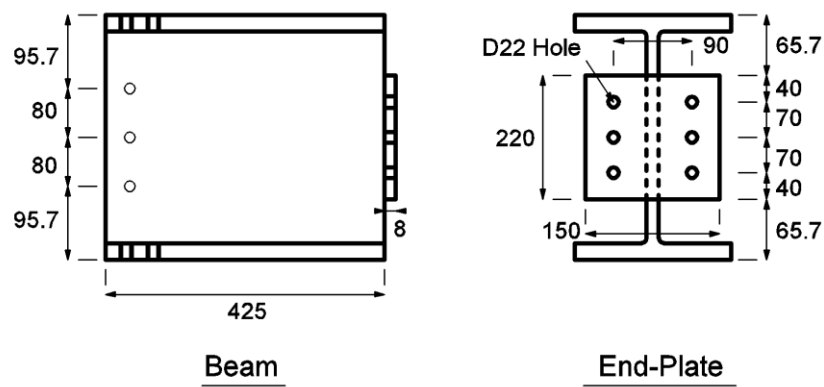


Figure 3-4 Geometric details of the end plate test specimens

Seventeen tests were conducted on end-plate connections. Four tests did not provide useful data for the validation purposes (FEP7, FEP9, FEP10 and FEP16) but the results from these tests are provided in Table 3-2. Tests FEP1, FEP4, FEP5, FEP6, FEP7 and FEP15 were used to validate the model - comparisons are provided in chapter 5.

Test	Peak connection resistance		Time to reach 6 degree rotation (s)	Failure mode	Post-test plate deformation (from load ram end of connection)
	Tensile (kN)	Moment (kNm)			
FEP1 8mm static	58.8	38.8	201	End-plate Fracture	

FEP2 8mm dynamic	97.7	64.5	0.037	End-plate Fracture	
FEP3 8mm dynamic	52.3	34.5	0.078	None	
FEP4 8mm dynamic	65.7	43.4	0.054	End-plate Fracture	
FEP5 8mm static	56.8	37.5	231	End-plate Fracture	
FEP6 8mm dynamic	84.2	55.6	0.046	End-plate Fracture	
FEP7 10mm dynamic	69.2	45.7	0.059	No failure	
FEP7 (Re test to failure statically)	92.8	61.2	NA	Fracture of endplate, beam web crushing and weld- endplate interface	

FEP8 10mm static	116.7	77.0	950	End-plate Fracture	
FEP9 8mm dynamic	47.7	31.3	0.075	No failure	
FEP9 (Re test to failure statically)	54.2	35.8	NA	End-plate Fracture	
FEP10 10mm dynamic	71.4	47.1	0.06	No failure	
FEP10 (Re test to failure statically)	89.5	59.1	NA	Asymmetric endplate fracture, bolt shear	
FEP11 10mm dynamic	113.0	74.6	0.038	Asymmetric endplate fracture, bolt shear	

FEP12 10mm dynamic	90.7	59.9	0.045	Asymmetric endplate fracture, bolt shear	
FEP13 10mm static	89.1	58.8	256	Weld end plate interface	
FEP14 8mm dynamic	45.0	29.7	0.085	No failure	
FEP15 10mm static	97.4	64.3	288	Weld end plate interface	
FEP16 8mm dynamic	NA	NA	NA	End-plate Fracture	
FEP17 10mm dynamic	87.1	57.5	0.047	End-plate Fracture, Weld end plate interface	

Table 3-2 Results from 17 experimental end-plate tests

(\* NA, indicates that no quantitative data was recorded for these tests due to instrumentation failure)

## 3.2 Numerical study

A finite element model of the tests described in the previous section was developed to facilitate efficient investigation of:

- The load-carrying and failure mechanisms of the connections.
- The effect of varying parameters such as material strength, size of connecting elements and ratio of rotation to axial extension.
- Changes to the connections that could improve the ductility and load-carrying performance.

A key issue in the presented work was that the relatively complex geometry of the experimental test arrangements should be modelled as realistically as possible, to enable assessment of the validity of assumptions in the analysis of the experimental work (e.g. the rigidity of the column, beam stub and beam stub mounting). This led to the development of a high-fidelity geometric finite element model, analysed using the LS-DYNA explicit dynamic FE code [58].

Considerable effort was expended on developing the model geometry, and identifying regions which required detailed meshing, more sophisticated material constitutive models and contact formulations (due to large deformations and failure occurring in these regions) and those which could be modelled using simpler modelling approaches.

These models were built with solid elements with typical element sizes varying from 10mm in regions experiencing little deformation, to 0.8mm in areas where high plastic deformation and/or failure occurred. The typical final model contains around 170,000 elements, 250 different parts and 360 contact interfaces. Model development progressed

in three steps: first, building the geometry of the model (explained in chapter 4), second, validating the model with the experiments (see chapter 5), and third, conducting the parametric studies on both connections as reported in chapters 6 & 7.

### **3.2.1 Material models**

One important parameter in every finite element model is choice of representative material property behaviour. High strain rate deformation is a part of many engineering applications from metal forming operations, to crash worthiness, impact and explosions [59], [60], [61]. Many plastic material models exist to model dynamic events with high rate of deformations and failures e.g. Johnson-Cook [62], Zerilli-Armstrong [63] and Cowper-Symonds [64]. Priyadarshini et al. [65] compared the behaviour of these three models and concluded that the Johnson-Cook model was suitable for analysis of medium-rate dynamic behaviour of steels, including fracture. The Armstrong-Zerilli model is more suitable for problems involving very high impact velocities and shock behaviour, whilst the Cowper-Symonds model simply factors the yield strength of the material by a user-defined, strain rate dependent dynamic increase factor.

The Johnson-Cook model is a visco-plastic material model which is commonly used for modelling of metals with large deformations, high strain rates and fracture and was first published in 1983 [62], [61]. This material model has been used in many different research areas, Borvik et al. [66] used it to study viscoplasticity and ductile damage for impact and penetration, Wen-ya et al. [67] for numerical simulation of linear friction welding of titanium alloy, Oscar & Eduardo [68] worked on impact performance of advanced high strength steel thin-walled columns, and Mićunović & Albertini [69] for the high strain rate property of stainless steel under tension and shear.

Many studies have been conducted to find the appropriate parameters for different materials for use in the Johnson-Cook material model [70][71][72][73][74].

The numerical models developed incorporated the Simplified Johnson Cook material model (see eq 1), which although less computationally expensive than the full Johnson Cook constitutive model is nonetheless still quite expensive. The main reason to use a Johnson-Cook material model is its inclusion of strain sensitivity in plastic deformation

thus allowing the tests to be analysed even where the strain rates vary over a large range [75]. The Simplified Johnson Cook material model was preferred to the full version for a number of reasons including difficulty in finding the correct magnitude for different parameters (like thermal or damage effects) for the full version of Johnson Cook material properties; instability in the model when running the model with the full Johnson Cook model; and it was assumed that adiabatic temperature increase (included in the full model but not the simplified one) is not high enough to result in significant plastic heating which would cause softening and reducing the yield stress [76].

$$\sigma_y = (A + B \cdot \varepsilon^n) \cdot (1 + C \cdot \ln \dot{\varepsilon}^*) \quad (1)$$

Where  $\sigma_y$  is the effective stress,  $\varepsilon$  is the effective plastic strain,  $\dot{\varepsilon}^*$  is the normalized effective plastic strain rate (typically normalized to a strain rate of  $1.0 \text{ s}^{-1}$ ),  $n$  is the work hardening exponent and  $A$ ,  $B$ ,  $C$  are constant.

A thorough search of peer-reviewed literature uncovered no J-C material data for S355 and S275 steel. A source for a similar American steel (ASTM A572 Grade 50 and A570 Grade 40) was found in a non-reviewed on-line source [77], presented by a numerical engineer from Lawrence Livermore National Laboratory, the institution which developed the DYNA code. The J-C parameters are provided in chapter 4. Clearly, caution must be exercised in using non-reviewed data, and so a series of DYNA models of uniaxial tension tests were analysed using these material constants (Figure 3-5). Examples of DYNA model results for S355 steel with quasi-static and very high rate loading are shown in Figure 3-6. These indicate that the dynamic increase factor (ratio of material strength at a loading rate of 2000 strain/s to that at a rate of 0.01 strain/sec) for the S355 steel at this loading rate is 1.5-1.8 in the range of strains 0.05-0.2. Experimental results from dynamic tests at similar rates presented in [78] for steel with static yield strengths of 217MPa and 430MPa, showed dynamic increase factors of approximately 1.7 and 1.3 respectively at strain rates of 1800strain/s, bounding the results from the model tests. It is well known that the dynamic increase factor for steel decreases with increasing static strength, and this provides confidence that the data from [77] can accurately capture the high rate strength increase.



Figure 3-5 LS-DYNA uniaxial tension test

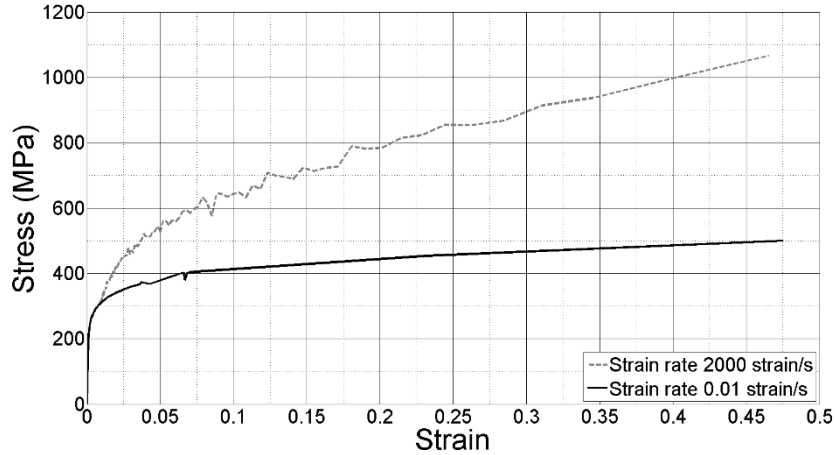


Figure 3-6 Stress strain curve for 275 steel for two different strain rates with J-C material model

Johnson-Cook parameters were found for most parts of the connections modelled but for the end-plate the welded area material properties were impossible to find. Many studies have been done on the properties of welded sections and different materials e.g. work done by Sreenivasan & Mannan [79] on impact properties of stainless steel weld, Xue et al. [80] on the response of welded HSLA 100 steel, and Lindgren [81] on numerical modelling of welding. But Johnson-Cook properties for fillet welds and the heat affected area around it were not available in the literature and for that reason those parameters were determined by a sequential calibration-validation approach in this research as explained in chapter 4.

### 3.2.2 Explicit and implicit solvers

Explicit solvers using very small time steps are mostly used for fast dynamic problems. Implicit solvers are preferred for slow dynamic and quasi-static problems as the number of time steps in explicit solvers becomes prohibitively large. To calculate the state of the system at  $t+\Delta t$  in explicit methods, the state of the system at the current time ( $t$ ) is used.

For implicit methods the state of the system at  $t+\Delta t$  is calculated based on the current *and later state* of the system. The mathematical function for an explicit method is:

$$Y(t+\Delta t) = F(Y(t)) \quad (2)$$

Current state of the system shown by  $Y(t)$  and later state by  $Y(t+\Delta t)$ , where  $\Delta t$  is a small time step). The mathematical equation for the implicit method is:

$$G(Y(t) + Y(t+\Delta t)) = 0 \quad (3)$$

In both equations it is necessary to calculate later state of the system ( $Y(t+\Delta t)$ ).

It is clear that implicit methods require an extra computation (eq.3), and they can be much harder to implement. Implicit methods are used because many problems arising in practice have relative long-duration dynamic response, for which the use of an explicit method requires impractically small time steps  $\Delta t$  to keep the error in the result bounded (i.e. avoid numerical instability). For such problems, to achieve a given accuracy, it takes much less computational time using an implicit method with larger time steps, even taking into account that need to solve an equation of the form (2) at each time step.

Software capable of conducting explicit analysis for solids are limited in numbers. Among them are LS-DYNA and Abaqus-Explicit. For this study, the LS-DYNA code was chosen, primarily due to the extensive body of previous fundamental research work which uses this code, and in particular, due to the wide range of robust contact algorithms available in the DYNA code. This has powerful solvers, both explicit and implicit, and has been widely used by many researchers for impact problems, such as by Borvik et al. [82] on the study of strength and ductility of Eldox 460E steel at high strain rates, elevated temperatures and various stress triaxialities.

Running analysis time in both explicit and implicit FE model depends upon (1) the number of calculations between each time step, (2) the time step size in both explicit and implicit analysis and (3) the element numbers and their contact with each other, which made it important to have efficient element sizes and give careful consideration to the contacts between the different parts.

In the explicit numerical integration method used for fast dynamic analyses the time steps depend on the smallest element dimension to ensure that the stress wave cannot propagate further than the length of any of the elements in each time step. Equation (4) shows how Ls-Dyna calculates the time step for this type of analysis:

$$\Delta t = 0.9 \times \frac{\Delta l}{c} \quad (4)$$

$\Delta t$  is the time step,  $\Delta l$  is the smallest element length,  $C$  is the wave velocity in the material and 0.9 is the factor that Ls-Dyna adopts to ensure numerical stability.

In the implicit numerical integration method, which was used for the quasi-static analyses, the time step could be larger than the explicit analysis thus giving the opportunity run analyses of a longer time frame. The magnitude of the time steps were defined manually at the beginning of the analysis but are changed automatically by the software to reach the convergence at each step.

### 3.2.3 Force and moment calculation method

The detail of force and moment are provided in the paper published by Tyas et al. [14], a brief explanation is provided in this section and Figure 3-7 provide the sketch of column movement. In dynamic analysis, the connection resistance was calculated by subtracting the translational inertial force accelerating the column from the applied load. The translational resistance of the connection was determined from dynamic force equilibrium:

$$F_C(t) = F_A(t) \cos \theta - m z_{CL}''(t) \quad (5)$$

Where  $F_C$  is the force generated at the initial centre of the connection,  $F_A$  is the applied force applied by the loading ram and measured by the load cell,  $\theta$  is the column rotation,  $m$  is the column mass and  $z_{CL}''$  is the acceleration of mass centre of column.

The resisted moment at the initial centre of the connection was also determined by dynamic moment equilibrium which shows below:

$$M_C(t) = F_A(t)x - m z_{CL}''(t)x_C \cos \theta(t) - I \ddot{\theta}(t) \quad (6)$$

$M_C$  is the applied moment at initial centre of the connection,  $F_A$  is the applied force applied by the loading ram and measured by the load cell,  $x$  distance between the line of action of applied load to the initial centre of the connection,  $m$  is the column mass,  $\ddot{z}_{CL}$  is the acceleration of mass centre of column,  $x_C$  is the distance between mass centre of column to the initial centre of connection,  $\theta$  is the column rotation,  $I$  mass moment of inertia of the column around its centre of mass and  $\ddot{\theta}$  is rotational acceleration.

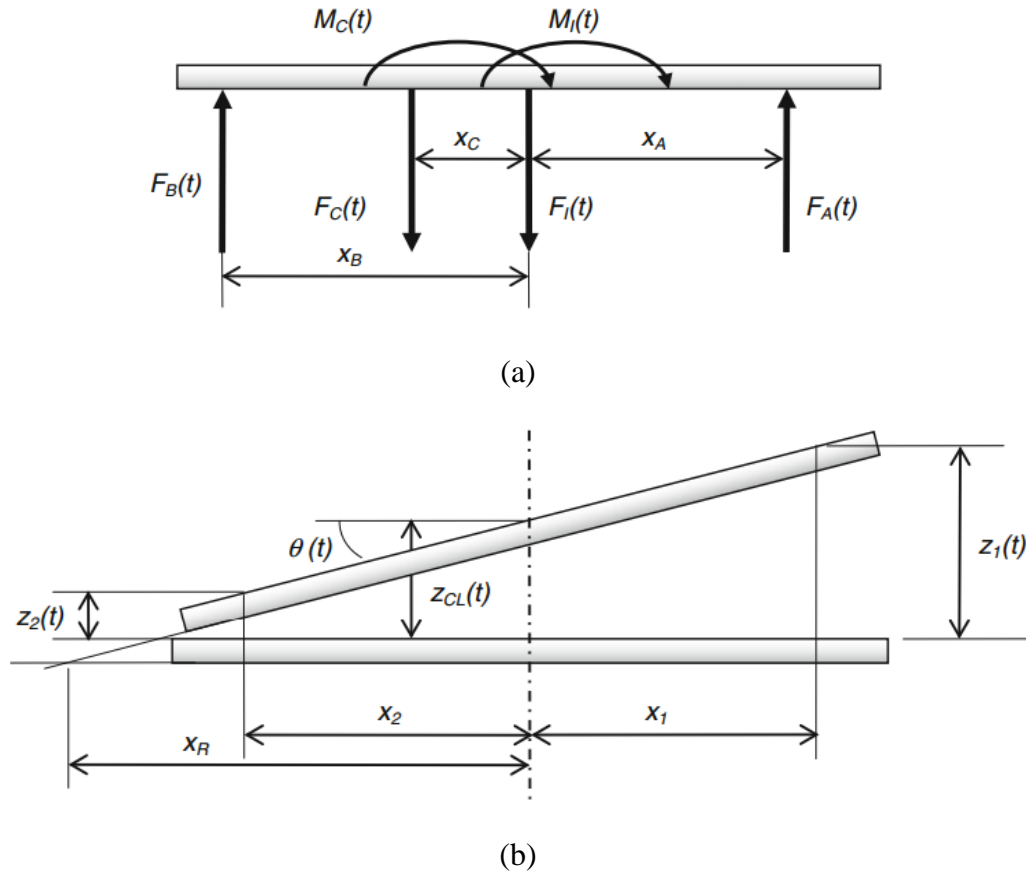


Figure 3-7 (a) Free-body force/moment diagram for flying column (b) Displacement/rotation diagram for flying column [14]

### 3.3 Conclusion

This chapter explained some general aspects of experimental and numerical studies, and next chapters will explain how these the model were developed (chapter4) then validated against experiments (chapter 5) and used for parametric studies to understand the connection behaviour under different loading rates, types and geometric changes (chapter 6,7).

## 4 Development of steel connection model using finite element method

This chapter describes how a finite element model was developed, from making the geometry up to meshing and applying boundary conditions. Development of the model from building the geometry and meshing up to defining the contacts and boundary condition were done in ANSYS environment, then solution were done by using LS-DYNA solver. As the connection model was complicated it was decided to divide the model into several smaller models and add them together to generate the final connection model. The advantage of this method was to have control over element sizes, shape and material properties. These smaller models were:

1. Column (Universal Column H-Section) with stiffener plates
2. Beam (Universal Beam I-Sections) including the splice connection
3. Bolts including the bolt body (head and threaded shank), nut and washers
4. Angle sections in web-cleat connections
5. Plate and the welds in end-Plate connections
6. Rigid plate at the load application points
7. Loading ram and load cell

Two terms used throughout this chapter require some explanation:

**Part:** defined in LS-DYNA as different groups of nodes and elements with all the elements in these groups having the same element type and material model. Contacts were defined between these Parts in the model.

**Component**, has the same concept as Parts but used in ANSYS, however it can contain different material type and also groups of key-points and volumes. Contacts and boundary conditions were defined by using these components.

To successfully assemble the complete joint the smaller models were added together. Parts and Components were introduced into the model and different types of contacts were generated between them. Finally, appropriate boundary conditions were applied at the

remote end of the beam and column to represent the supports and loading conditions. The details of these different steps are provided in this chapter and verification and validation of the model are described in Chapter 5. Figure 4-1 shows the complete model in LS-DYNA with different colours representing the different Parts in the model.

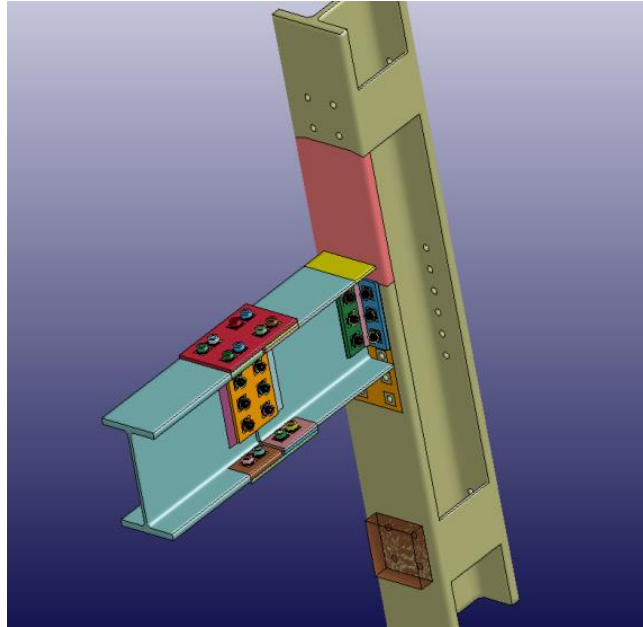


Figure 4-1 Final model of the connection, beam and column

## **4.1 Universal column H-section with stiffener plates**

As explained in Chapter 3, in the experiments reported by Tyas et. al. [14] a steel H-Section (254x254x167UKC S355 steel) was used as the column in the experimental programme. This was designed to be significantly stronger and stiffer than the test connections, in order to prevent any permanent or even significant elastic deformation in the section.

### **4.1.1 Building the geometry of the column**

Figure 4-2 shows the different parameters used to model the column section; the model geometry was defined using a purpose written code which can easily accommodate changes in sections as the dimensions are defined as variables which can be entered by the user.

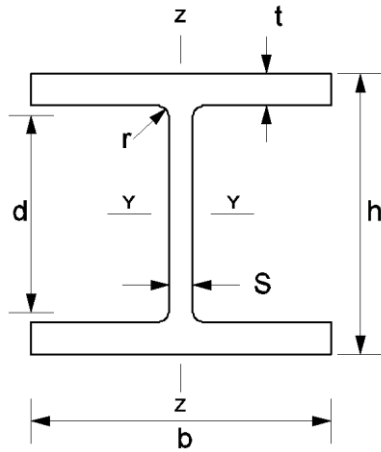


Figure 4-2 Drawing of column section dimensions

Column stiffener plates were added to the model, as they were in the experiments, but to simplify the model the plates were attached to the column section by merging nodes at the boundaries rather than modelling the welds or contact interfaces explicitly. Eight rollers, attached to the column, were used to reduce the friction as the column moved across the top of the rigid supporting rig. These rollers were added to the model by applying constraints and small masses at relevant points on the column model; for simplification they were assumed to be frictionless.

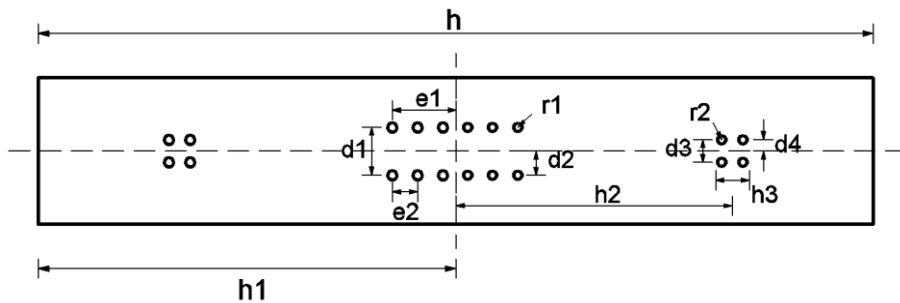


Figure 4-3 Drawing of the column's flange

Figure 4-3 shows the column dimensions on the flange and Figure 4-4 shows the column dimensions on the web and stiffener plates. The values for these variable dimensions are available in Table B- 1 in the appendix B.

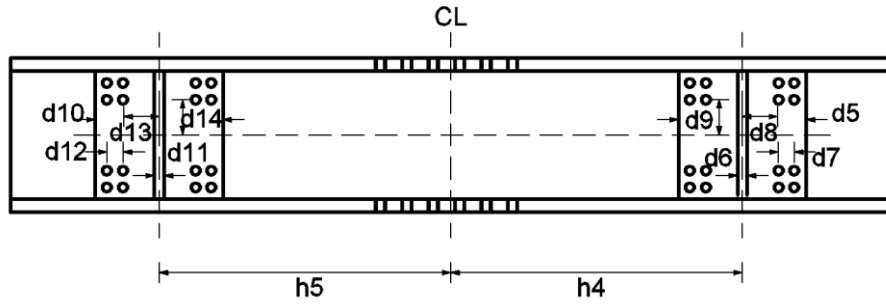


Figure 4-4 Drawing of the column web and stiffener plates

The column was divided into different sections, as shown in Figure 4-5, and then key-points were defined in each section to create the model. This helped to simplify the modelling process of column and plates, an example of one of these sections is provided in Figure 4-6.

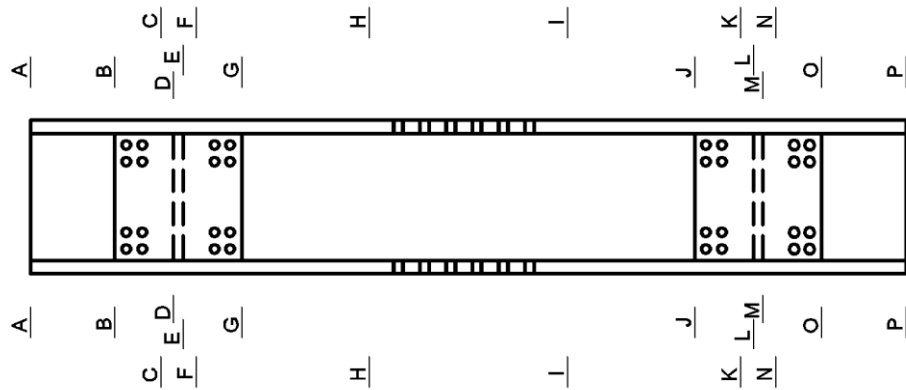


Figure 4-5 Dividing the column to different sections

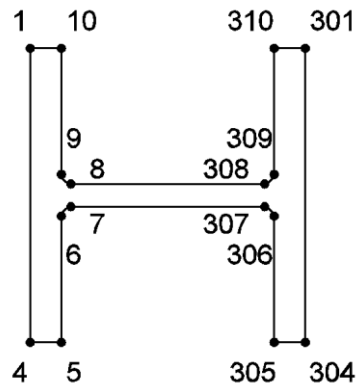


Figure 4-6 Column first section's key-points (the rest of these sections and their key-points are provided in Appendix A)

By connecting the key-points with volumes, the column geometry was developed as illustrated in Figure 4-7. The figure also shows the stiffener plates connected to the column.

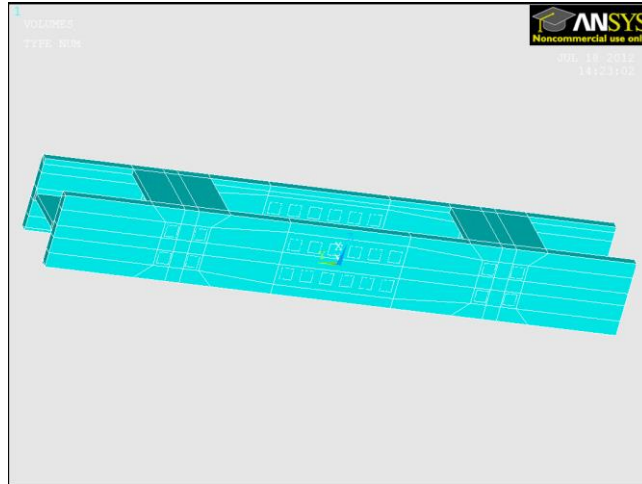


Figure 4-7 Column geometry made by volumes

To generate the bolt holes on the column it was decided to build them by controlling the meshing size and shape, to prevent any small elements forming in automatic meshing. For that reason, first square holes were removed from the column volumes as shown in Figure 4-8.

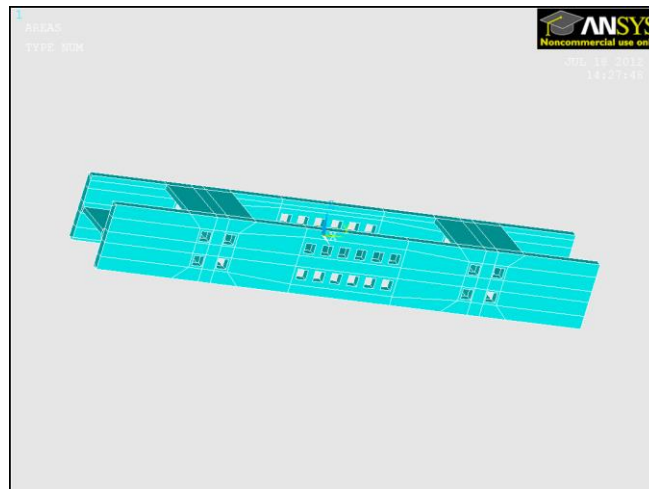


Figure 4-8 Column volumes with square holes

Each square bolt hole was then made into a circle with 24 different volumes, the inner circle made the bolt hole and the outer square was attached to the column model with square holes in it. Figure 4-9 shows the column with a round hole attached.

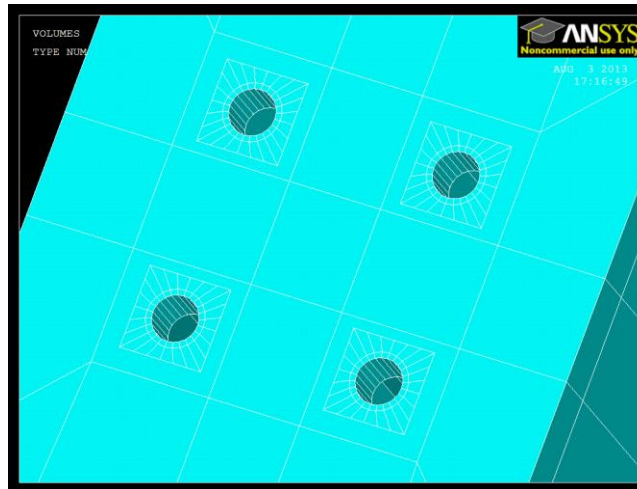


Figure 4-9 Four bolt holes attached to the column

#### 4.1.2 Material properties and mesh generation of the column

Different Components of volumes were introduced into the column model to give control over the mesh size of different locations on the column. Also after the meshing was completed, different Components were introduced containing nodes and elements which used to build the contacts between them. An example of these Components is provided in Figure 4-10 with each Component shown in a different colour.

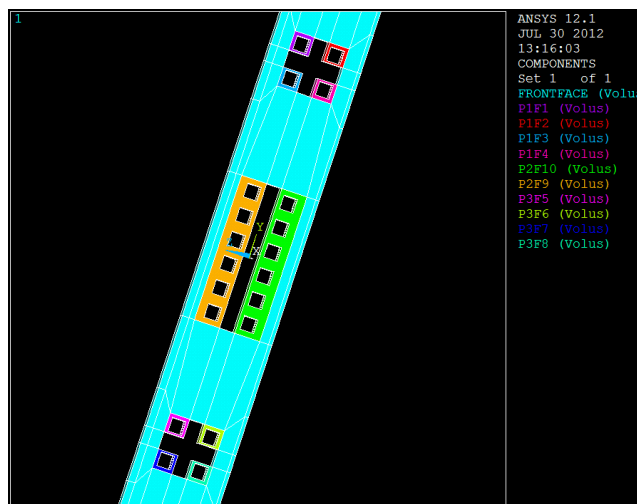


Figure 4-10 Example of different Components on the column

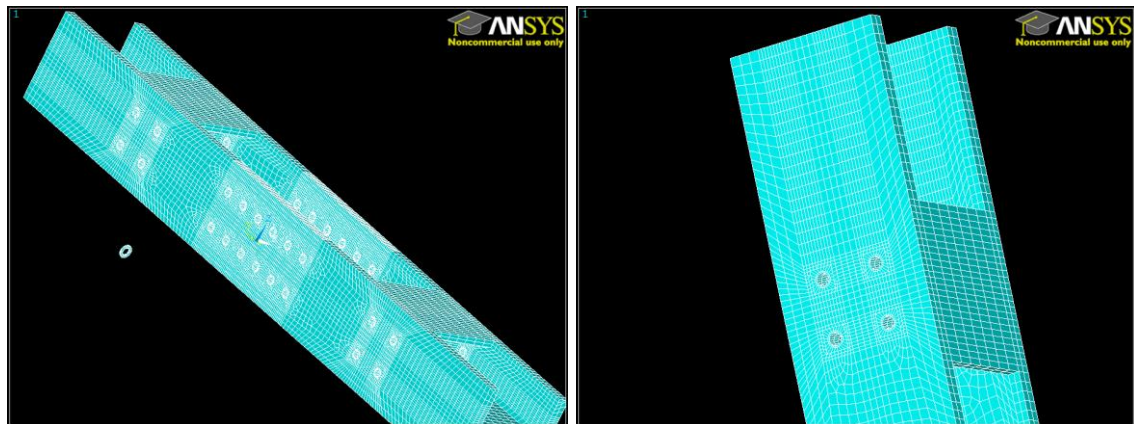
Elastic material (“\*MAT\_ELASTIC”) was used for modelling the column, as the column experienced no plastic deformation during testing. Table 4-1 shows the parameters used for the isotropic elastic column material.

Poisson's Ratio	Mass Density	Young's Modulus
0.3	7850 (kg/m <sup>3</sup> )	210E09 (Pa)

Table 4-1 Material properties for the column

Running analysis time in an explicit dynamic FE model depends upon (1) the number of calculations between each time step, (2) the time step size in both explicit and implicit analysis and (3) the element numbers and their contact with each other, which made it important to have efficient element sizes and give careful consideration to the contacts between the different parts.

Automatic block mesh was used to mesh the column model, with hierarchy in meshing of different Components to control the size and shapes of the elements. This hierarchy began from volumes around bolt holes up to the column web and flanges. These elements had SOLID164 element type, single integration points and elastic material properties. The column mesh can be seen in Figure 4-11.



(a) (b)  
Figure 4-11 Pictures of column after meshing

## 4.2 Universal beam I-sections and the splice connection

As explained in Chapter 3, two I-sections were connected end to end to act as the beam in the experiment. One of these was a relatively strong, stiff I-section beam stub which was permanently connected to the reaction frame. The test sample (356x171UKB45) was connected to the free end of this permanent stub beam using a flange and web spliced connection (with the other end of the test beam connected to the column flange by either

the end plate or web cleat connections under study). This configuration allowed the test beam and connection to be replaced without having to disassemble large sections of the loading rig.

#### 4.2.1 Building the geometry of the beams

The permanent stub-beam and splice were modelled in detail as it was not clear from the experimental data how their response might affect the overall behaviour of the system. Figure 4-12 shows the different parameters used to make the beam finite element model.

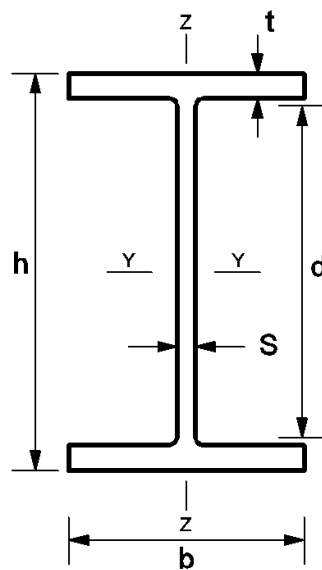


Figure 4-12 Drawing of beam section dimensions

Figure 4-13 shows the configurations of the two beams and their splice connection. Two plates were used to connect the webs and four plates were used to connect the flanges.

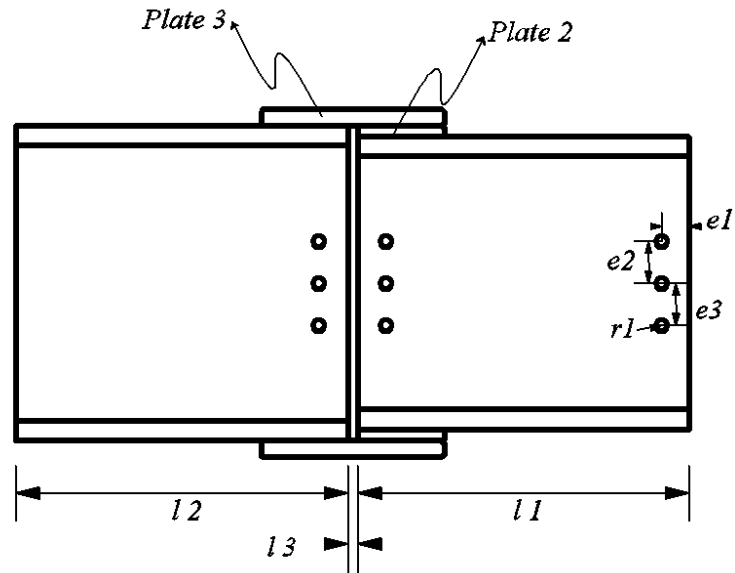


Figure 4-13 Side drawing of beams and splice dimensions

Plate 3 connected the beam flanges and plate 2 was a pack to space out the difference in height between the two I sections. Plate 3 is detailed in Figure 4-14. The values for these variable dimensions are available in Table B- 1 in the appendix B.

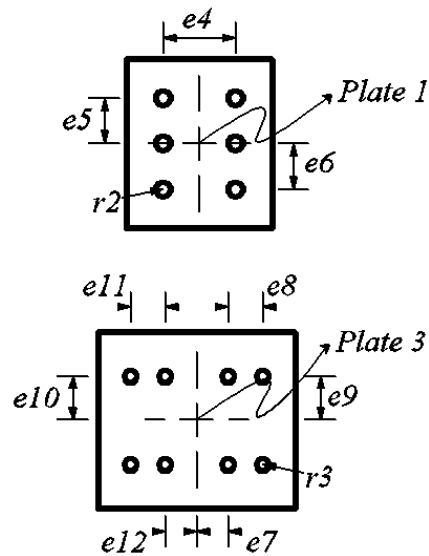


Figure 4-14 Flange plate of splice

Figure 4-15 shows the geometry of the splice, which has six plates: two of them connect the beam webs (Plate1) and the other four connect the beam flanges (Plate 2&3). As

shown in the figure, six bolts were used to connect beam webs and sixteen more to connect the beam flanges. The plates were thick enough to prevent any permanent deformation making them re-useable for different experiments.

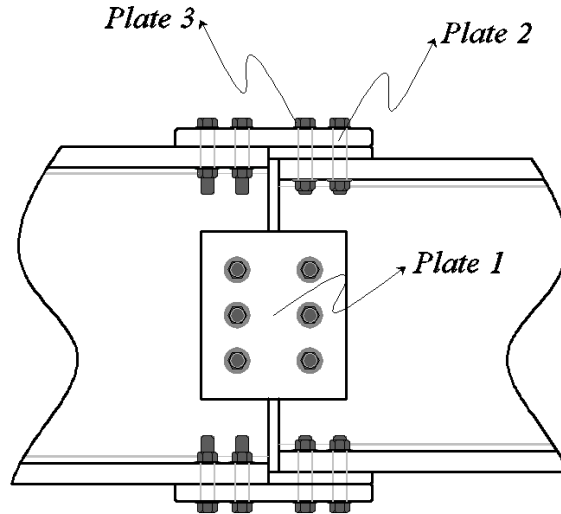


Figure 4-15 Beam splice plates

The gap between the beams was closed as much as it was possible in the experiments to prevent any rotation of the beams inside the splice.

Following the same procedure as the column, the beams were divided into different sections. Figure 4-16 shows the permanent stub beam (the length between sections A and D) fixed to the rigid rig at section A. The test beam was the length between sections E and I. When modelling the web-cleat connections holes were added to the beam web between the section at H and I. Other sections (B, C, F and G) were used to generate the splice plates and connect them to the beams.

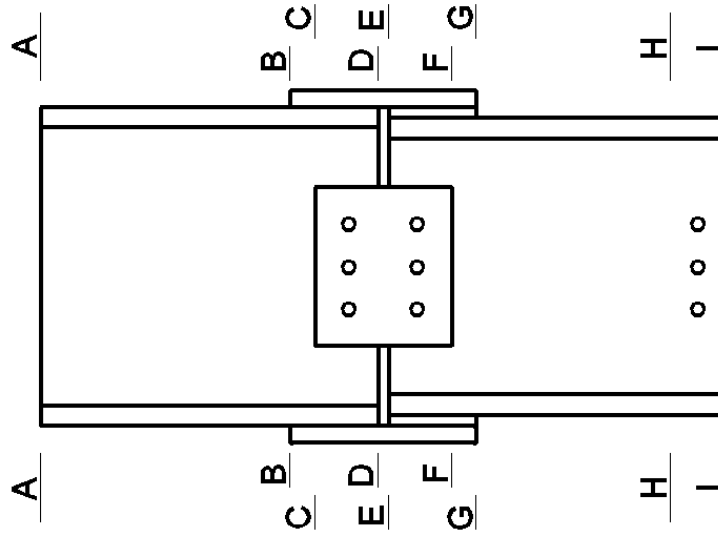


Figure 4-16 Beam section divisions

Figure 4-17 shows the key points on section A- A. These points were decided upon to provide the correct shape of beams with the least number of volumes and complications.

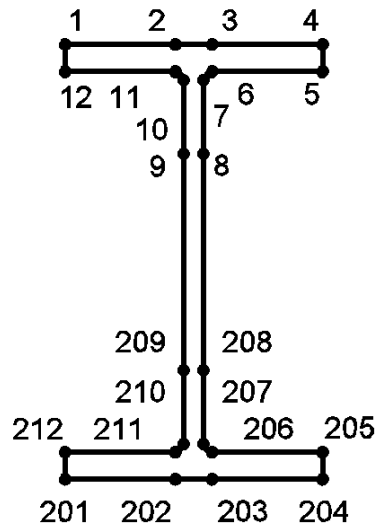


Figure 4-17 Section A- A, example of key points numbering (the rest of these sections and their key-points are provided in Appendix A)

By connecting the key points by volumes, the geometry of the beams and splice plates were developed. Figure 4-18 show beams and plates geometry developed in ANSYS.

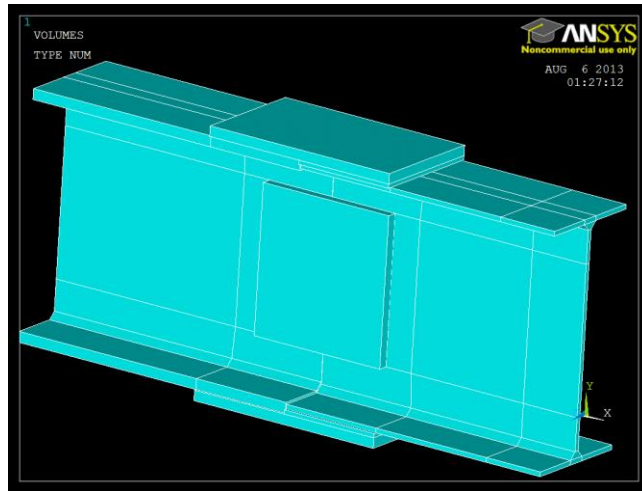
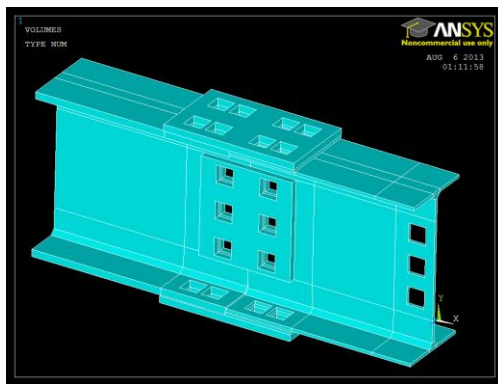


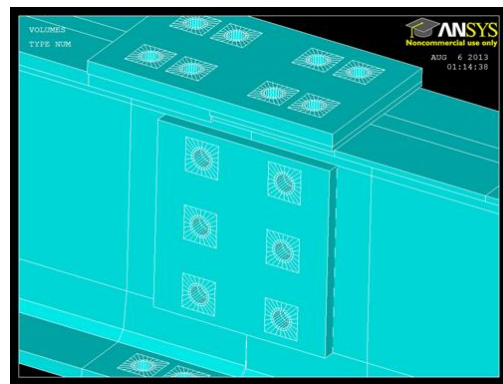
Figure 4-18 Beam & splice geometry in ANSYS

The holes were generated in the same way as described earlier in this chapter

Figure 4-19.



(a)



(b)

Figure 4-19 (a) Beam with square holes (b) Bolt holes attached to the beams and plates

#### 4.2.2 Material properties and mesh generation of the beam

Building Components had two advantages (1) control over the mesh sizes of different locations of the beam (2) defining the contacts between different groups of nodes and elements. An example of the different Components is provided in Figure 4-20, with the different colours representing different Components.

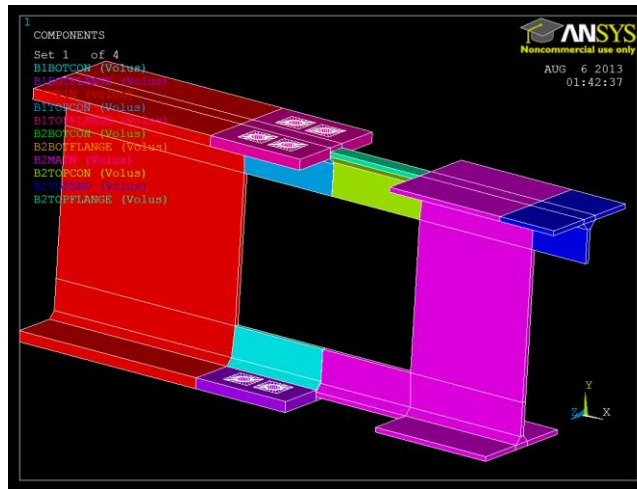


Figure 4-20 Sample of different Components on the beams

The Simplified Johnson-Cook material model (see Chapter 3) was used for the beams, with parameters shown in Table 4-2.

Poisson's Ratio	Density	Young's Modulus	A
0.3	7833 (Kg/m3)	2.07E11 (Pa)	1.6642D08 (Pa)
B	N	C	Psfail
4.8578E08 (Pa)	0.16981	0.022	0.5962

Table 4-2 Simplified Johnson Cook material model for the beam

As no significant deformation was foreseen in the splice plates, it was decided to use a less computationally expensive material, “\*MAT\_PLASTIC\_KINEMATIC”. This material uses an isotropic and kinematic hardening plasticity model. Table 4-3 shows the parameters used in the model.

Poisson's Ratio	Density	Young's Modulus
0.3	7833 (Kg/m3)	2.07E11 (Pa)
Yield stress	Tangent modulus	Hardening parameter
0.350E+09	0.445E+09	1.00

Table 4-3 Plastic Kinematic parameters for the splice plates

A finer mesh was applied to the beam web in the vicinity of the test connection for the web cleat models, as this was the region in which failure was anticipated. Also as the

beam top flange could impact the column flange as the column rotated, a finer mesh was used in that area. This was done to solve problems with hourglassing in earlier models, with a coarser mesh in this region. Figure 4-21 shows the example of the end of the test beam for the web cleat models.

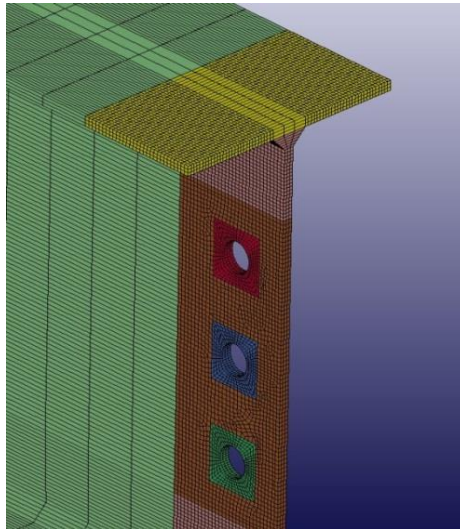
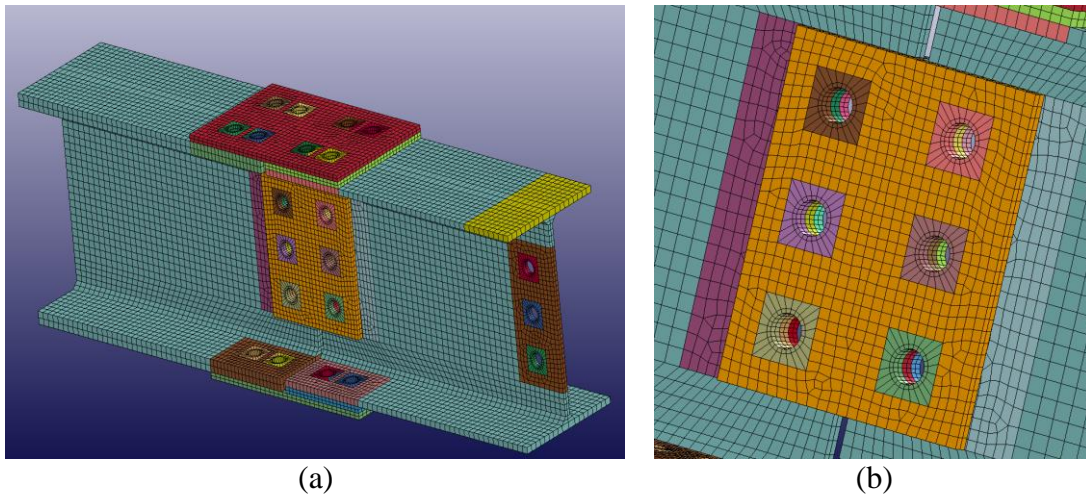


Figure 4-21 Finer meshing at the end of the beam which was connected to the Web-cleat connection

After meshing the important sections of the beam, other sections were meshed with larger elements to reduce the number of elements and analysis time. Figure 4-22 shows the beam splice mesh and different colours are the Parts of the beam.



(a) (b)  
Figure 4-22 Beam mesh and splice mesh

The ANSYS block meshing was used to mesh the beam and SOLID164 assigned as its element type with single integration points for most sections of the beams and splice, however in beam web areas close to the connection full integrated elements were used.

### 4.3 Modelling bolts, nuts and washers

As explained in Chapter 3, thirty one M20 bolts were used in the experiment and each bolt has a nut and two washers.

#### 4.3.1 Building the geometry of the bolt

Figure 4-23 below shows the bolt geometry and the parameters used to build the model. The values for these variable dimensions are available in Table B- 1 in the appendix B.

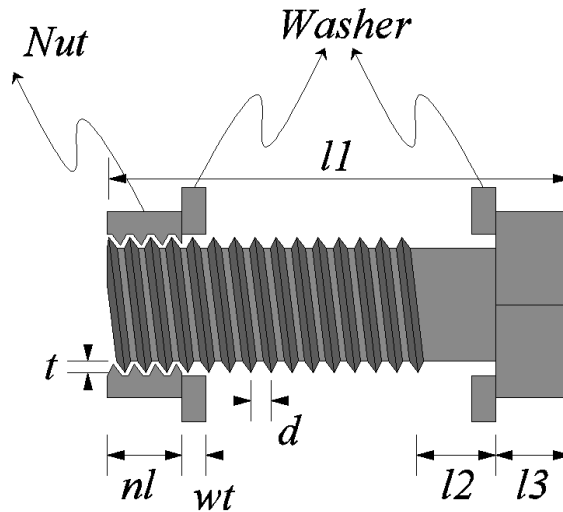


Figure 4-23 Bolt drawing and its dimensions

Figure 4-24 shows the parameters of the bolt head, nut and washer used to build the model.

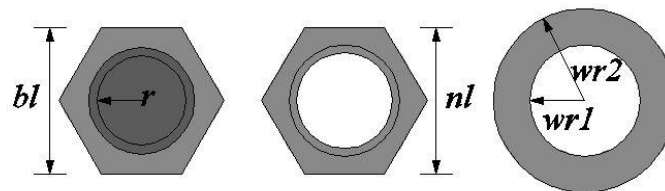


Figure 4-24 Bolt Head (R), Nut (M), Washer (R)

Figure 4-25 shows different sections of the bolt from which the model was developed by using nodes and elements. Automatic meshing was not used as it was important to control the element size and time step in the model.

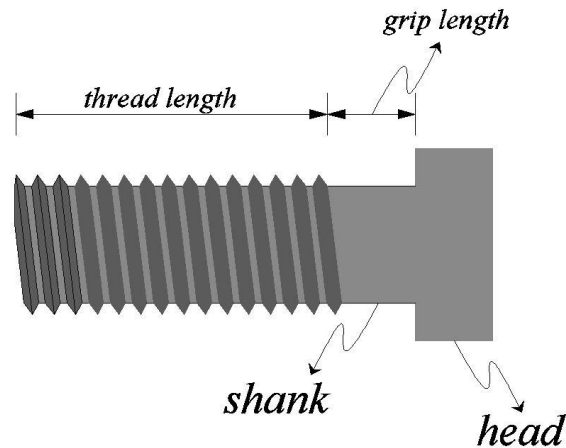


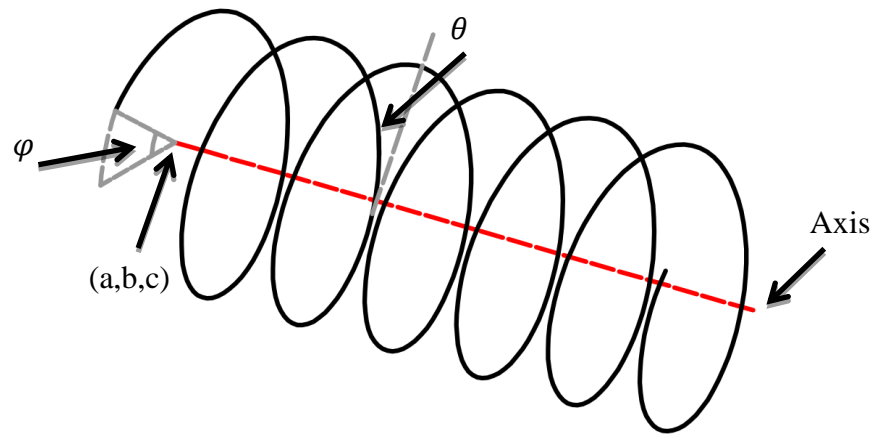
Figure 4-25 Bolt different parts

### 4.3.2 Building the bolt model by nodes and elements

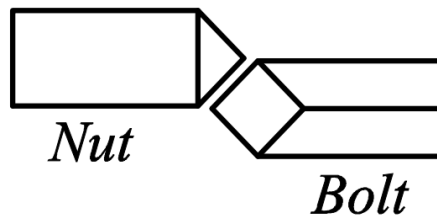
The threaded part of the bolt shank was the most complicated part of the model to create. To generate the model a series of elements were connected together side by side on the perimeter of a helix with key point coordinates defined by using the formula in equation (3) below:

$$k(x, y, z) = a + \frac{2\pi}{\theta}i, b + \cos(\theta i + \varphi), c + \sin(\theta i + \varphi) \quad (3)$$

$k$  is the key point,  $a$ ,  $b$  and  $c$  are constants to show the coordinates of helix centre,  $\theta$  is each slice angle,  $\varphi$  is the out of phase which can rotate the helix around its axes and  $i$  is a counter number which starts from 1 and ends with a number which depends on the length of the threaded shank. Figure 4-26 (a) shows the perimeter of the helix and some of the parameters used in EQ (3) (b) shows the section which is rotated around the helix.



(a)



(b)

Figure 4-26 (a) Helix line (b) Element section

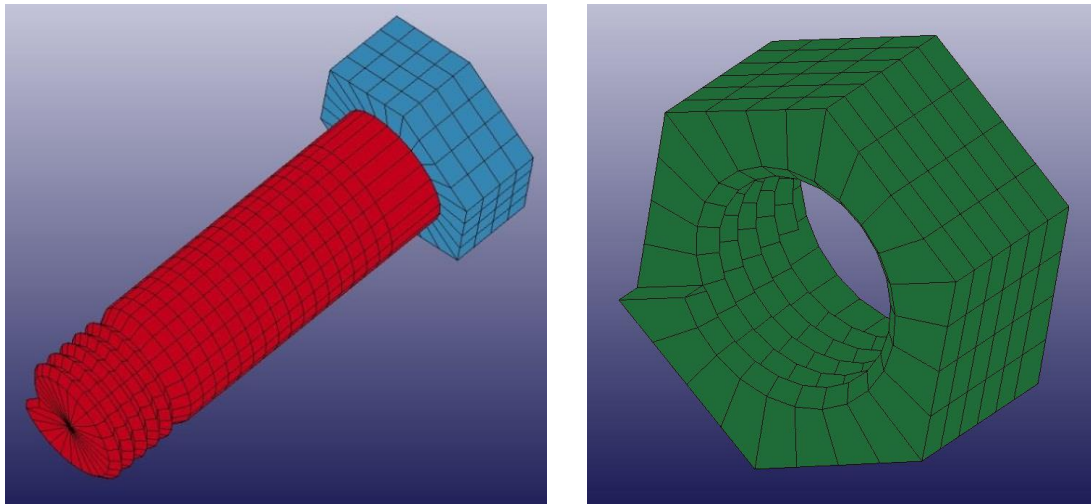
SOLID164 and material “\*MAT\_SIMPLIFIED\_JOHNSON\_COOK” were used to make the solid elements by connecting the key points around the helix. Table 4-4 shows the parameters for the material properties and the Figure 4-27 shows the solid element and how it looks after rotating around the helix.

Poisson's Ratio	Density	Young's Modulus	A
0.3	7833 (Kg/m3)	2.07E11 (Pa)	7.3285D08 (Pa)
B	N	C	Psfail
7.1698E08 (Pa)	0.243821	0.022	0.6329

Table 4-4 Johnson cook material for bolt 8.8

By rotating the section shown in Figure 4-26 (b) around the helix, the bolt shaft was made (shown in re colour in Figure 4-27 (a)). The bolt head was a hexagonal shape; the washers were made of circle sections. The nut was a helix at the inner surface and hexagonal on

the outside section. Figure 4-27 (a) shows the bolt shaft and head developed by the nodes and elements, (b) shows the bolt nut with a helix inside and hexagonal on the outside.



(a) (b)  
Figure 4-27 (a) Bolt grip and head (b) Bolt nut

Washers were modelled with similar solid elements and material properties however, because of hourglass problems in initial model, it was necessary to have small elements on the thickness and increase the density to keep the time step constant.

Figure 4-28 shows the bolt model with all five Parts - the bolt shank, head, nut and its two washers. The washer on the bolts contacting to the angles were subjected to more deformation in the tests and had smaller elements than the other one like the yellow washer shown in the figure.

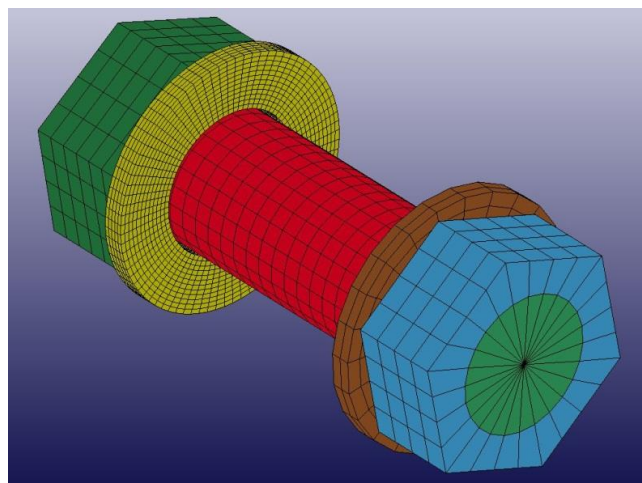


Figure 4-28 Complete bolt model

#### 4.4 Angle sections (for Web-cleat connections)

In web cleat connections, two angles were used to connect the beam web to the column flange.

##### 4.4.1 Building the geometry of the angles

Figure 4-29 shows a drawing of the angles and provides the dimensions. The values for these variable dimensions are available in Table B- 1 in the appendix B.

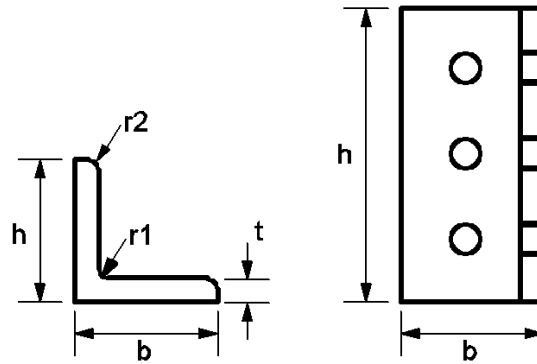


Figure 4-29 Angle parameters

Each angle was divided into two sections as shown in Figure 4-30.

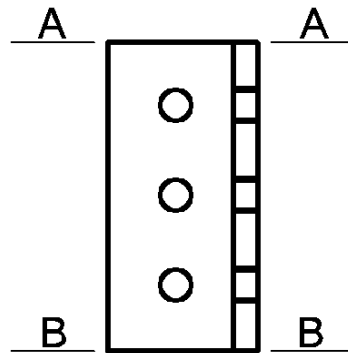
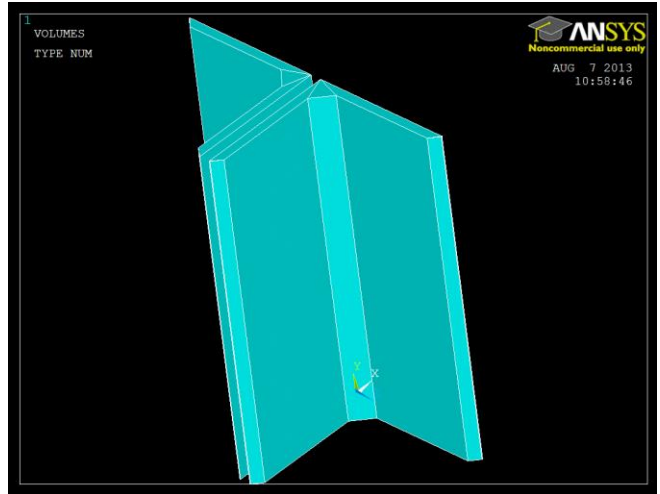
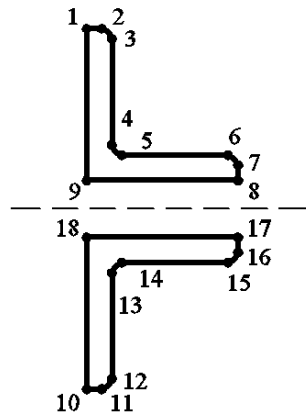


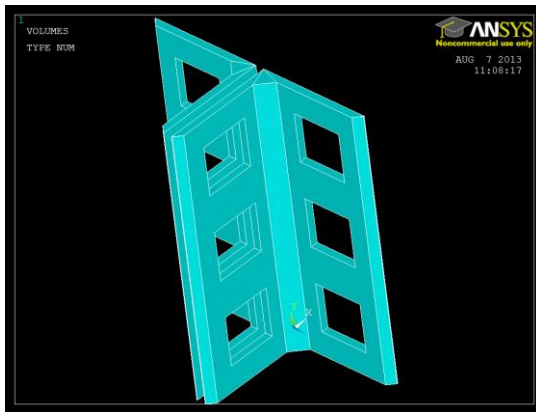
Figure 4-30 Angle sections

Key points were assigned to the sections and volumes were generated by connecting these key points as shown in Figure 4-31 (a) and (b).



(a) (b)  
Figure 4-31 (a) Angle section key points (b) Angle geometry

The bolt holes were generated as described previously. Figure 4-32 shows the angles before and after adding these bolt holes.



(a) (b)  
Figure 4-32 (a) Angles with square holes (b) Angles with the bolt holes

#### 4.4.2 Material properties and mesh generation of the beam

Different Components were introduced to help with meshing the angles and later used to build different parts. The different colours in Figure 4-33 represent these Components.

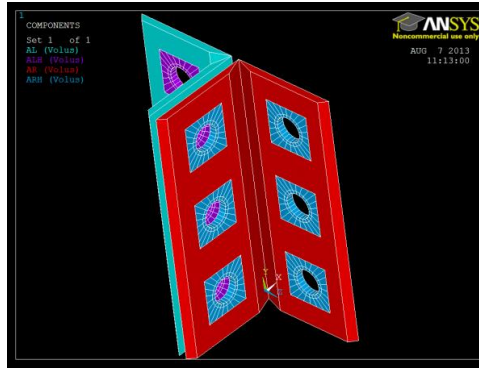


Figure 4-33 Sample of different Components on the angles

SOLID164 and material “\*MAT\_SIMPLIFIED\_JOHNSON\_COOK” were used to mesh the angles. This material was chosen because of its rate sensitivity and failure characteristics, which enabled the angles’ behaviour to be realistically modelled. Table 4-5 shows the parameters for the S275 steel of the angles and Figure 4-34 shows the angles after meshing and ready to use in the completed model of the connection.

Poisson’s Ratio	Density	Young’s Modulus	A
0.3	7833 (kg/m <sup>3</sup> )	2.07E11 (Pa)	8.8565D07 (Pa)
B	N	C	Psfail
4.7404E08 (Pa)	0.158132	0.022	0.4737

Table 4-5 Angle material properties

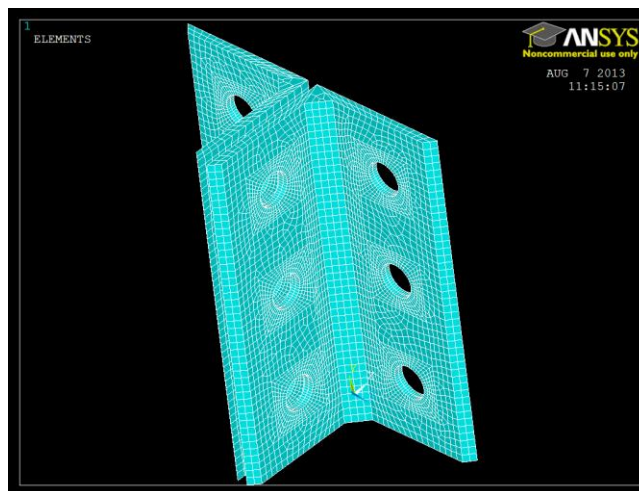


Figure 4-34 Angles after meshing

## 4.5 End-plate and welding (for end- plate connections)

To analyse the behaviour of the end plate connection, models of the plate and its welds were developed for use with other Parts of the connection model.

### 4.5.1 Building the geometry of the plate and welding

Figure 4-35 (a) shows the dimensions of the end-plate from above, and (b) are the dimension from the side. The values for these variable dimensions are available in Table B- 1 in the appendix B.

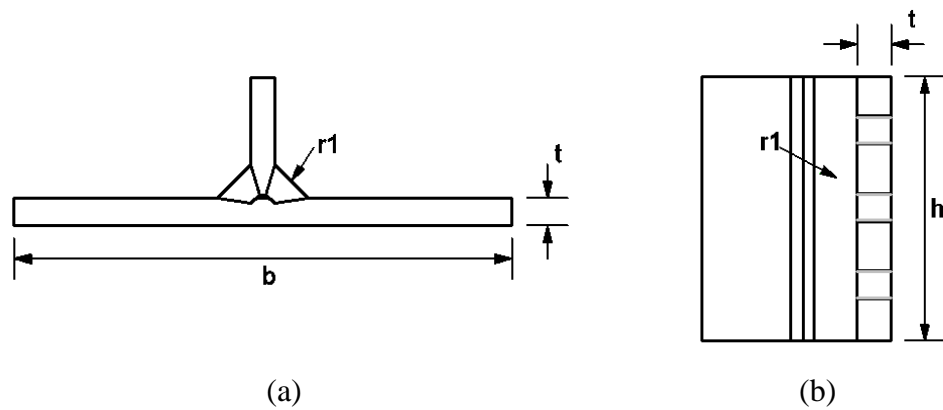


Figure 4-35 End plate connected to the beam

Key points were implemented on two sections of the plate; an example is provided in Figure 4-36.

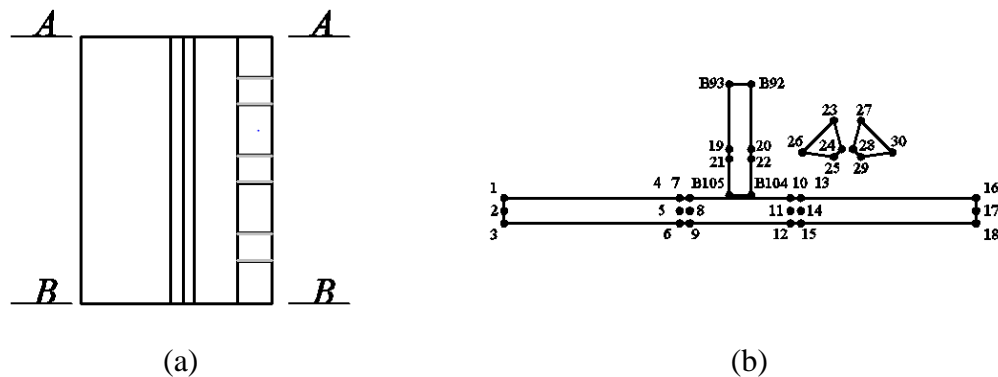


Figure 4-36 (a) End-Plate sections (b) End plate key points for section A- A

#### 4.5.2 Material properties and mesh generation of the plate

Bolt holes were built in the same way as previously described for the column and beams. Figure 4-37 shows the developed model of the end plate before meshing and the different colours show the Components which were used to mesh and build up the different parts.

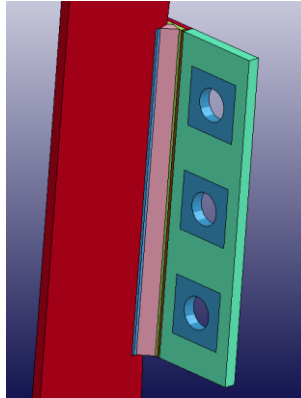


Figure 4-37 End plate Components

The welding process causes changes in the microstructure of the material adjacent to the weld. An x-ray from a welded T-stub can show the different areas of heat affected zones as they are shown in Figure 4-38. Figure 4-39 shows the drawing of the welded end plate and its different areas including the heat affected zones which were used in the model.

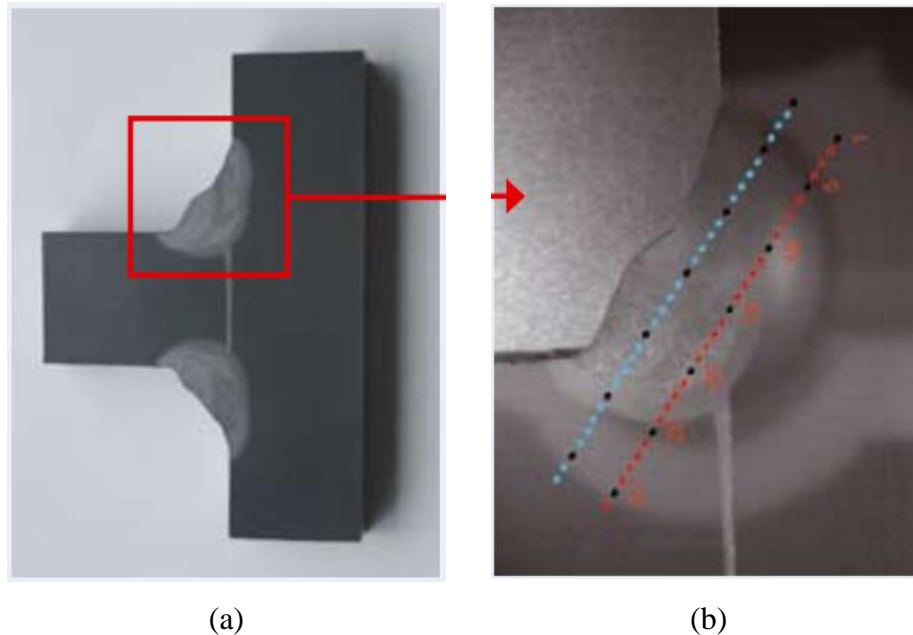


Figure 4-38 (a) Welded T-Stub, (b) Closer look to heat affected zones [83]

SOLID164 and material “\*MAT\_SIMPLIFIED\_JOHNSON\_COOK” were used to mesh the end plate and its welding areas. The welds and three sub-sections of the HAZ were modelled as separate Components, to enable different material properties to be used in different regions (Figure 4-40).

As discussed in Chapter 3.2.1, whilst considerable amounts of data exist in the published literature for the fracture toughness of welds and HAZ, there is very little published data on strain rate-dependent constitutive model data, and no data was found on the rate dependent elasto-plastic stress-strain behaviour of welds in construction grade steels. Since developing such data experimentally was beyond the scope of this study, a model calibration-validation approach was developed as described below.

Firstly, a static stress-strain curve, based on the parent metal properties was assumed. Then the value of plastic strain at failure was adjusted until the model results matched those of a static test of an endplate connection. Then, having fixed these static values, the value of the strain rate parameter “*C*” was varied until the model matched the behaviour of a dynamic test on an endplate connection. This concluded the “calibration” stage. The material model values determined by this calibration approach are shown in Table 4.6. For the “validation” stage, the material model parameters were fixed at the calibrated values, and the model used to predict the behaviour of connections at different load rates, with the results compared to experimental test data at the same loading rates. (See Chapter 5.4 for a further results and discussion.)

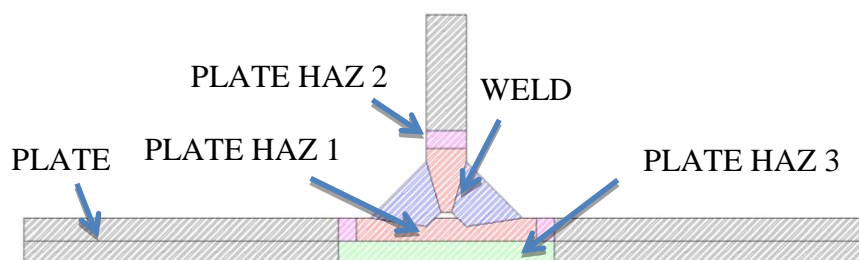


Figure 4-39 Drawing to show different zones in the end-plate

PLATE & WELD	Poisson's Ratio	Density	Young's Modulus	A
	0.3	7833 (kg/m <sup>3</sup> )	2.07E11 (Pa)	8.8565E07 (Pa)
	B	N	C	Psfail
	4.7404E08 (Pa)	0.158132	0.022	0.5962
HAZ 1	B	N	C	Psfail
	4.7404E08 (Pa)	0.158132	0.22	0.19
HAZ 2	B	N	C	Psfail
	4.7404E08 (Pa)	0.158132	0.22	0.21
HAZ 3	B	N	C	Psfail
	4.7404E08 (Pa)	0.158132	0.22	0.24

Table 4-6 End plate and welding material properties

The psfail parameter, which is provided in Table 4-6, is the strain to failure of each element and is based on the tensile test study explained in section 3.2.1; the whole tensile bar failed with around 0.3 strain to failure. These numbers are in accordance with studies conducted by other researchers e.g. Može et al. [57] developed a tensile test finite element model and validated it against experiments. The specimen was built from mild steel with a yield stress of 313MPa, and tensile strength of 425MPa, the standard tensile test coupon fractured at 37%. ABAQUS material input for this model was the true stress and plastic strain and values up to 700MPa and 0.67 strain to failure were used for each element. A similar study by Draganić et al. [57] on construction steel used 0.45 as the strain to failure to be able to validate their model with the experiment.

The end plates, HAZ and welds were meshed by brick elements as shown in Figure 4-40. Different colours show the Parts used to build the contacts between the end-plate and column flange.

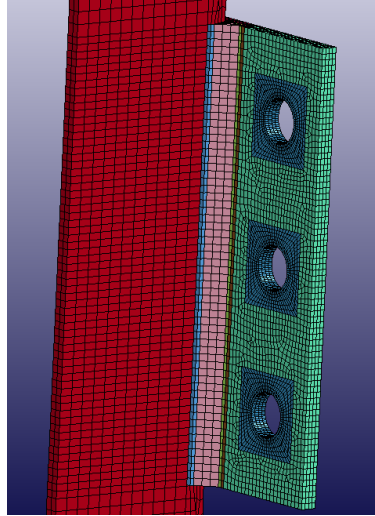
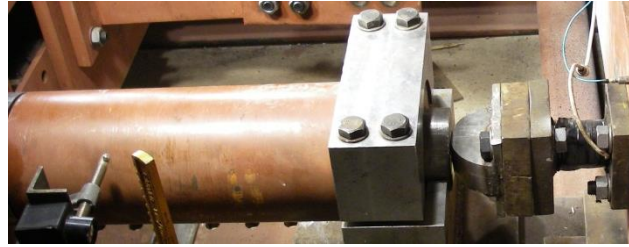


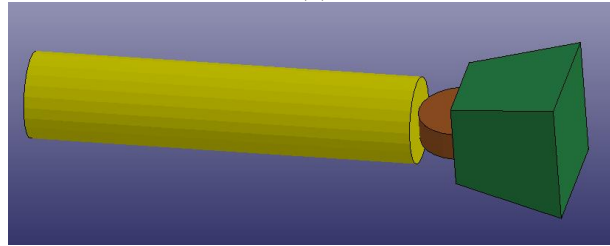
Figure 4-40 End plate mesh

#### **4.6 Rigid plate or load application**

As explained in Chapter 3, load was applied to the column in the experimental work by using a loading ram forcing the loading cell installed at the end of the column. The initial modelling strategy was to explicitly model this loading ram and the load cell, and then apply to the model the experimentally-recorded displacement-time history of the loading ram. Figure 4-41 shows the loading ram and cell arrangement in experiment and the model. The mass of loading ram and load cell were the same as it was in the experiments and for computational efficiency, a rigid material model was used for both. However, this strategy proved unsuitable; small differences in the inertia of the column between the model and the experiment meant that, in the model, this displacement control led to transient separation of the loading ram and load cell, resulting in spurious secondary impacts on the loading.



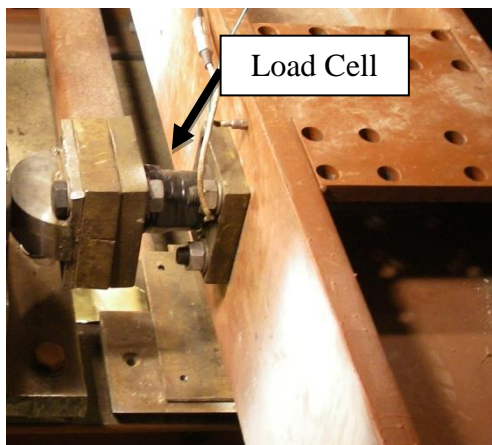
(a)



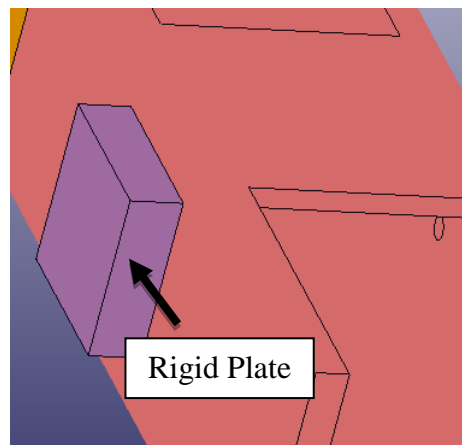
(b)

Figure 4-41 Loading Ram and load cell (a) Experiment (b) Model

Hence, it was decided to build a rigid plate in the model (to capture the inertia of the load cell and bearing) and apply the force which was measured by the load cell as pressure on top of this plate. Figure 4-42 shows the load cell and rigid plate in the model; both of them combined had a mass of 25kg matching the values of the load cell and connection plate in the experimental work and once more a rigid material model was used. The load recorded in an experimental test was applied as a uniform pressure over the face of the rigid plate.



(a)



(b)

Figure 4-42 Force plate & load cell (a) Experiment (b) Model

## 4.7 Parts and Components

Parts and Components are required for defining the contacts in the model. Two different contact types were used: Automatic Surface to Surface (ASTS) which needed node Components, and Eroding Surface to Surface (ESTS) which needed element Parts. About 260 different Parts and Components were defined in the models to have control, on the numbers of elements in each contact and their type.

Different colours in Figure 4-43 shows the Parts and Components defined in the column. Element Parts were defined for bolt holes and the main body, node Components on the column flange in the area between the bolt holes and above them.

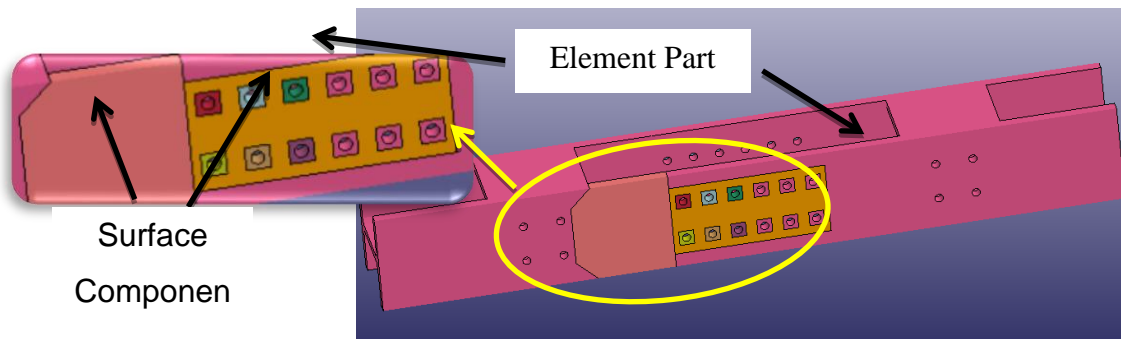


Figure 4-43 Example of column Parts

85 different Parts and Components were defined in beams and their splice connection and shown by different colours in Figure 4-44. Most of them were the element Parts needed to define the Eroding Surface to Surface (ESTS) for bolt holes and also the section of the beam which was connected to the angles. Also there were node Components that used to define the Automatic Surface to Surface (ASTS) contacts in the splice between the beams and plates.

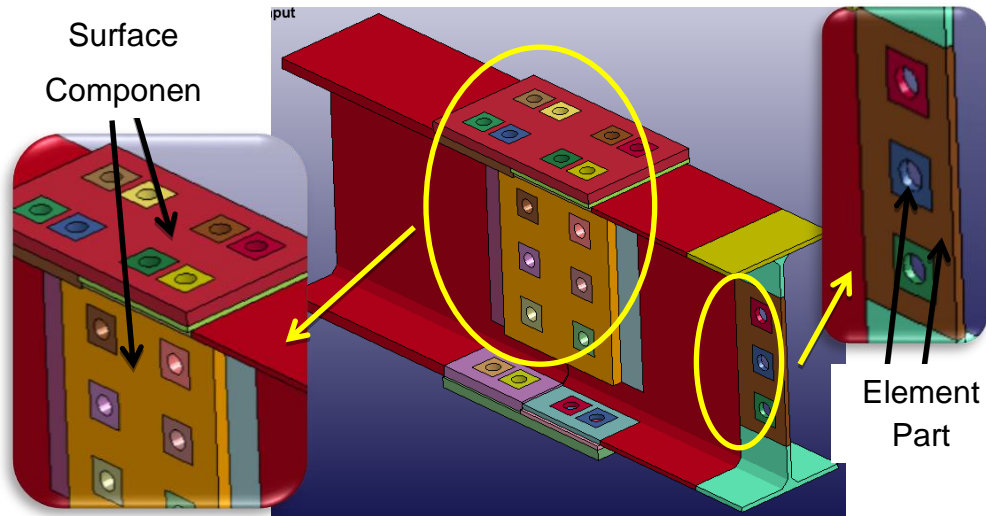


Figure 4-44 Example of beam Parts & Component

Angles were made up of fifteen element Parts, three for main segment of the angles and twelve for bolt holes as shown in Figure 4-45 which used to define the Eroding Surface to Surface (ESTS) contacts between the angles and the bolts. Also there were two node Components to define the Automatic Surface to Surface (ASTS) contacts between the column flange, beam web and the angles.

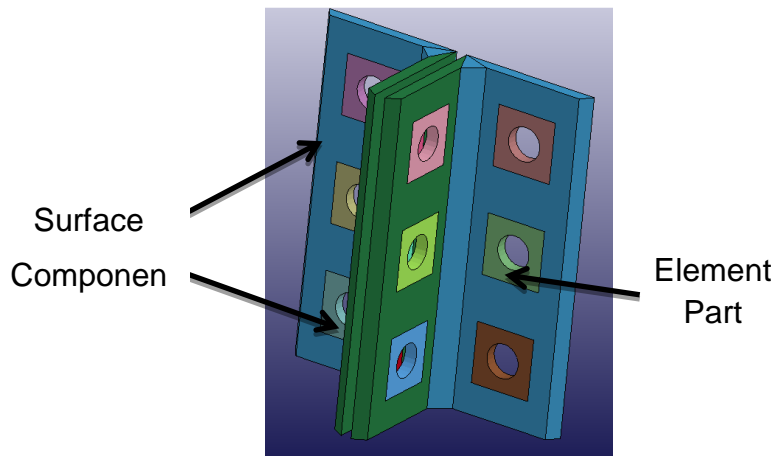


Figure 4-45 Example of angles Parts & Components

Each bolt had five different element Parts as shown in Figure 4-46. Thirty one bolts were developed in the model which makes the number of bolt Parts one hundred and fifty five which were used to define Eroding Surface to Surface (ESTS) contacts.

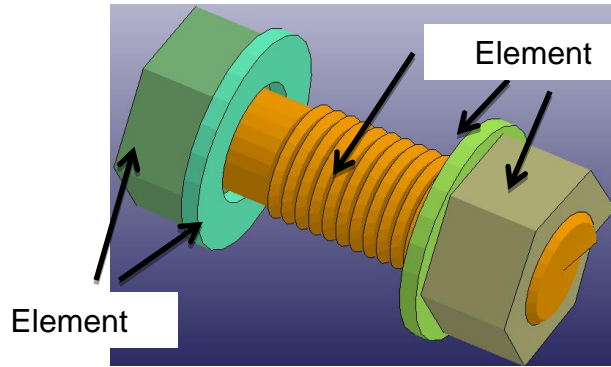


Figure 4-46 Example of Five different Parts of the bolt

The force plate, loading ram and load cell, also had different element Parts as shown in Figure 4-47.

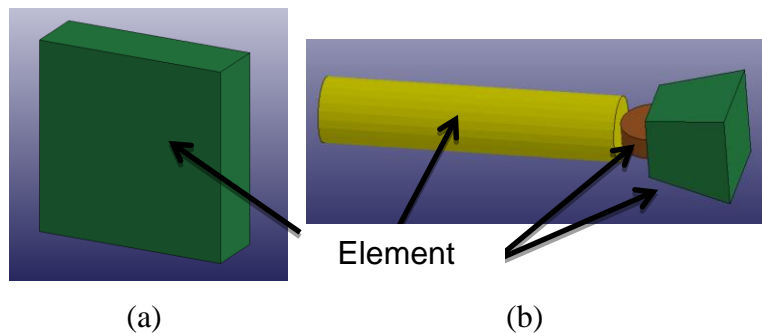
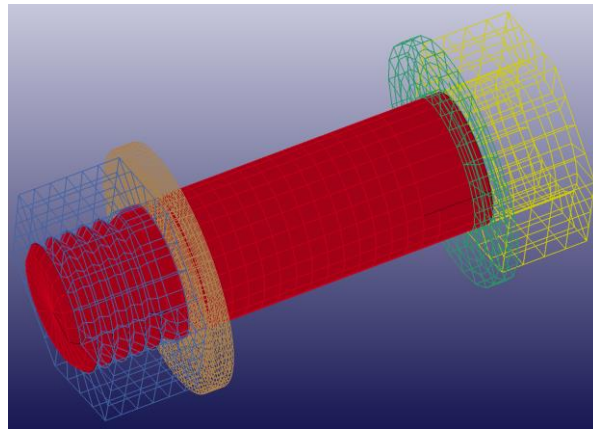


Figure 4-47 Example of (a) Force plate (b) Loading ram and load cell

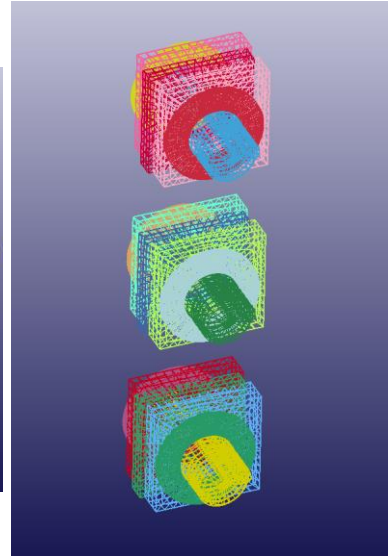
## 4.8 Contacts

Two different types of contacts were used in dynamic (explicit) modelling process, one was Eroding Surface to Surface (ESTS) contact which gives the opportunity to develop penetration and failure. Second was Automatic Surface to Surface (ASTS) contact were used in the areas which no penetration and failure was expected by sliding over one another.

Eroding Surface to Surface (ESTS) does not exist in quasi-static (implicit) then it was decided to change these contact types to Single Surface to Surface contacts. However the previous areas with Automatic Surface to Surface (ASTS) contacts remained the same, as this contact works perfectly in implicit analysis. In total there were 365 different contacts in the model to have more realistic behaviour of the connection. Figure 4-48 shows the examples of Eroding Surface to Surface (ESTS) contacts, the frames with different colours shows the Parts in contact with each other.



(a)



(b)

Figure 4-48 Example of (a) ESTS contacts between the bolt parts  
(b) ESTS contacts between bolts and beam web

Figure 4-49 shows an example of Automatic Surface to Surface (ASTS) contact between the angle and column flange, with two different colours showing the Parts in contact.

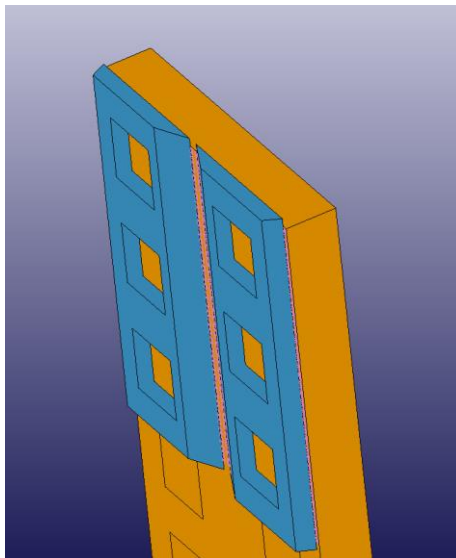


Figure 4-49 Example of ASTS contacts between the angle and column flange

## 4.9 Boundary conditions

In the experiments (Chapter 3), the beam end was connected to the rigid rig with a high capacity moment and tension resistant splice connection. However, initial model results indicated that the explicit modelling of the permanent beam stub was unnecessary. As a result, in later models, it was decided simply to fix three translational and three rotational degrees of freedom at the end of the test beam. In the experimental tests, eight single ball-rollers were used under the column to allow it to translate freely with effectively no friction (the force required to set the ~400kg column in motion was recorded at <10N). Rather than explicitly model these rollers, it was decided simply to apply a vertical translational constraint boundary condition at these locations, and to model their inertia by adding suitable additional mass of these points in the model. The overall boundary conditions for the finalised model are shown in Figure 4-50.

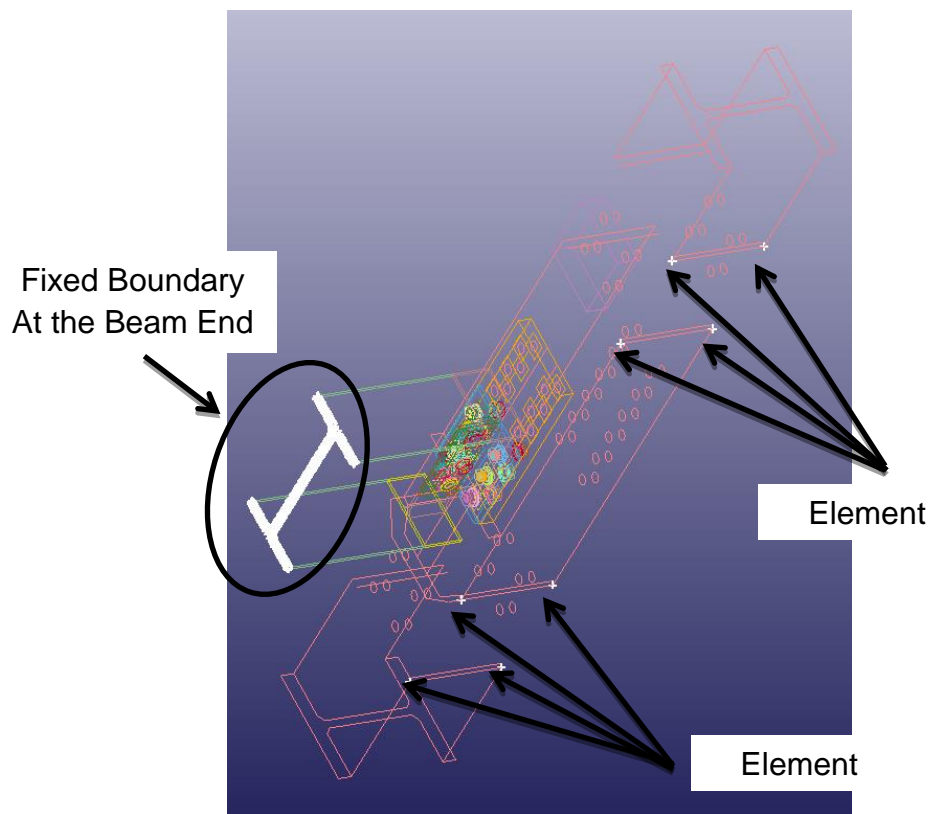


Figure 4-50 Boundary condition around the model

## **4.10 Conclusion**

This chapter provided the details of how each section of the model has been developed. Correct meshing size and shape, time-step, defining the Components and Parts, defining the contacts and material properties were the important steps to model the connection correctly and efficiently. After this step all these sections were added together to build the connection model and got validated against experimental results which is provided in Chapter 5.

## 5 Finite element model of connections

### 5.1 Free column validation

As a first stage in the model validation it was important to assess whether the inertia of the column had been modelled correctly. The column and associated parts had a relatively complex geometry, and consequently the rotational inertia could not be determined analytically. In the experimental work (Tyas et al [14]) the column rotational inertia was found by applying an eccentric dynamic load in the absence of a connection (the “free acceleration test”), recording the translational and rotational displacement and determining the mass moment of inertia from these results. A similar approach was taken with the numerical model, with the same dynamic load applied. Figure 5-1 shows the column movement and rotation in the model at different times.

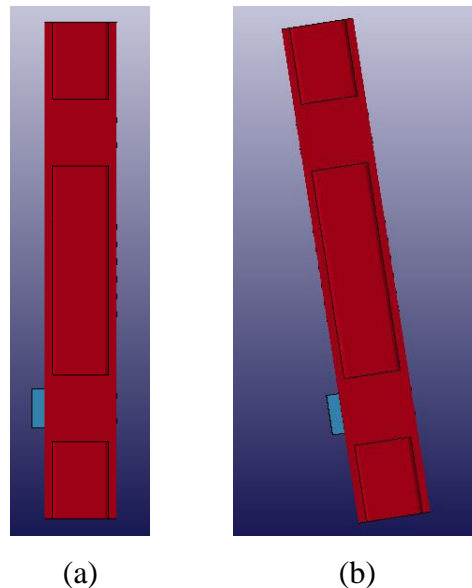


Figure 5-1 (a) Initial position of the column (b) Column at 40ms

The total mass of the column was 411kg which included the column itself, stiffeners, rollers and the load cell. The length of the column was 1.999m and the load was applied at 0.44m from the end of the column.

Displacements of the column were measured by different methods in the experimental work; one of them was measuring displacement with unidirectional laser gauges as

explained in Chapter 3.1. Figure 5-2 shows the experimentally determined load applied to the column with a magnitude of 35kN and duration of 0.4s; after 0.4s the column hit an end stop and measurements were not suitable for validation.

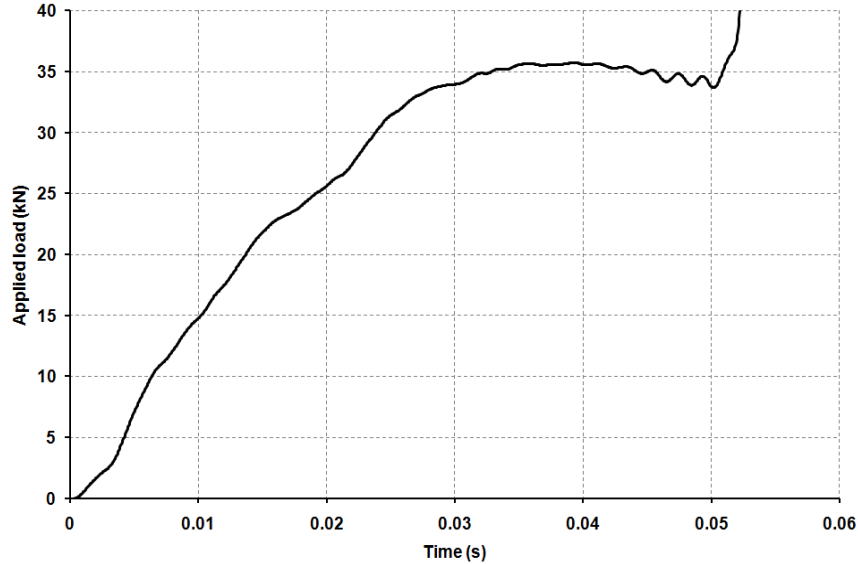


Figure 5-2 Applied load to the free column against time

Displacement of the two ends of column was measured experimentally by laser gauges installed at each end, as explained in Chapter 3.1. By analysing the free column model displacements (by using line equation) of the same locations as the laser gauges were calculated and the comparison is provided in Figure 5-3. As shown by the figure, the correlation between the model and experiment was excellent.

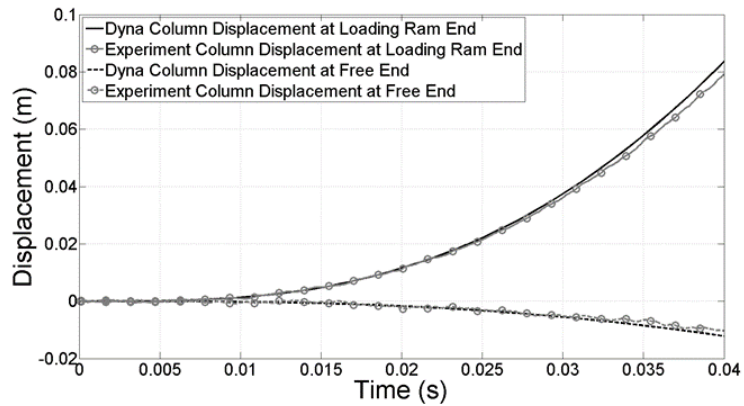


Figure 5-3 Displacement time history of the free column

## 5.2 Instabilities problems in dynamic analysis

Fast dynamics may frequently can cause instabilities in models, for example hourglass instability which is a numerical problem in finite element models especially with fast and large deformations. Hourglassing is a so-called “zero energy deformation mode” in which numerical instabilities cause spurious vibration of the nodes of elements in a way which does not result in strains in the elements themselves. The practical effect of this is to artificially soften the regions of the model experiencing hourglassing, resulting in spuriously high deformations, and eventually, breakdown of the model through gross element deformation. Figure 5-4 (a) shows the washer after having an hourglass instability problem and (b) shows that the washer behaves reasonably under the same loading condition after making three different corrections as mentioned below:

1. The mesh size was made smaller but this decreases the time step in explicit analysis. However, to prevent this change in time step the washer’s density was increased (the extra mass could be ignored as few washers had this problem and their contribution to total inertia was small enough to be ignored)
2. The number of integration points was increased from single to fully integrated in those areas with this problem
3. Damping was added to the washers to reduce the internal energy generated by the contacts (extra damping caused no effect on parts around the washer)

The major down side of these changes was increasing the running time of the model; however this extra time was the cost of having a model with no instability. These changes had no major effect on the behaviour of other parts of the structure but the behaviour of these washers became smoother and enabled large deformation of them to be captured. Figure 5-5 shows how much a washer was deformed under the high localized loading applied by the bolt nut. These deformations highlight the importance of washers and how they prevent the bolts from passing through the angle holes.

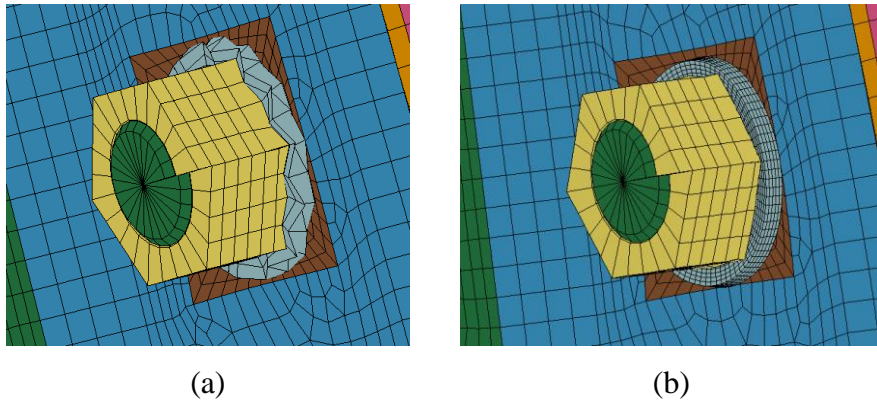


Figure 5-4 (a) Washer with instability problem (b) Washer with no instability problem

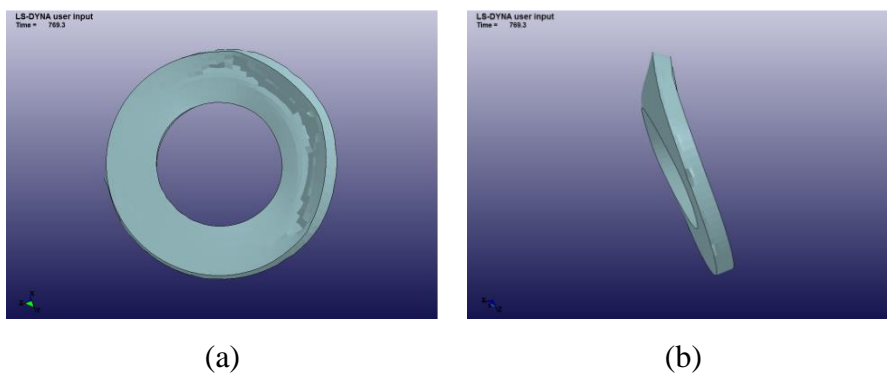


Figure 5-5 Washer deformation (a) Front view (b) Side view

The beam web also had some instability problems as the bolt moved inside the holes before contacting with the sides and sheared through the beam web. In Figure 5-6 the red and brown colour show those parts of the beam web in contact with the bolt (shown in blue). To prevent the instability in the beam web three steps were taken:

1. The bolt threads on the bolt shank in contact with the web were removed. These threads caused high concentration of force as the tips came into contact and made the elements in that area unstable.
2. The number of integration points in the beam web was increased and the mesh size reduced without any change in time step.
3. Damping was added to the beam web to prevent instabilities but without changing the behaviour or adding extra stiffness into the model.

These changes were made carefully to prevent any effect on the qualitative behaviour of the connection.

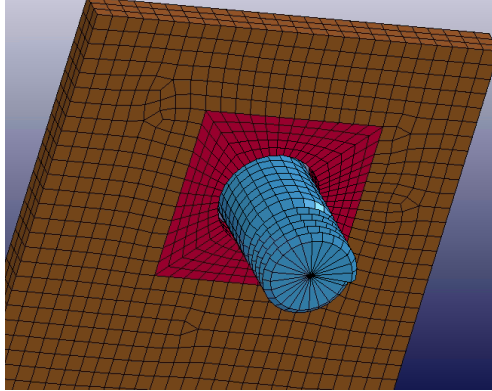


Figure 5-6 Bolt and beam web

### 5.3 Web-cleat connection

By adding all the sections explained in Chapter 4 the web-cleat model was developed. To validate this model first all instabilities problems and complications were resolved then the model results were compared with *dynamic* and *static* results both *qualitatively* and *quantitatively*.

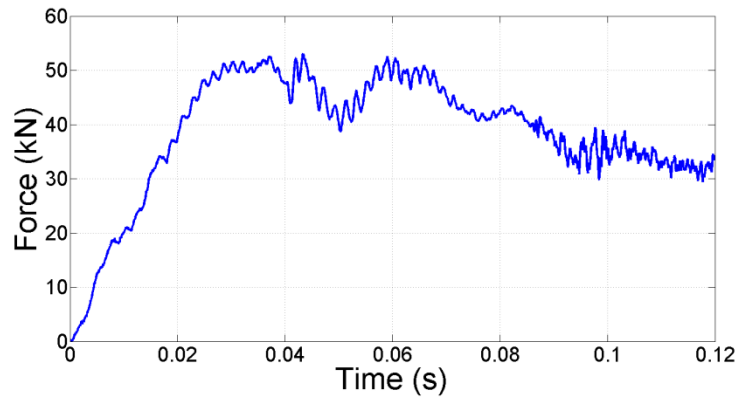
The reason to do validation against both dynamic and static loading was to have a model which could be used over a wide range of loading from static up to fast dynamic. Also having qualitative validation was as important as quantitative, because how connections deform and fail was equally important as the correct time history results. It is important to note that the same model was used for both static and dynamic process with some small changes, as explained in chapter 4.

In the dynamic tests, WC5, 4 and 7, the results for rotation time history and the connection moment and axial force vs rotation from the models follow the experimental data very closely. Also the model had excellent correlation with experiments qualitatively in terms of deformations and failure.

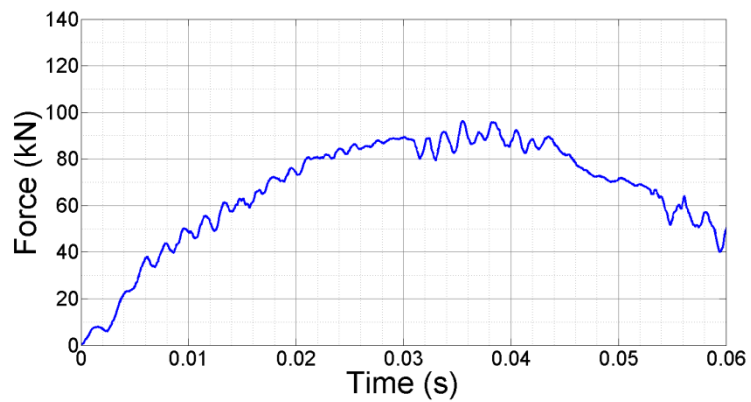
For static tests, WC6 and 9, the results for rotation time history and the connection moment and axial force vs rotation from the models follow the experimental data but with some important differences which are discussed in the following section.

### 5.3.1 Quantitative validation against dynamic tests 4, 5 and 7

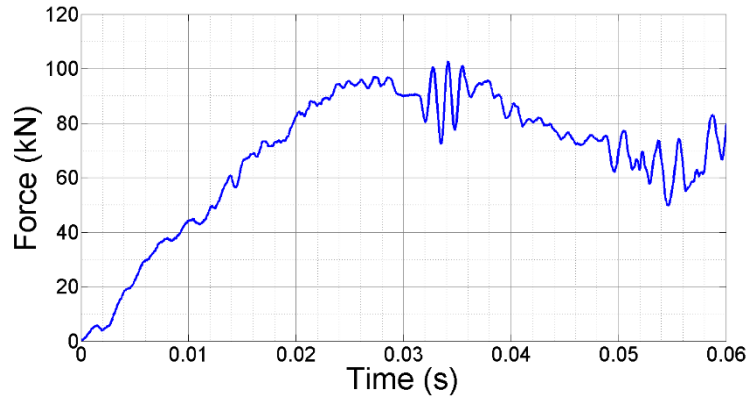
After validation of the column alone, other parts were added to the model, including the beams, splices and connection angles. The remote end of the beam was fixed in all degrees of freedom - force was then applied to the rigid plate connected to the column. Three dynamic tests were used to validate the model. WC 4 and 5 had an 8mm angle connection and WC7 had a 10mm thick angle. The applied force-time data from the experimental work for these three tests are shown in Figure 5-7.



(a)



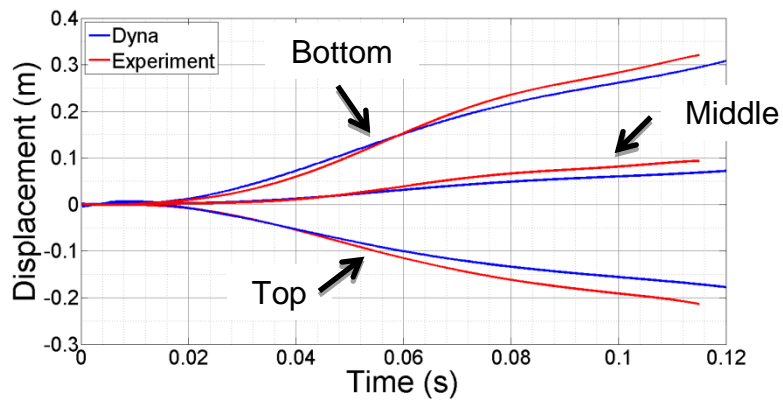
(b)



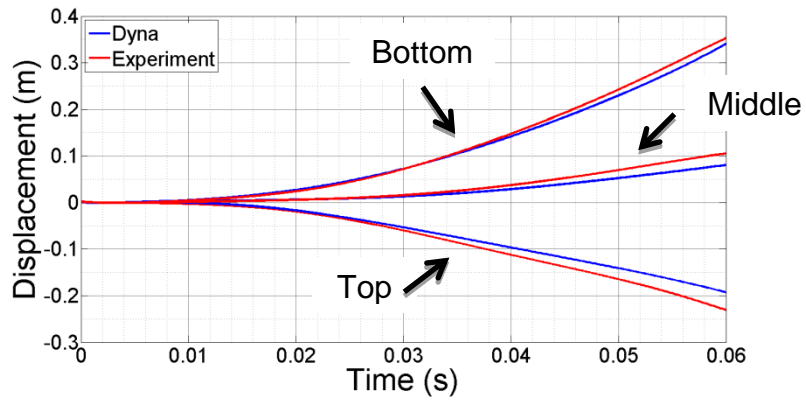
(c)

Figure 5-7 Applied force time history (a) Test WC5 (b) Test WC4 (c) Test WC7

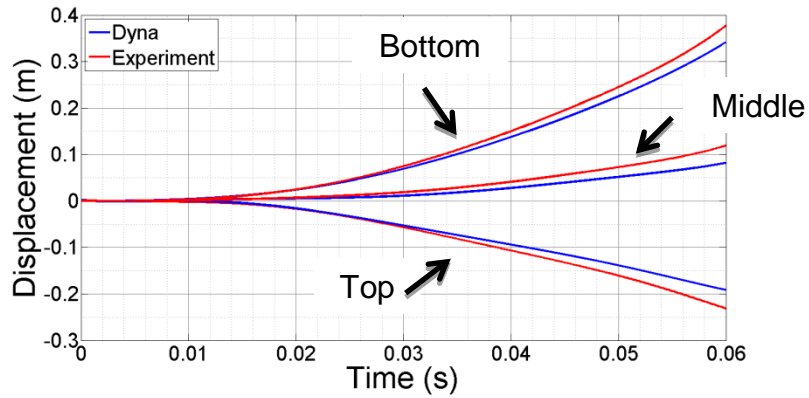
Figure 5-8 shows the displacement-time histories for these three points from experimental data from WC4, 5 and 7, and from the corresponding points on the column in the numerical analyses.



(a)



(b)



(c)

Figure 5-8 Displacement time history (a) Test WC5 (b) Test WC4 (c) Test WC7

The experimental and numerical model data show good, but not perfect correlation. To further investigate the significance of the difference between the displacement time histories from the experiments and models, a free column acceleration model (i.e. no connection present, with the column free to translate and rotate under the dynamic loading) was analysed with the applied load from test WC7. The intention of this analysis was to separately quantify the effect of solely the inertial resistance and thereby give an indication of the absolute contribution of the connection, and hence to better quantify the significance of the difference between the model and the experimental work. Figure 5-9 shows the displacements at two ends and the centre of the column. These indicate that the error between the experiment and model is a small percentage of the absolute connection resistance.

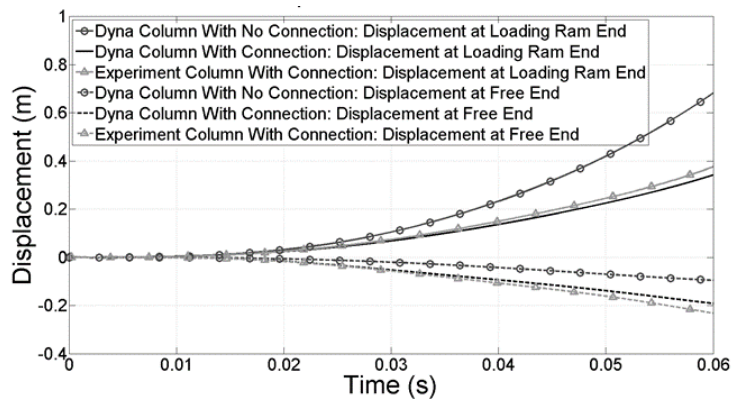
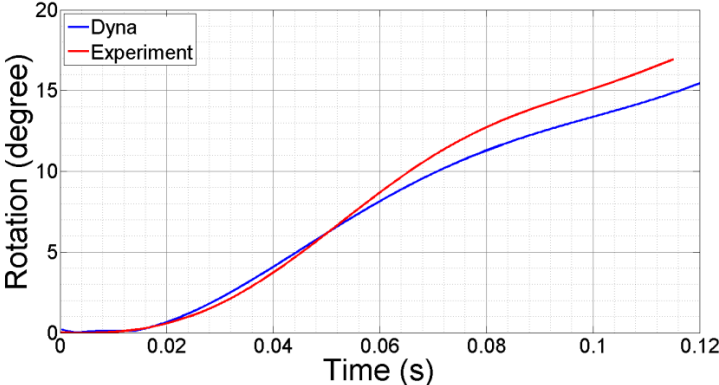
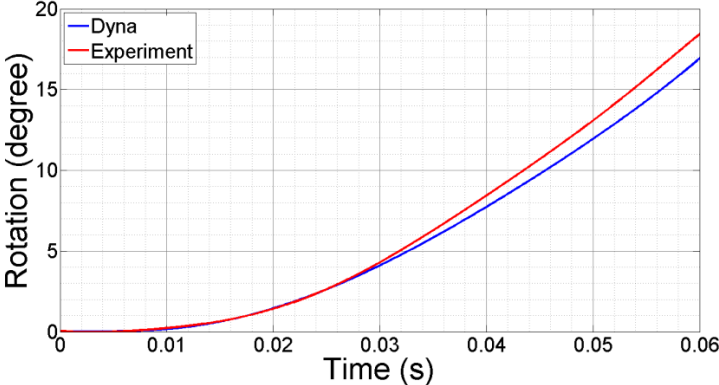


Figure 5-9 WC7 – Column rotation vs time: comparison of results from experimental connection test, model connection test and model with same applied load but no connection

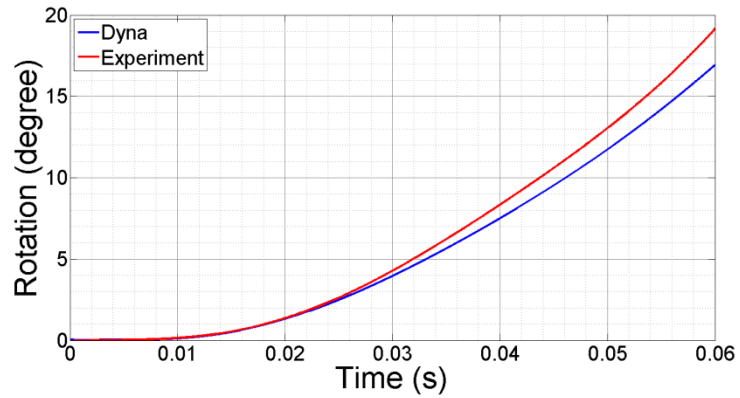
Figure 5-10 shows the rotation of the column against time. Comparison between experiments and numerical modelling shows that they follow each other very closely and have the same general trends, with the model and experimental data only diverging at relatively large rotations.



(a)



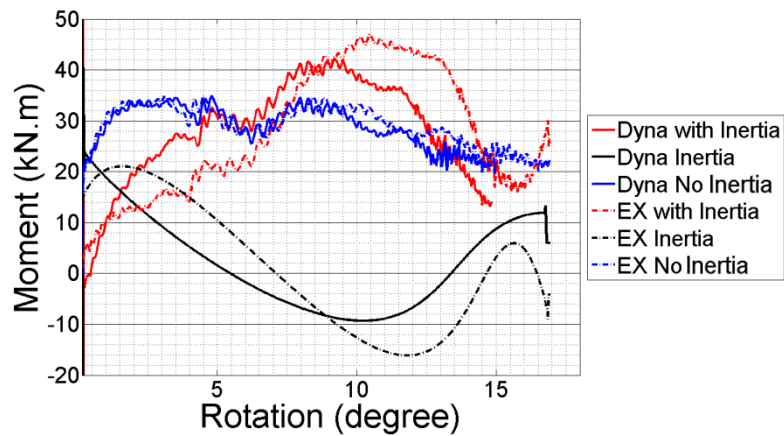
(b)



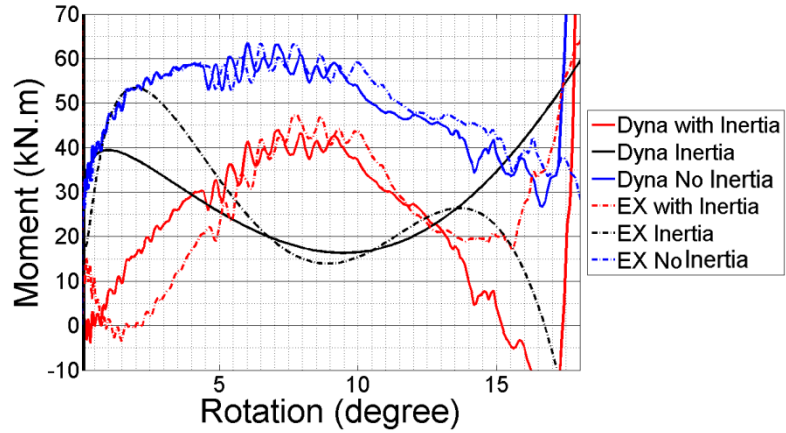
(c)

Figure 5-10 Rotation time history (a) Test WC5 (b) Test WC4 (c) Test WC7

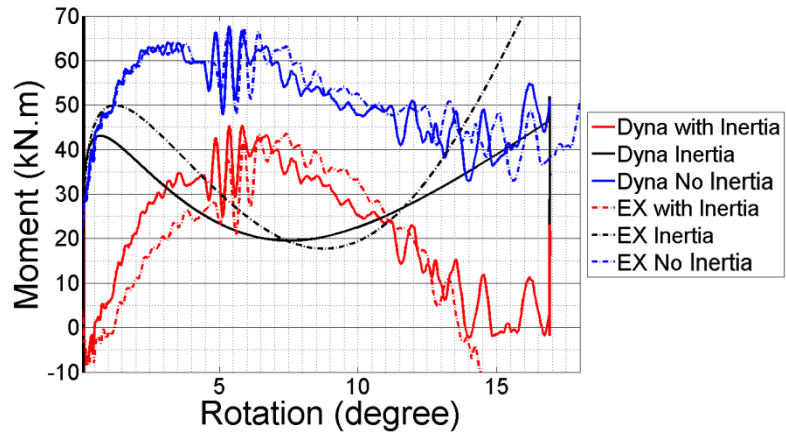
The moment resistance of the connection was calculated by the formula provided in Section 3.2.3. This involved subtracting the inertial moment of the column from the applied moment. Figure 5-11 shows moment rotation diagrams for models and experiments WC4, 5 and 7, the dotted lines are results from experiments and continuous lines are results from LS-DYNA analysis. Blue lines are the total moment applied to the column without considering any inertial effect, black lines are just the moment generated by the column inertia and the red lines are the difference between the two which shows the resistance moment of the connection. The results are reasonably close.



(a)



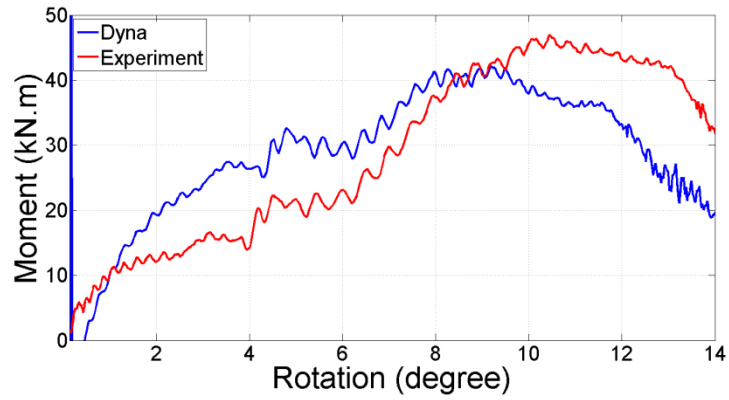
(b)



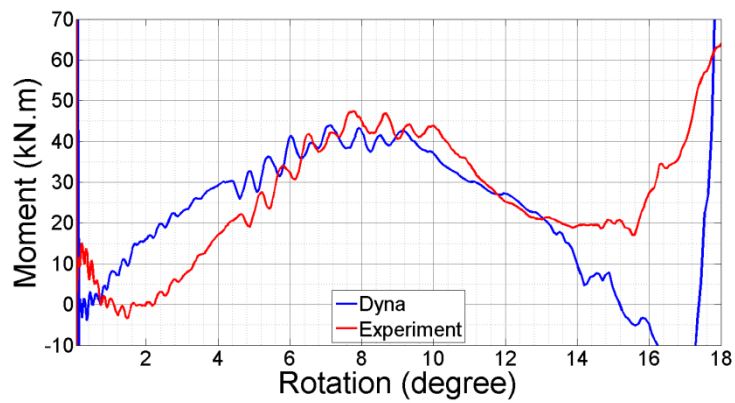
(c)

Figure 5-11 Moment rotation diagrams (a) Test WC5 (b) Test WC4 (c) Test WC7

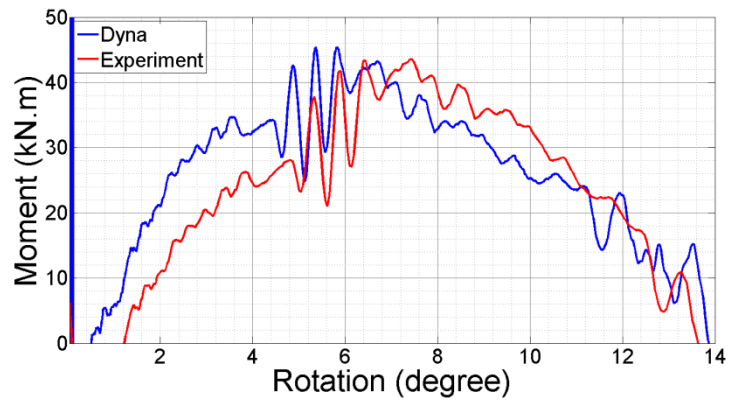
For clarity, Figure 5-12 shows just the connection moment against rotation. In all three cases the moment resisted was about 40kN.m, however experiments with 8mm angles reached this resistance with higher rotation i.e. more ductility for the same resistance.



(a)



(b)

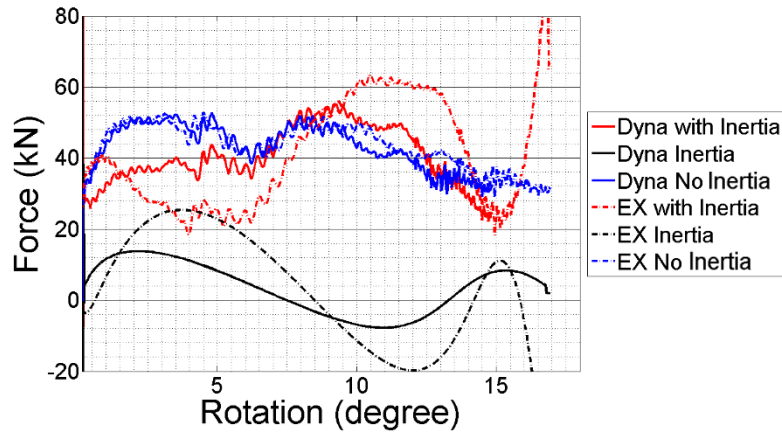


(c)

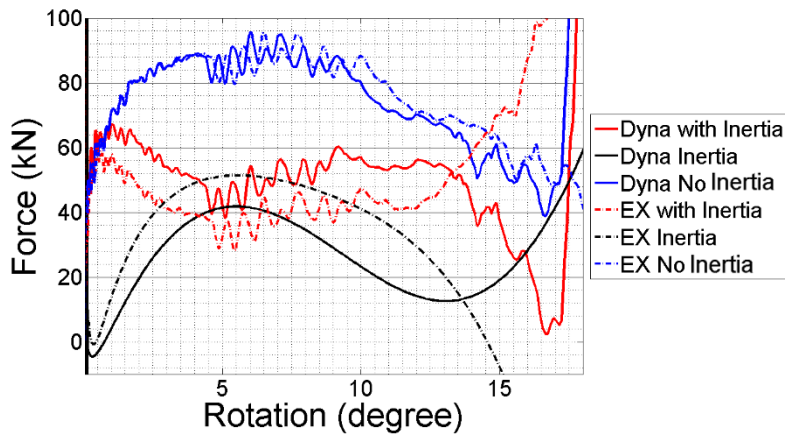
Figure 5-12: Moment rotation diagrams (a) Test WC5 (b) Test WC4 (c) Test WC7

The same principle, that of subtracting the inertial resistance from the applied load, was also used to determine the axial resistance in the connection, explained in Section

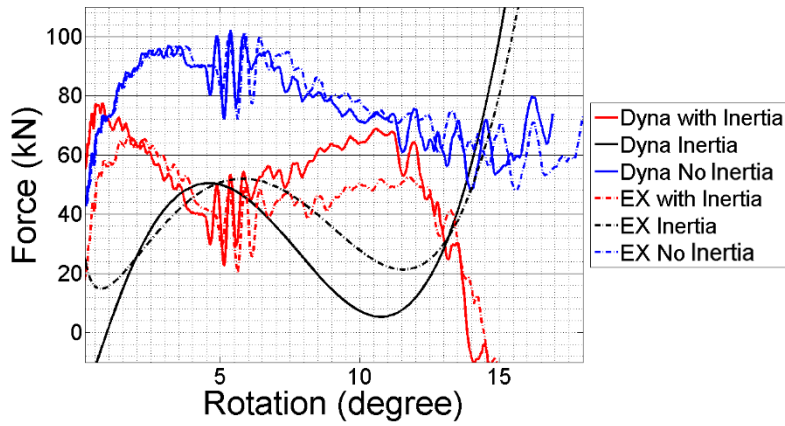
3.2.3. Figure 5-13 shows Force-Rotation diagrams for all three cases. As in the case of the moment-rotation, results are again close for experiments and the LS-DYNA model.



(a)



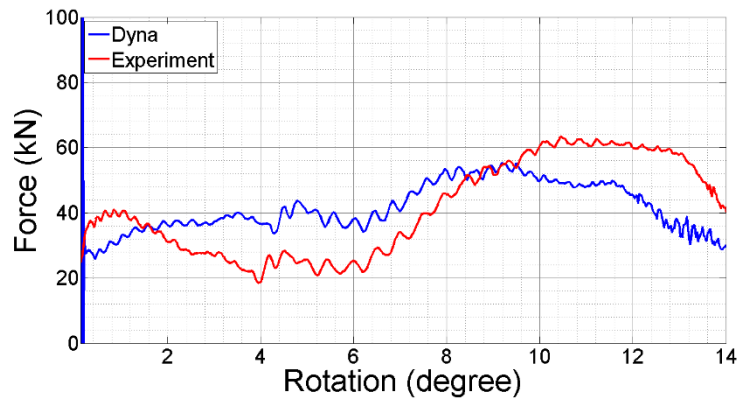
(b)



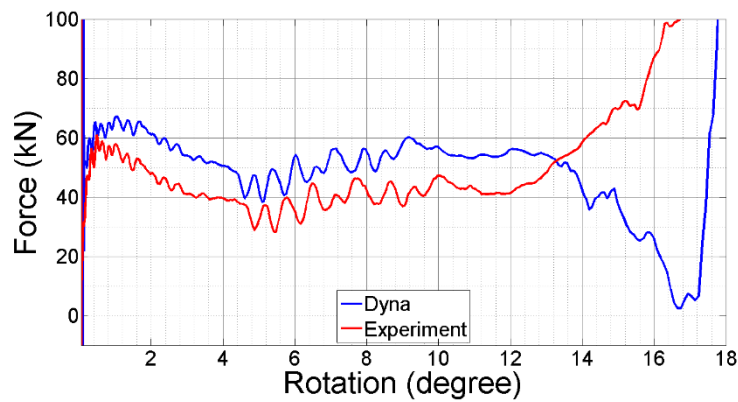
(c)

Figure 5-13 Force rotation (a) Test WC5 (b) Test WC4 (c) Test WC7

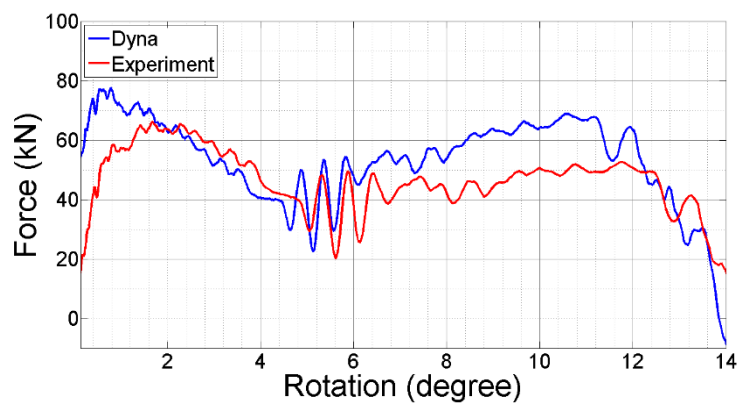
Figure 5-14 shows the connection resisted force against rotation. In all three cases the maximum force resisted was around 60kN but the ductility varied with 8mm angles delivering more ductility than the 10mm thick angle.



(a)



(b)



(c)

Figure 5-14 Force rotation (a) Test WC5 (b) Test WC4 (c) Test WC7

### **5.3.2 Qualitative validation against dynamic tests 4, 5 and 7**

As much as it is important to correctly predict resistance of the connection in terms of numbers, it is also important to have correlation in terms of qualitative behaviour. For that reason some comparisons were made of the deformation of the connection in both modelling and experiment.

Figure 5-15 shows the final stage of the beam web after connection failure, in both model and test WC4 and WC7. Also Figure 5-16 shows how the angles were deformed in test WC4 and compares the model against the experiment. Excellent qualitative correlation is evident between the experimental and numerical results.

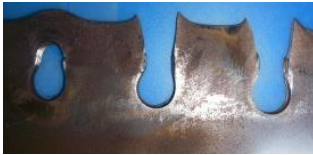
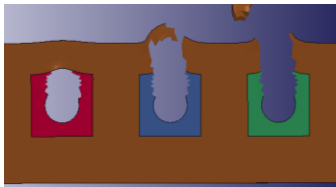
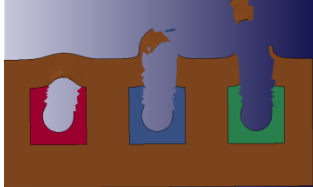
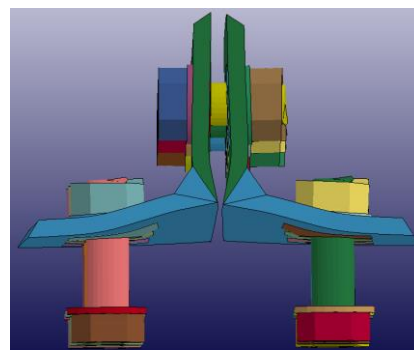
Test	WC4	WC7
Exp		
Model		

Figure 5-15 Post-test web failure



(a)



(b)

Figure 5-16 Post-test angle deformation for test WC4 (a) Experiments (b) Ls-Dyna

Images from the high speed video and the model for tests WC5 and WC7 are presented in Figure 5-17 and Figure 5-18. These indicate that, qualitatively the deformations and displacements in the connection were very similar in the model and the experimental test at similar times and rotations, with failure occurring through shear of the beam web due to bearing of the connection bolts in all cases.

Time (s)	Rotation (degree)	Experiment	Model	Model (beam web and bolts)
0 (model)	0 (a)			
0 (exp)				
0.037 (model)	3.25 (b)			
0.0358 (exp)				
0.055 (model)	7.5 (c)			
0.0565 (exp)				
0.096 (model)	14.7 (d)			
0.113 (exp)				
0.117 (model)	17 (e)			
0.130 (exp)				

Figure 5-17 – Test WC5 deformation of connection at key points.

(a) Pre-test (b) Beam flange strikes column (c) First element failed in model (d) Web completely failed adjacent to first bolt in model (e) Web completely failed adjacent to second bolt in model.

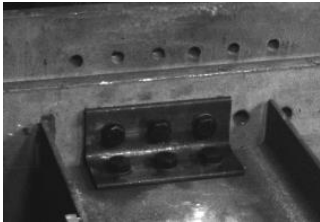
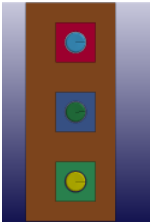
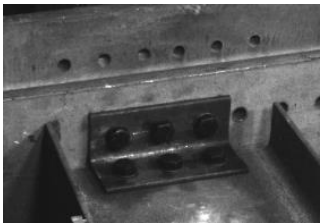
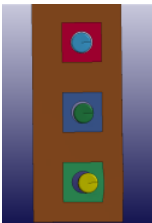
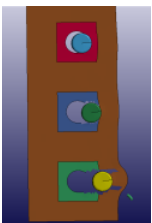
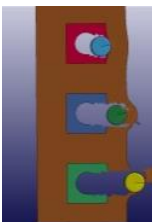
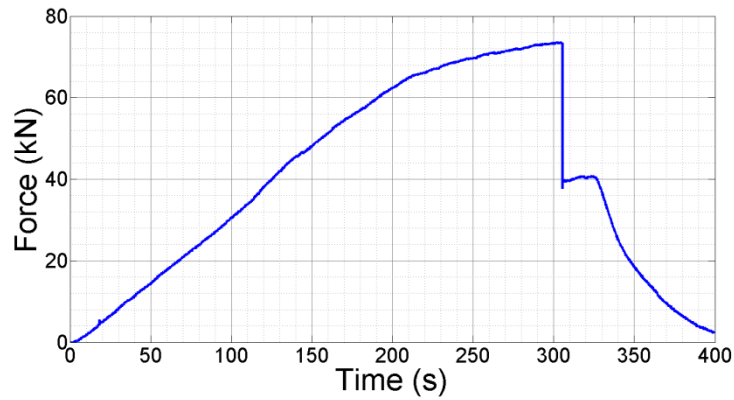
Time (s)	Rotation (degree)	Experiment	Model	Model (beam web and bolts)
0 (model)	0 (a)			
0 (exp)				
0.029 (model)	4 (b)			
0.029 (exp)				
0.034 (model)	5.25 (c)			
0.033 (exp)				
0.047 (model)	10.5 (d)			
0.045 (exp)				
0.055 (model)	14 (e)			
0.052 (exp)				

Figure 5-18 – Test WC7 deformation of connection at key points.

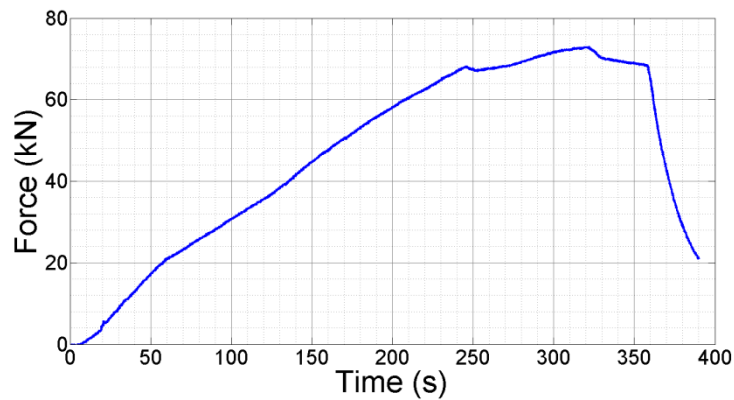
(a) Pre-test (b) Beam flange strikes column (c) First element failed in model (d) Web completely failed adjacent to first bolt in model (e) Web completely failed adjacent to second bolt in model. .

### 5.3.3 Quantitative validation against static tests 6 and 9

Tests WC6 and WC9, both quasi-static with 8mm angles, were used for validation purposes in the static loading cases. The models were analysed with implicit solvers and some minor changes to the code used for the dynamic analysis. Figure 5-19 (a) shows the force time history for test WC6. The maximum applied load was around 67kN reached in 300 seconds. Also Figure 5-19 (b) shows the applied force time history in test WC9. This load reached approximately 70kN in 350 seconds. (Note that in the experimental work, some seal leakage meant that the rate of increase of the load dropped off towards the end of the loading. Furthermore, the abrupt drop in loading was due to the sudden displacement of the column on connection failure.)



(a)



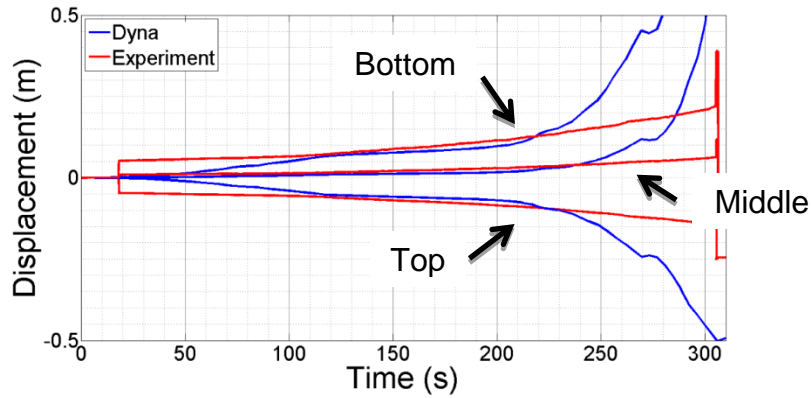
(b)

Figure 5-19 Applied force time history (a) Test WC6 (b) Test WC9

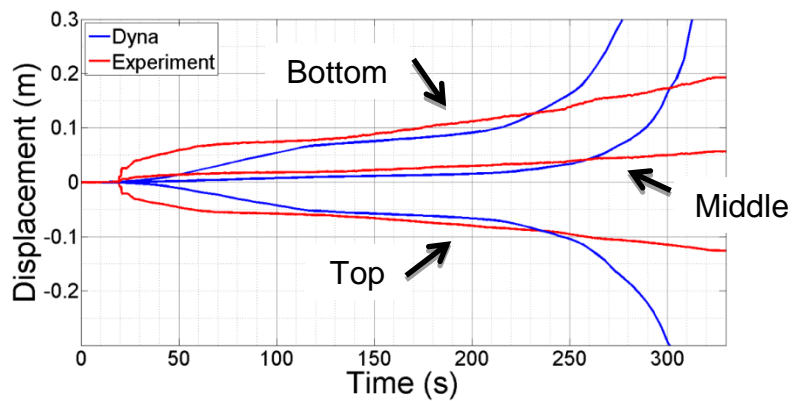
Displacements were measured by the laser gauges at three points on the column, as before. By the same method the displacement of those three points were measured from finite

element model results. Figure 5-20 shows the displacements time history and compares the results between experiments and finite element model.

As can be seen in Figure 5-20 and Figure 5-21, the correlation between the static experiments and the corresponding numerical models is, at first sight, less good than that in the dynamic models. Considering test WC6 as an example, there is a significant difference in the rotation-time from the model and the experimental work, predominantly due to two features. Firstly, the early slip of the connection from its pre-loaded position to the position in which the column flange and beam flange are in contact and prying commences – this occurs at slightly different times in the model and experiment. This is due to differences in the frictional pre-slip resistance of the connection. However, this is of minimal importance; the purpose of this study was to assess the ultimate behaviour of the connections and the accurate modelling of early slip is of secondary interest. Secondly, in the experimental test, the connection failed suddenly and catastrophically at a rotation of ~12 degrees. This occurred 305 seconds after the onset of loading, at an applied load of 72kN and applied moment of 48kNm. In the model, failure of the beam web occurred in the vicinity of the bolt closest to the loading ram, and commenced at 220s after the onset of loading, at an applied load of ~65kN and moment of 43kNm. Thereafter, the connection rapidly lost stiffness and the rate of deformation with time increased relative to that seen in the experimental test. It is believed that this difference may be due to the way in which failure is modelled in the finite element model. In the model, failed elements are eroded and removed from the mesh, whereas in the experimental tests, fractured steel in the web was still present and jammed between the deformed angle cleats, giving some additional resistance, even after the beam web had failed in shear. Despite these differences in initial failure, it is noteworthy that in the model the web adjacent to the first bolt was completely ruptured at a rotation of 12 degrees, a similar rotation to that at which the experimental connection catastrophically failed. This strongly suggests that the final connection failure in the experimental work was induced by the loss of resistance of the beam web material adjacent to the bolt closest to the loading ram.



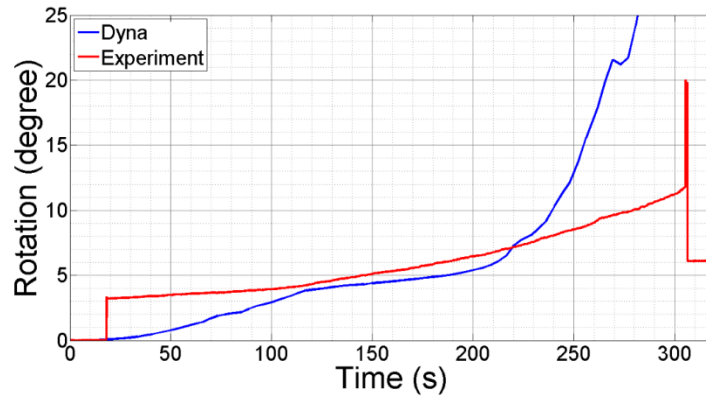
(a)



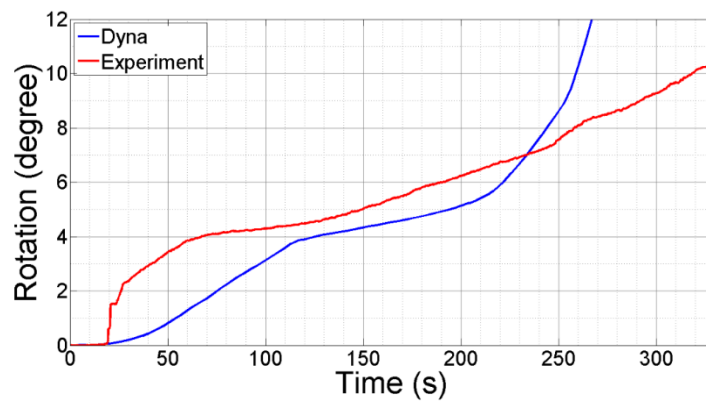
(b)

Figure 5-20 Displacement time history (a) Test WC6 (b) Test WC9

Figure 5-21 shows the rotation time history of both tests, however as mentioned for displacement-time histories there was a difference between the finite element model and experimental test data, for the two reasons discussed previously. In experiment test WC 6, there was a frictional hold of the bolts at low applied force, followed by a sudden slip to around 3 degrees at 20s after the onset of loading, with an applied load of 5kN and moment of 3.5kNm. In the model, by contrast, there was a continuous slippage from the onset of loading to the onset of prying at 4 degrees rotation.



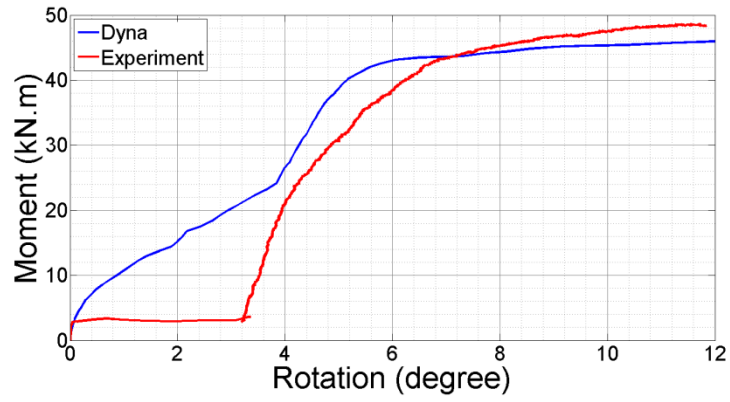
(a)



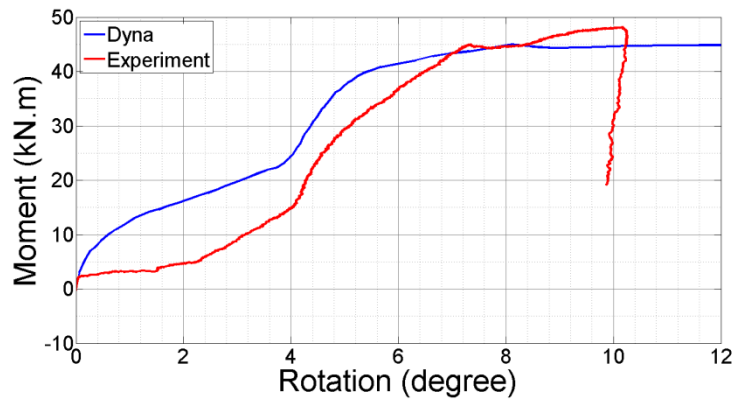
(b)

Figure 5-21 Rotation time history (a) Test WC6 (b) Test WC9

Figure 5-22 shows the moment rotation diagrams for both tests and compares the results from the finite element model and experimental tests. Although there were difference in the development of the resistance and rotation as discussed previously, the ultimate moment resistance of the model and experimental connections was very close in both cases.



(a)



(b)

Figure 5-22 Moment rotation diagram (a) Test WC6 (b) Test WC9

### 5.3.4 Qualitative validation against static tests 6 and 9

Figure 5-23 shows the final stage of the beam web after connection failure, in both model and test WC6. Also Figure 5-24 shows how the angles were deformed in test WC6 and compares the model against the experiment. Excellent qualitative correlation is evident between the experimental and numerical results.



Figure 5-23 Final deformation of beam web (a) Experiments (b) Ls-Dyna

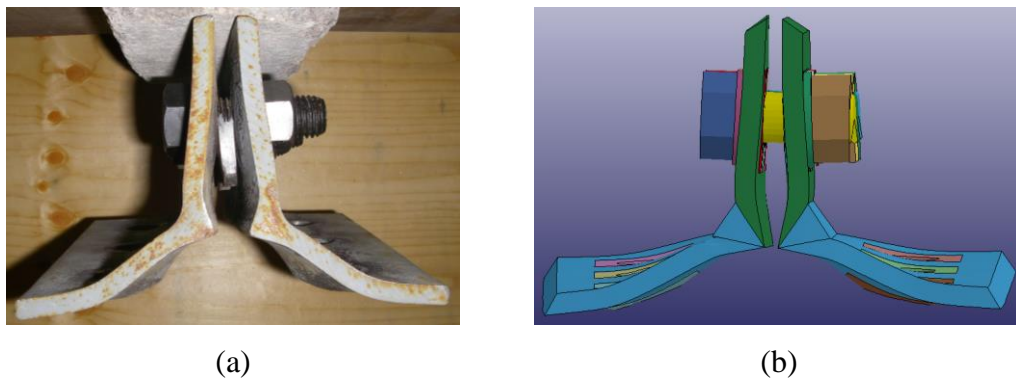


Figure 5-24: Post-test angle deformation (a) Experiments (b) Ls-Dyna

Images from the high-speed video and the model from models and tests WC6 are presented in Figure 5-25. These indicate that, qualitatively the deformations and displacements in the connection were very similar in the model and the experimental test at close times and rotations, with failure occurring through shear of the beam web due to bearing of the connection bolts in all cases.

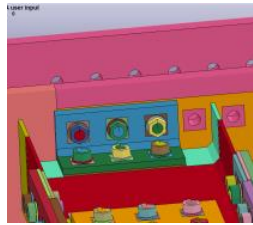
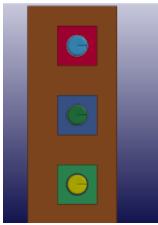
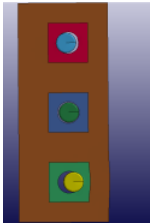
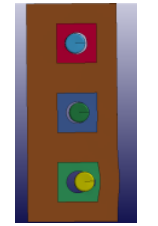
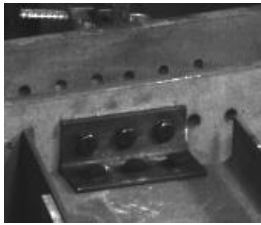
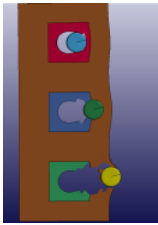
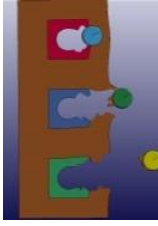
Time (s)	Rotation (degree)	Experiment	Model	Model (beam web and bolts)
0 (model)	0 (a)			
0 (exp)				
140 (model)	4 (b)			
120 (exp)				
201 (model)	5.5 (c)			
160 (exp)				
248 (model)	12 (d)			
305 (exp)				
265 (model)	20 (e)	NA (Connection failed catastrophically at shortly after 12 degree rotation image shown above)		
Exp N/A				

Figure 5-25– Test WC6 deformation of connection at key points.

(a) Pre-test (b) Beam flange strikes column (c) First element failed in model (d) Web completely failed adjacent to first bolt in model (e) Web completely failed adjacent to second bolt in model.

### 5.3.5 Simplified model of Web-cleat connection

The permanent beam stub and splice were found in early models to play a negligible role in total behaviour of the connection and as their inclusion added significantly to the run-time of the models these were removed from the final model for parametric studies (Chapter 6). This reduced the CPU time by around half to typically around 10 hours; this simplified model is shown in Figure 5-26.

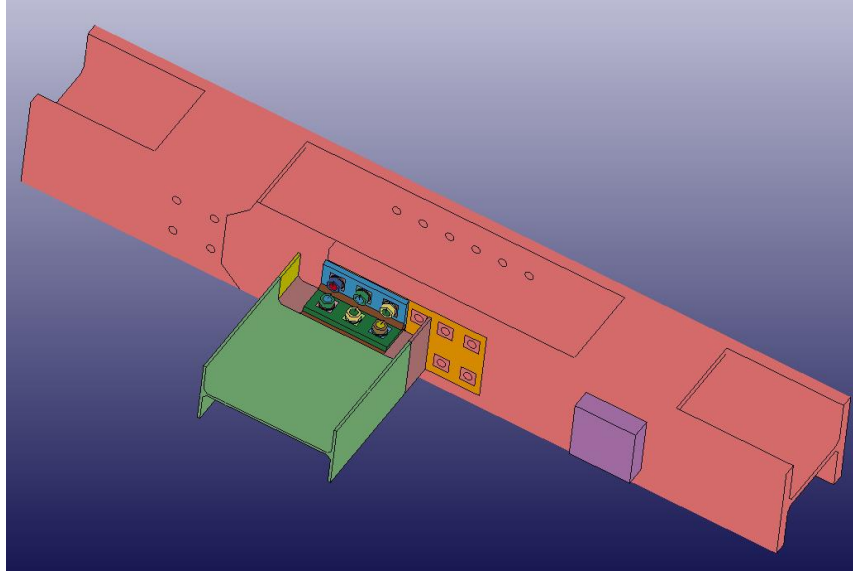


Figure 5-26 Simplified model after removing the splice

## 5.4 End-plate connections

By adding all the sections defined in chapter 4 the End-Plate model was developed and validated under different types of loading as described in this section. To validate this model first *complications* were resolved then model results were compared with *dynamic* and *static* results both *qualitatively* and *quantitatively*.

An important point to remember was that the same model was used for both static and dynamic process with some small changes as mentioned in chapter 4.

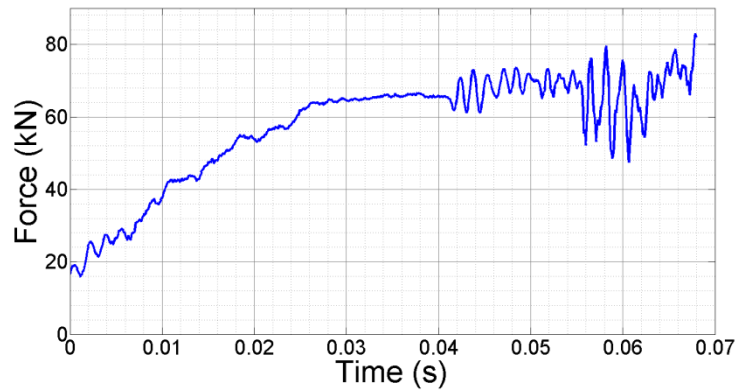
### 5.4.1 Complications regarding connection failure

The main complication in making the End-Plate connection was the material properties around the welded area. Despite an exhaustive literature survey, no constitutive model data was found on dynamic behaviour of either weld material or HAZ for construction grade steel (Chapter 3). Furthermore, experimental work to derive these properties was beyond the scope of this study. As a consequence, as explained in Section 4.6, the constitutive model data and the subsequent structural analysis of the connection were studied by a calibration-followed by-validation process. The welded area was divided into three different heat affected areas and their material properties were calibrated such that the numerical model of overall connection behaviour matched experimental results for one test. The robustness of the resulting model was assessed by validating it against data from different experimental tests.

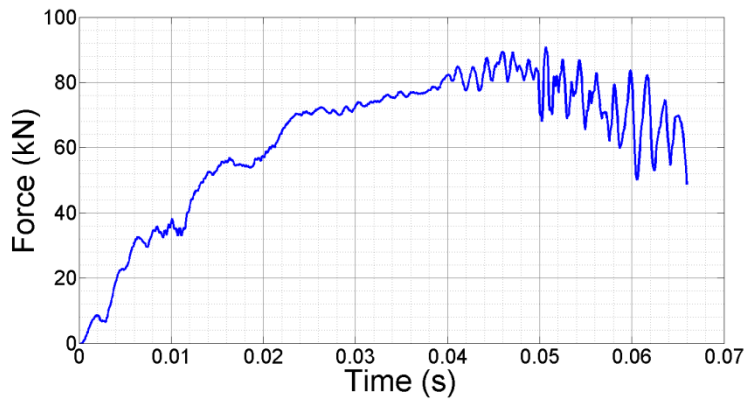
To find the parameters of material properties in the *calibration* stage, the model results were compared with static test EP1 to find the strain to failure of these heat affected areas, then model results with the correct strain failure were compared to a dynamic test EP4 to find the C value, which is the parameter to control the strain rate in Johnson-Cook material properties. The parameters for these materials are provided in Chapter 4, table 4-6. After this calibration of the material for both static and dynamic analysis, the model was then validated against four other tests.

### 5.4.2 Quantitative validation against dynamic tests 4, 6 and 11

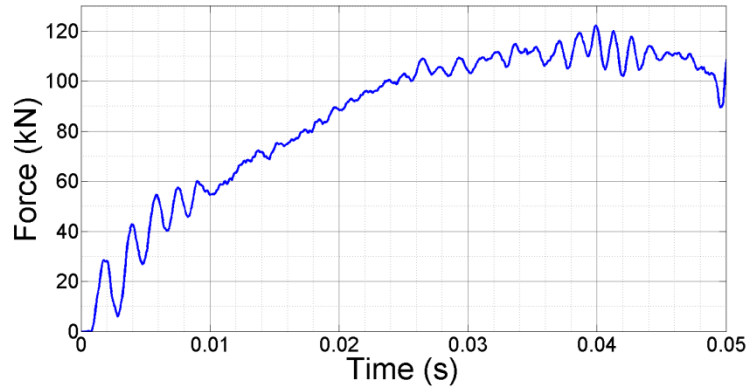
After validation of the column other parts were added to the model e.g. beams, slices and connection angles. One end of the beam was fixed in all degree of freedoms; force was applied to the rigid plate connected to the column. Three dynamic tests were used to validate the model. First, test EP4 was used to find the dynamic parameters of material properties of heat affected zones. This test had an 8mm thick end-plate connection. Figure 5-27 (a) shows the applied load time history of this experiment with the maximum load of 70 kN around 45ms. Following successful validation in this instance, the model was checked against all other experimental data. Next two dynamic tests (EP6 and EP11) with 8 and 10mm thick end-plates respectively were modelled. Figure 5-27 (b) is the test EP6 force time history which reached a maximum 90kN in 50ms and (c) is the test EP11 load time history which reached 120kN in 40ms.



(a)



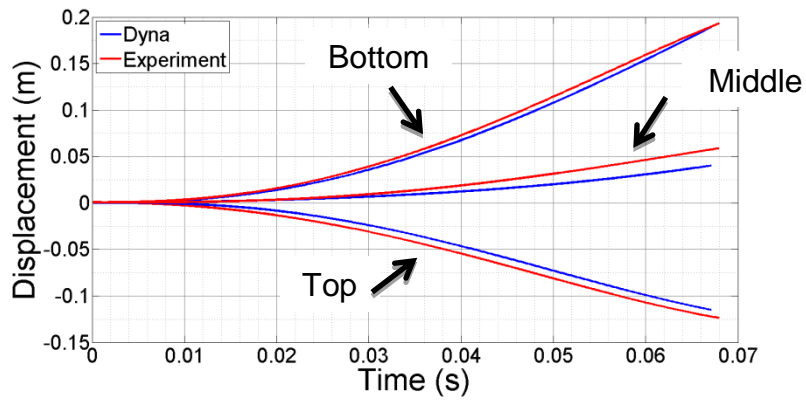
(b)



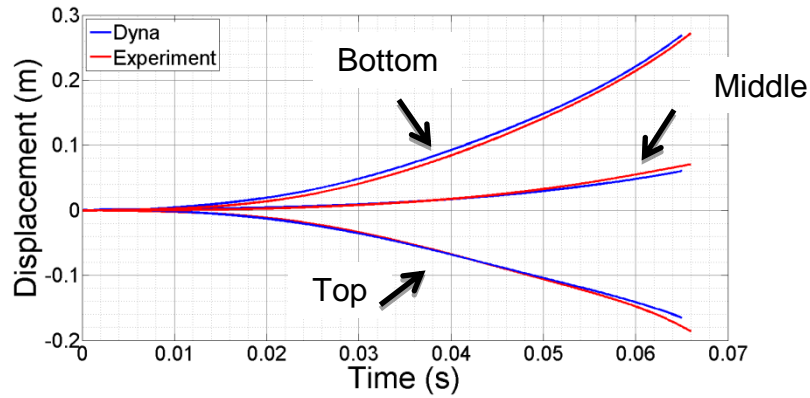
(c)

Figure 5-27 Applied force time history (a) Test EP4 (b) Test EP6 (c) Test EP11

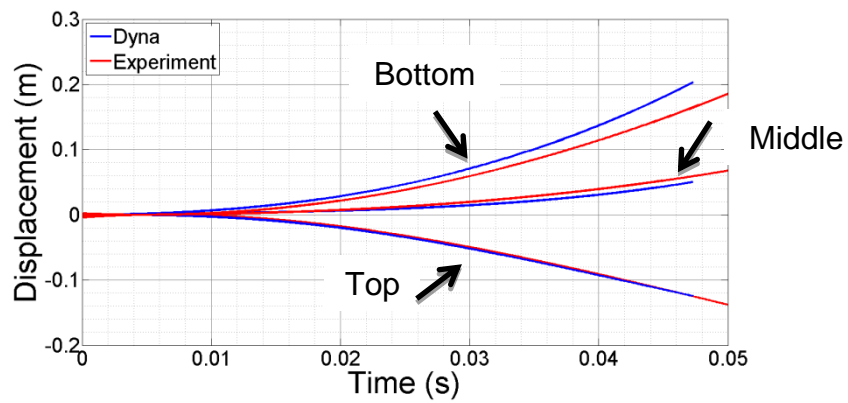
The same method was used to measure the displacement of the column in the end-plate analysis as was used for the web-cleats (Section 5.3.1). Figure 5-28 shows the displacement-time history of three points measured by the laser gauge for EP4, EP6 and EP11 in the experimental tests, and from the corresponding points in the numerical analysis.



(a)



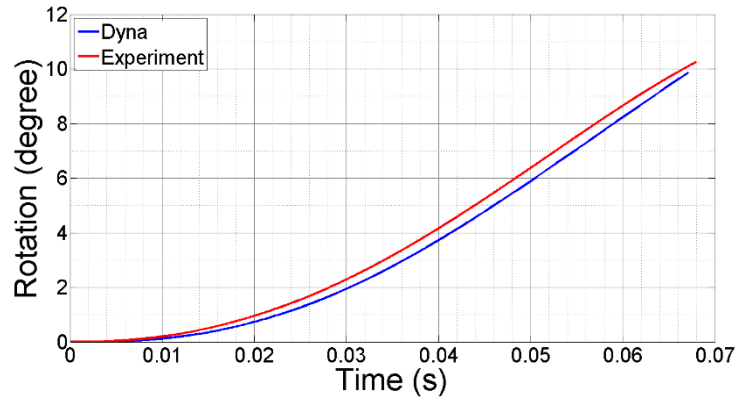
(b)



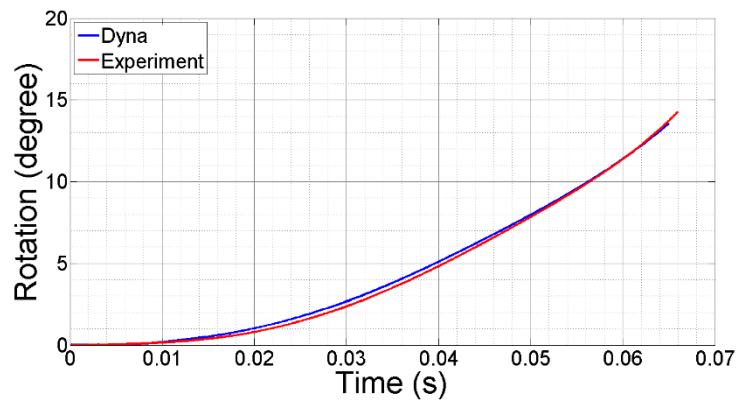
(c)

Figure 5-28 Displacement time history (a) Test EP4 (b) Test EP6 (c) Test EP11

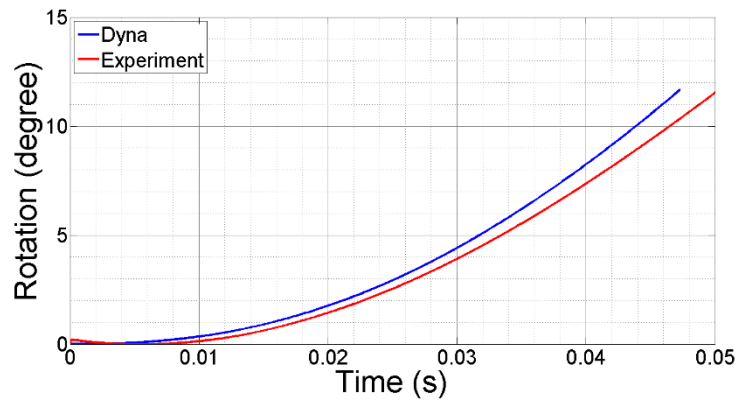
Figure 5-29 shows the rotation of the column against time. As 8mm thick end-plate experiments (EP1 and EP4) were used for calibration of the model, comparison between experiments and numerical modelling showed excellent correlation for test EP4 and EP6 which also had 8mm thick plate, however there was a small difference in EP11 which has 10mm thick endplates.



(a)



(b)

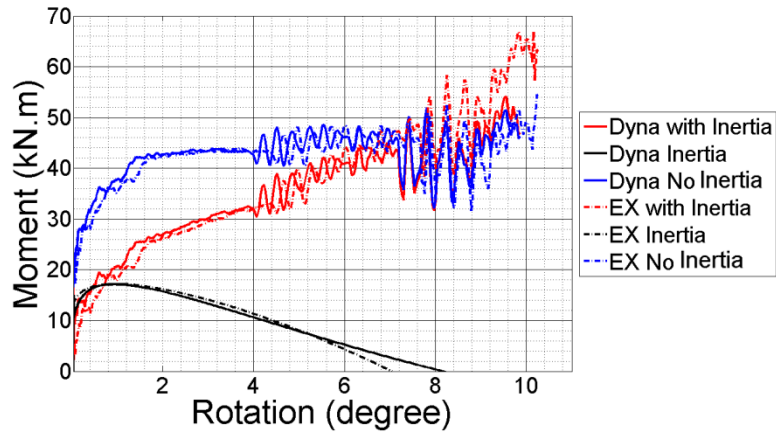


(c)

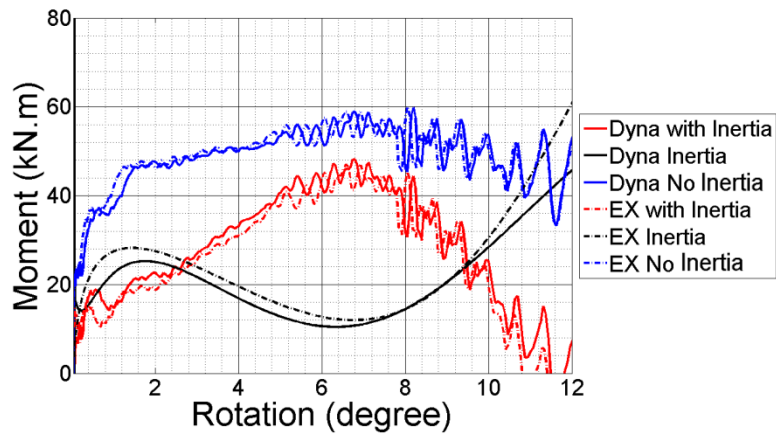
Figure 5-29 Rotation time history (a) Test EP4 (b) Test EP6 (c) Test EP11

Moment resistance of the connection was calculated using the formula described in Section 3.2.3. Figure 5-30 shows moment rotation diagrams for both experiment and

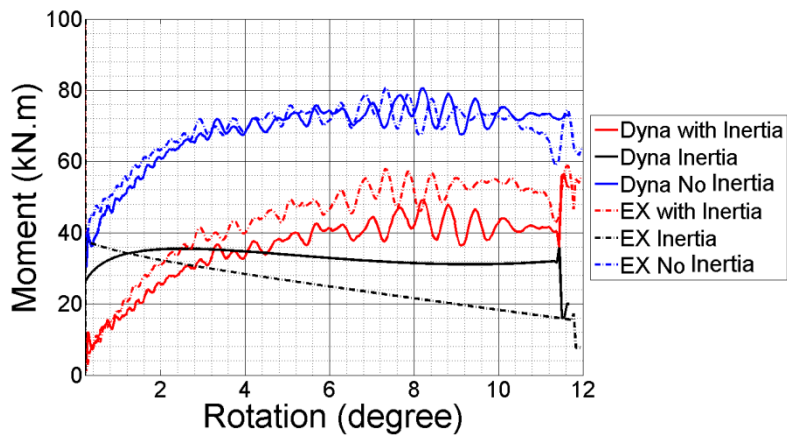
LS\_DYNA model of EP4, EP6 and EP11. There is an excellent correlation between experiment and numerical analysis results for both 8 and 10mm thick end-plates.



(a)



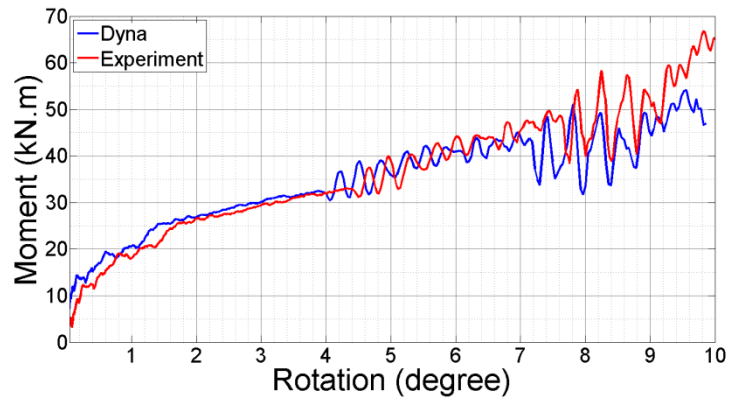
(b)



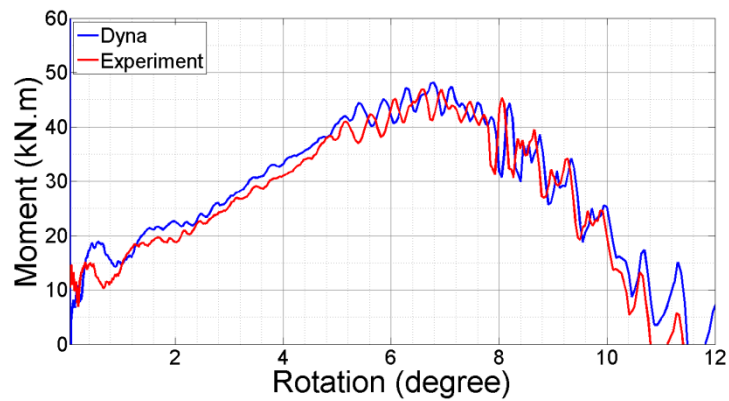
(c)

Figure 5-30 Moment rotation (a) Test EP4 (b) Test EP6 (c) Test EP11

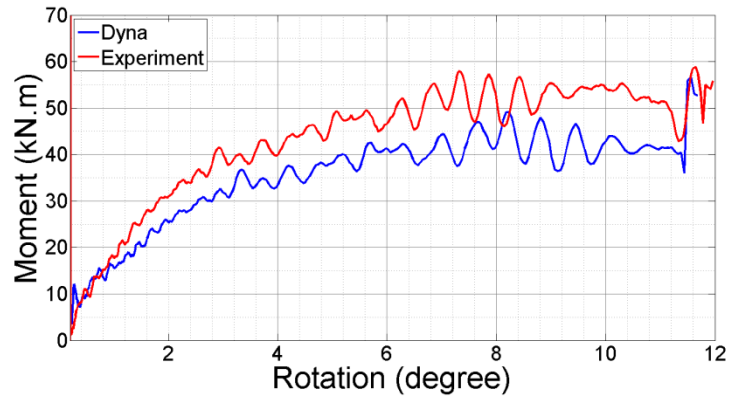
Figure 5-31 shows the total moment resisted by the connection, there was a close correlation between the results for the 8mm thick end-plate, however there was a small difference with 10mm thick plate. The maximum moment resistance was around 45kNm for the 8mm thick end-plate, and around 50kNm for the 10mm thick plate, and the thicker plate reached the maximum moment with less column rotation.



(a)



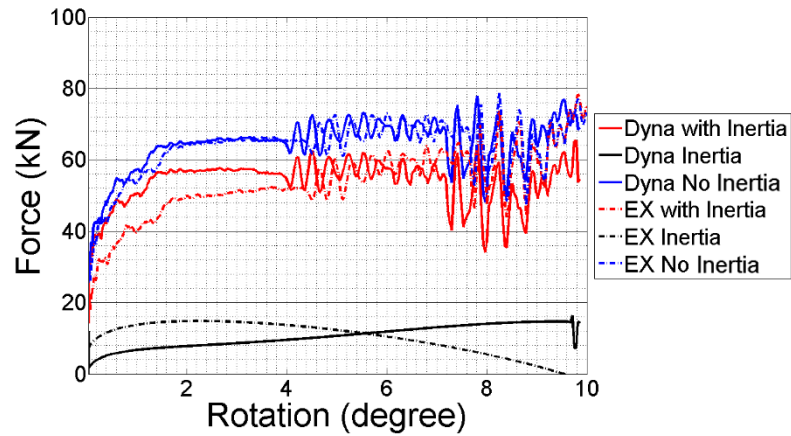
(b)



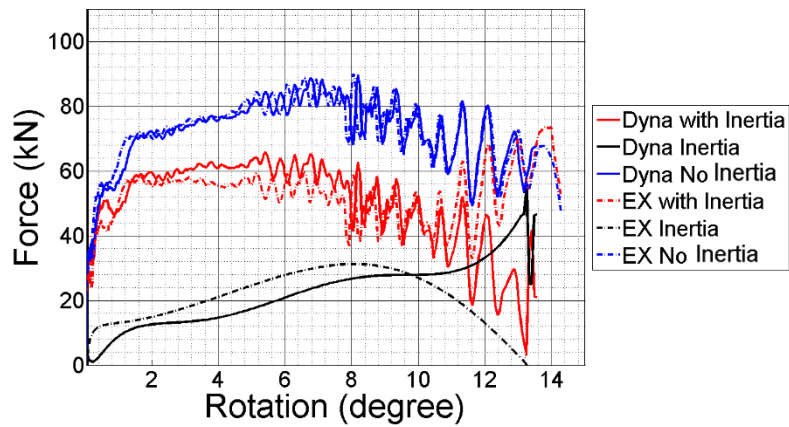
(c)

Figure 5-31 Moment rotation (a) Test EP4 (b) Test EP6 (c) Test EP11

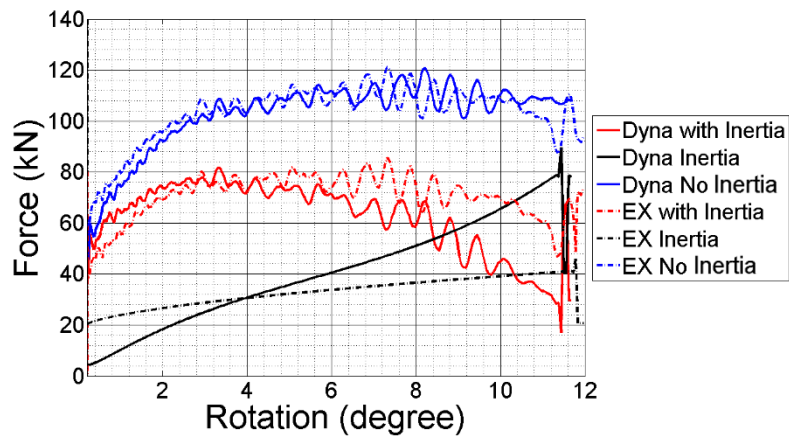
The same method was used to calculate the force resistance of the connection (Section 3.2.3). Figure 5-32 shows force-rotation diagrams for all the arrangements (EP4, EP6 and EP11). The results show excellent correlation between experiments and the LS-DYNA connection model.



(a)



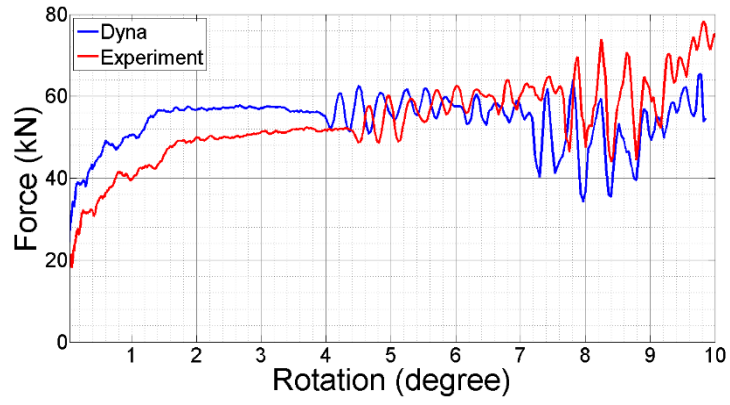
(b)



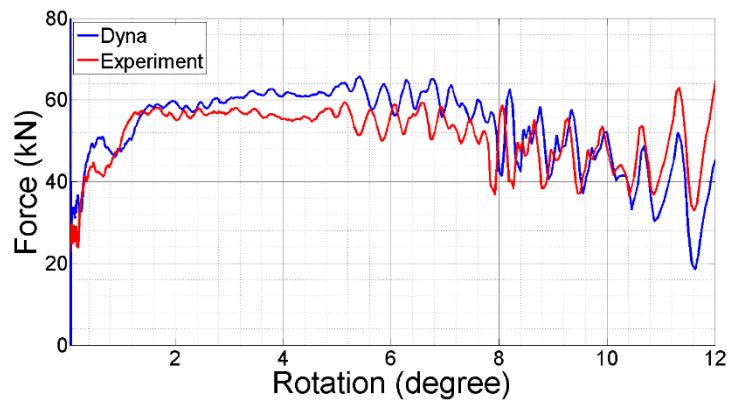
(c)

Figure 5-32 Force rotation (a) Test EP4 (b) Test EP6 (c) Test EP11

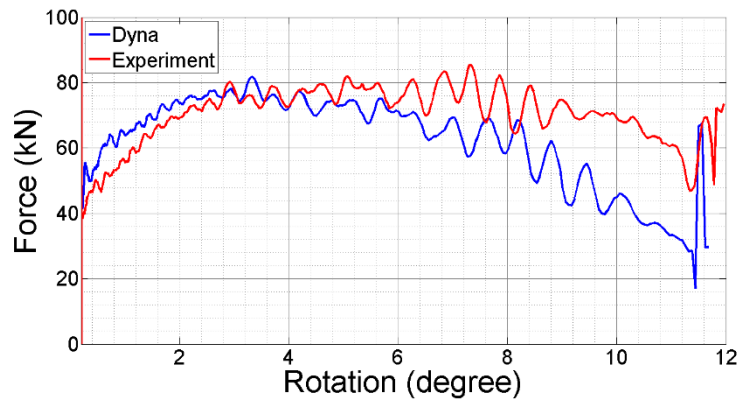
Figure 5-33 provides the total force resistance of the connection vs rotation and shows that the connection reached its maximum resistance with less rotation when the plate was thicker. The force resisted in the 8mm thick end-plate connection was around 60kN and 80kN for the 10mm thick end-plate connection.



(a)



(b)



(c)

Figure 5-33 Force rotation (a) Test EP4 (b) Test EP6 (c) Test EP11

### 5.4.3 Qualitative validation against dynamic tests 4 and 11

Comparing the connection's deformation between experiments and numerical modelling was also important in the validation process. Figure 5-34 shows the final stage of the end-plate and the beam web after connection failure in test EP6. Figure 5-35 shows how the end-plate was deformed after the failure in the same test. The correlation between experiment and the model was excellent.

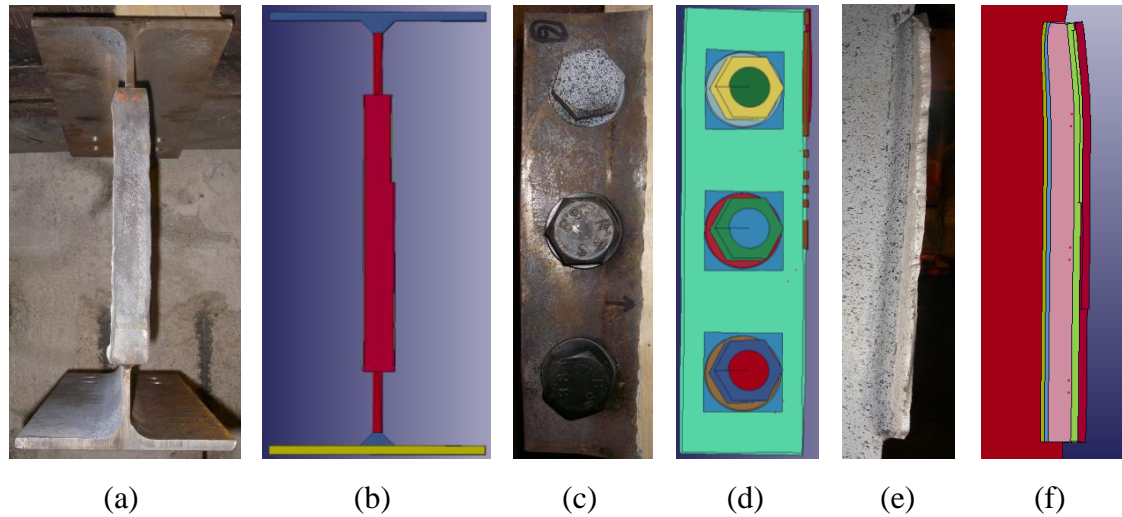


Figure 5-34 Deformed shape of plate and beam web in test EP6 after the failure (a) Exp. beam web front view (b) Model beam web front view (c) Exp. End-plate (d) Model end-plate (e) Exp. Beam web (f) Model beam web

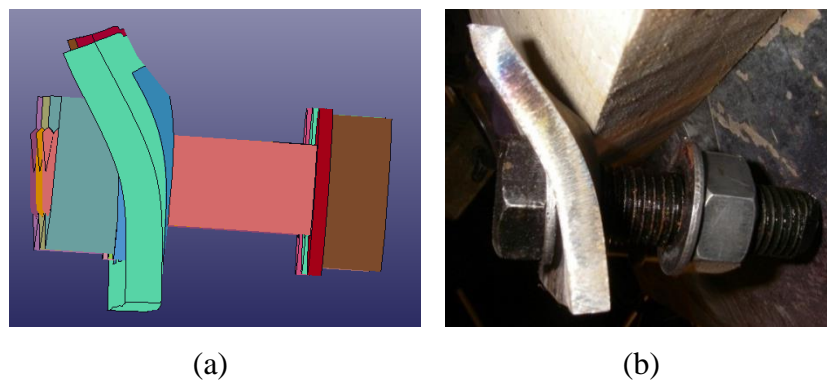


Figure 5-35 End- plate deformation after the failure in test EP6 (a) Model (b) Experiment

Figure 5-36 and Figure 5-37 present images from the high speed video and the model for tests EP6 and EP11. Model and experiment had a good correlation this present the

possibility to study the effect of the connection failure caused by crack opening in the end-plate. This is discussed more in detail in Chapter 8.

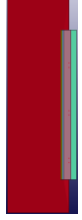
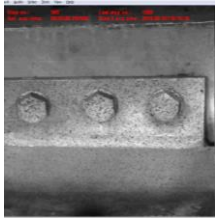
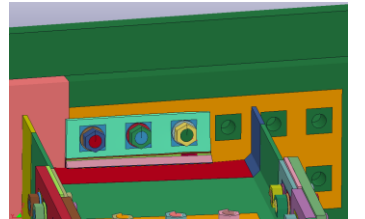
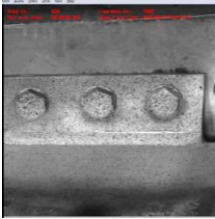
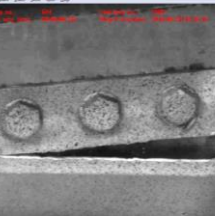
Time (ms)	Rotation (degree)	Experiment	Model	Model (beam web and plate)
0 (model)	0 (a)			
0 (exp)				
41.5 (model)	5.6 (b)			
42.7 (exp)				
44 (model)	6.5 (c)			
45.2 (exp)				
49 (model)	7.9 (d)			
50 (exp)				
70 (model)	N/A (e)			
70 (exp)				

Figure 5-36 Test EP6 deformation of connection at key points.

(a) Pre-test (b) Beam flange strikes column (c) First element failed in model (d) End plate crack went through (e) End plate cracked completely.

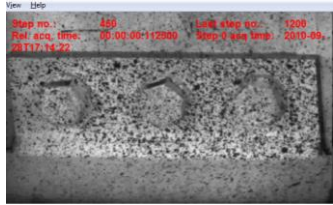
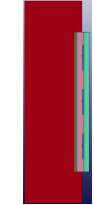
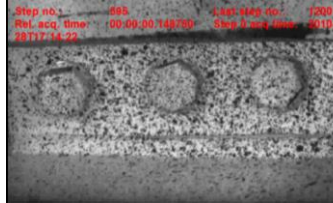
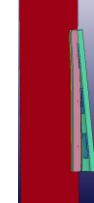
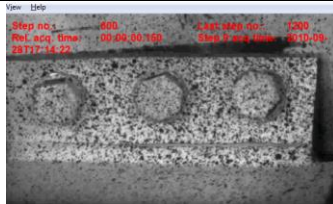
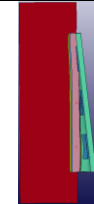
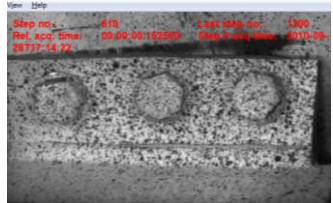
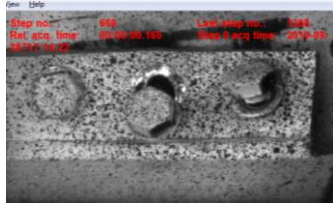
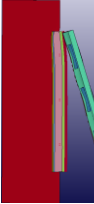
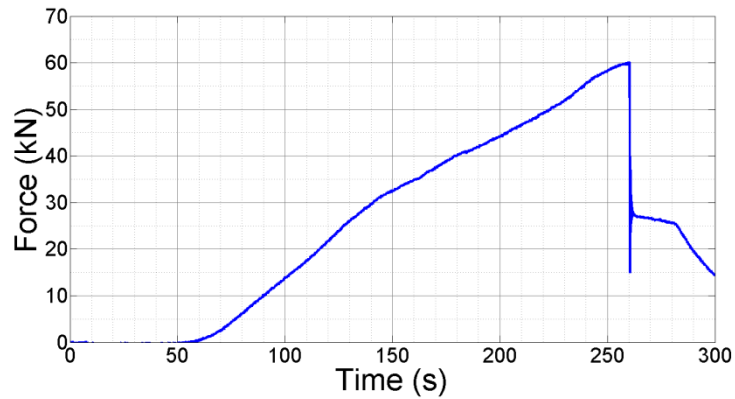
Time (ms)	Rotation (degree)	Experiment	Model	Model (beam web and plate)
0 (model)	0 (a)			
0 (exp)				
33 (model)	5.6 (b)			
36 (exp)				
35 (model)	6.2 (c)			
38.0 (exp)				
38.5 (model)	7.6 (d)			
41.5 (exp)				
55 (model)	?? (e)			
55 (exp)				

Figure 5-37 Test EP11 deformation of connection at key points.

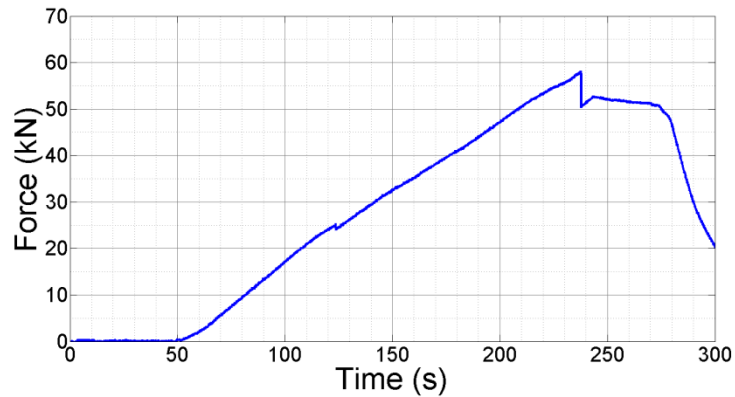
(a) Pre-test (b) Beam flange strikes column (c) First element failed in model (d) End plate crack went through (e) End plate cracked completely.

#### 5.4.4 Quantitative validation against static tests 1, 5 and 15

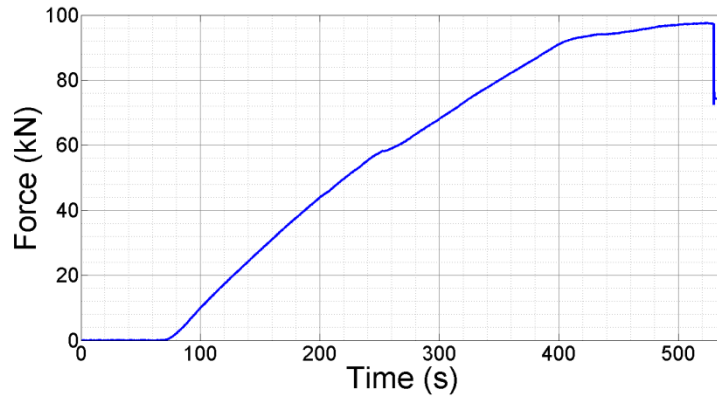
The end-plate connection model was validated against three different tests, experiment EP1 and EP5 both had 8mm thick plate and EP15 had a 10mm thick plate. The applied force time histories of these tests are provided in Figure 5-38. The maximum force for EP1 and 5 was about 60kN and 100kN for EP15.



(a)



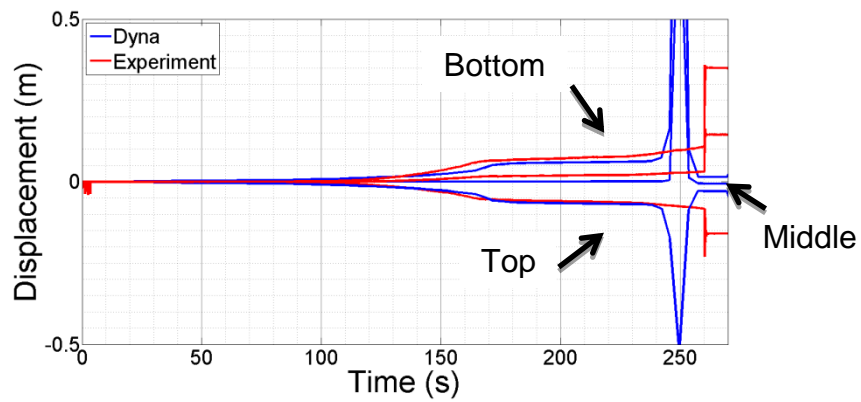
(b)



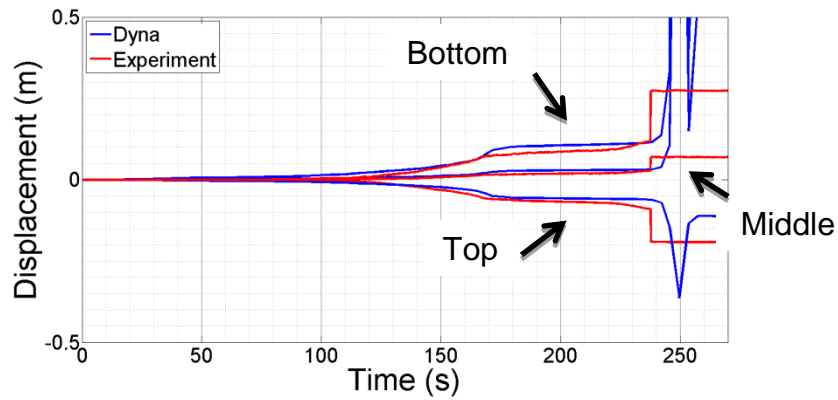
(c)

Figure 5-38 Applied force time history (a) Test EP1 (b) Test EP5 (C) Test EP15

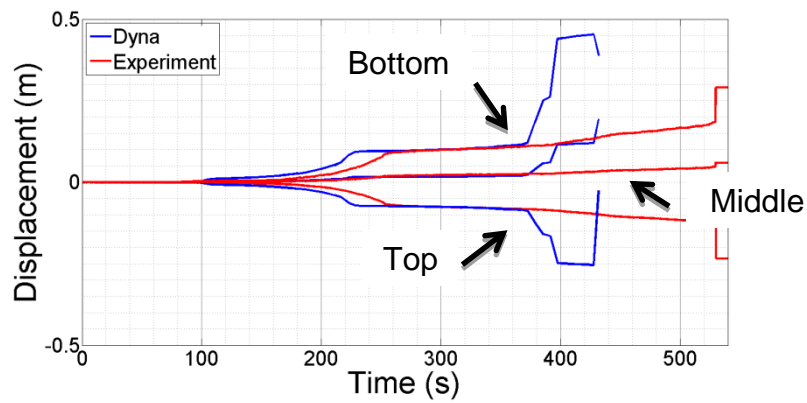
Same method of measurement was used in the experiment and the model, and column displacements are provided in Figure 5-39. There was a good correlation for the 8mm thick end-plate connections but there was a difference in the 10mm thick plate connection results. As explained before, the material model for this connection was based on EP1 which had an 8mm thick test and caused this difference in 10mm thick end-plate model.



(a)



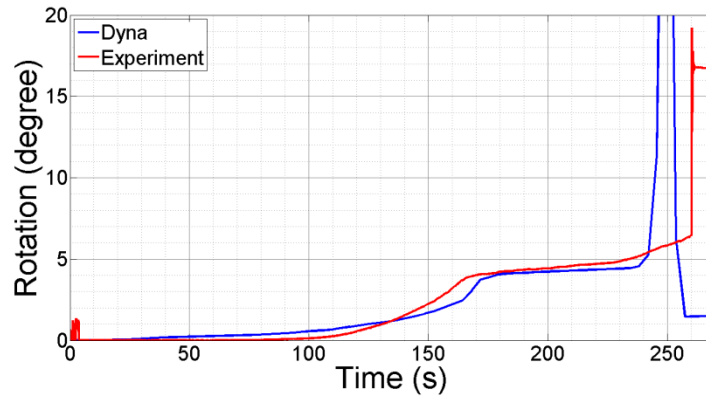
(b)



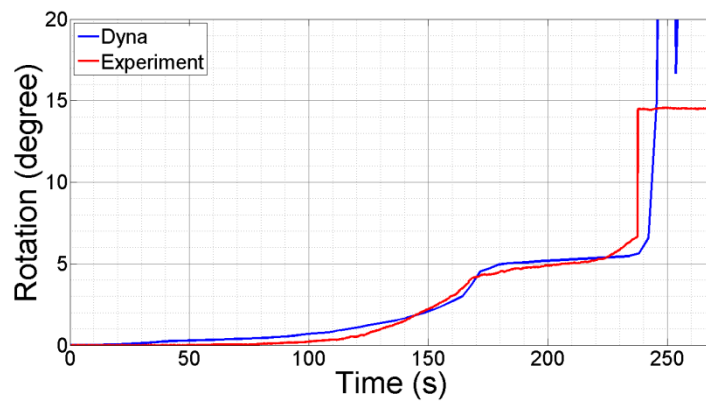
(c)

Figure 5-39 Displacement time history (a) Test EP1 (b) Test EP5 (C) Test EP15

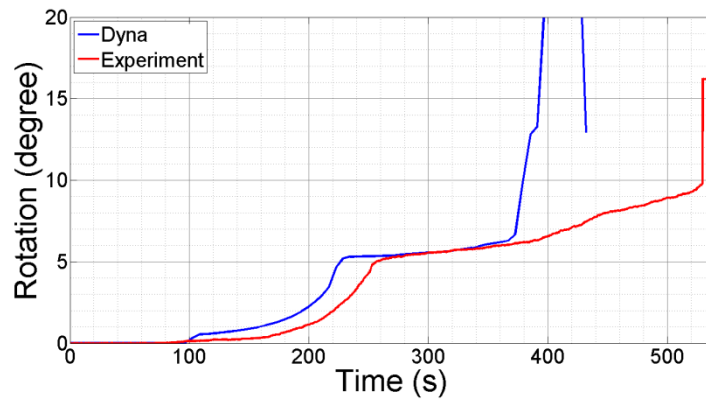
Results for column rotation vs time are presented in Figure 5-40. The connection began to fail at around 380s in the numerical model and 520s in the experiment. However, the force applied to the connection increased by only a small amount between these two times. Excellent correlation between the model and experiments was found for the 8mm thick end-plate.



(a)



(b)

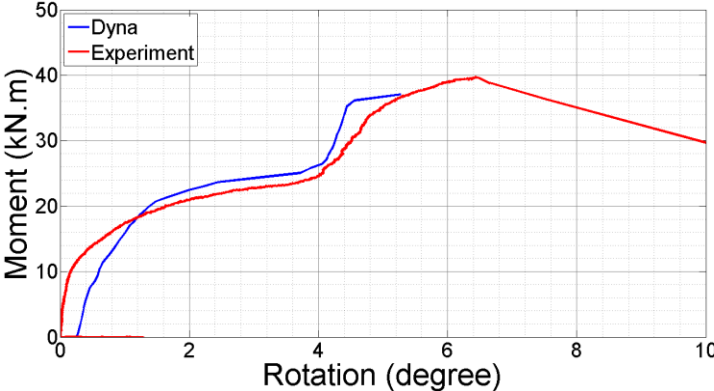


(c)

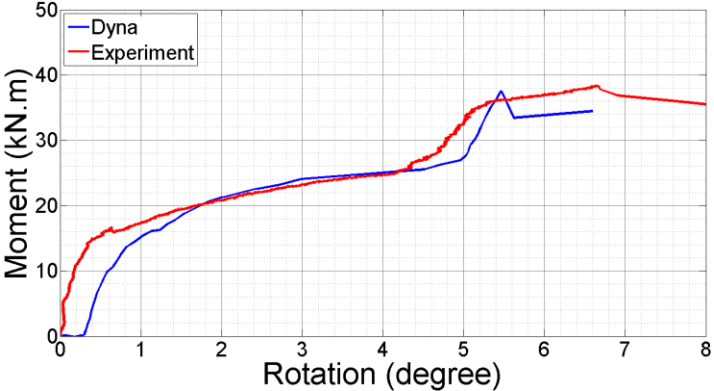
Figure 5-40 Rotation time history (a) Test EP1 (b) Test EP5 (c) Test EP15

Moment resistance of the connection had an excellent correlation between the model and experiment. Figure 5-41 provides the moment resistance against column rotation for all three tests (EP1, EP5 and EP15). The shift in time of failure (see curve (c)) did not change

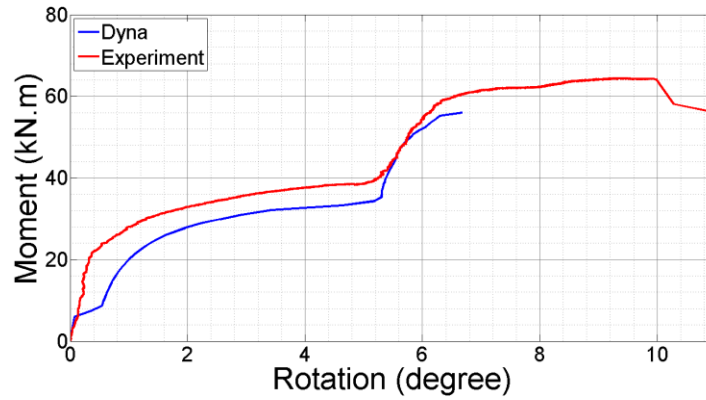
the resistance of the connection for the 10mm thick end-plate as the applied force changed little after 380s. After failure the column picked up acceleration in the experiments. However, as the failure was gradual in the model the drop did not happen as in the experiments and the curve has been discontinued after the failure point. The rotation time history shows the time of failure for both experiments and models.



(a)



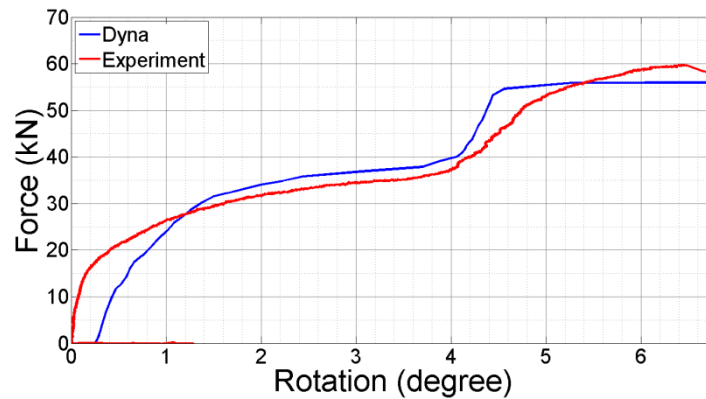
(b)



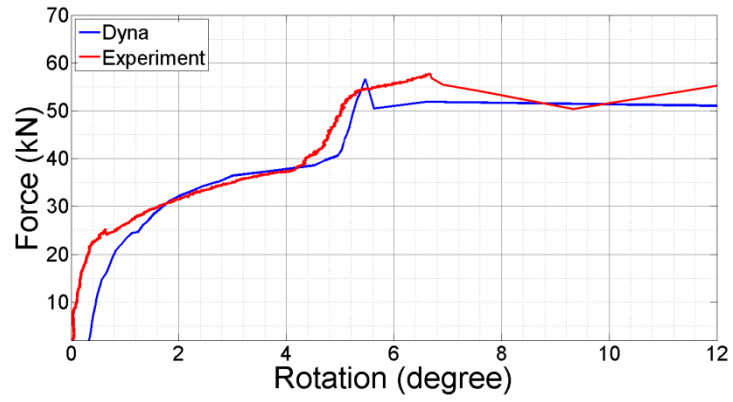
(c)

Figure 5-41 Moment rotation (a) Test EP1 (b) Test EP5 (C) Test EP15

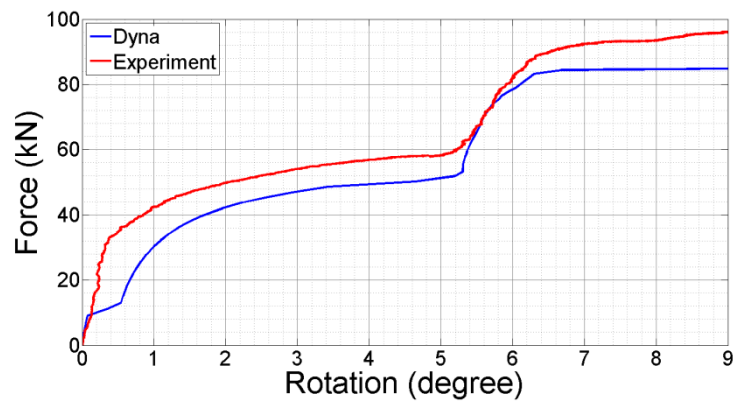
Figure 5-41 provides the results of force resisted plotted against rotation of the connection for both experiments and the numerical model. Again, good correlation can be seen. The shift in failure time of the connection for the 10mm thick end-plate is not evident in the force resistance-rotation plot as the change in load over time varied little after 380s.



(a)



(b)



(c)

Figure 5-42 Force rotation (a) Test EP1 (b) Test EP5 (C) Test EP15

#### 5.4.5 Qualitative validation against static tests 1, 5 and 15

There was a good correlation of connection deformation between the numerical model and the experiment for the static tests, as was the case for the dynamic tests. Figure 5-43 to Figure 5-45 show the good correlation of the end-plate deformation after connection failure in both test EP5 and the numerical model.

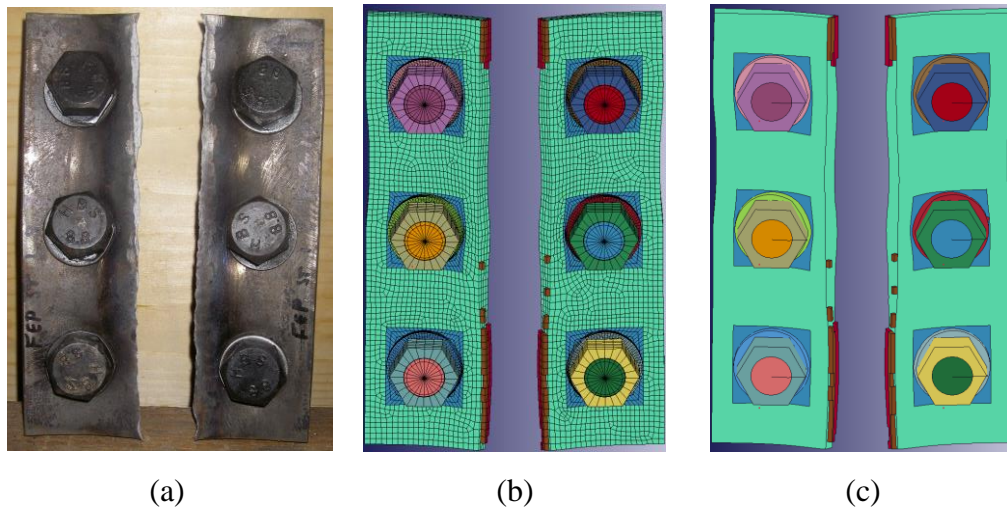


Figure 5-43 Test EP5 End plate deformation (a) Experiment (b) Meshed model (c) Unmeshed model

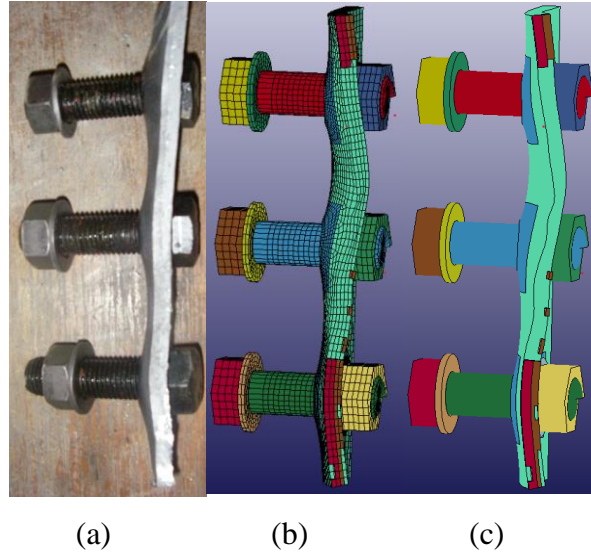


Figure 5-44 Test 5 End plate deformation side view (a) Experiment (b) Meshed model (c) Unmeshed model

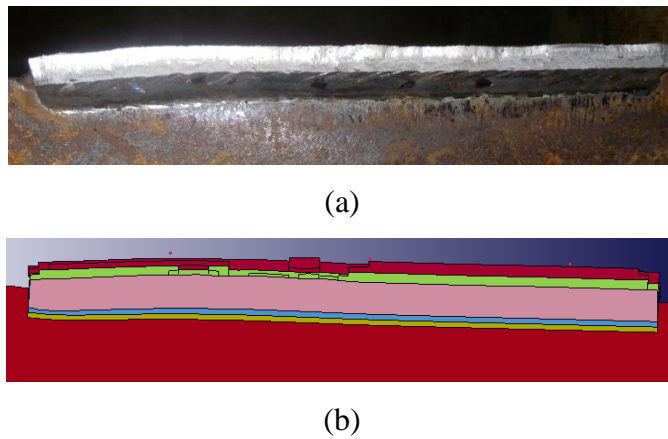


Figure 5-45 Test EP5 welding deformation (a) Experiment (b) Finite element model

A qualitative comparison between the numerical model and experiment is provided in Figure 5-46 and Figure 5-47 for both EP1 and EP15. These figures describe how the connection failed at different stages of time and column rotation. They also give details of when the cracked opened in the end-plate. There were differences in time and rotation for EP15, as explained in Section 5.4.4.

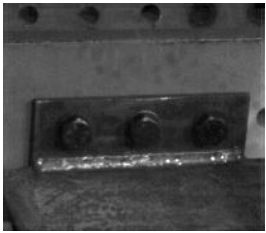
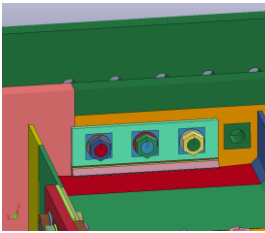
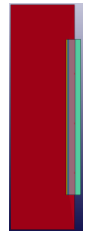
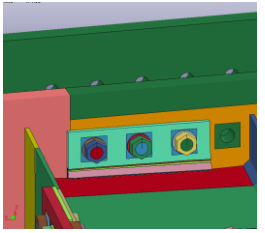
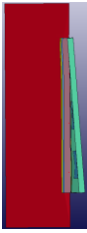
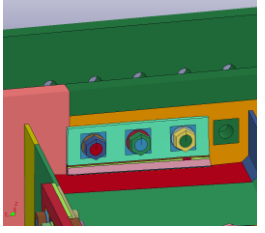
Time (s)	Rotation (degree)	Experiment	Model	Model (Beam web, End-plate)
0 (model)	0 (a)			
0 (exp)				
171 (model)	3.6			
163 (exp)	3.8			
176 (model)	3.9 (c)			
173 (exp)				
238 (model)	4.5 (d)			
210 (exp)				
241 (model)	6			
264 (exp)	6.3			

Figure 5-46 Test EP1 deformation of connection at key points.

(a) Pre-test (b) Beam flange strikes column (c) First element failed in model (d) End plate crack went through (e) End plate cracked completely.

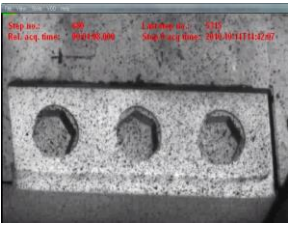
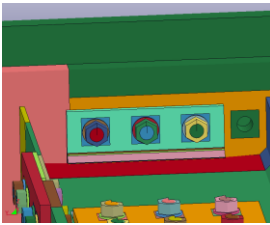
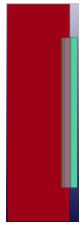
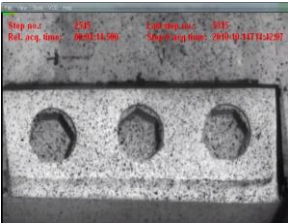
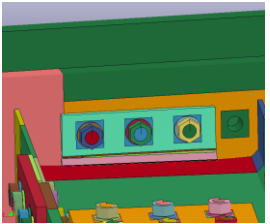
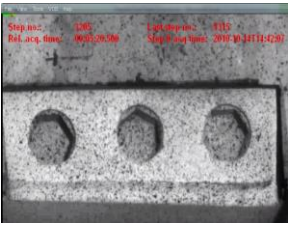
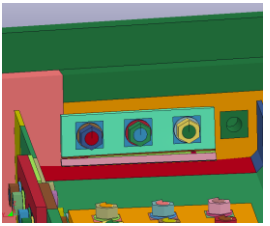
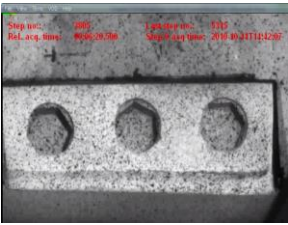
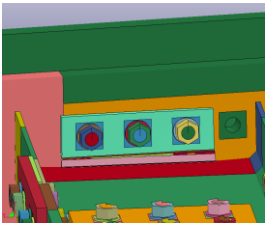
Time (s)	Rotation (degree)	Experiment	Model	Model (Beam web, End-plate)
0 (model)	0 (a)			
0 (exp)				
229 (model)	5.3			
186 (exp)	4.9			
307 (model)	5.8 (c)			
261 (exp)				
366 (model)	6.1 (d)			
302 (exp)				
409 (model)	6.5			
463 (exp)	9.8			

Figure 5-47 Test EP15 deformation of connection at key points.

(a) Pre-test (b) Beam flange strikes column (c) First element failed in model (d) End plate crack went through (e) End plate cracked completely.

#### 5.4.6 Simplified model of End-plate connection

As the beam stub and splice had an insignificant influence on the behaviour of the connection, they were removed from the model which reduced the run time significantly. This simplified model was used in the parametric studies and required a running time of approximately 10 hours (Chapter 6). This simplified model is shown in Figure 5-48.

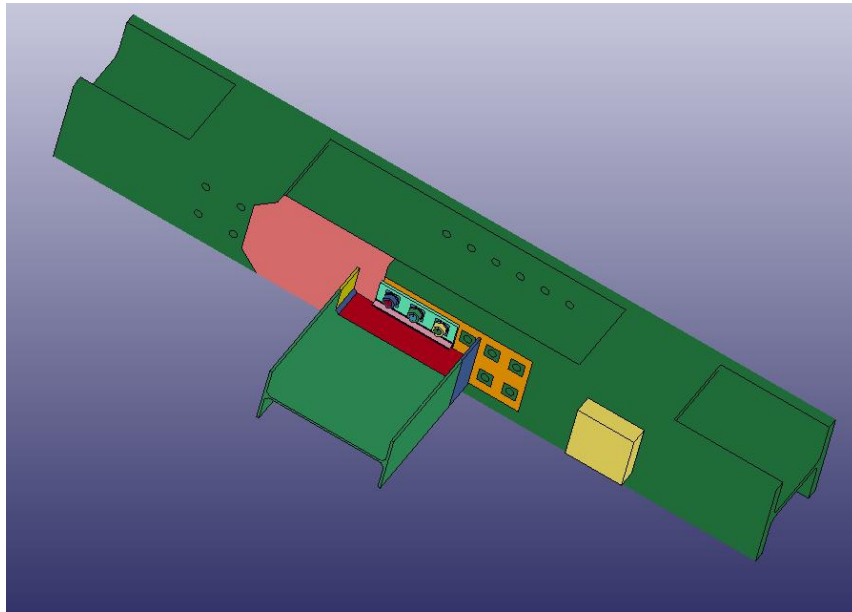


Figure 5-48 Simplified model after removing the splice

### 5.5 Conclusion

This chapter has described the validation process of numerical models of end-plate and web-cleat connections. Developing a validated model was a main aim of this research and demonstrated that it is possible to model this very complex behaviour with reasonable accuracy. These validated models have been used to conduct detailed parametric studies of the connection behaviour under different loading rates, types and connection geometries the results of which are presented in Chapters 6 and 7.

## 6 Parametric study of Web-cleat connection behaviour

After validating the models with experimental results, the next stage involved parametric studies of loading rates and connection geometry. A key objective of this thesis was to investigate how connections respond to fast dynamic loadings and to determine their behaviour at different loading rates. One benefit of the developed model was the ability to run *both* implicit and explicit analyses which gave the opportunity to study the connection behaviour under a range of loading rates from quasi-static (1 kN/s applied load) up to impact or fast dynamic (7000 kN/s was the fastest loading rate applied in this study). The reason for using two solvers came from the limitation inherent in running a quasi-static analysis with an explicit solver i.e. the typical time-step in explicit analysis was around  $1.5E-07$  s which means that many thousands of hours of CPU time would be required for explicit analyses of models with hundreds of seconds of run time.

Analysis time is a crucial aspect in parametric studies and for this reason the spliced support beam was removed as discussed in Section 5.3.6. This reduced the run time by approximately 50%, with no significant effect on the results. To run each analysis a PC with four 3.6 GHz CPUs and a total of 24 GB memory was used; running time was typically 12 hours for 100ms of analysis and around 6 days for 1s of dynamic analysis with the explicit solver. Using the same PC for the quasi-static analysis, model times of up to 350s took around 12 hours with the implicit solver. In total 280 different analyses were conducted on the web-cleat connection model with different types of loading, loading rates and different dimensions; results are presented in this chapter.

Four different loading types were used as shown in Figure 6-1; (a) shows the original loading used in the experiment which was applied to one end of the column and generated a combination of translation and rotation in the connection, (b) shows the connection in pure tension as two equal forces applied to both ends of the column with the same direction away from the connection, (c) shows the connection in pure moment as two equal forces applied to both ends of the column with opposite directions, (d) is a loading type where two forces were applied to both ends of column with the top force half the magnitude of the bottom one with same directions away from connection; this generates

a combination of rotation and translation in the connection that is somewhere between cases (a) and (c).

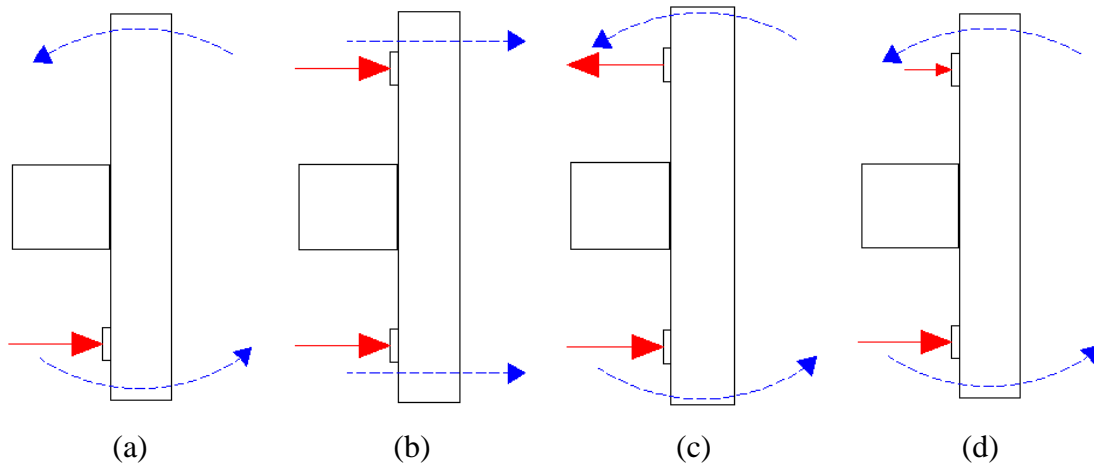


Figure 6-1 Different types of loading, red arrows are the forces and blue lines shows the direction of the column displacement (a) Type1, one applied force (b) Type 2, two applied forces equal in same direction (c) Type 3, two equal forces but opposite in direction (d) Type 4, two applied forces in the same direction but one force half the magnitude of the other

Loads applied to the model varied linearly with time starting from zero. Based on the loading rate and analysis time it reached a maximum e.g. if the rate of load was 5000kN/s (denoted “5000”) and running time was 100ms, the maximum load would be 500 kN. Figure 6-2 shows an example of loading rates applied to the connection in loading type1.

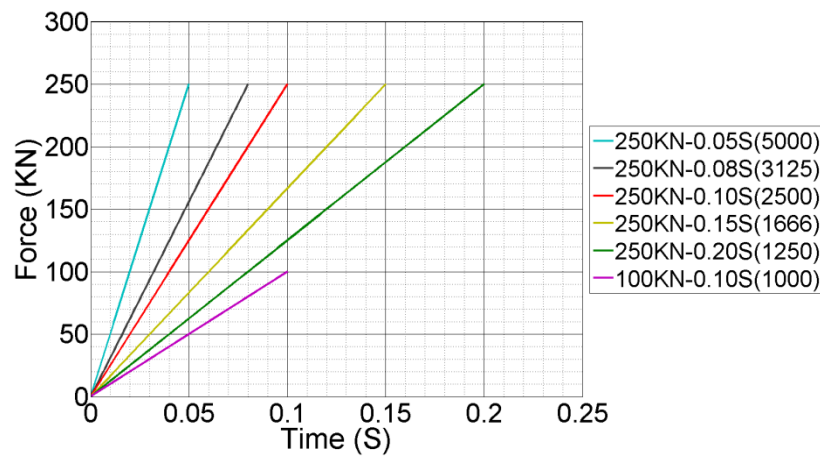


Figure 6-2 Example of different loading rates

The geometry of the web-cleat connections was varied by changing the angle leg thickness, bolt and washer sizes, end distances, pitch and gauge. Also different loading types and rates were applied to the connection. A summary of the final results is provided at the end of this chapter and a brief overview in the following text:

- Different loading types changed the axial force and moment resistance of the structure as by applying moment the axial force resisted in the connection dropped dramatically.
- Thinner angle legs resulted in more ductility to the whole connection; however the resistance remained more or less similar for all thicknesses.
- Using similar size but stronger bolts made the connection less ductile by a very small amount.
- Replacing the size 20 washers with size 24 changed the behaviour but was insignificant in overall ductility or resistance.
- Increasing the bolt diameter reduced the connection ductility.
- Changing the bolt gauge changed the force and moment resistance of the connection minimally; a larger bolt gauge increased the overall connection ductility and vice versa.
- Having different bolt pitches changed the ductility, however the changes in force and moment resistance were small.

## **6.1 Influence of different loading types and rates**

The main objective of this research was to study the effect of different rates of loadings on connection response. A series of parametric studies was conducted on the connection with different loading rates, varying the applied load from quasi-static (1 kN/s) up to fast dynamic (7000 kN/s).

A second objective was to study the response of the connections with different ratios of applied axial force and moment. Four different applied loading types were used as described in Figure 6-1.

### **6.1.1 Column displacement in time**

A simple way to gain a qualitative understanding of the effect of loading rate is to consider the displacement of each end of the flying column, as shown in Figure 6-3 for loading type 1 and with 10mm thick angles. The units for the rates of loading shown in the legend is kN/s e.g. 5000 is denotes 5000kN/s resulting in a peak load of 250 kN applied to the connection at 50ms.

There is a clear qualitative change in the connection response at a loading rate of around 500-1000kN/s. At lower rates, there are two pauses in the movement of the column as, firstly, the bolts bear against the bolt holes and start to provide initial moment resistance, and a little later as the column and beam flanges make contact and some prying effect commences. These two effects manifest themselves as brief plateaus on the displacement-time curves. At faster rates, these momentary plateaus are not seen, as the momentum of the beam-column rotation drives through this resistance.

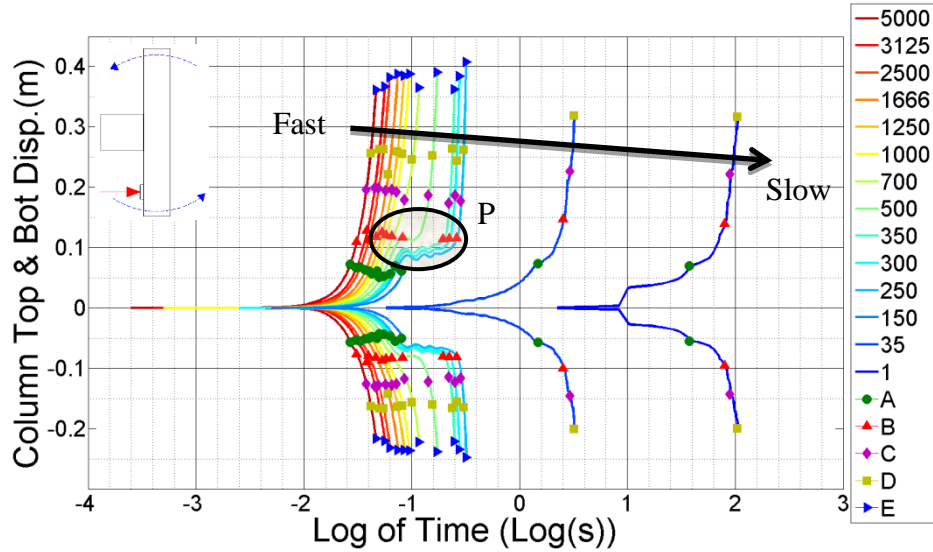


Figure 6-3 Column displacement time history LT1 10mm angle  
 (Coloured dots indicate the points at which: A- the beam and column flanges made contact and prying action commenced, B- 1<sup>st</sup> element in the model was eroded in vicinity of 1<sup>st</sup> bolt, C- Beam web totally failed in vicinity of 1<sup>st</sup> bolt, D- Beam web totally failed in vicinity of 2<sup>nd</sup> bolt, E- Beam web totally failed in vicinity of 3<sup>rd</sup> bolt)

With applied loading in pure tension (LT2), all bolts failed at approximately the same time, as expected (Figure 6-4). There was a small rotation in the column due to accumulated numerical round-off errors, which led to a slight but insignificant rotation as shown by the difference in displacement of both ends of the column.

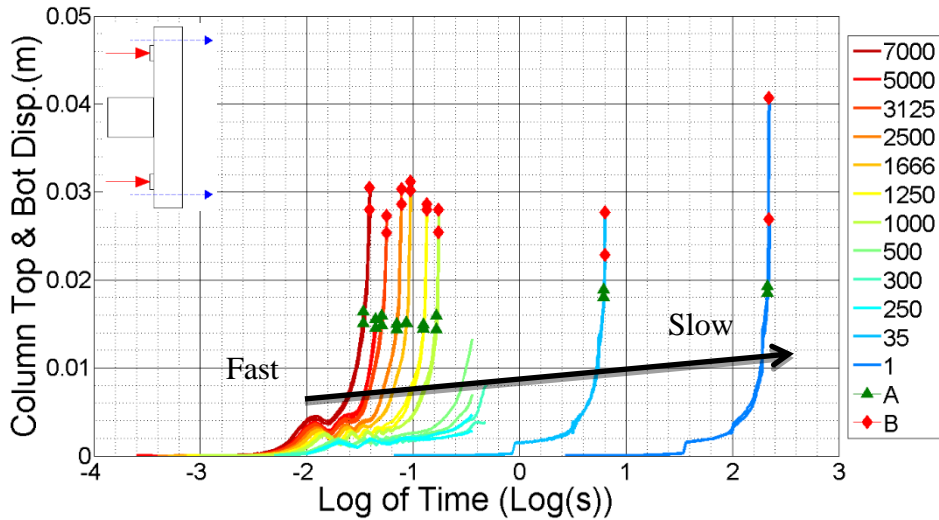


Figure 6-4 Column displacement time history LT2 10mm angle  
 (Coloured dots indicate the points at which: A- 1<sup>st</sup> element in the model was eroded in vicinity of 1<sup>st</sup> bolt, B- Beam web totally failed in vicinity of all bolts)

Figure 6-5 shows the displacement time history of the column when pure moment (LT3) was applied to the connection, whilst Figure 6-6 shows the effect of LT4, with a moment-to-axial force between those of LT1 and LT3. Again, the plateau due to prying action is clear at lower rates of loading, but not distinct at higher rates.

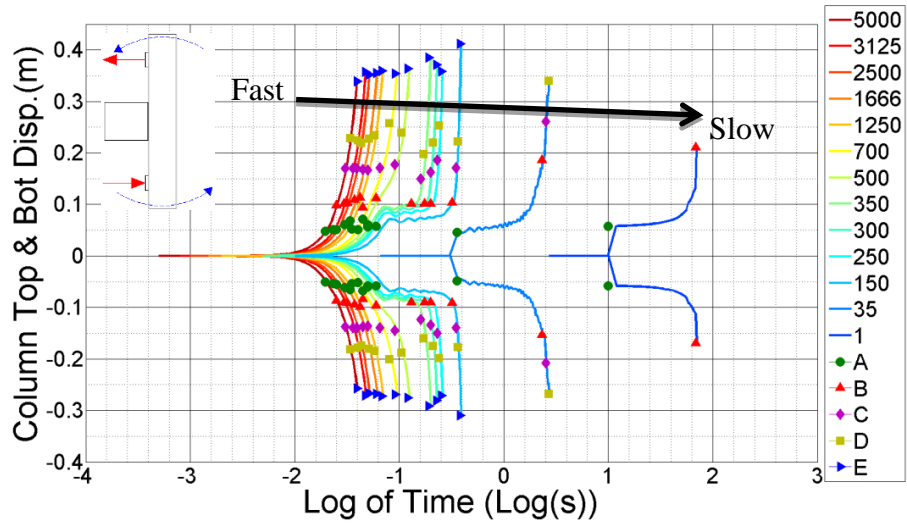


Figure 6-5 Column displacement time history LT3 10mm angle  
 (Coloured dots indicate the points at which: A- the beam and column flanges made contact and prying action commenced, B- 1<sup>st</sup> element in the model was eroded in vicinity of 1<sup>st</sup> bolt, C- Beam web totally failed in vicinity of 1<sup>st</sup> bolt, D- Beam web totally failed in vicinity of 2<sup>nd</sup> bolt, E- Beam web totally failed in vicinity of 3<sup>rd</sup> bolt)

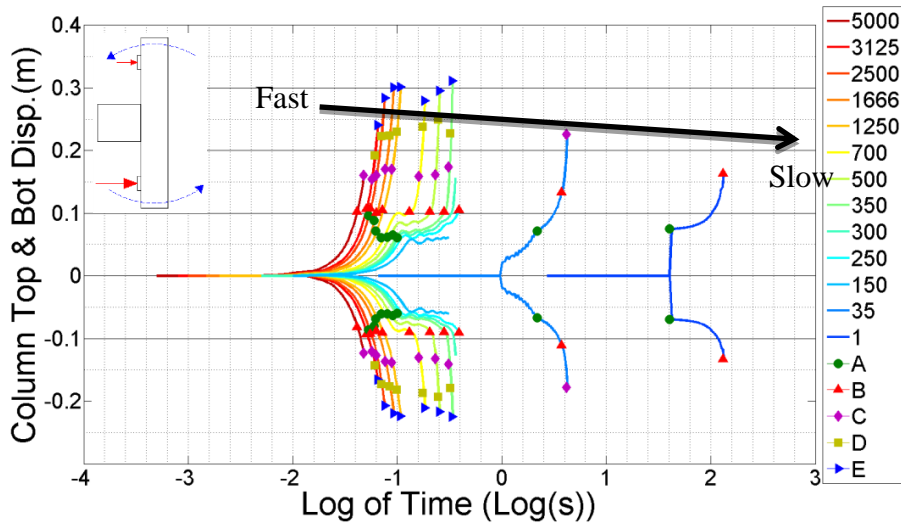


Figure 6-6 Column displacement time history LT4 10mm angle  
 (Coloured dots indicate the points at which: A- the beam and column flanges made contact and prying action commenced, B- 1<sup>st</sup> element in the model was eroded in vicinity of 1<sup>st</sup> bolt, C- Beam web totally failed in vicinity of 1<sup>st</sup> bolt, D- Beam web totally failed in vicinity of 2<sup>nd</sup> bolt, E- Beam web totally failed in vicinity of 3<sup>rd</sup> bolt)

### 6.1.2 Column response due to connection reaction

The way the flying column moved was dependent on the applied force and also how the connection resisted that force. Plotting the column rotation against its translation reveals the effect of the connection. Figure 6-7 shows the results of column rotation against column translation caused by different loading types and loading rates. In the case of pure tension (LT2) loading the column did not rotate, however in other cases combinations of rotation and translation were observed. Loading type four showed that loading rates changed the connection behaviour, as the load was applied slowly the behaviour was more similar to the pure moment (LT3) loading and as the rate of loading increased it became more like the pure tension case as the column momentum made the column translate faster and more than the lower loading rate and avoided the impact between the beam and the column flange which resulted in less prying in the angles. Three loading types (LT1, LT2, and LT3) showed no significant rate effect (drawn by straight lines in the figure) but loading type 4 had a load rate effect as shown by the dotted lines. The shaded area in Figure 6-7 gives the combination of rotations and translation for the connection is still resisting load and has not failed totally.

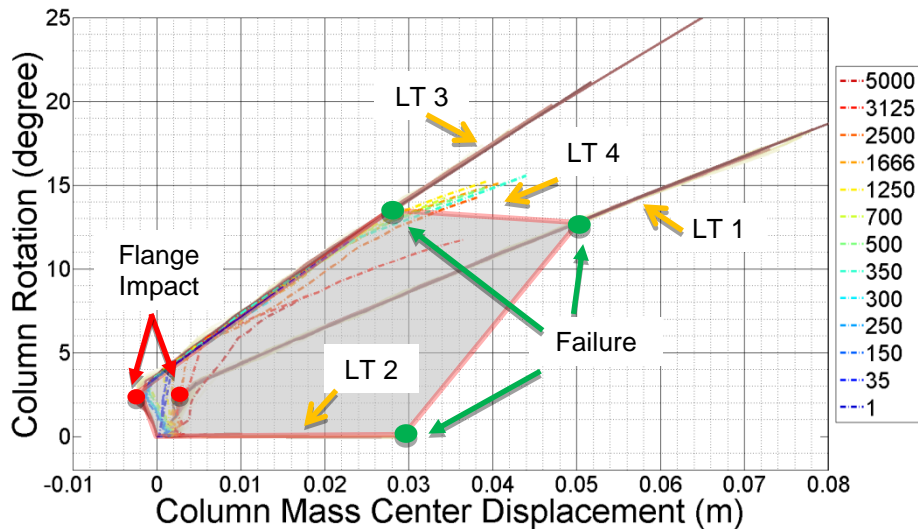
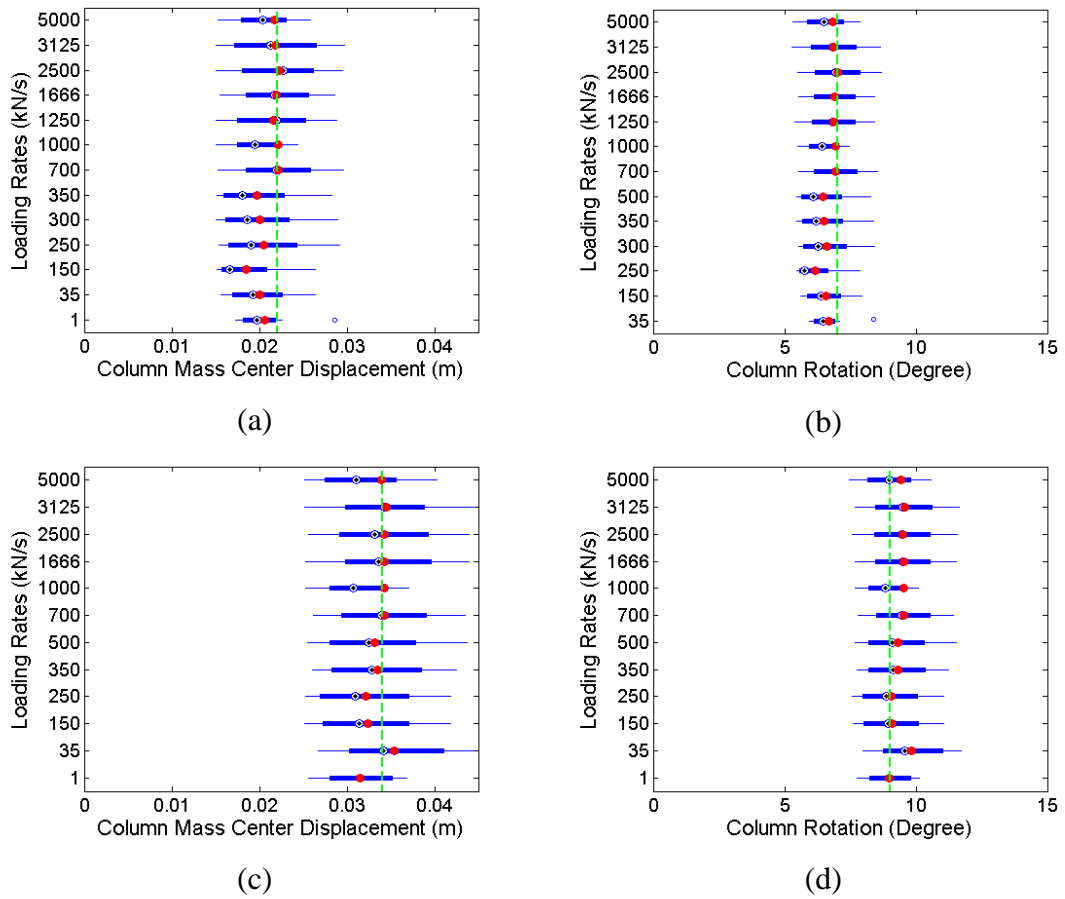


Figure 6-7 Mid bolt and column displacement LT1-4 10mm angle. Green points show the total connection failure

Figure 6-8 shows the median and mean value of the column rotation and translation for three different thicknesses. These values are calculated based on the column movement from the first element failure until the time that the first bolt pulls through the beam web. The comparison shows that the column has lower average displacement and rotation with a 10mm angle than with the other two. Also, 8 and 6mm thick angles both have similar averages. The connection with 10mm thick angles is less ductile than the others, both of which have similar ductility.



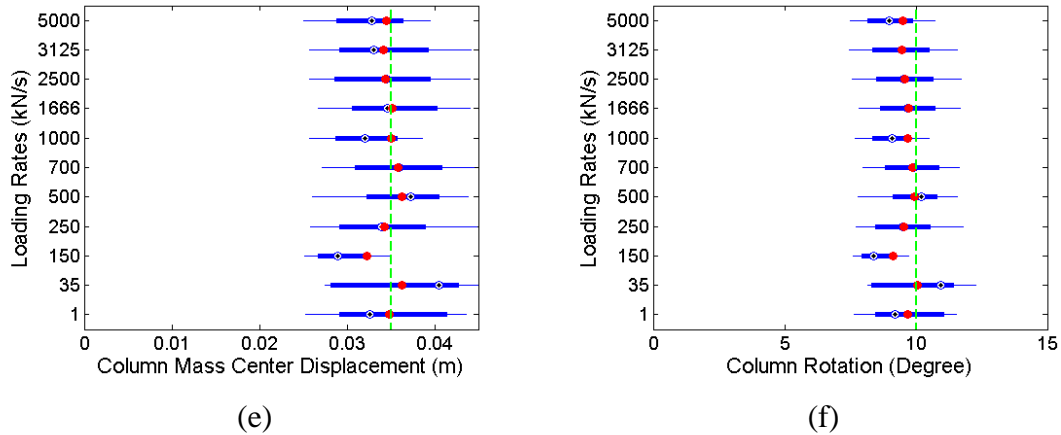


Figure 6-8 Median and mean value of column rotation and translation (a,b) 10mm thick angle, (c,d) 8mm thick angle and (e,f) 6mm thick angle

### 6.1.3 Deformation of the Angle-cleats

Understanding the angles' behaviour as one of the main components of the connection is an important key to understanding the whole joint behaviour. Figure 6-9 indicates the effect of load (and hence, deformation) rate on the deformation of the angles. This graph shows the relationship between the translational displacement of the central bolt in the beam web and the centre of the column; effectively, this is a measure of the deformation of the angle cleats. One loading case (LT2, pure tension) is shown for simplicity, but similar, if less pronounced effects were seen with other load cases. The graph shows the effect of strain rate on the response of the connection in the later stages of deformation, with the faster loading rates leading to less deformation of the angles.

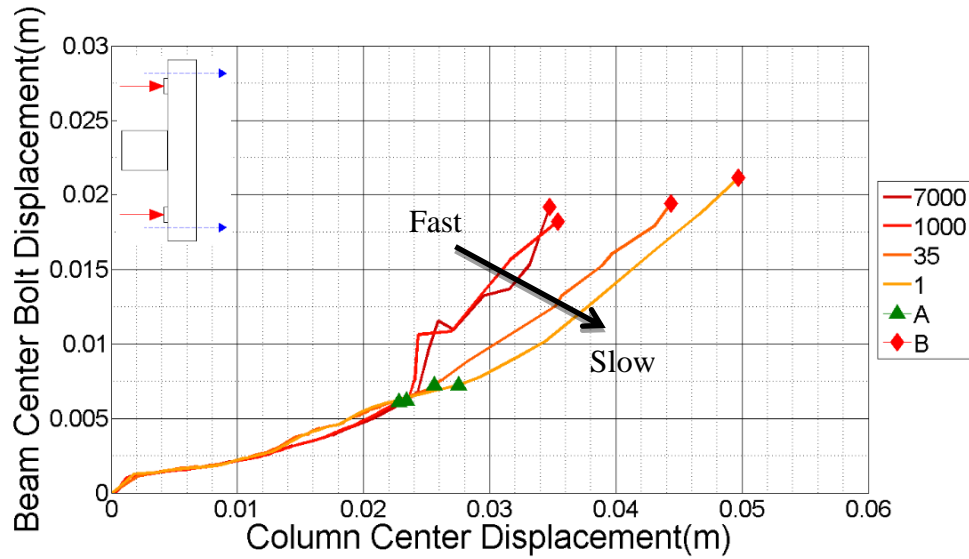


Figure 6-9 Mid bolt and column displacement LT2 8mm angle  
 (Coloured dots indicate the points at which: A- 1<sup>st</sup> element in the model was eroded in vicinity of 1<sup>st</sup> bolt, B- Beam web totally failed in vicinity of all bolts)

Comparison between different angle sizes showed that, as expected, 6mm thick angles exhibited greater deformation than 8 or 10mm angles. Figure 6-10 shows the relationship between the translational displacement of the central bolt in the beam web and the centre of the column; effectively, this is a measure of the deformation of the angle cleats. Only loading case (LT1 – combined rotation and translation) is shown, but similar effects were seen with other load types. This graph shows that there is little rate-dependency in the deformation of the angles. Deformation is dominated by the static strength and stiffness of the different thickness angle legs.

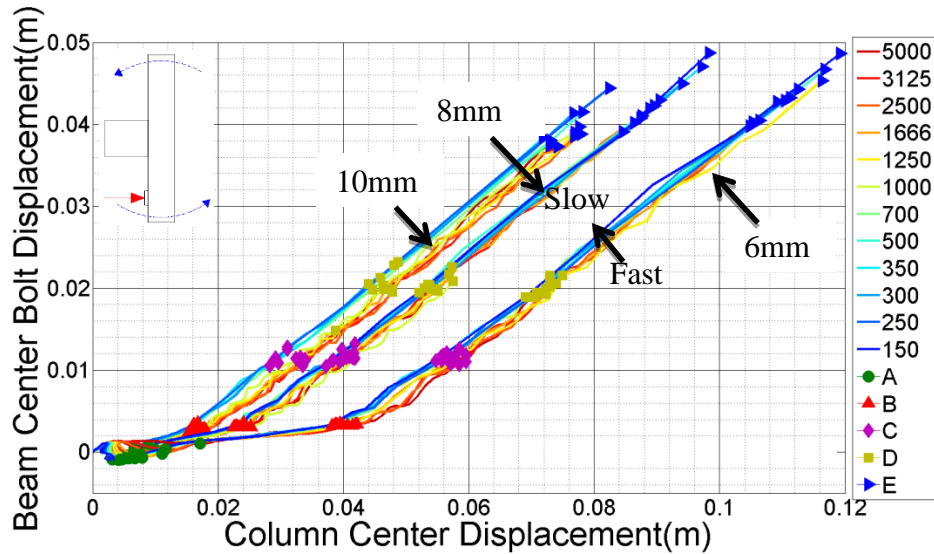


Figure 6-10 Mid bolt and column displacement LT1 10 & 8 & 6mm angle  
 (Coloured dots indicate the points at which: A- the beam and column flanges made contact and prying action commenced, B- 1<sup>st</sup> element in the model was eroded in vicinity of 1<sup>st</sup> bolt, C- Beam web totally failed in vicinity of 1<sup>st</sup> bolt, D- Beam web totally failed in vicinity of 2<sup>nd</sup> bolt, E- Beam web totally failed in vicinity of 3<sup>rd</sup> bolt)

#### 6.1.4 Connection force resistance

Figures 6-11 to 6-14 show how the relationship between the axial resistance of the connections and the axial displacement of the centre of the column varies with loading rate and load type. In all of these graphs, quasi-static results (in which the effect of inertia was negligible) are included as well as dynamic results, where inertia was very significant. In these dynamic results, the connection resistance was calculated as set out in Section 3.2.3 by subtracting the translational inertial force accelerating the column from the applied load. This process resulted in relatively “noisy” traces for the dynamic resistance, due to the difficulty in precisely capturing the inertial effect. This should be borne in mind when comparing the dynamic and quasi-static traces.

Figure 6-11 shows the results for the 10mm angle cleat for LT1. For clarity, only a sub-set of the results for the different loading rates is shown – the other results essentially follow the same trends, as did the results for other angle leg thicknesses. This graph shows that the axial resistance and stiffness of the connection is more or less rate-independent until web failure occurs in the vicinity of the most heavily loaded bolt (closest to the loaded

end of the column). Thereafter, the axial resistance of the connection falls rapidly in the faster-loaded connections, whilst it is maintained in the quasi-static loading case. In the latter case, this is relatively easy to understand. The rotation of the connection means that, effectively, only one bolt is actively contributing to the axial resistance at any given time (the bolt closest to the loaded end), which, due to the deformation of the connection, is fully bearing against the beam web. When this heavily loaded bolt fails, the next one (the central bolt of the three) takes up the same bearing and, having a similar capacity, gives a similar axial resistance until it fails. In the dynamic loading case, the re-distribution of load following the first bolt failure is dynamic and appears to produce an earlier failure of the second and third bolts, leading to a progressive fall off in axial resistance.

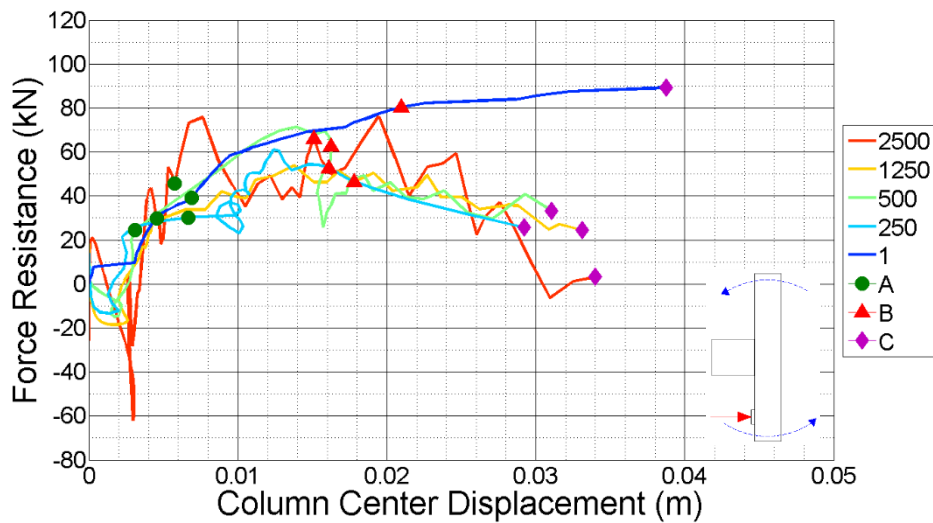


Figure 6-11 Force and column displacement LT1 10mm angle  
 (Coloured dots indicate the points at which: A- the beam and column flanges made contact and prying action commenced, B- 1<sup>st</sup> element in the model was eroded in vicinity of 1<sup>st</sup> bolt, C- Beam web totally failed in vicinity of 1<sup>st</sup> bolt)

Figure 6-12 shows the resistance under pure tension (LT2) loading for three different angle thicknesses and loading rates. All three angle sizes had resistance around 400kN, which is close to the ultimate static value of this connection in web shear failure. The angle leg thickness had little effect on the ultimate resistance but, as expected, the ductility was inversely related to the ductility. There was no significant rate effect.

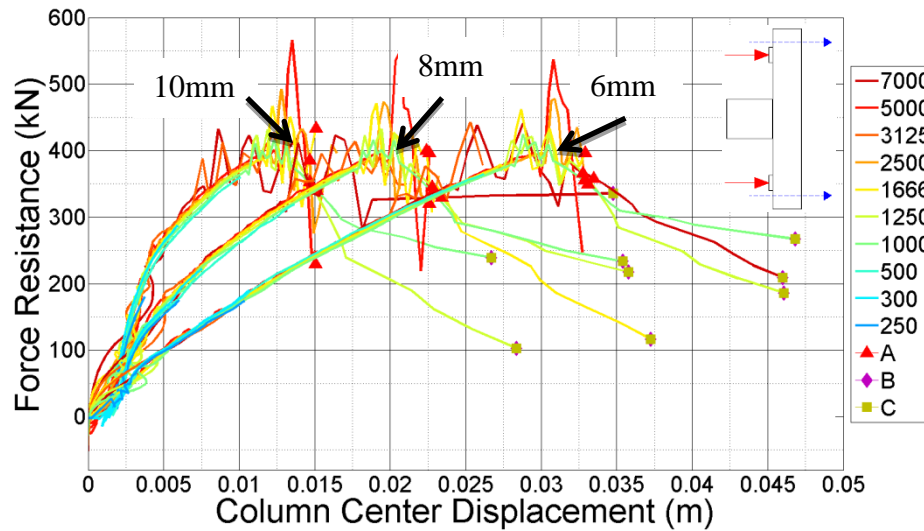


Figure 6-12 Force and column displacement LT2 10 & 8 & 6mm angle  
 (Coloured dots indicate the points at which: A- 1<sup>st</sup> element in the model was eroded in vicinity of 1<sup>st</sup> bolt, B- Beam web totally failed in vicinity of 1<sup>st</sup> bolt, C- Beam web totally failed in vicinity of 2<sup>nd</sup> bolt)

In the case of pure moment (LT3), two equal forces with opposite directions were applied to both ends of the column. In the static loading case, and ignoring the effect of the prying between the beam flange and column flange, this applied couple should generate no axial force. However, as shown in Figure 6-13, as the loading rate increases a compression force develops in the connection which was because of the inertia and the impact of the beam flange to the column.

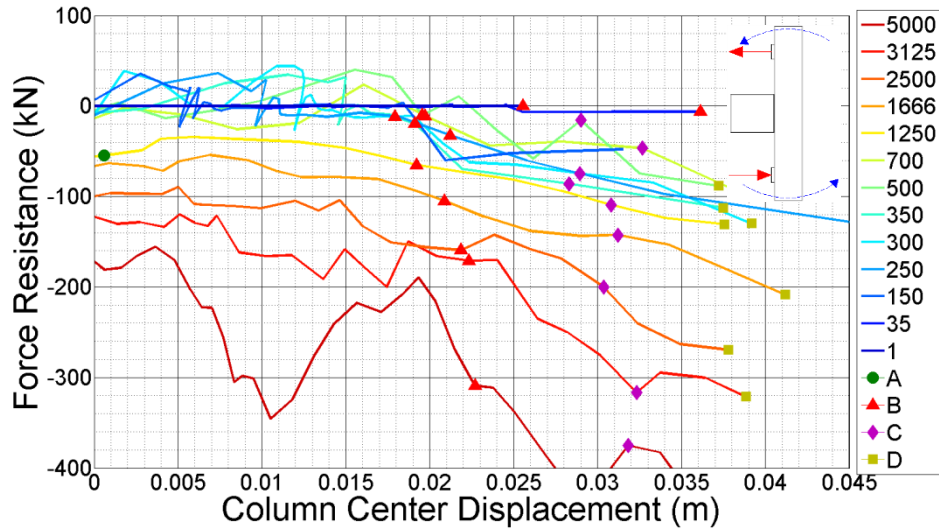


Figure 6-13 Force and column displacement LT3 6mm angle  
 (Coloured dots indicate the points at which: A- the beam and column flanges made contact and prying action commenced, B- 1<sup>st</sup> element in the model was eroded in vicinity of 1<sup>st</sup> bolt, C- Beam web totally failed in vicinity of 1<sup>st</sup> bolt, D- Beam web totally failed in vicinity of 2<sup>nd</sup> bolt)

The connection force resistance under type 4 loading was around 140 to 180 kN, after the flange impact and before the first element failure. Results are provided in Figure 6-14 for different loading rates from quasi-static up to fast dynamic. As mentioned before, connection behaviour was sensitive to loading rates when this type of loading was applied, in static and higher dynamic loading the resistances were close which show that the connection behaved more in tension. However, at lower dynamic rates the resistance dropped after the first element failure which could be because the connection was resisting more moment and rotation as column inertia was important in determining the tension and rotation applied to the connection.

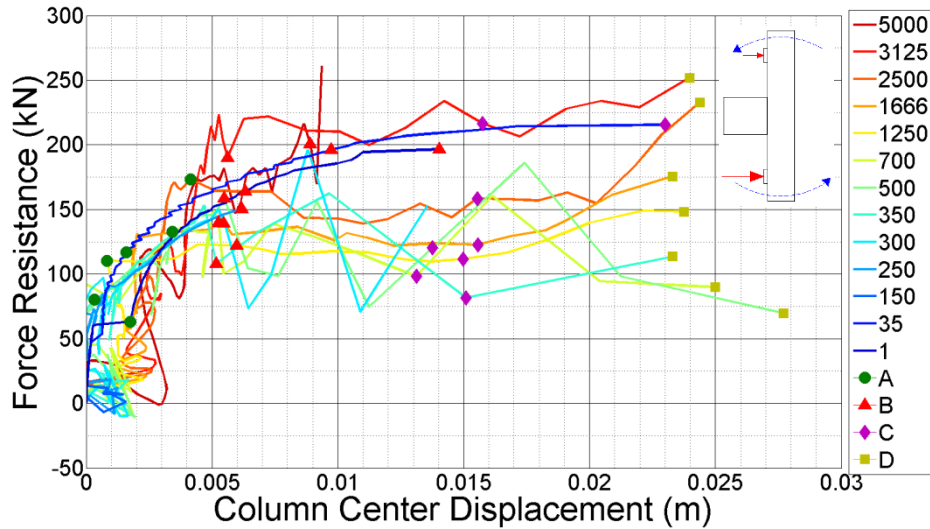


Figure 6-14 Force and column displacement LT4 10mm angle  
 (Coloured dots indicate the points at which: A- the beam and column flanges made contact and prying action commenced, B- 1<sup>st</sup> element in the model was eroded in vicinity of 1<sup>st</sup> bolt, C- Beam web totally failed in vicinity of 1<sup>st</sup> bolt, D- Beam web totally failed in vicinity of 2<sup>nd</sup> bolt)

### 6.1.5 Connection moment resistance

As with connection axial resistance, the moment resistance was determined by subtracting the inertial moment of the column from the applied moment (see Section 3.2.3). Figures 6-15 and 6-16 show how the relationship between the moment resistance and rotation of the connections varies with loading rate and load type.

Figure 6-15 shows the results for load type LT1. As with the axial resistance graph (Figure 6-11), only a small number of loading rates are shown for clarity. This graph again shows that, as with the axial resistance vs displacement, the dynamic connection behaviour closely follows the quasi-static behaviour up until failure begins to occur in the beam web. Thereafter, there is a significant fall off in moment resistance for the dynamic connection as the beam web in the vicinity of the first bolt fails entirely.

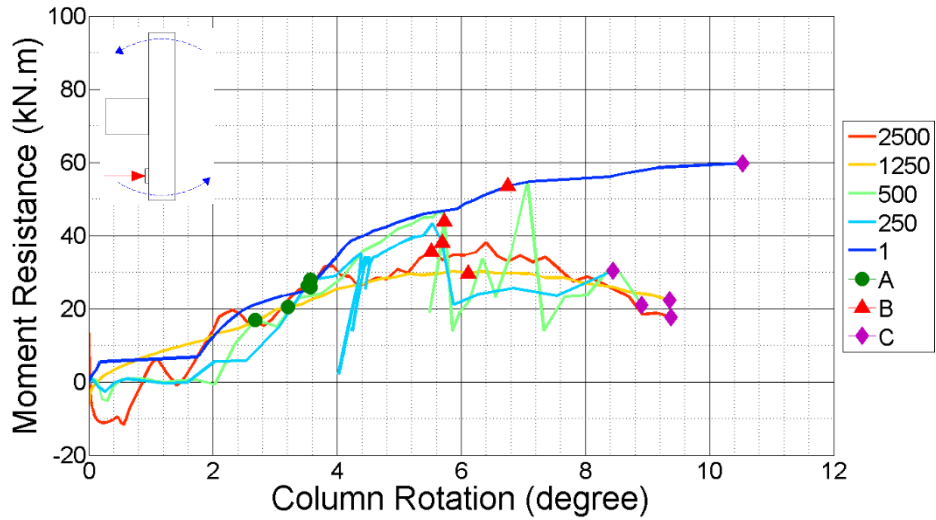


Figure 6-15 Moment and column rotation LT1 10mm angle, rates were in kN/s  
 (Coloured dots indicate the points at which: A- the beam and column flanges made contact and prying action commenced, B- 1<sup>st</sup> element in the model was eroded in vicinity of 1<sup>st</sup> bolt, C- Beam web totally failed in vicinity of 1<sup>st</sup> bolt)

Figure 6-16 provides the results for pure moment loading type (LT3) for six different rates, with intermediate ones omitted for clarity. Once again, the pre-failure behaviour is effectively rate independent (ignoring the difference in initial bolt slip between the quasi-static and dynamic analyses) with the dynamic connection resistance falling after the onset of beam web failure.

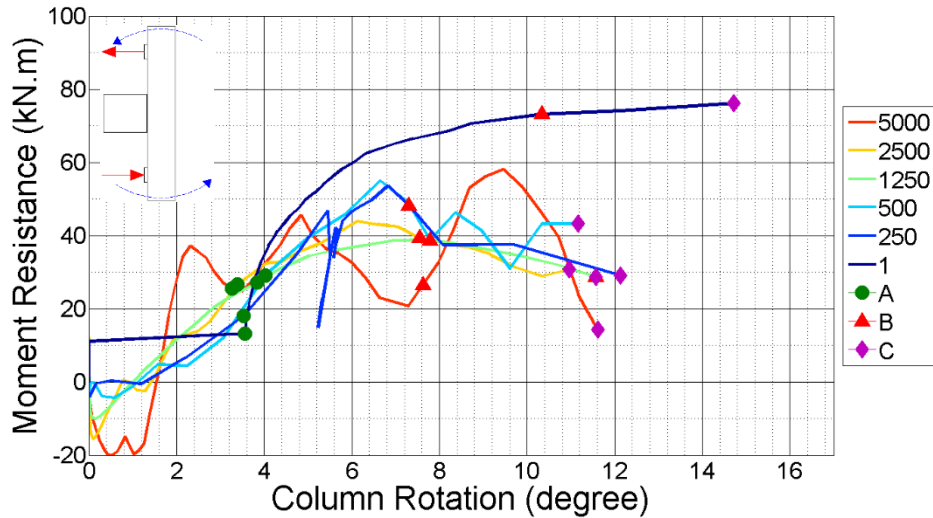
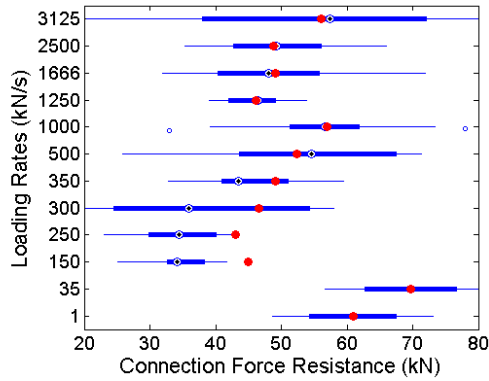


Figure 6-16 Moment and column rotation LT3 8mm angle  
(Coloured dots indicate the points at which: A- the beam and column flanges made contact and prying action commenced, B- 1<sup>st</sup> element in the model was eroded in vicinity of 1<sup>st</sup> bolt, C- Beam web totally failed in vicinity of 1<sup>st</sup> bolt, D- Beam web totally failed in vicinity of 2<sup>nd</sup> bolt)

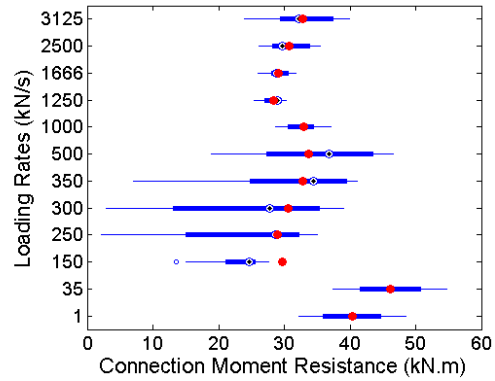
### 6.1.6 Median and mean values of force and moment resisted in the connection

Median and mean values of force and moment were calculated to understand the range of connection resistance, however as original results had some noise it is not possible to find any accurate trends from these figures. These calculations were performed on the data from the time of beam flange and column impact up to just after first element failure for the loading types of LT1 and LT3, and just before and after first element failure in the case of pure tension loading (LT2).

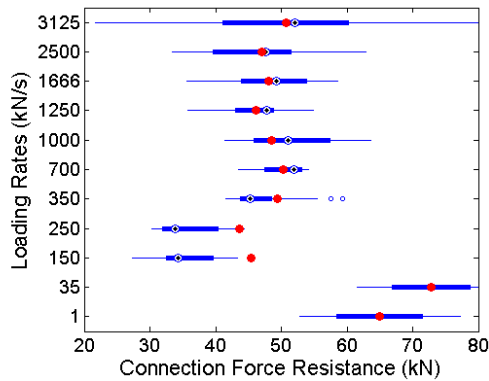
Figure 6-17 provides the median and mean values of force and moment in the case of loading type one for different rates of loading. Moment resistance around 35 kN.m and force resistance around 50 kN were similar for all three thicknesses (10 & 8mm results).



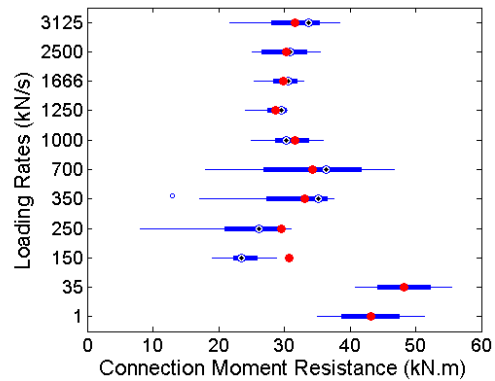
(a)



(b)



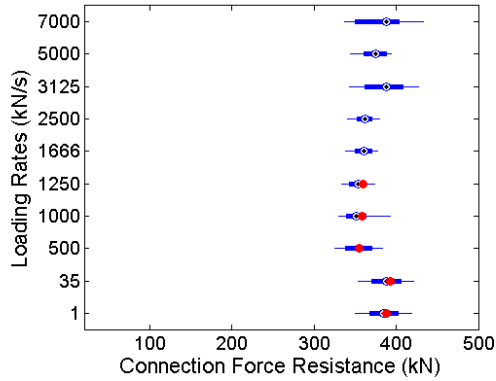
(c)



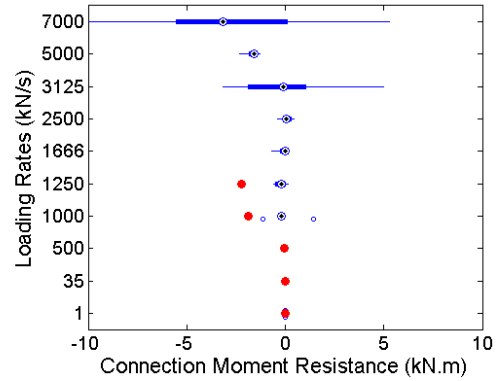
(d)

Figure 6-17 Median and mean value of the force and moment resistance for LT1 (a,b) 10mm thick angle (c,d) 8mm thick angle

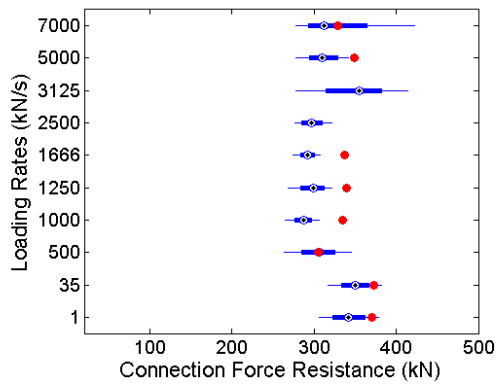
By applying pure tension loading type (LT2) the force resisted in the connection was between 350 to 400 kN and independent of angle thickness and loading rate. As expected, the moment resisted in the connection was close to zero, with only a very small resistance moment generated through some small rotations due to numerical round-off errors. Results from these analyses are provided in Figure 6-18 for two different thicknesses and loading rates in the case of pure tensioning load type.



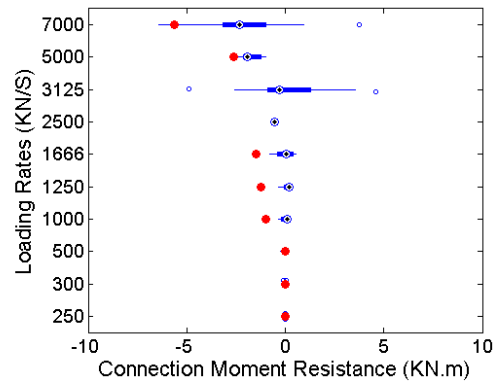
(a)



(b)



(c)



(d)

Figure 6-18 Median and mean value of the force and moment resistance for LT2 (a,b) 10mm thick angle (c,d) 8mm thick angle

As explained earlier, a compression force was developed in the connection through prying effects as the connection was loaded with an applied pure moment loading type (LT3) and high rates. The net axial force generated in the connection varied between 0-200 kN. The moment resisted in the connection was around 40 kN for three different angle thicknesses and loading rates as shown by the data provided in Figure 6-19 for 10 and 8mm thick angles.

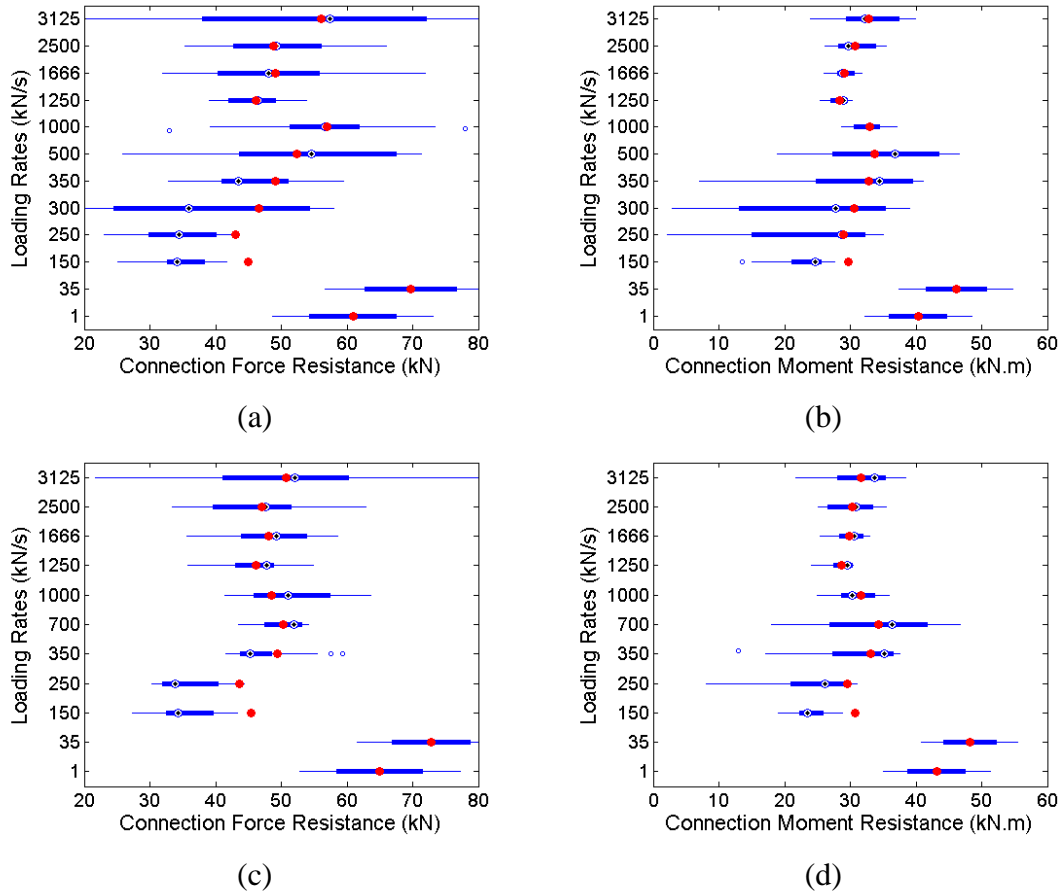


Figure 6-19 Median and mean value of the force and moment resistance for LT3 (a,b) 10mm thick angle (c,d) 8mm thick angle

## 6.2 Influence of bolt strength on connection behaviour

Although the failure of the angle cleat connections was always through web beam shear failure, it was noted that in many cases there was significant plastic bending of the bolts. To check the effect of this phenomenon on the overall connection behaviour a series of models was analysed in which the bolt strength was arbitrarily increased by a factor of 5 to preclude any plastic deformation of the bolts. The results indicated that this reduction in bolt deformation had a marginal but not significant effect on the connection behaviour and resistance. Illustrative examples are shown in Figure 6-20 and Figure 6-21.

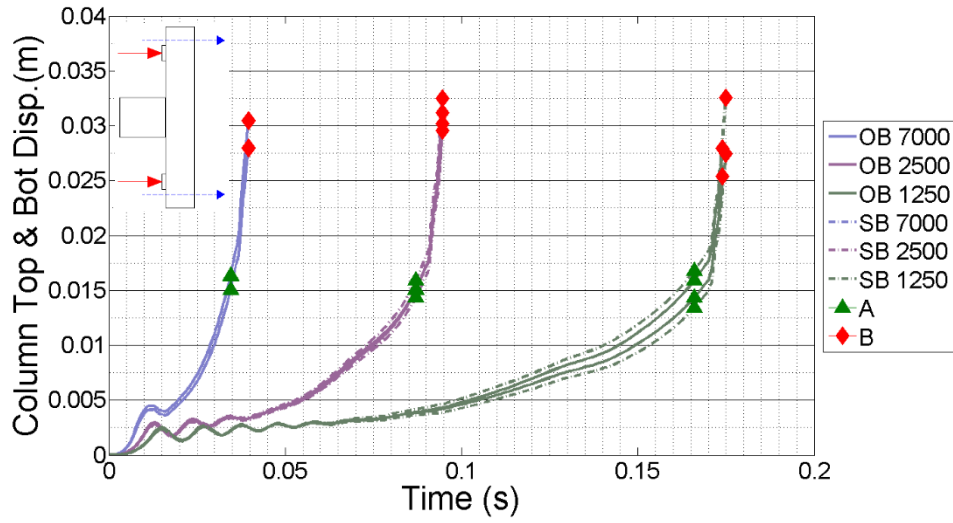


Figure 6-20 Column displacement time history for strong bolt LT2 10mm angle, OB is original bolt and SB is stronger bolt simulations.  
 (Coloured dots indicate the points at which: A- 1<sup>st</sup> element in the model was eroded in vicinity of 1<sup>st</sup> bolt, B- Beam web totally failed in vicinity of all bolts)

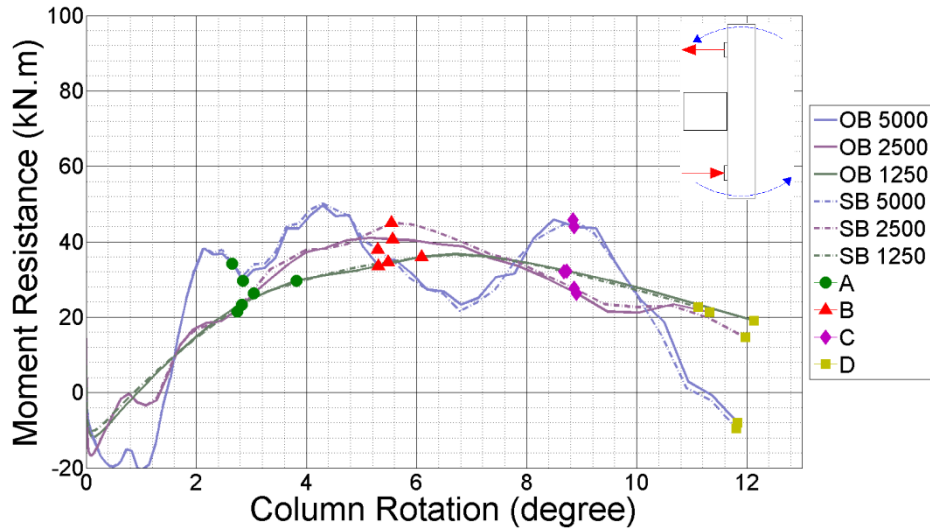
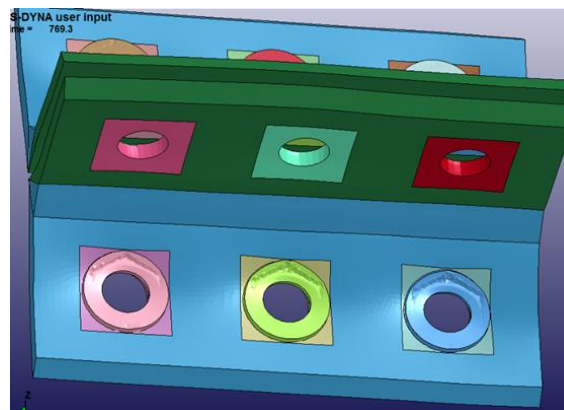


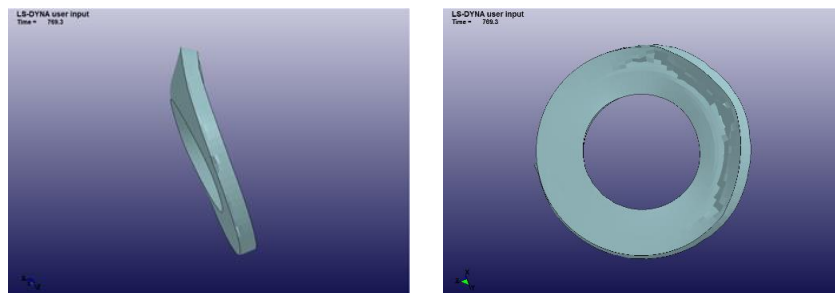
Figure 6-21 Moment & column disp for strong bolt LT3 6mm angle, OB is original bolt and SB is stronger bolt simulations.  
 (Coloured dots indicate the points at which: A- the beam and column flanges made contact and prying action commenced, B- 1<sup>st</sup> element in the model was eroded in vicinity of 1<sup>st</sup> bolt, C- Beam web totally failed in vicinity of 1<sup>st</sup> bolt, D- Beam web totally failed in vicinity of 2<sup>nd</sup> bolt)

### 6.3 Effect of washer size on connection behaviour

The main objective of this parametric study was to assess the influence of washer size on overall connection deformation and its resistance. Whilst the washer may generally be considered a non-structural part of the connection, results indicated that it could be of critical importance in determining different failure modes. In this case, the ductility of the connection was to a great extent governed by the plastic flexural deformation of the legs of the angle cleats. It was considered that this might be affected by the washer size, which could locally affect the lever arm over which the angle cleat legs could bend (Figure 6-22). The models were run as in section 6.2, but with size 24 washers used without any change in the material properties. For this study three different dynamic loading rates were used for two different loading types (LT3 and LT4) with three thicknesses of the angles. As with the bolt strength, no significant effect was found when the washer size was increased. Illustrative results are shown in Figures 6-23 and 6-24.



(a)



(b)

Figure 6-22 (a) Angles and washers deformation (b) Washers deformation

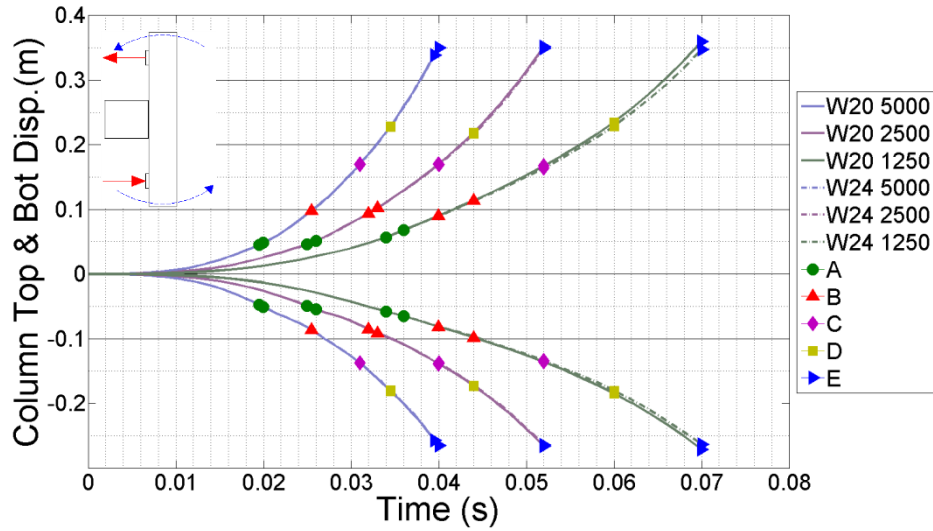


Figure 6-23 Column displacement time history for washer size 24 LT3 10mm angle; W20 is original washer size 20 and W24 is the washer size 24 simulations.  
 (Coloured dots indicate the points at which: A- the beam and column flanges made contact and prying action commenced, B- 1<sup>st</sup> element in the model was eroded in vicinity of 1<sup>st</sup> bolt, C- Beam web totally failed in vicinity of 1<sup>st</sup> bolt, D- Beam web totally failed in vicinity of 2<sup>nd</sup> bolt, E- Beam web totally failed in vicinity of 3<sup>rd</sup> bolt)

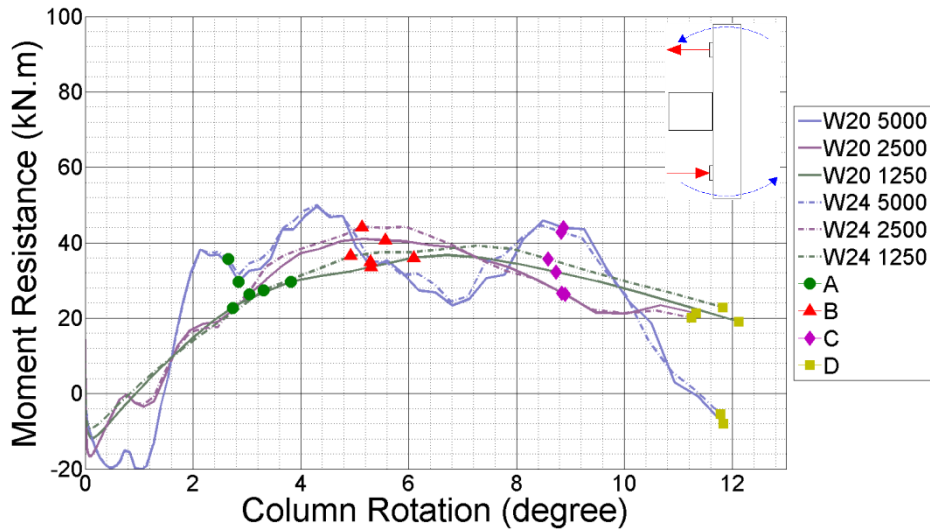


Figure 6-24 Moment & column displacement for washer size 24 LT3 6mm angle; W20 is original washer size 20 and W24 is the washer size 24 simulations.  
 (Coloured dots indicate the points at which: A- the beam and column flanges made contact and prying action commenced, B- 1<sup>st</sup> element in the model was eroded in vicinity of 1<sup>st</sup> bolt, C- Beam web totally failed in vicinity of 1<sup>st</sup> bolt, D- Beam web totally failed in vicinity of 2<sup>nd</sup> bolt, E- Beam web totally failed in vicinity of 3<sup>rd</sup> bolt)

## 6.4 Effect of bolt size on connection behaviour

The main objective of this study was to understand the influence of bolt size on overall connection deformation and its resistance. M24 bolts were used with all other model parameters left unchanged. For this study three different dynamic loading rates were used as well as two different loading type (LT2 and LT3) and three thicknesses of the angles.

### 6.4.1 Column displacement in time

Figure 6-25 shows the displacement time history of each end of the column under loading type LT2 (pure applied tension) with 10mm thick angles. Results are shown for the connection with the original M20 bolt size (denoted “B20”) and for bolt size M24 (denoted “B24”). There is clear evidence that the increased bolt diameter leads to a stiffer response as the loading rate increases. Bigger bolts had less bending and also shortened the lever arm in the angle leg. These cause the overall behaviour of the connection to be less ductile but stronger. Also, as the connection became more rigid in pure tension, 2500 and 1250 kN/s loading rate runs stopped as the model became unstable, but the results provided here are before any instabilities happened in the model.

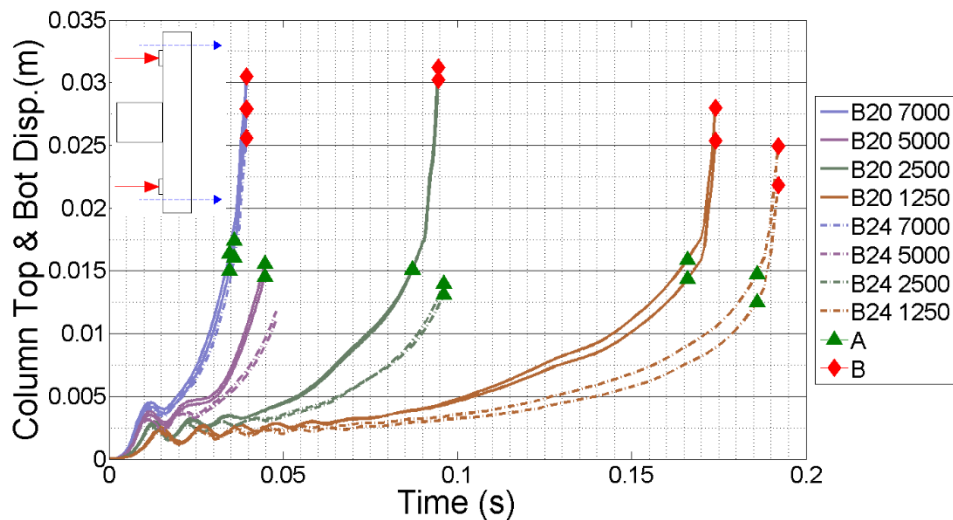


Figure 6-25 Column displacement time history for bolt M24 LT2 10mm angle, B20 is original bolt size 20 and B24 is the bolt size 24 simulations.  
(Coloured dots indicate the points at which: A- 1<sup>st</sup> element in the model was eroded in vicinity of 1<sup>st</sup> bolt, B- Beam web totally failed in vicinity of all bolts)

Figure 6-26 shows connection displacement vs time data for the models with load type LT3 (pure applied moment). Again there is a tendency for the connections to behave more stiffly with increased bolt size, and for the effect to become more pronounced with increasing loading rate; however, neither effect is as pronounced as in the case of LT2 pure tension loading.

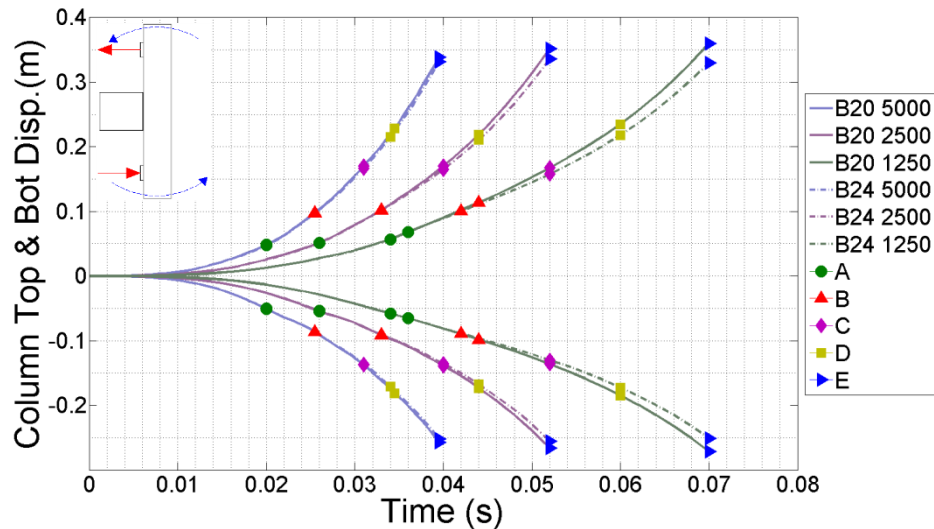


Figure 6-26 Column displacement time history for bolt M24 LT3 10mm angle, B20 is original bolt size 20 and B24 is the bolt size 24 simulations.

(Coloured dots indicate the points at which: A- the beam and column flanges made contact and prying action commenced, B- 1<sup>st</sup> element in the model was eroded in vicinity of 1<sup>st</sup> bolt, C- Beam web totally failed in vicinity of 1<sup>st</sup> bolt, D- Beam web totally failed in vicinity of 2<sup>nd</sup> bolt, E- Beam web totally failed in vicinity of 3<sup>rd</sup> bolt)

#### 6.4.2 Connection force resistance

Figure 6-27 shows the connection axial resistance vs translation for pure tension (LT02) with 10mm thick angle cleats and different bolt diameters. Only two loading rates (1250 and 7000 kN/s) are shown for clarity. In overall bolt size had no significant effect irrespective of loading rate on connection resistance.

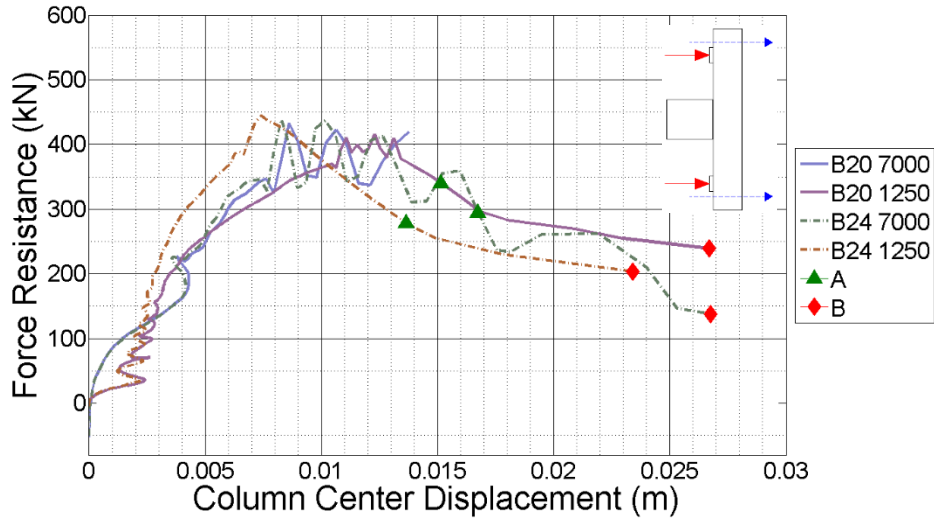


Figure 6-27 Force and column displacement for bolt M24 LT2 10mm angle, B20 is original bolt size 20 and B24 is the bolt size 24 simulations.  
 (Coloured dots indicate the points at which: A- 1<sup>st</sup> element in the model was eroded in vicinity of 1<sup>st</sup> bolt, B- Beam web totally failed in vicinity of all bolts)

### 6.4.3 Connection moment resistance

Figure 6-28 shows the relationship between the connection's moment of resistance and the column rotation for different rates of loading rates with M20 (denoted B20) and M24 (denoted B24) bolts for applied load type LT03 (pure applied moment). The figure shows that the increased bolt diameter has little effect on the connection resistance or ductility.

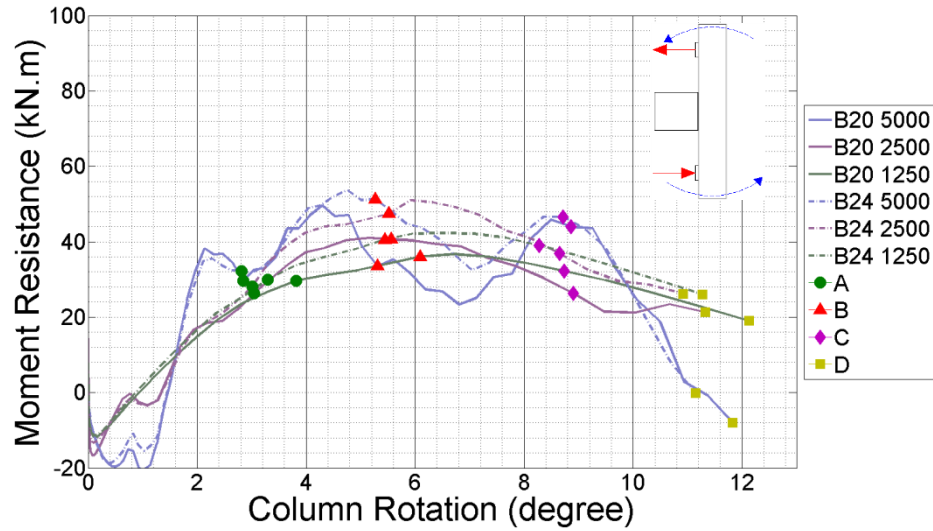


Figure 6-28 Moment and column Rotation for bolt M24 LT3 10mm angle, B20 is original bolt size 20 and B24 is the bolt size 24 simulations.  
 (Coloured dots indicate the points at which: A- the beam and column flanges made contact and prying action commenced, B- 1<sup>st</sup> element in the model was eroded in vicinity of 1<sup>st</sup> bolt, C- Beam web totally failed in vicinity of 1<sup>st</sup> bolt, D- Beam web totally failed in vicinity of 2<sup>nd</sup> bolt)

### 6.5 Influence of bolt gauge on connection behaviour

The main objective of this study was to understand the influence of bolt gauge on overall connection deformation and its resistance. For this reason two different bolt gauges were used one of them 1cm bigger and other one had 1cm less bolt gauge than the original 9cm bolt gauge. In this study three different dynamic loading rates were used as well as two different loading type (LT2 and LT3) and three thicknesses of the angles.

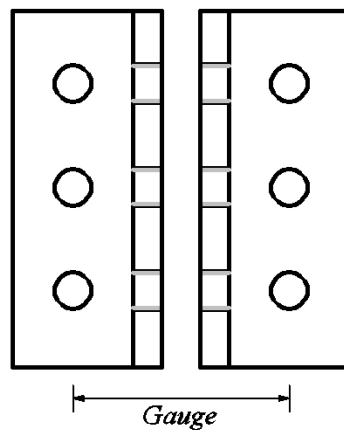


Figure 6-29 Drawing of the bolt gauge

### 6.5.1 Column displacement in time

Column displacement was measured at both ends. By measuring how much the column translated or rotated, the response of the connection could be understood. For example, changing the bolt gauge from 90mm to 80mm, stiffened the angle and effectively transferred the force faster to the beam web, thus causing the connection to resist a greater force (i.e. for a longer in time) but with less ductility. However changing the bolt gauge from 90mm to 100mm caused the angles to deform more and transfer the load to the beam web with more delay resulting in overall behaviour that was more ductile. Figure 6-30 shows the column displacement time history at both its ends in pure tension loading type (LT2) with 10mm thick angles; different colours denote a loading rate the magnitude of which is provided in the legend. Two simulations were conducted, one for the connection with the original bolt gauge (OBG) which was 90mm and another with a lower bolt gauge of 80mm (LBG). The results show that the connection with the lower bolt gauge reacted more stiffly and failed with lower column displacement. As with the bolt diameter, the increase in stiffness is more marked at higher loading rates.

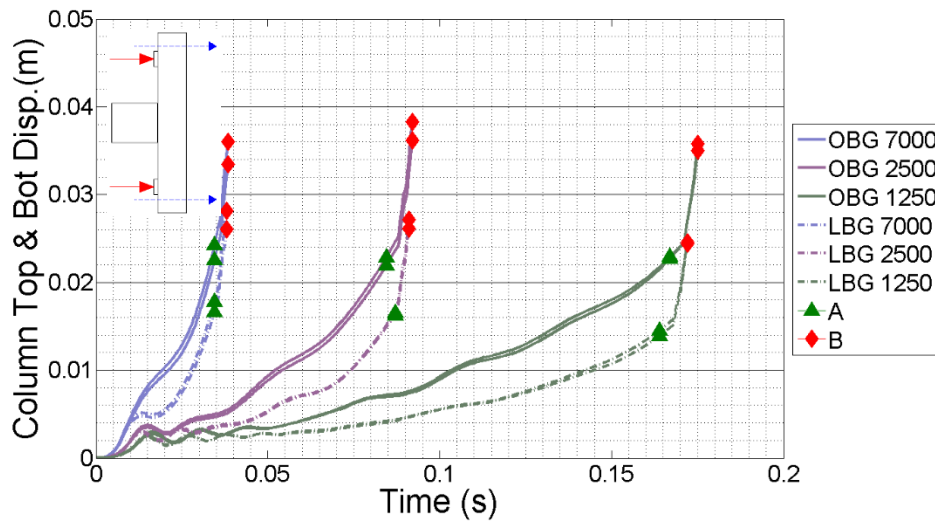


Figure 6-30 Column displacement time history for BG less LT2 8mm angle, OBG is original bolt gauge (90mm) and LBG is the lower bolt gauge (80mm) simulation.

(Coloured dots indicate the points at which: A- 1<sup>st</sup> element in the model was eroded in vicinity of 1<sup>st</sup> bolt, B- Beam web totally failed in vicinity of all bolts)

Increasing the bolt gauge to 100mm (MBG model) improved the ductility of the angle as evidenced by the column displacement results provided in Figure 6-31 for pure tension

loading type (LT2) and three different loading rates. Increasing the bolt gauge resulted in greater angle deformation and consequently, increased connection ductility.

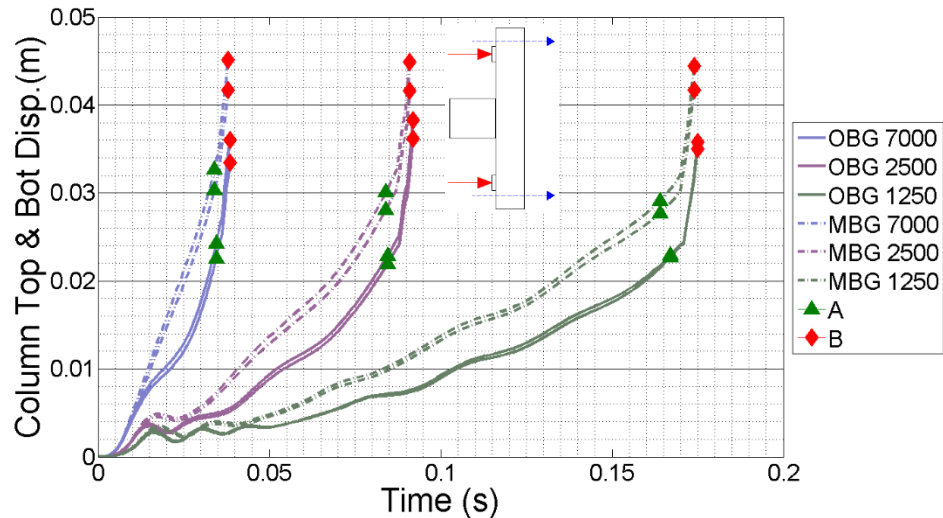


Figure 6-31 Column displacement time history for BG more LT2 8mm angle, OBG is original bolt gauge and MBG is the maximum bolt gauge simulation.  
 (Coloured dots indicate the points at which: A- 1<sup>st</sup> element in the model was eroded in vicinity of 1<sup>st</sup> bolt, B- Beam web totally failed in vicinity of all bolts)

### 6.5.2 Deformation of the Angle-cleats

Figure 6-32 shows the results for the displacement of the central bolt in the beam web vs the displacement of the centre of the column. Effectively this is a measure of the deformation of the angles. The data shown is for the 8mm thick angles. This confirms that the deformation of the angles increases with bolt gauge, but, unlike the overall connection ductility, it is effectively insensitive to loading rate.

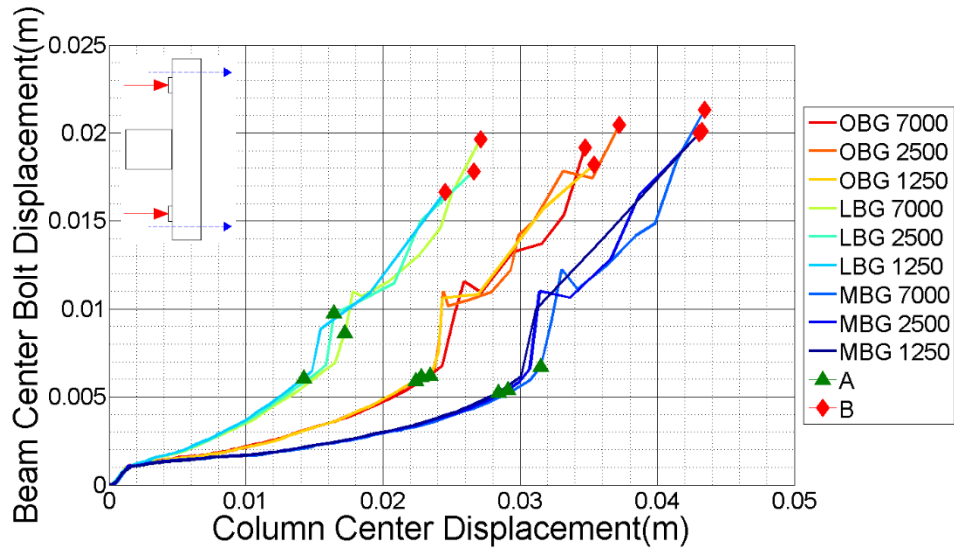


Figure 6-32 Bolt and column displacement for BG more & less LT2 8mm angle, OBG is original bolt gauge and LBG is the less bolt gauge simulations.  
(Coloured dots indicate the points at which: A- 1<sup>st</sup> element in the model was eroded in vicinity of 1<sup>st</sup> bolt, B- Beam web totally failed in vicinity of all bolts)

### 6.5.3 Connection force resistance

Increasing or decreasing the bolt gauge did not change the force resistance of the connection, however ductility was inversely related to the bolt gauge as the deformation in the angle changed. This implies that the limit to the axial resistance of the connection came from the beam web. Results are provided in Figure 6-33 for three different loading rates and an 8mm thick angle under pure tension loading.

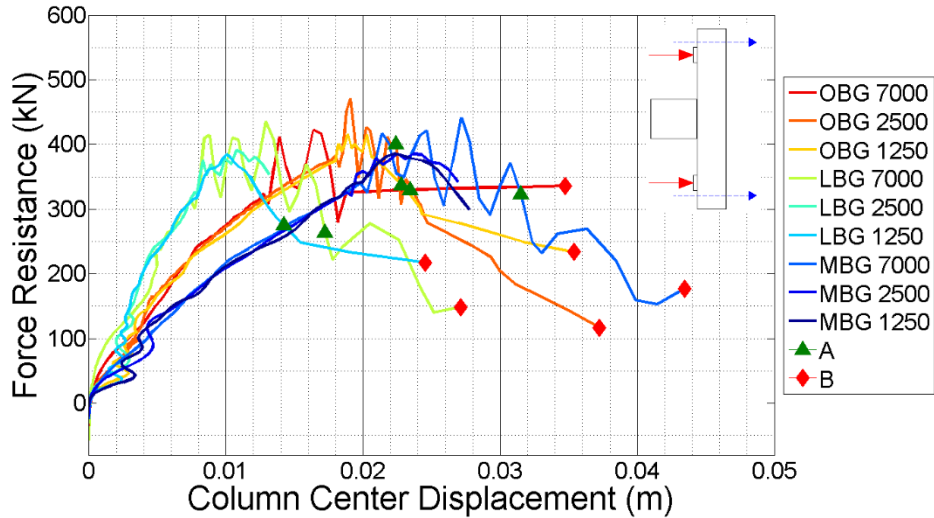


Figure 6-33 Force and column displacement for BG more & less LT2 8mm angle, OBG is original bolt gauge and LBG is the least bolt gauge simulation.  
(Coloured dots indicate the points at which: A- 1<sup>st</sup> element in the model was eroded in vicinity of 1<sup>st</sup> bolt, B- Beam web totally failed in vicinity of all bolts

#### 6.5.4 Connection moment resistance

There was no significant effect on moment-rotation behaviour arising from changes in load rate or bolt gauge. However, a smaller bolt gauge reduced the prying effect in the angle leg attached to the column and less rotation was observed at each stage of the failure; opposite results were observed as the bolt gauge was increased. Results are provided in Figure 6-34 and Figure 6-35 for both cases of bolt gauge and 8mm thick angle under different loading rates and pure moment loading.

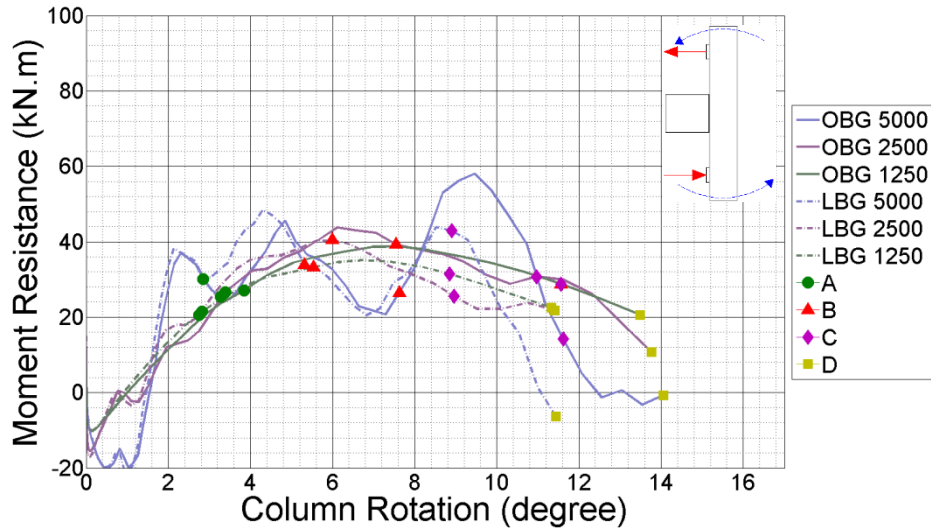


Figure 6-34 Moment and column rotation for BG less LT3 8mm angle, OBG is original bolt gauge and LBG is the least bolt gauge simulation.  
 (Coloured dots indicate the points at which: A- the beam and column flanges made contact and prying action commenced, B- 1<sup>st</sup> element in the model was eroded in vicinity of 1<sup>st</sup> bolt, C- Beam web totally failed in vicinity of 1<sup>st</sup> bolt, D- Beam web totally failed in vicinity of 2<sup>nd</sup> bolt)

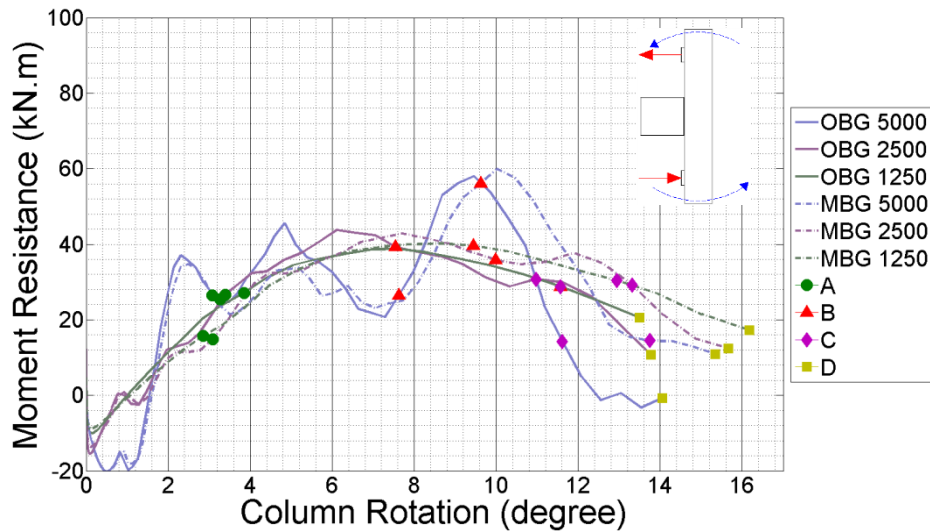


Figure 6-35 Moment and column rotation for BG more LT3 8mm angle, OBG is original bolt gauge and MBG is the maximum bolt gauge simulation.  
 (Coloured dots indicate the points at which: A- the beam and column flanges made contact and prying action commenced, B- 1<sup>st</sup> element in the model was eroded in vicinity of 1<sup>st</sup> bolt, C- Beam web totally failed in vicinity of 1<sup>st</sup> bolt, D- Beam web totally failed in vicinity of 2<sup>nd</sup> bolt)

## 6.6 Influence of bolt pitch on connection behaviour

The main objective of this study was to understand the influence of bolt pitch on overall connection deformation and resistance. For this reason two different bolt pitches were used one of them 10mm greater (MBP) and other one 10mm less (LBP) than the original 7cm bolt pitch. For this study three different dynamic loading rates were used as well as two different loading type (LT2 and LT3) and three thicknesses of the angles.

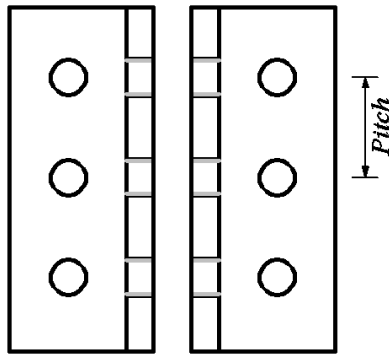


Figure 6-36 Drawing of the bolt locations

### 6.6.1 Column displacement in time

Figures 6-37 and 6-38 show the results of column displacement vs time with increased and reduced bolt pitch (LBP and MBP), under pure tension loading type (LT2), different loading rates and 8mm thick angles. Overall, bolt pitch had little effect on connection ductility.

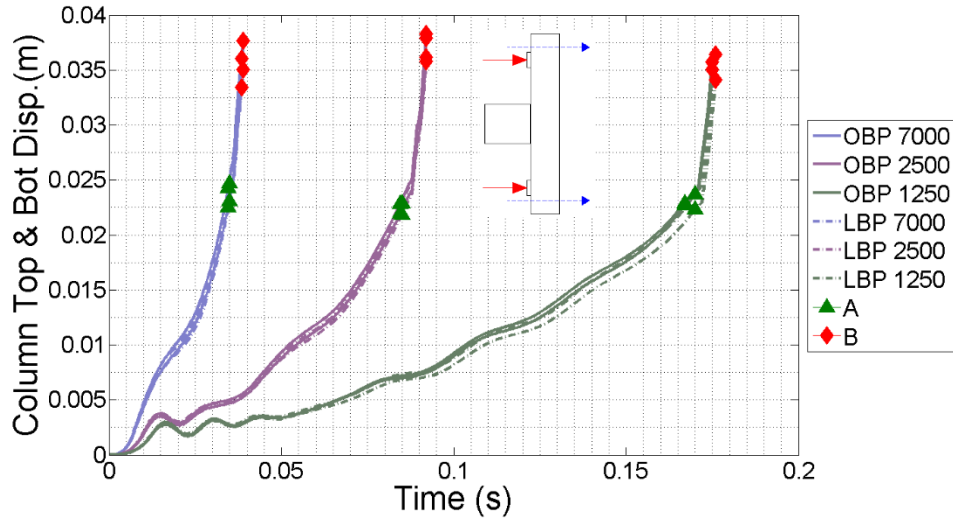


Figure 6-37 Column displacement time history for BP less LT2 8mm angle, OBP is original bolt pitch and LBP is the less bolt pitch simulations.  
 (Coloured dots indicate the points at which: A- 1<sup>st</sup> element in the model was eroded in vicinity of 1<sup>st</sup> bolt, B- Beam web totally failed in vicinity of all bolts)

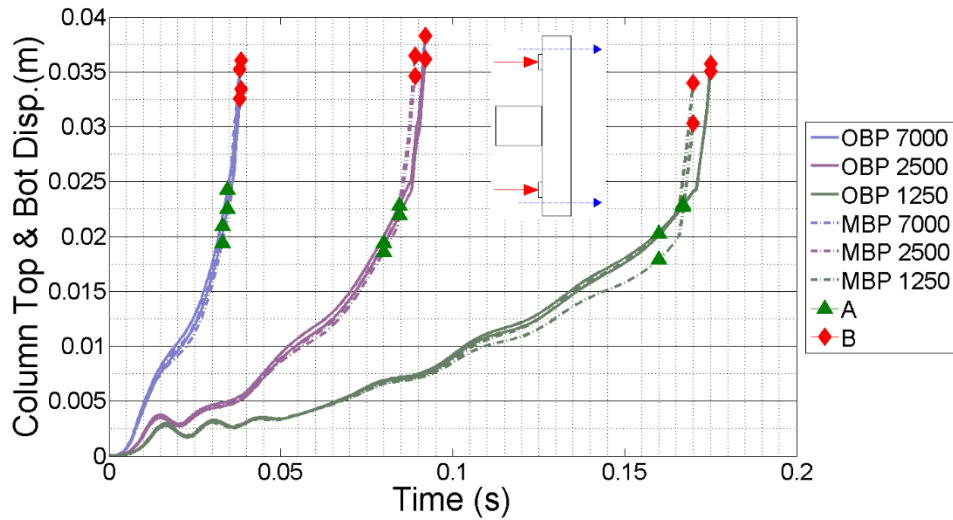


Figure 6-38 Column displacement time history for BP more LT2 8mm angle, OBP is original bolt pitch and MBP is the more bolt pitch simulations.  
 (Coloured dots indicate the points at which: A- the beam and column flanges made contact and prying action commenced, B- 1<sup>st</sup> element in the model was eroded in vicinity of all bolts)

### 6.6.2 Deformation of the Angle-cleats

Figure 6-39 and Figure 6-40 provide the results for less and more bolt pitch compared with the original case under pure moment loading type (LT3) and three different loading rates.

Reducing the bolt pitch caused no change in connection reaction and did not change the ductility and increasing the bolt pitch had a small effect.

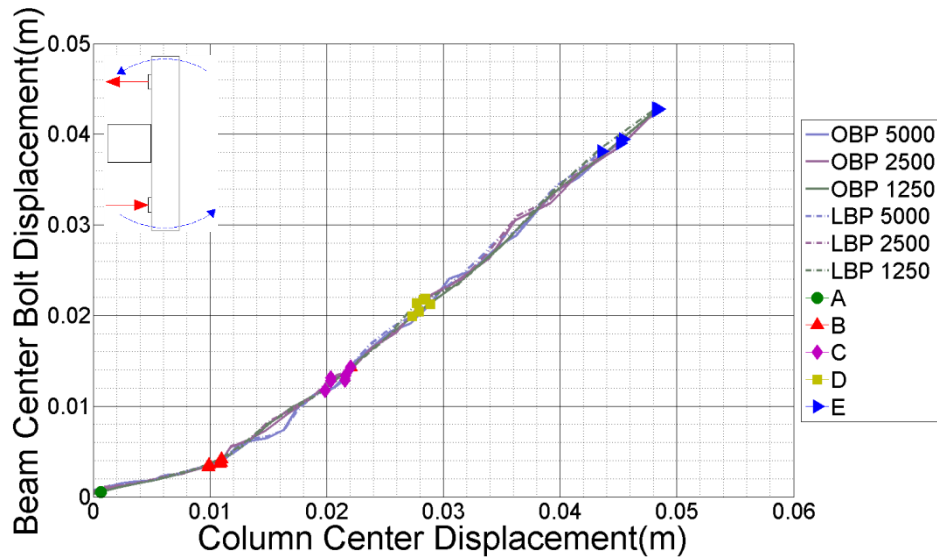


Figure 6-39 Bolt and column displacement for BP less LT3 8mm angle, rates were in kN/s. OBP is original bolt pitch and LBP is the less bolt pitch simulations.

(Coloured dots indicate the points at which: A- the beam and column flanges made contact and prying action commenced, B- 1<sup>st</sup> element in the model was eroded in vicinity of 1<sup>st</sup> bolt, C- Beam web totally failed in vicinity of 1<sup>st</sup> bolt, D- Beam web totally failed in vicinity of 2<sup>nd</sup> bolt, E- Beam web totally failed in vicinity of 3<sup>rd</sup> bolt)

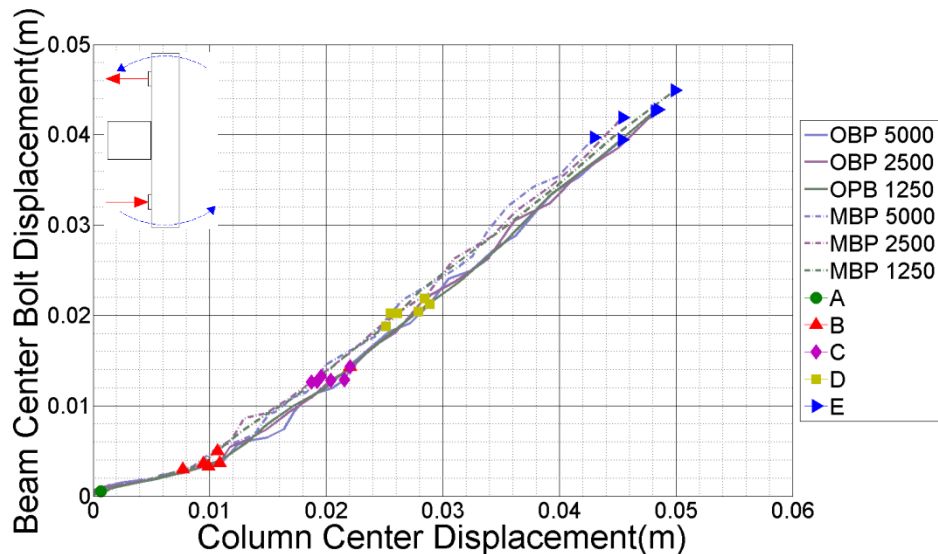


Figure 6-40 Bolt and column displacement for BP more LT3 8mm angle, rates were in kN/s. OBP is original bolt pitch and MBP is the more bolt pitch simulations.

(Coloured dots indicate the points at which: A- the beam and column flanges made contact and prying action commenced, B- 1<sup>st</sup> element in the model was eroded in vicinity of 1<sup>st</sup> bolt, C- Beam web totally failed in vicinity of 1<sup>st</sup> bolt, D- Beam web totally failed in vicinity of 2<sup>nd</sup> bolt)

### 6.6.3 Connection force resistance

As changing the bolt pitch had no significant effect on angle deformation, it also did not change the force resistance of the connection or its translational ductility. Results are provided in Figure 6-41 and Figure 6-42 for the 8mm thick angle under pure tension and different loading rates.

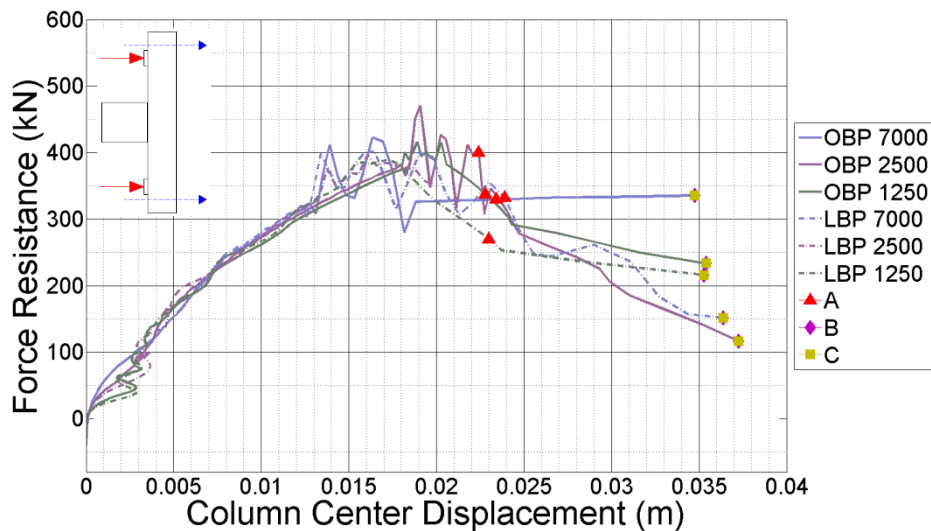


Figure 6-41 Force and column displacement for BP less LT2 8mm angle, OBP is original bolt pitch and LBP is the least bolt pitch simulations.

(Coloured dots indicate the points at which: A- the beam and column flanges made contact and prying action commenced, B- 1<sup>st</sup> element in the model was eroded in vicinity of 1<sup>st</sup> bolt, C- Beam web totally failed in vicinity of 1<sup>st</sup> bolt)

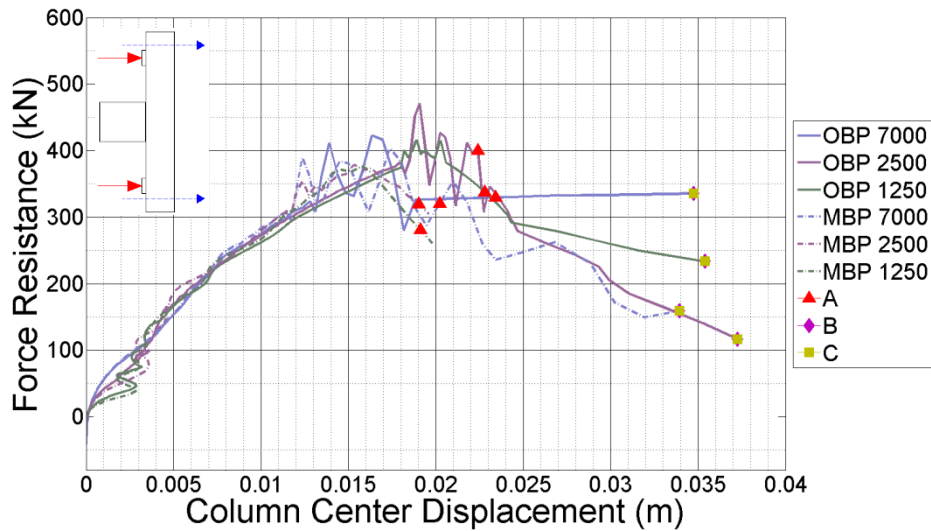


Figure 6-42 Force and column displacement for BP more LT2 8mm angle, OBP is original bolt pitch and MBP is the maximum bolt pitch simulations.  
 (Coloured dots indicate the points at which: A- the beam and column flanges made contact and prying action commenced, B- 1<sup>st</sup> element in the model was eroded in vicinity of 1<sup>st</sup> bolt, C- Beam web totally failed in vicinity of 1<sup>st</sup> bolt)

#### 6.6.4 Connection moment resistance

Angles deformation did not change and as the result connection had no significant change in its moment resistance or its rotational ductility either. Figure 6-43 and Figure 6-44 provide the results for an 8mm thick angle under pure moment loading and different loading rates.

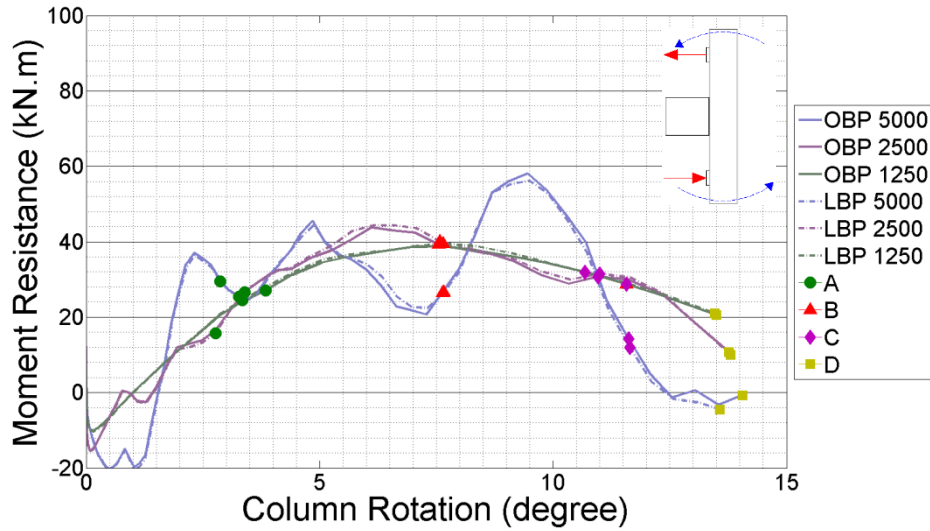


Figure 6-43 Moment and column displacement for BP less LT3 8mm angle, OBP is original bolt pitch and LBP is the least bolt pitch simulation.  
 (Coloured dots indicate the points at which: A- the beam and column flanges made contact and prying action commenced, B- 1<sup>st</sup> element in the model was eroded in vicinity of 1<sup>st</sup> bolt, C- Beam web totally failed in vicinity of 1<sup>st</sup> bolt, D- Beam web totally failed in vicinity of 2<sup>nd</sup> bolt)

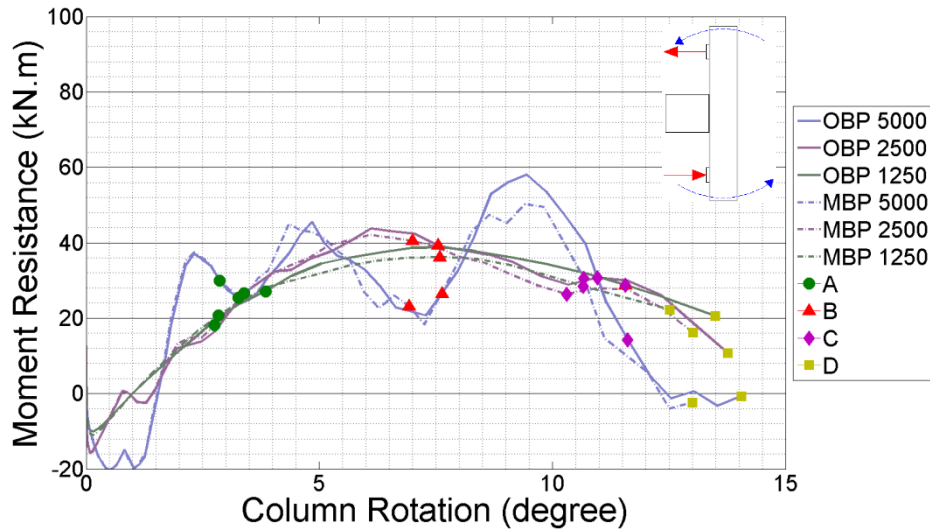


Figure 6-44 Moment and column displacement for BP more LT3 8mm angle, OBP is original bolt pitch and MBP is the maximum bolt pitch simulation.  
 (Coloured dots indicate the points at which: A- the beam and column flanges made contact and prying action commenced, B- 1<sup>st</sup> element in the model was eroded in vicinity of 1<sup>st</sup> bolt, C- Beam web totally failed in vicinity of 1<sup>st</sup> bolt, D- Beam web totally failed in vicinity of 2<sup>nd</sup> bolt)

## 6.7 Summary

Table 6-1 provides a short comparison between all the parametric studies conducted on web-cleat connections. This table demonstrates how different geometry or loading rates and types change different aspects of connection behaviour e.g. the column time histories, angle deformations, and force and moment resistance.

<i>Web Cleat Connection</i>	
	Description
Influence of Different Loading Types and Rates	<ul style="list-style-type: none"> <li>• <i>Column displacement in time (Section 6.2.1)</i>: The connection behaviour and angle prying changed from fast to slow loading rates around rate of 700 kN/s as deformation in the angle as increased in quasi-static loading rates.</li> <li>• <i>Column response due to connection reaction (Section 6.2.2)</i>: Loading types LT1, LT2 and LT3 were loading rate independent, however LT4 was rate dependent.</li> <li>• <i>Angle deformation (Section 6.2.3)</i>: Angles deformed more in quasi-static loadings regardless of the thickness. The thinnest angle (6mm) showed the most difference between fast and slow loading rates.</li> <li>• <i>Connection force resistance (Section 6.2.4)</i>: Pure tension loading enabled more force to be resisted than the other loading cases as rotation was not applied to the connection. Force resistance of the connection did not change much as the loading rate changed. Changes in angle thickness did not change the resistance, but a 6mm thick angle gave the highest translation in the column and ductility for different loading types and rates. Pure moment loading type (LT3) generated a compressive force in the connection which was a result of column inertia, however other cases generated only a tension force.</li> <li>• <i>Connection moment resistance (Section 6.2.5)</i>: Moment resistance of the connection changed with the loading type but loading rates did not change the overall resistance of the connection as the inertia effect of the column cancelled out the dynamic effect. Material response was different in dynamic and static situations which caused small differences between results.</li> </ul>
Influence of Bolt Strength	<p>There was no significant change in column displacement, angle deformation or force and moment resistance of the connection (Section 6.3).</p>

Effect of Washer Size	<p>There was no significant change in column displacement, angle deformation or force and moment resistance of the connection (Section 6.4).</p>
Effect of Bolt Size	<ul style="list-style-type: none"> <li>• <i>Column displacement in time</i> (Section 6.5.1): As the loading rate decreased, the angles became more flexible and angles deformations were higher with stronger bolts.</li> <li>• <i>Angle deformation</i> (Section 6.5.2): Having bigger bolts caused the angle to deform less and behave with less ductility.</li> <li>• <i>Connection force resistance</i> (Section 6.5.3): Force resistance of the connection did not change by having bigger bolts but translation was reduced except for the highest loading rate which had similar translation as the original case.</li> <li>• <i>Connection moment resistance</i> (Section 6.5.4): Connection had more moment resistance as the angles deformed less and also the bolts themselves had less deformation.</li> </ul>
Influence of Bolt Gauge	<ul style="list-style-type: none"> <li>• <i>Column displacement in time</i> (Section 6.6.1): Much less ductile as the gauge was reduced, displacement reduced and failed with less displacement, and more ductile as the gauge was increased, displacement improved and failed with more displacement.</li> <li>• <i>Angle deformation</i> (Section 6.6.2): Less ductile as reducing the gauge caused the angles to deform less and pass the force to beam web sooner than the original bolt gauge, and more ductile as increasing the gauge caused the angles to deform more and pass the force to beam web later than the original bolt gauge.</li> <li>• <i>Connection force resistance</i> (Section 6.6.3): Reducing the bolt gauge did not increase the force resistance in the connection however it reduced the column translation and made it more rigid, also adding the bolt gauge did not increase the force resistance in the connection however it improved the column translation and made it more ductile.</li> <li>• <i>Connection moment resistance</i> (Section 6.6.4): Less bolt gauge did not increase the moment resistance in the connection however it reduced the column rotation and made it more rigid, and also adding the bolt gauge did not increase the moment resistance in the connection however it improved the column rotation and made it more ductile.</li> </ul>

Influence of Bolt Pitch	<ul style="list-style-type: none"> <li>• <i>Column displacement in time</i> (Section 6.7.1): Reducing the bolt pitch made the connection slightly stiffer and the column displaced less. Increasing the pitch caused the column to move less than the original case and decreased the ductility as stress was distributed badly in the angle.</li> <li>• <i>Angle deformation</i> (Section 6.7.2): Less bolt pitch made no change in angle deformation or ductility, however more bolt pitch made the angles to deform less and their ductility was reduced.</li> <li>• <i>Connection force resistance</i> (Section 6.7.3): Having more or less bolt pitch did not change the force resistance, however had less column translation.</li> <li>• <i>Connection moment resistance</i> (Section 6.7.4): More and less bolt pitch had same moment resistance and rotation to failure. These two had no effect on moment and rotation resistance of the connection.</li> </ul>
-------------------------	---

Table 6-1 Summarize the parametric conclusions

The final results of the parametric studies are provided in Table 6-2, which shows the translation and rotation of the column at the time of total failure of the connection. The force and moment resistance are the maximum resisted in the connection before the failure (two numbers separated by “/” shows the maximum and minimum for different range of loading rats).

Web Cleat Connection							
Angle leg thickness & Loading Type		Translation (mm)	Rotation (Degree)	Force (kN)	Moment (kN.m)		
Influence of Different Loading Types and Rates	10mm	1	16	6	60/85	40/60	
		2	15	0	400/450	0	
		3	5	6	-250/0	40/80	
		4	6	6	150/200	20/40	
	8mm	1	25	8	55/80	40/60	
		2	22.5	0	400/450	0	
		3	10	7	-250/0	40/80	
		4	10	7	150/200	20/40	
	6 mm	1	40	11	55/80	40/60	
		2	32.5	0	400/450	0	
		3	20	11	-250/0	40/80	
		4	20	11	150/200	20/40	
Influence of Bolt Strength	10mm	2	14	0	400	0	
		3	4	5	-300/0	40	
	8mm	2	22	0	400	0	
		3	10	7	-300/0	40	
	6mm	2	32	0	400	0	
		3	20	11	-300/0	50	
Effect of Washer Size	10mm	3	4	5	-300/0	40	
		4	6	5	120/200	30	
	8mm	3	10	7	-300/0	40	
		4	12	7	120/175	30	
	6mm	3	20	11	-300/0	50	
		4	22	10	120/175	30	
Effect of Bolt Size	10mm	2	14	0	400	0	
		3	4	6	-300/0	50	
Influence of Bolt Gauge	More	8mm	2	20	0	380	0
		8mm	3	8	10	-300/0	50
	Less	8mm	2	22	0	380	0
		8mm	3	10	6	-300/0	40
Influence of Bolt Pitch	More	8mm	2	22	0	380	0
		8mm	3	18	7	-300/0	40
	Less	8mm	2	16	0	380	0
		8mm	3	4	8	-300/0	40

Table 6-2 Web-cleat connection results from parametric studies

## **6.8 Conclusion**

This chapter provides an insight into the effects of loading and geometry changes on connection behaviour. In general loading rate did not change the behaviour significantly, however loading type could change the resistance, for instance loading the connection in pure tension showed the maximum tensile resistance. Making the bolt and washer stronger did not change the ductility or resistance significantly.

Using a bigger bolt size reduced the ductility and added resistance to the connection capacity. Increasing the bolt gauge increased the ductility but reduced the resistance, reducing the bolt gauge had the opposite effect. Changing the bolt pitch had a small effect on both ductility and resistance of the connection.



## 7 Parametric study of End-plate connection behaviour

This chapter presents a parametric study on end-plate connections investigating loading rates and connection geometry. The same loading rates and loading types were used as those explained in Chapter 6. The explicit time-step for these analyses was around  $1.1E-07$  resulting in an analysis time of 11 hours for 100ms and 6 days for 1s of dynamic analysis. Running time for the quasi-static model was around 12 hours for 350s of analysis. In total 230 different analyses were conducted on this type of connection.

The geometry of the end-plate connections was varied by changing the plate thickness, bolt and washer sizes, end distances, pitch and gauge. Also different loading types and rates were applied to the connection. A summary of the final results is provided at the end of this chapter but a brief overview is:

- Force and moment resistance of the connection were affected by different loading types as by applying moment the force resisted in the connection dropped dramatically.
- Less thickness in the plate increased the ductility and reduced the resistance of the whole connection.
- Using similar size but stronger bolts had no significant effect on the connection behaviour but slightly increased resistance and reduced ductility. Increasing the washer size had a similar effect.
- Using a larger diameter bolt increased the connection resistance but reduced its ductility.
- Bolt gauge directly affected ductility but reducing the bolt gauge did not change the resistance; increasing the bolt gauge reduced the resistance.
- Bolt pitch had an inverse relationship with ductility; however force and moment resistance showed no significant change.

## 7.1 Influence of different loading types and rates

This study on End-Plate connection models aimed to investigate (1) connection behaviour under different loading rates and (2) connection response under different loading types.

### 7.1.1 Column displacement in time

Plotting the displacement of each end of the column gives a qualitative understanding of the effect of loading rate. Figure 7-1 shows the results for 10mm thick end-plate and loading type 1 under different rates of loading. There is a qualitative change in connection response when the loading rate was between 350-1250kN/s.

Two impacts occurred, first as the column started to rotate and the top of the end-plate contacted with the beam web and caused some moment resistance to the connection, then as the beam flange struck the column flange and prying commenced. At lower rates of loading the time between these two impacts was obviously longer and made a plateau as shown in Figure 7-1. At higher loading rates the time between these two impacts was brief and no plateau was made.

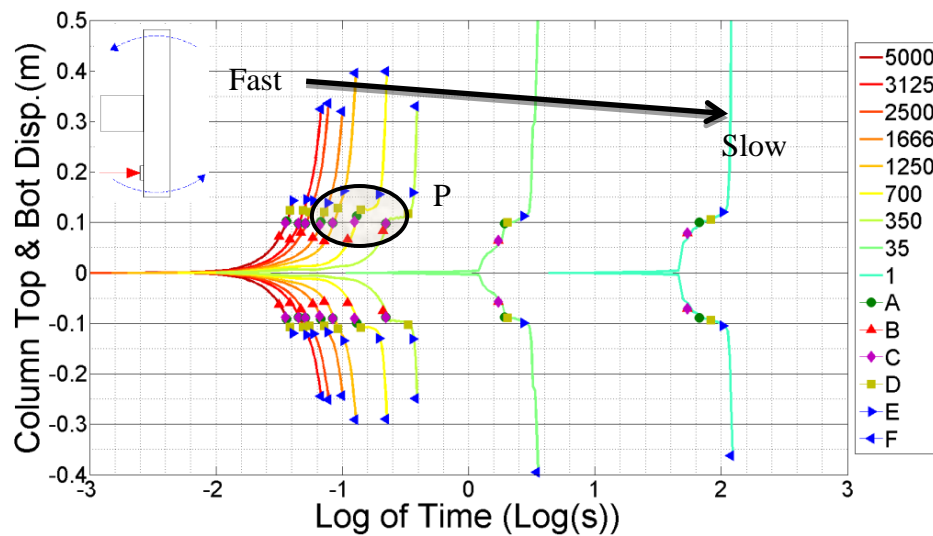


Figure 7-1 Column displacement time history LT1 10mm

(Coloured dots indicate the points at which: A- the beam and column flanges made contact and prying action commenced, B- failure at the top of the welding, C- 1<sup>st</sup> element was eroded at crack opening, D- Crack opened half way through the plate thickness, E- Crack fully opened through the plate thickness, F- Crack went through whole length of the end plate)

Applying the pure tension (LT2 loading arrangement) to the connection made it stronger, and analyses with higher rates did not reach failure (Figure 7-2). As expected, a crack was opened through the plate length at the same column displacement however there was a small rotation in the column due to accumulated numerical round-off errors, which led to a slight but insignificant rotation as shown in the displacement of both ends of the column.

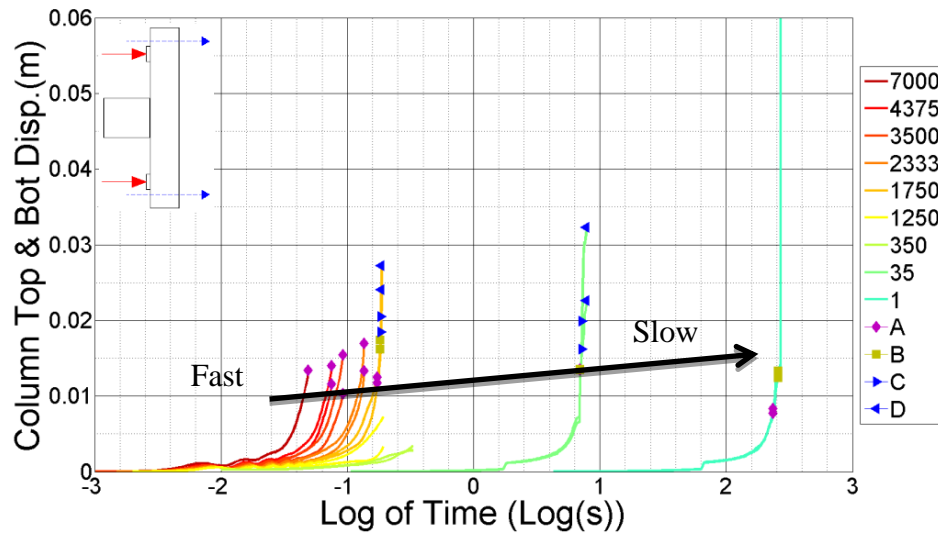


Figure 7-2 Column displacement time history LT2 10mm  
 (Coloured dots indicate the points at which: A- failure at the top of the welding, B- 1<sup>st</sup> element was eroded at crack opening, C- Crack opened half way through the plate thickness, D- Crack fully opened through the plate thickness)

Figure 7-3 and Figure 7-4 provide the results of column displacement time history when the connection was under loading types 3 and 4. The plateau due to the prying effect did not developed in loading type 4, which meant that the effect of flange impact was not significant in all loading rates.

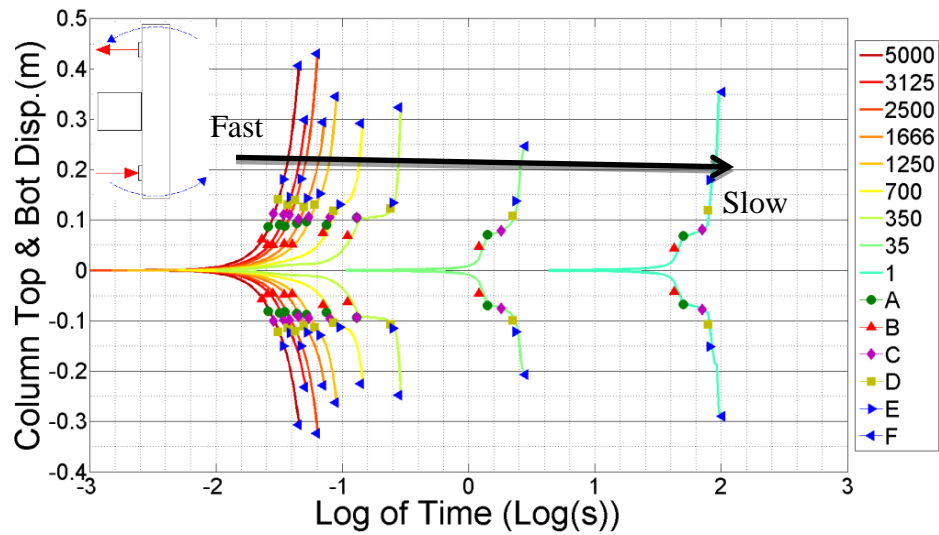


Figure 7-3 Column displacement time history LT3 10mm  
 (Coloured dots indicate the points at which: A- beam and column flanges made contact and prying action commenced, B- failure at the top of the welding, C- 1<sup>st</sup> element was eroded at crack opening, D- Crack opened half way through the plate thickness, E- Crack fully opened through the plate thickness, F- Crack went through whole length of the end plate)

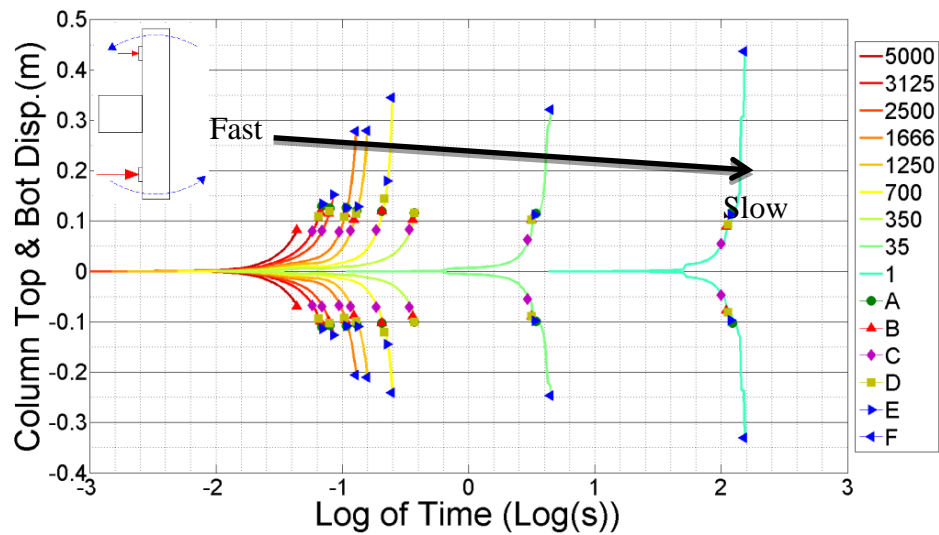


Figure 7-4 Column displacement time history LT4 10mm  
 (Coloured dots indicate the points at which: A- beam and column flanges made contact and prying action commenced, B- failure at the top of the welding, C- 1<sup>st</sup> element was eroded at crack opening, D- Crack opened half way through the plate thickness, E- Crack fully opened through the plate thickness, F- Crack went through whole length of the end plate)

### 7.1.2 Column response due to connection reaction

Plotting the column rotation against translation shows the effect of different loading types on connection behaviour.

Figure 7-5 shows the results of column rotation against column translation caused by different loading types and loading rates. Under pure tension (LT2) the column did not rotate. Applying the pure moment case (LT3) the column flange impact happened with smaller translation than the others. Loading type 4 had the highest translation at the time of flange impact, however all three cases (LT1, 3 and 4) behaved more or less similarly after the column impact and all had similar translation and rotation at failure. The area highlighted in Figure 7-5 gives the combination of rotations and translation under which the connection remains intact.

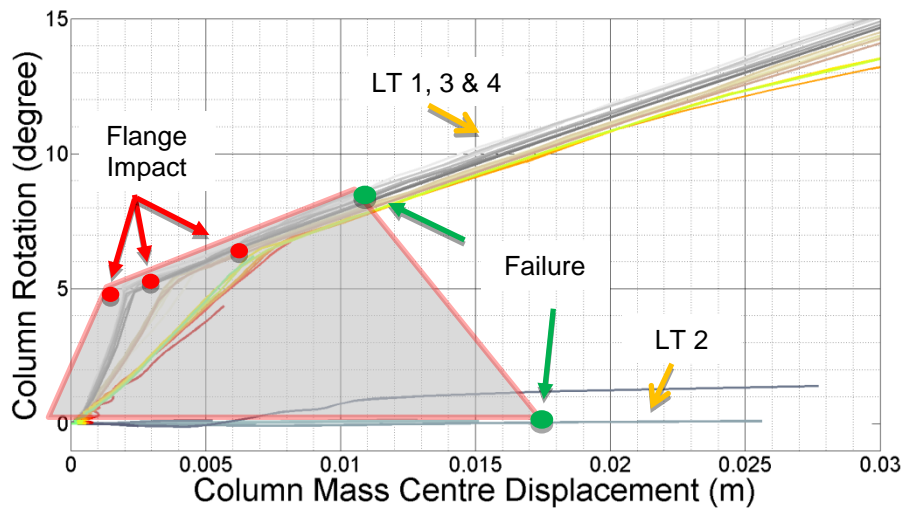


Figure 7-5 Column rotation against displacement LT1-4 10mm

Having a thinner end-plate delayed the flange impact between the beam and column, and the failure happened with more column translation and rotation as the 8mm plate deformed more. Results for column rotation and translation are provided in Figure 7-6 for both 10 and 8mm thicknesses, under loading type 1.

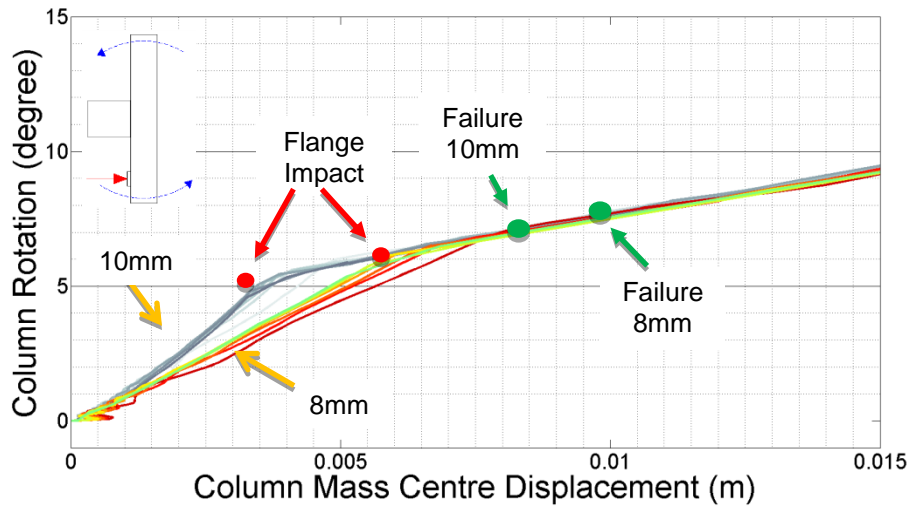
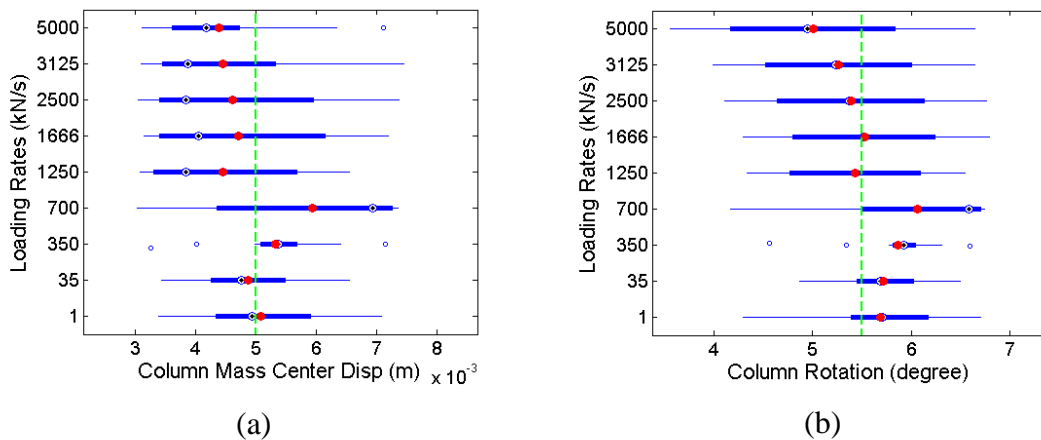
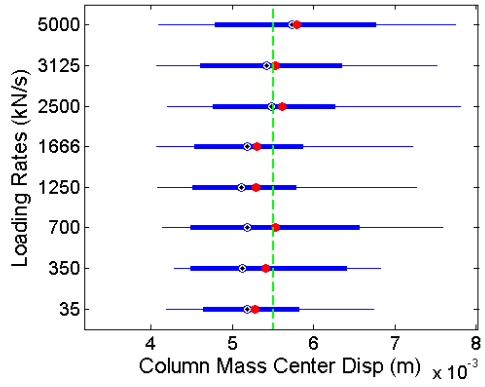


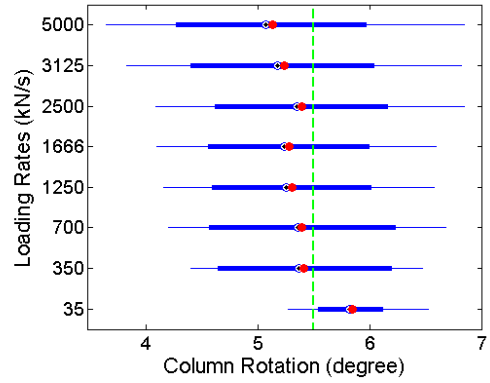
Figure 7-6 Column rotation against displacement LT1 10-8mm

Figure 7-7 and Figure 7-8 show the median and mean value of the column rotation and translation for two different thicknesses and loading types (LT1 and 2). These values are calculated based on the column movement from first element failure until the time that the first crack progresses through the end plate. Column rotation and translation averages were slightly less in the 10mm thick end-plate. Pure tension loading (LT2) had no rotation and much lower translation compared to other loading types and the connection behaved in a less ductile manner but was stronger in this loading condition.



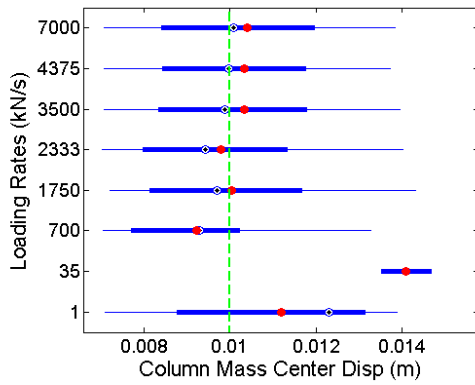


(c)

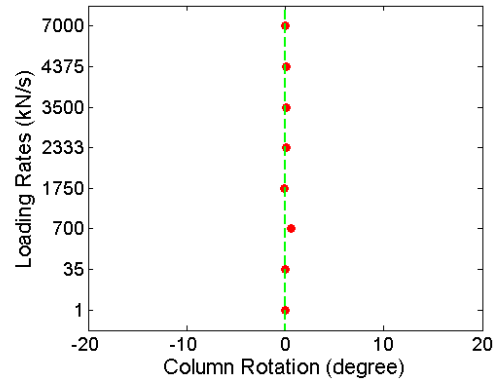


(d)

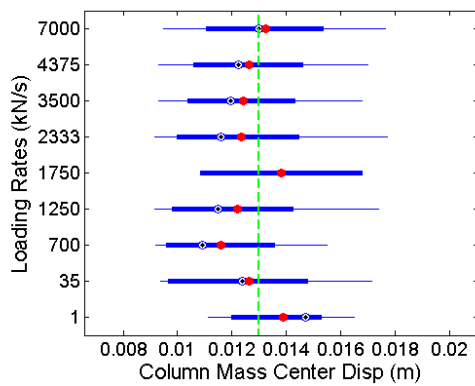
Figure 7-7 Median and mean value of column rotation and translation for LT1 (a,b) 10mm thick plate (c, d) 8mm thick plate



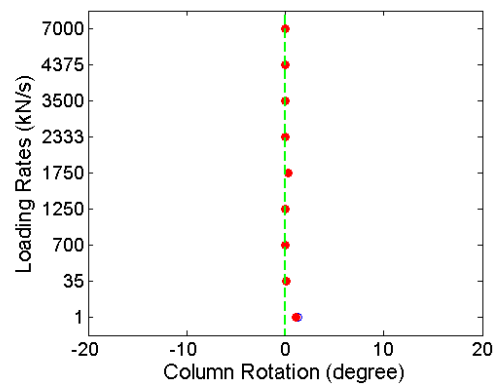
(a)



(b)



(c)



(d)

Figure 7-8 Median and mean value of column rotation and translation for LT2 (a,b) 10mm thick plate (c, d) 8mm thick plate

### 7.1.3 Deformation of the End-plate

Plate deformation was measured from displacement points on the end-plate, one close to the welding and one at the free end (Figure 7-9).

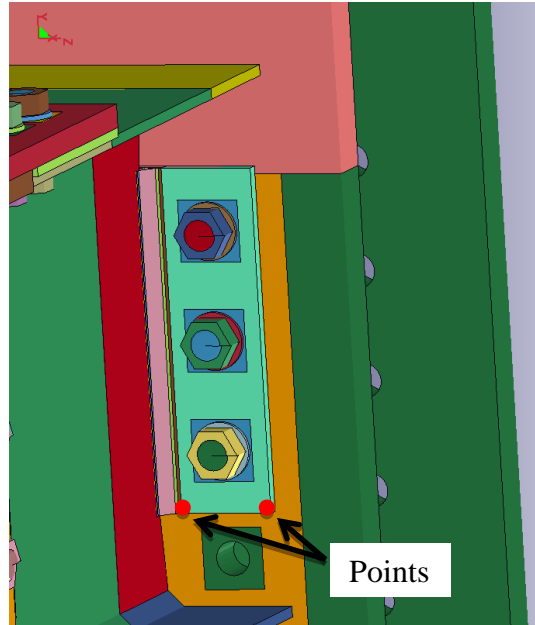


Figure 7-9 two measured points on the end-plate

Figure 7-10 and Figure 7-11 provide the displacement of these two points for the end-plate connection under loading type 1 and 3 with different plate thicknesses. Loading rate had an effect on the plate deformation (static results were not smooth as the dynamic analysis had bigger output intervals). Reducing the plate thickness increased the plate deformation and connection ductility.

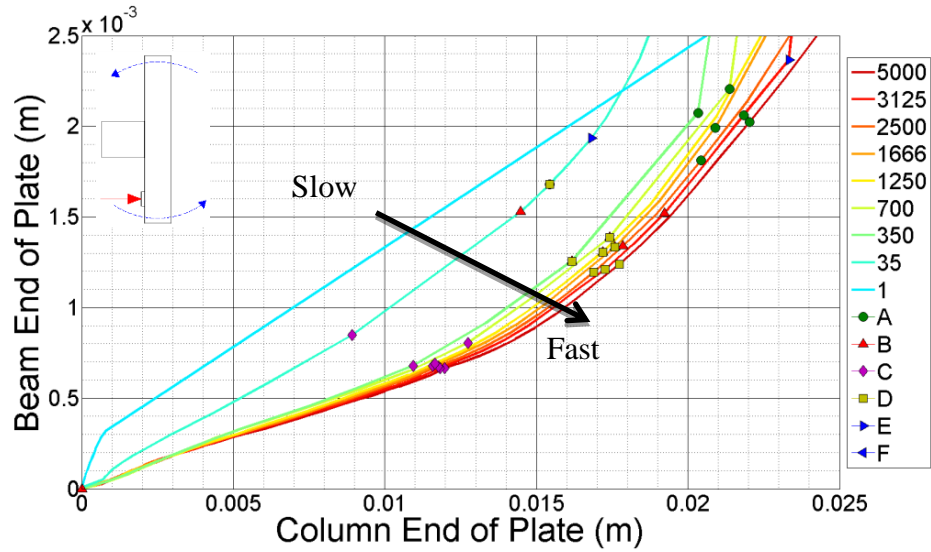


Figure 7-10 Displacement of the two corner LT1 8mm  
 (Coloured dots indicate the points at which: A- beam and column flanges made contact and prying action commenced, B- failure at the top of the welding, C- 1<sup>st</sup> element was eroded at crack opening, D- Crack opened half way through the plate thickness, E- Crack fully opened through the plate thickness, F- Crack went through whole length of the end plate)

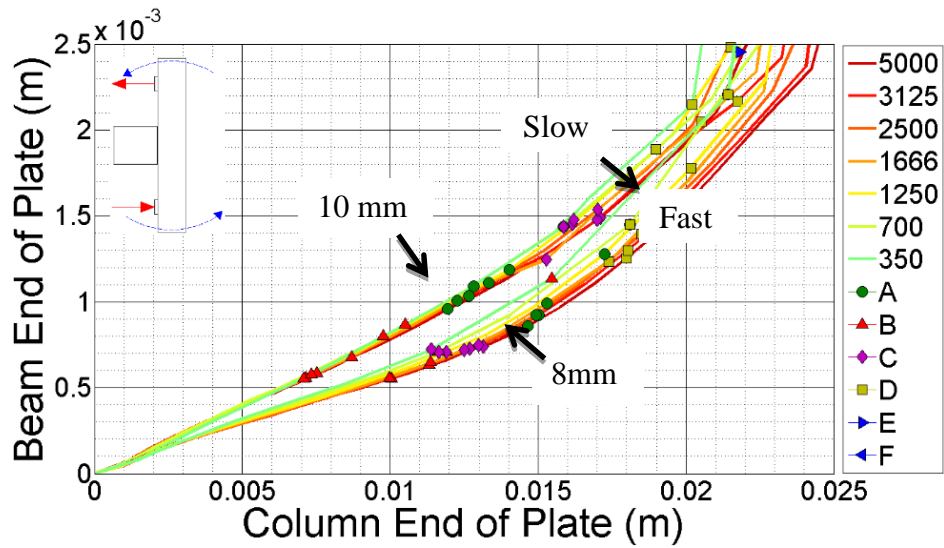


Figure 7-11 Displacement of the two corner LT3 8mm  
 (Coloured dots indicate the points at which: A- beam and column flanges made contact and prying action commenced, B- failure at the top of the welding, C- 1<sup>st</sup> element was eroded at crack opening, D- Crack opened half way through the plate thickness, E- Crack fully opened through the plate thickness, F- Crack went through whole length of the end plate)

#### **7.1.4 Connection force resistance**

Figure 7-12 to Figure 7-15 show the relationship between the axial resistance of the connection and central column axial displacement when loading rates and load types vary. Connection resistance in the dynamic tests was calculated as set out in Section 3.2.3 by subtracting the translational inertial force accelerating the column from the applied load.

Results for 10mm thick end-plate and loading type 1 are shown in Figure 7-12. To make the graph clearer only a sub-set of results for different loading rates is provided but other results follow the same trends. This graph shows that connection axial resistance and stiffness was more or less rate-independent until some elements were failed at the top of the welding, which was the time that the plate top impacted on the beam web. After this stage, the force resistance and column axial displacement increased as the loading rates increased. In the dynamic analysis, as the crack opened half way through the plate thickness, the column developed acceleration and caused the crack to travel faster along the plate length, so the force resistance in the connection dropped after this stage to the lower level of the quasi-static runs.

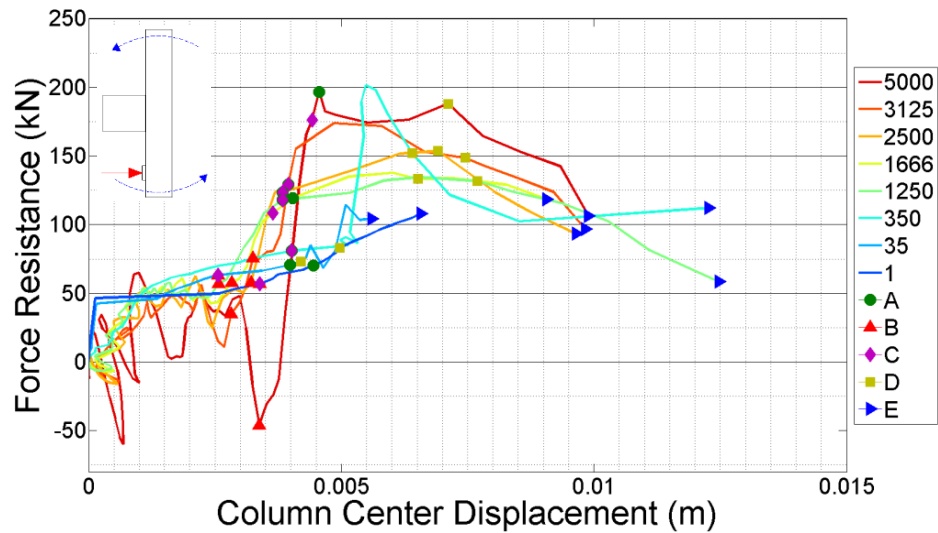


Figure 7-12 Force and column displacement LT1 10mm  
 (Coloured dots indicate the points at which: A- beam and column flanges made contact and prying action commenced, B- failure at the top of the welding, C- 1<sup>st</sup> element was eroded at crack opening, D- Crack opened half way through the plate thickness, E- Crack fully opened through the plate thickness)

Figure 7-13 shows the resistance of the 10mm thick plate connection under pure tension (LT2) and different loading rates. As the connection behaved stronger in this type of loading some analyses with high loading rates were impossible to fail as these models became unstable. As the pattern of these dynamic results show, the resistance increased as the loading rate increased. Thinner end-plates had lower resistance but the influence of the loading rate was the same.

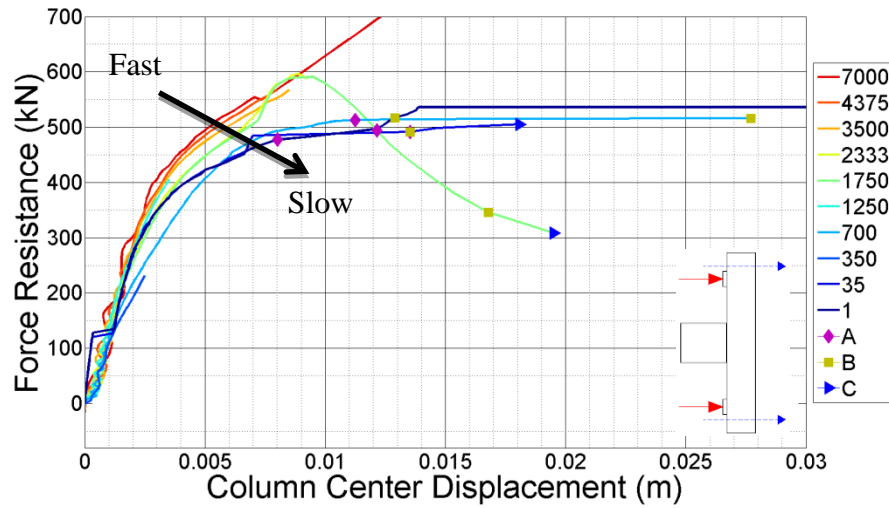


Figure 7-13 Force and column displacement LT2 10mm  
 (Coloured dots indicate the points at which: A- beam and column flanges made contact and prying action commenced, B- failure at the top of the welding, C- 1<sup>st</sup> element was eroded at crack opening)

Figure 7-14 shows the axial force in the connection under pure moment (LT3) and different loading rates. In principal under static loading, applied coupled loads should generate no axial force. However, as mentioned before, and provided in the graph, as the loading rate gets faster a compression force develops into the connection which was because of the inertia and the impact of the beam flange to the column. After having the impact between the plate and beam web (point B) this compression force was reduced as the column slowed down and its acceleration dropped, however after a crack opening in the plate column acceleration raised and compression increased again.

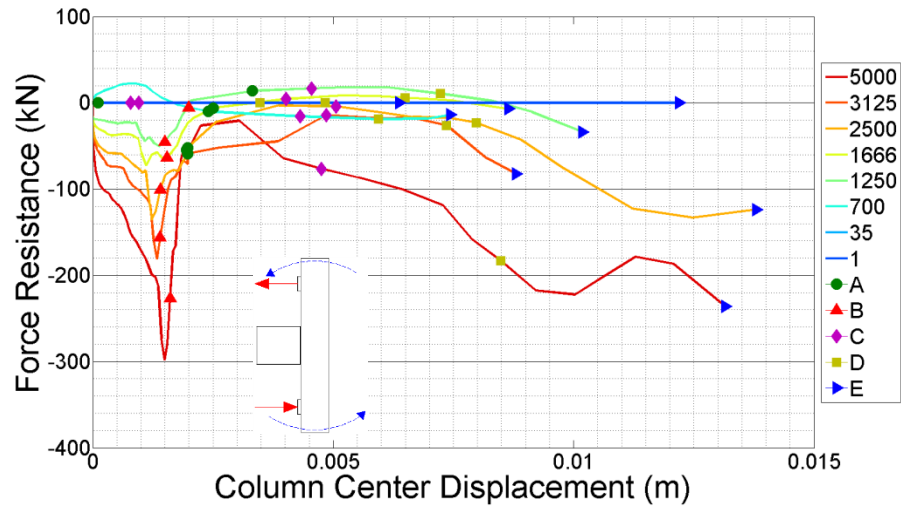


Figure 7-14 Force and column displacement LT3 10mm  
 (Coloured dots indicate the points at which: the A- beam and column flanges made contact and prying action commenced, B- failure at the top of the welding, C- 1<sup>st</sup> element was eroded at crack opening, D- Crack opened half way through the plate thickness, E- Crack fully opened through the plate thickness)

Figure 7-15 shows the force resistance of 10mm thick end-plate connection under loading type 4 and different loading rates. Like the web-cleat connection, the end-plate connection was sensitive to loading rates with this type of loading. The magnitude of the resistance increased as the rate of loading was increased too, also this magnitude was between the pure tension (LT2) and loading type 1.

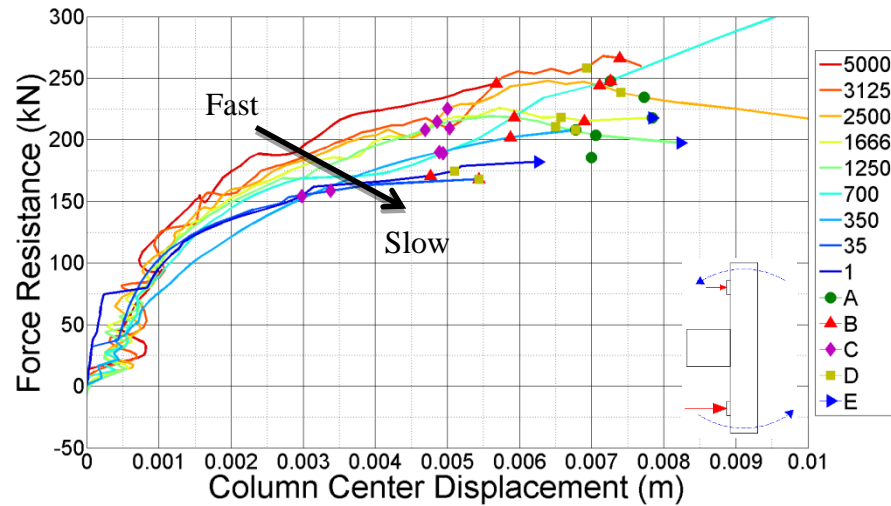


Figure 7-15 Force and column displacement LT4 10mm  
 (Coloured dots indicate the points at which: A- beam and column flanges made contact and prying action commenced, B- failure at the top of the welding, C- 1<sup>st</sup> element was eroded at crack opening, D- Crack opened half way through the plate thickness, E- Crack fully opened through the plate thickness)

### 7.1.5 Connection moment resistance

As previously mentioned (in Section 3.2.3), the moment resistance was determined by subtracting the inertial moment of the column from the applied moment. Figure 7-16 shows the relationship between moment resistance of the 10mm thick end-plate and column rotation under loading type 1 and different loading rates. There was no significant change in moment resistance of the connection when different loading rates were applied but the dynamic analysis resistance dropped after a crack opened halfway through the plate thickness and the column picked up more acceleration.

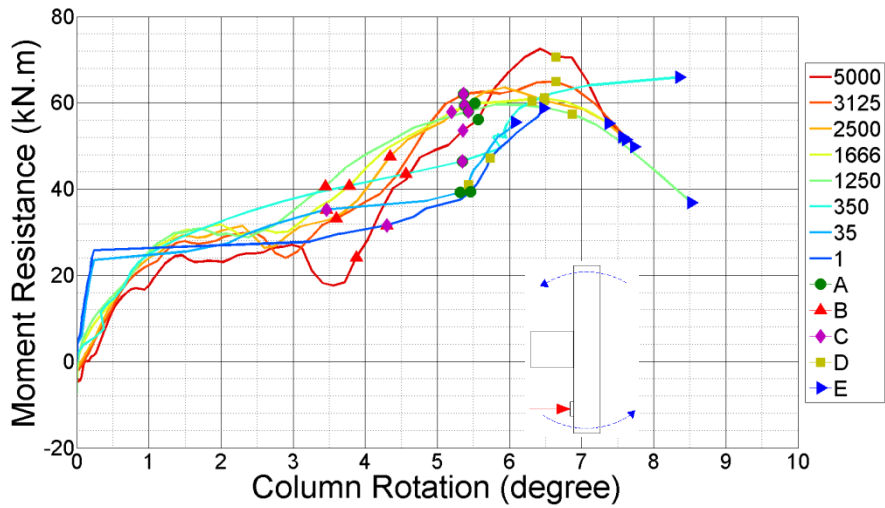
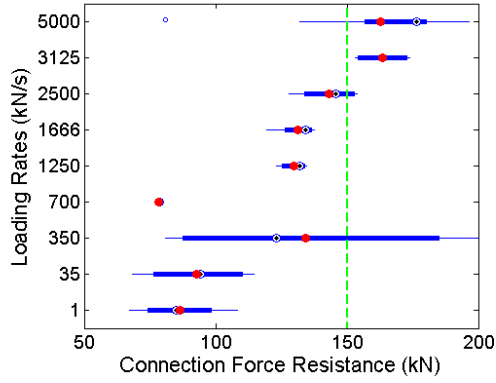


Figure 7-16 Moment and column rotation LT1 10mm  
 (Coloured dots indicate the points at which: A- beam and column flanges made contact and prying action commenced, B- failure at the top of the welding, C- 1<sup>st</sup> element was eroded at crack opening, D- Crack opened half way through the plate thickness, and E- Crack fully opened through the plate thickness)

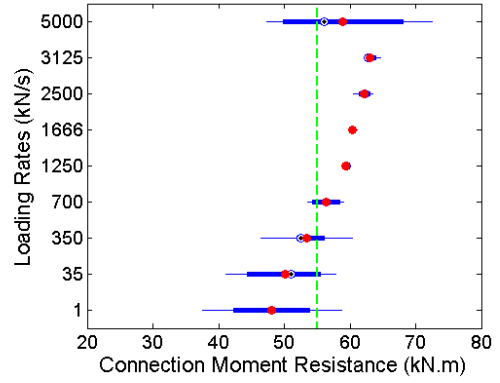
### 7.1.6 Median and mean values of force and moment resisted in the connection

Median and mean values were used to in understanding the range of connection resistance. The calculations were performed on the data from the time of plate impact to the beam web up to just after the crack started to open. Figure 7-17 and Figure 7-18 provide these values for both 10 and 8mm thick plate connections under different loading rates and types (LT1, 2).

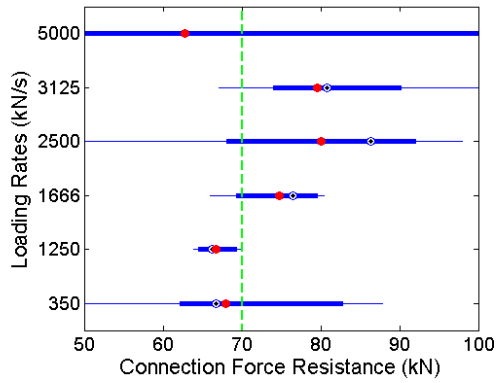
The 8mm thick plate connection had less resistance than the 10mm thick plate connection and also more ductility. No moment resistance was observed in the case of pure tension loading type, as expected. In general, rotation of the connection reduced the resistance, which is important when assessing connection behaviour and structural integrity.



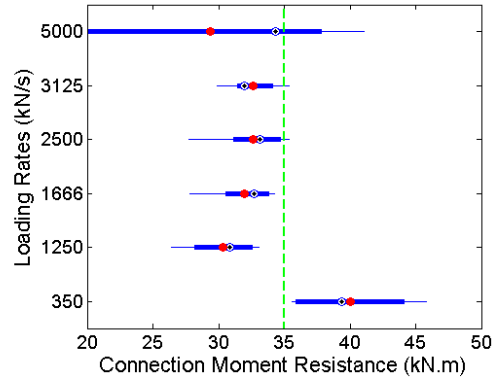
(a)



(b)

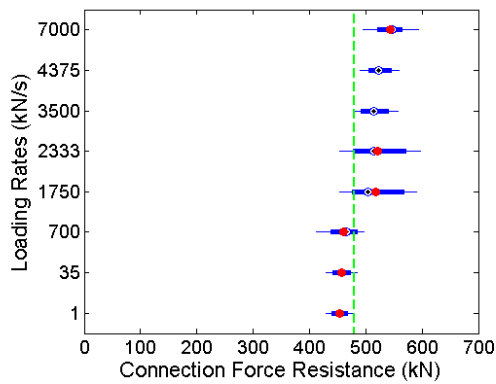


(c)

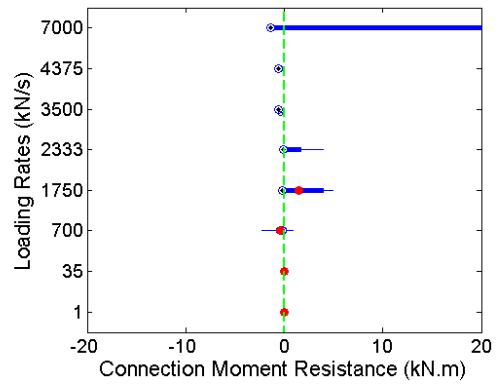


(d)

Figure 7-17 Median and mean value of the force and moment resistance for LT1 (a,b) 10mm thick plate (c,d) 8mm thick plate



(a)



(b)

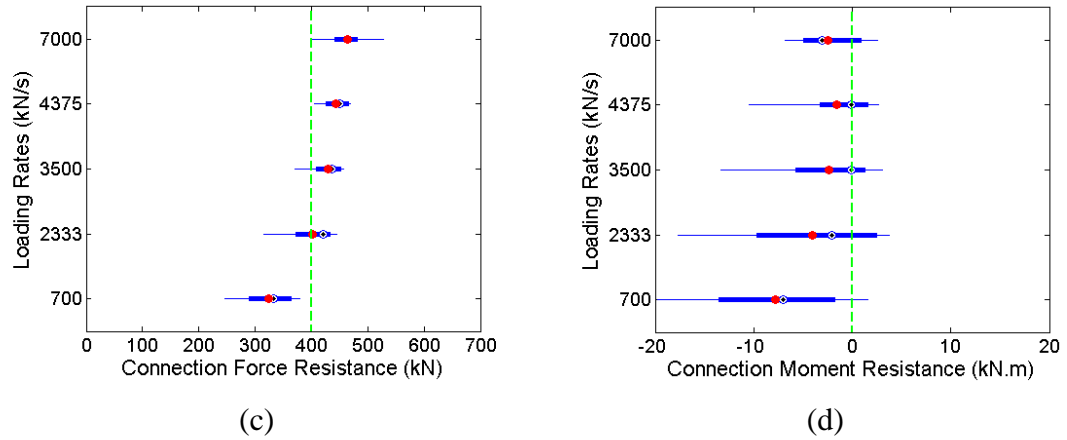


Figure 7-18 Median and mean value of the force and moment resistance for LT2 (a,b) 10mm thick plate (c,d) 8mm thick plate

## 7.2 Influence of bolt strength on connection behaviour

As discussed in Section 6.3, bolt deformation can be significant particularly if plastic bending occurs. To check the effect of this phenomenon on connection behaviour a series of models was analysed with bolt strength increased by 5 times that of the original M20 bolt strength. The results indicated that this reduction in bolt deformation had a marginal but not significant effect on the connection behaviour and resistance. Illustrative examples are shown in Figure 7-19 and Figure 7-20.

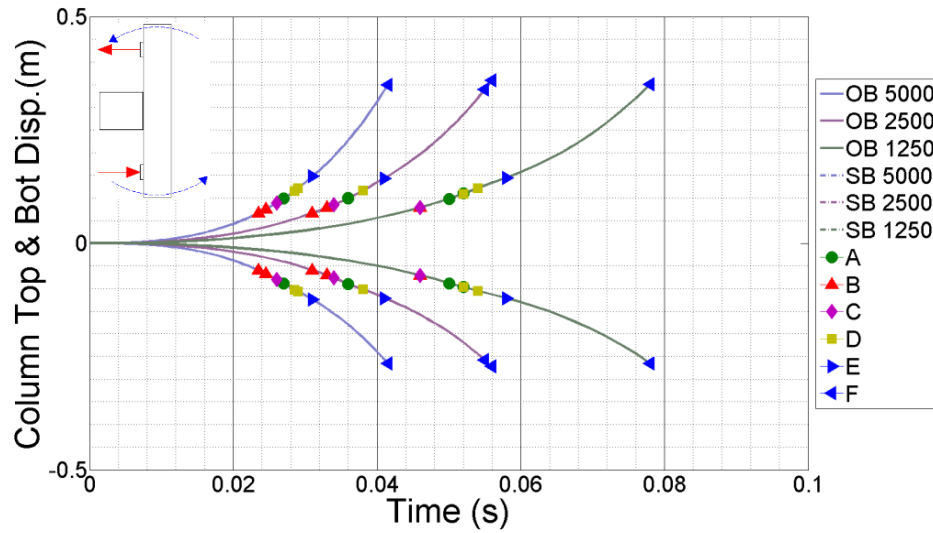


Figure 7-19 Column displacement time history for strong bolt LT3 8mm, OB is original bolt and SB is stronger bolt simulations.

(Coloured dots indicate the points at which: A- beam and column flanges made contact and prying action commenced, B- failure at the top of the welding, C- 1<sup>st</sup> element was eroded at crack opening, D- Crack opened half way through the plate thickness, E- Crack fully opened through the plate thickness, F- Crack went through whole length of the end plate)

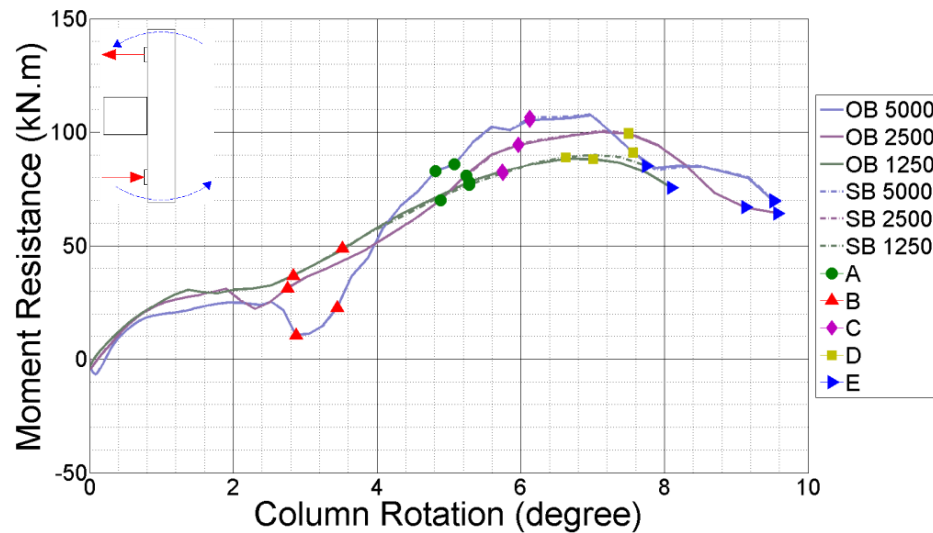


Figure 7-20 Moment and column rotation by strong bolt LT3 10mm, OB is original bolt and SB is stronger bolt simulations.

(Coloured dots indicate the points at which: A- beam and column flanges made contact and prying action commenced, B- failure at the top of the welding, C- 1<sup>st</sup> element was eroded at crack opening, D- Crack opened half way through the plate thickness, E- Crack fully opened through the plate thickness)

### 7.3 Effect of washer size on connection behaviour

Washer size could have an effect on plate behaviour and because of that a series of analyses was conducted just changing the washer size from 20 to 24. For this study three different dynamic loading rates were used as well as two different loading type (LT2 and LT3) and two thicknesses of the plate. No significant influence was observed as the washer size increased. Illustrative results are shown here in Figure 7-21 and Figure 7-22.

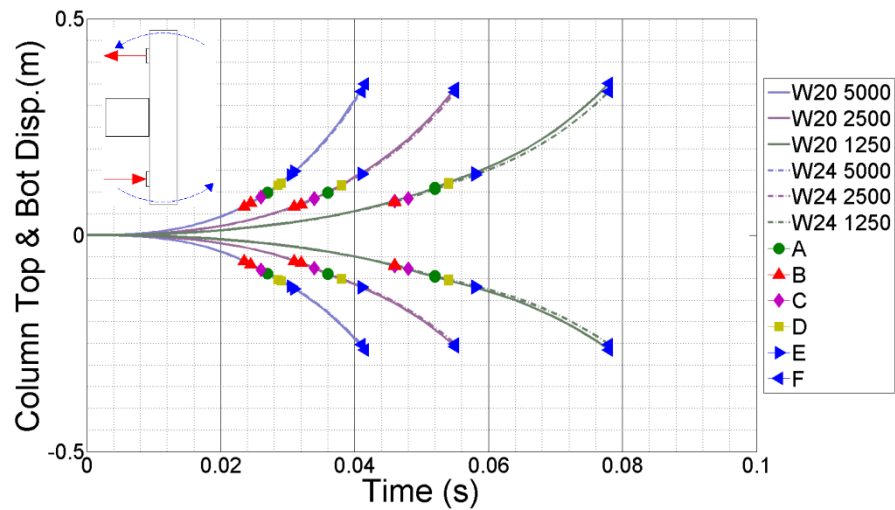


Figure 7-21 Column displacement time history by washer size 24 LT3 8mm; W20 is original washer size 20 and W24 is the washer size 24 simulations.

(Coloured dots indicate the points at which: A- beam and column flanges made contact and prying action commenced, B- failure at the top of the welding, C- 1<sup>st</sup> element was eroded at crack opening, D- Crack opened half way through the plate thickness, E- Crack fully opened through the plate thickness, F- Crack went through whole length of the end plate)

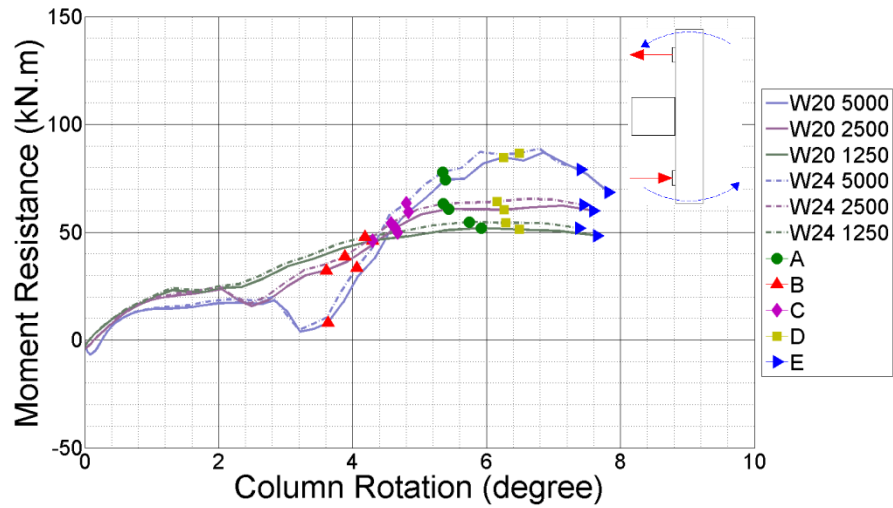


Figure 7-22 Moment and column rotation by washer size 24 LT3 8mm; W20 is original washer size 20 and W24 is the washer size 24 simulations.

(Coloured dots indicate the points at which: A- beam and column flanges made contact and prying action commenced, B- failure at the top of the welding, C- 1<sup>st</sup> element was eroded at crack opening, D- Crack opened half way through the plate thickness, E- Crack fully opened through the plate thickness)

## 7.4 Effect of Bolt Size on Connection Behaviour

To understand the influence of bolt size on connection behaviour, M20 bolts were replaced by M24 bolts in the model. For this study three different dynamic loading rates were used as well as two different loading types (LT2 and LT4) and two thicknesses of the plate, illustrative results are discussed in detail here.

### 7.4.1 Column displacement in time

Figure 7-23 and Figure 7-24 present the displacement of each end of the column when the connection (with an 8mm thick endplate) was under pure tension (LT2) and loading type four (LT4). Results are shown for the connection with the original M20 bolt size (denoted “B20”) and for bolt size M24 (denoted “B24”). Overall, using bigger bolts made the connection stronger but less ductile, and the connection did not fail even under pure tension loading type (LT2)

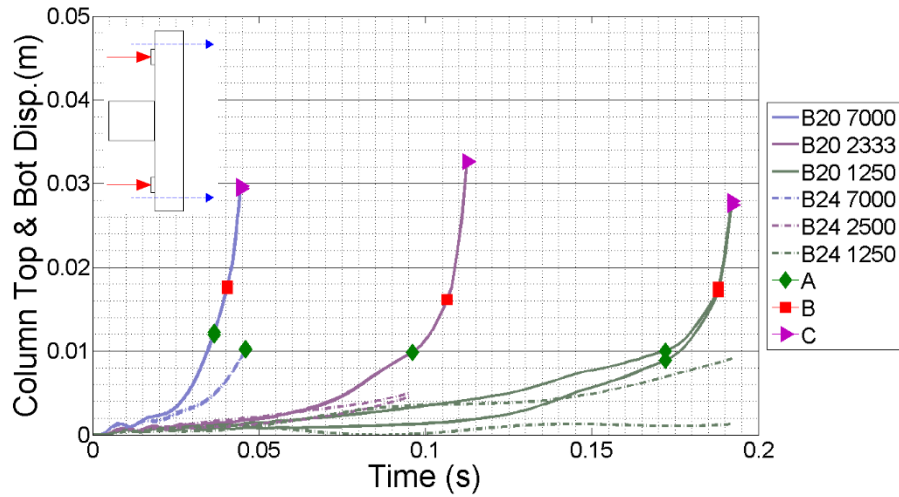


Figure 7-23 Column displacement time history by bolt M24 LT2 8mm, B20 is original bolt size 20 and B24 is the bolt size 24 simulations.  
 (Coloured dots indicate the points at which: A- 1<sup>st</sup> element was eroded at crack opening, B- Crack opened half way through the plate thickness, C- Crack fully opened through the plate thickness)

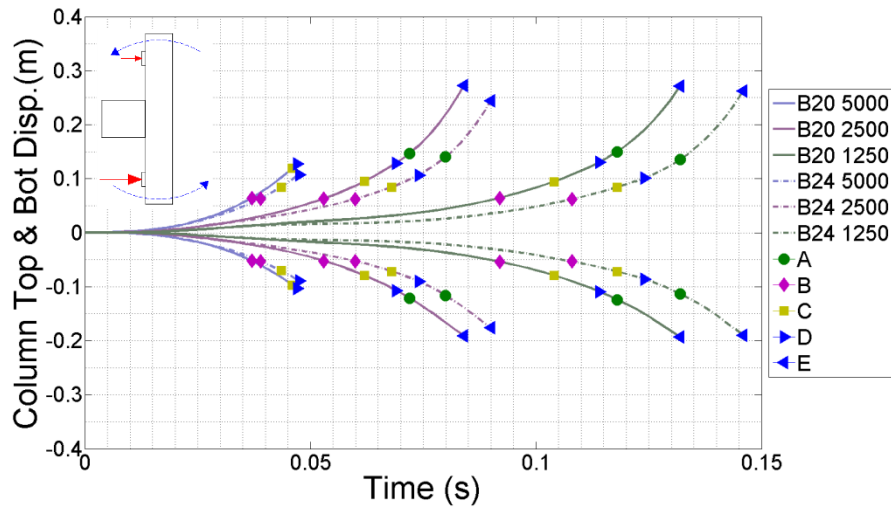


Figure 7-24 Column displacement time history by bolt M24 LT4 8mm, B20 is original bolt size 20 and B24 is the bolt size 24 simulations.  
 (Coloured dots indicate the points at which: A- beam and column flanges made contact and prying action commenced, B- failure at the top of the welding, C- 1<sup>st</sup> element was eroded at crack opening, D- Crack opened half way through the plate thickness, E- Crack fully opened through the plate thickness)

### 7.4.2 Deformation of the End-plate

Deformation of the end-plate was measured by the same method as explained in Section 7.2.3. Figure 7-25 shows the displacement of two points on the end-plate, and illustrate that plate deformation reduced dramatically. Less bolt gauge made the end-plate deform less and caused the connection to behave more rigidly.

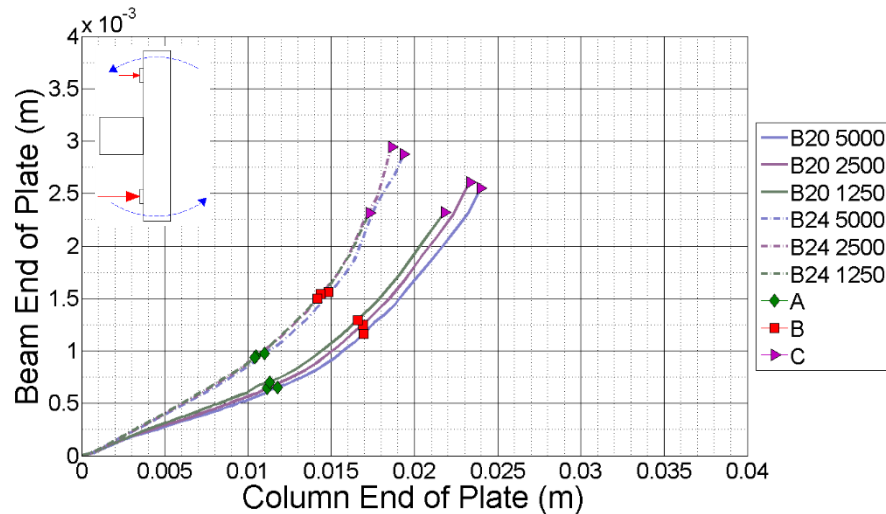


Figure 7-25 Displacement of the two corner by bolt M24 LT4 8mm, B20 is original bolt size 20 and B24 is the bolt size 24 simulations.

(Coloured dots indicate the points at which: A- Having failure at the top of the welding, B- 1<sup>st</sup> element was eroded at crack opening, C- Crack opened half way through the plate thickness)

### 7.4.3 Connection force resistance

Figure 7-26 shows the connection axial force resistance against translation for pure tension loading (LT2), for different loading rates, an 8mm thick end-plate and different bolt sizes. The force resistance was increased for the larger bolt size and the connection did not reach the failure stage.

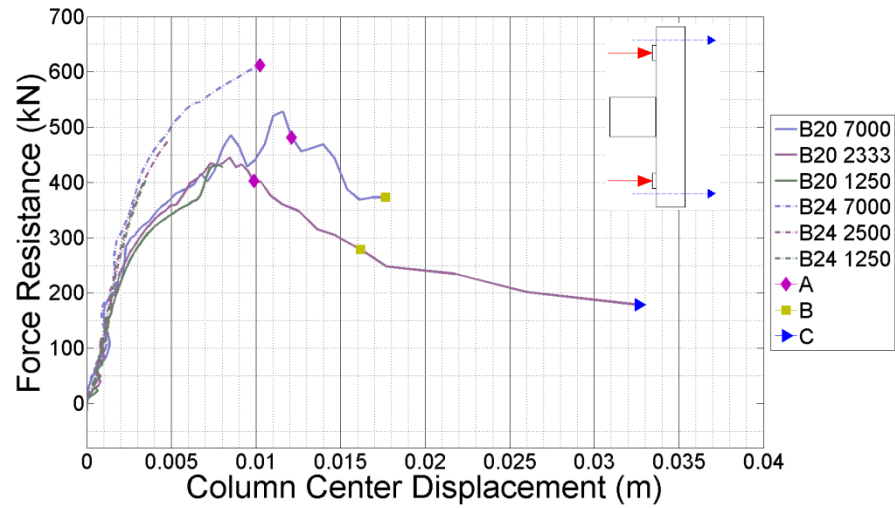


Figure 7-26 Force and column displacement by bolt M24 LT2 8mm, B20 is original bolt size 20 and B24 is the bolt size 24 simulations.  
 (Coloured dots indicate the points at which: A- Having failure at the top of the welding, B- 1<sup>st</sup> element was eroded at crack opening, C- Crack opened half way through the plate thickness)

#### 7.4.4 Connection moment resistance

Figure 7-27 shows the moment resisted by the connection plotted against the column rotation, under loading type four (LT4), for different loading rates, bolt sizes and an 8mm thick end-plate. The moment resistance increased with bolt size and the column had slightly less rotation when the failures happened.

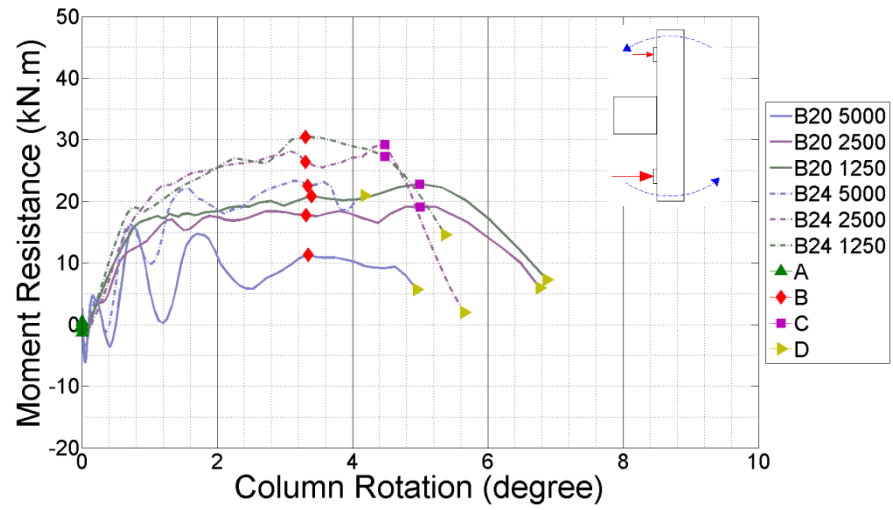


Figure 7-27 Moment and column rotation by bolt M24 LT4 8mm, B20 is original bolt size 20 and B24 is the bolt size 24 simulations.

(Coloured dots indicate the points at which: A- beam and column flanges made contact and prying action commenced, B- failure at the top of the welding, C- 1<sup>st</sup> element was eroded at crack opening, D- Crack opened half way through the plate thickness)

## 7.5 Influence of bolt gauge on connection behaviour

A study was conducted of the influence of changing the bolt gauge in end-plate connections. Two different plate thicknesses, two different loading types (LT2 and LT3) and three different loading rates were considered with bolt gauges changed by +/-10mm from the original bolt gauge of 90mm.

Figure 7-28(b) shows the shear stress developed in the plate at a loading rate of 3500kN/s under loading type two for the case with the original bolt gauge. The shear stress developed for the other cases is shown in (a) and (c).

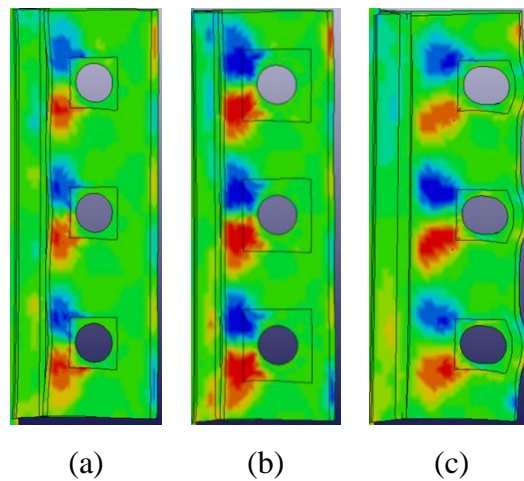


Figure 7-28 Shear stress generated in the connection  
(a) less (b) original (c) more bolt gauge

Changing the bolt gauge also changed the plate deformation. More deformation occurred with a larger bolt gauge. A plot of the deformations are provided in Figure 7-29 in which the green area between the bolt holes and the beam web shows the plastic area; this green area was the smallest in the case of less bolt gauge.

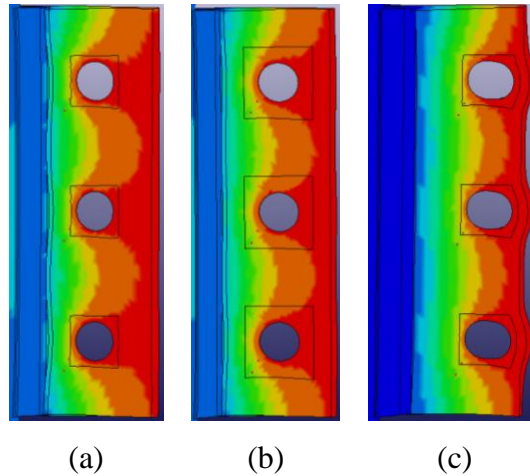


Figure 7-29 End plate deformation contour plot  
 (a) less (b) original (c) more bolt gauge

### 7.5.1 Column displacement in time

By reducing the bolt gauge the connection became rigid and the column moved less in time. Figure 7-30 shows the column displacements at two ends for simulations with the original 90mm bolt gauge (OBG) and 10mm less bolt gauge (LBG), under pure tension loading type (LT2) and three different loading rates and an 8mm thick end-plate. The connection became more brittle and it failed with less column displacement.

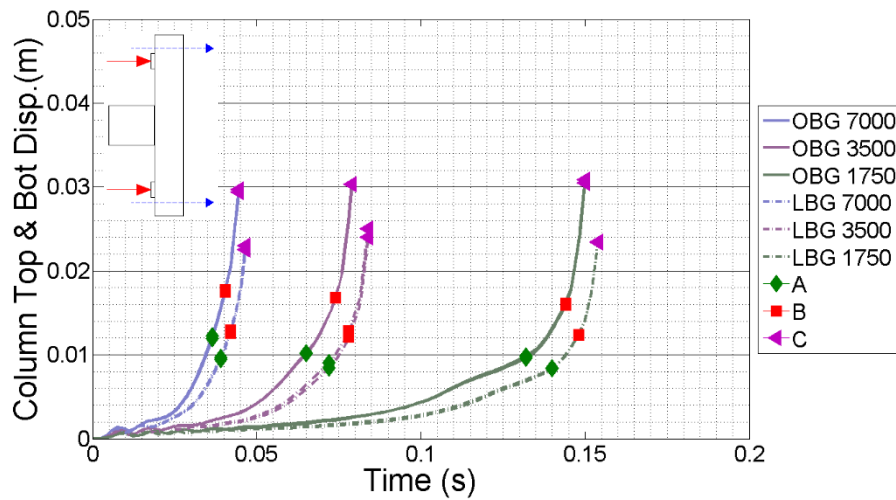


Figure 7-30 Column displacement time history by BG less LT2 8mm, OBG is original bolt gauge (90mm) and LBG is the lower bolt gauge (80mm) simulation.  
 (Coloured dots indicate the points at which: A- beam and column flanges made contact and prying action commenced, B- failure at the top of the welding, C- Crack opened half way through the plate thickness)

As expected, adding 10mm to the bolt gauge distance caused the connection to behave in a more ductile fashion and with less rigidity. Figure 7-31 provides the column displacement time history in the case of pure tension and an 8mm thick end plate for the connection with the original 90mm bolt gauge (OBG) and 10mm more bolt gauge (MBG).

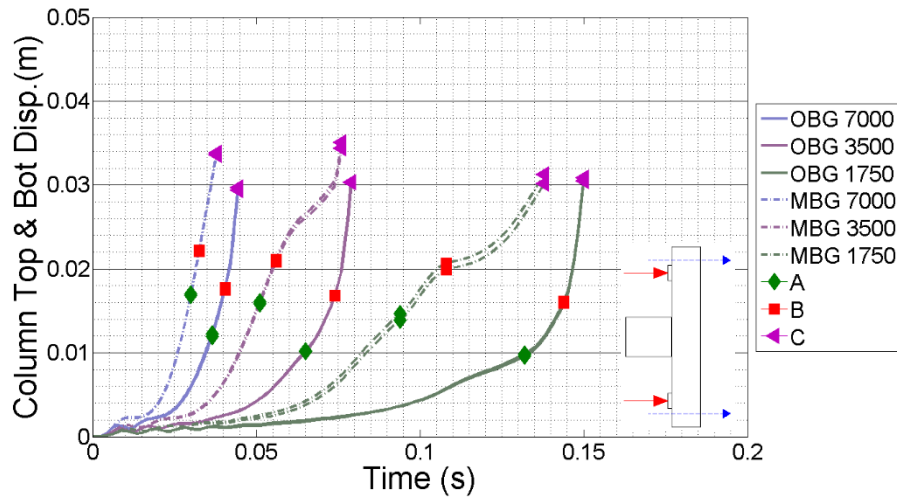


Figure 7-31 Column displacement time history by BG more LT2 8mm, OBG is original bolt gauge and MBG is the maximum bolt gauge simulation.

(Coloured dots indicate the points at which: A- beam and column flanges made contact and prying action commenced, B- failure at the top of the welding, C -Crack opened half way through the plate thickness)

### 7.5.2 Deformation of the End-plate

Figure 7-32 provides the results for both cases of adding and reducing the bolt gauge by 10mm (MBG and LBG). As expected having more bolt gauge increased the plate deformation and increased the connection ductility, however reducing the bolt gauge did not change the plate deformation significantly and the connection became more rigid by a small amount. The influence of reducing the bolt gauge was greater for angle deformations in web-cleat connections (Section 6.6.2) than end-plate connections, and the reason was the type of the failure, because in the case of the web-cleat connection the beam web was the cause of failure and this mode was able to resist more shear than the plate tearing failure mode.

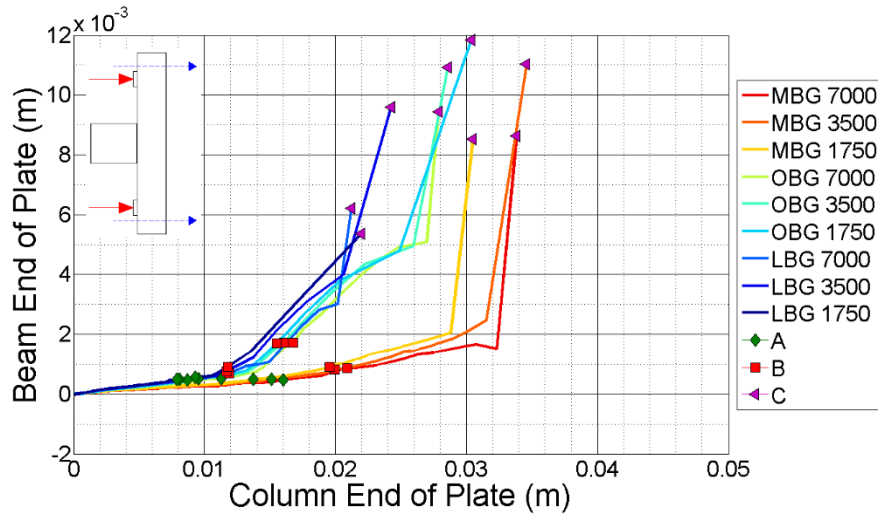


Figure 7-32 Displacement of the two corner by BG less and more LT2 8mm, OBG is original bolt gauge (90mm), MBG is the maximum bolt gauge simulation and LBG is the lower bolt gauge (80mm) simulation.

(Coloured dots indicate the points at which: A- 1<sup>st</sup> element was eroded at crack opening, B- Crack opened half way through the plate thickness, C- Cracked fully opened through the plate thickness)

### 7.5.3 Connection force resistance

At the highest loading rate reducing the bolt gauge did not change the resistance of the connection, however at lower rates it reduced the force resistance. Having a higher loading rate means less time for the plate to deform and resistance becomes controlled by plate failure alone. Figure 7-33 provides the results for force resistance vs column centre translation for 10mm less bolt gauge (LBG) with different loading rates, pure tension loading (LT2) and an 8mm thick end plate.

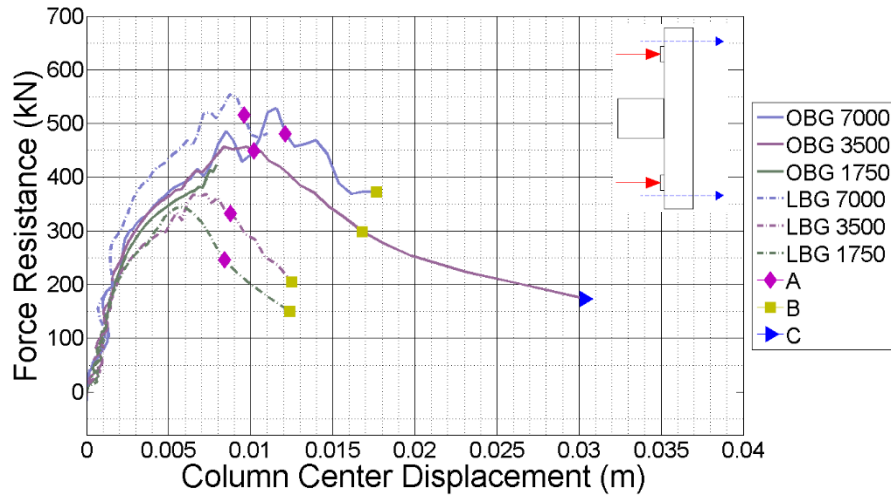


Figure 7-33 Force and column displacement by BG less LT2 8mm, OBG is original bolt gauge (90mm) and LBG is the lower bolt gauge (80mm) simulation.  
 (Coloured dots indicate the points at which: A- 1<sup>st</sup> element was eroded at crack opening, B- Crack opened half way through the plate thickness, C- Cracked fully opened through the plate thickness)

10mm more bolt gauge (MBG) gave the connection more ductility, and similar to the less gauge case, under high loading rate the connection had the same resistance. Figure 7-34 provides the results for the increased bolt gauge case (MBG) under pure tension losing type (LT2), with different loading rates and an 8mm thick end-plate connection.

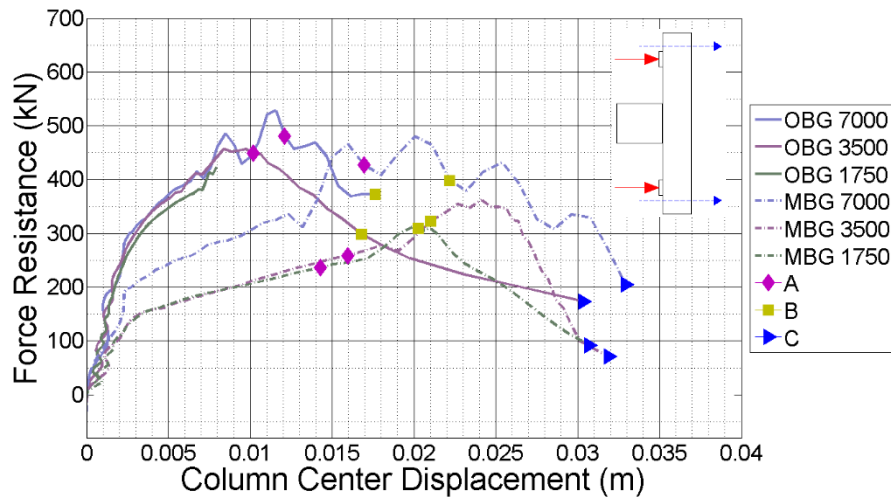


Figure 7-34 Force and column displacement by BG more LT2 8mm, OBG is original bolt gauge and MBG is the maximum bolt gauge simulation.  
 (Coloured dots indicate the points at which: A- 1<sup>st</sup> element was eroded at crack opening, B- Crack opened half way through the plate thickness, C- Cracked fully opened through the plate thickness)

#### 7.5.4 Connection moment resistance

Having less bolt gauge had an insignificant effect on connection moment resistance, however adding 10mm to the bolt gauge distance gave the connection more ductility but maintained the same moment resistance. Figure 7-35 and Figure 7-36 compare the 10mm less bolt gauge (LBG) and more bolt gauge (MBG) cases with the original (90mm) position under pure moment loading type with a range of loading rates and 8mm thick end-plate connection.

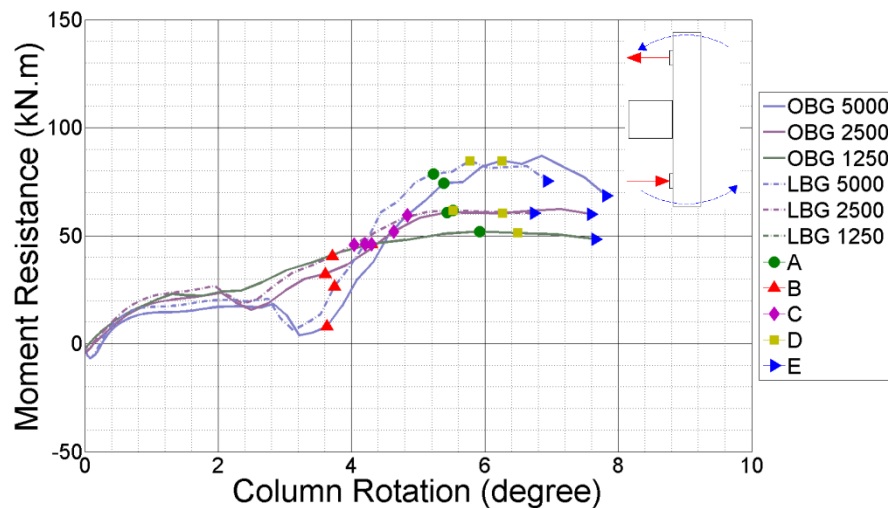


Figure 7-35 Moment and column rotation by BG less LT3 8mm, OBG is original bolt gauge (90mm) and LBG is the lower bolt gauge (80mm) simulation.

(Coloured dots indicate the points at which: A- beam and column flanges made contact and prying action commenced, B- failure at the top of the welding, C- 1<sup>st</sup> element was eroded at crack opening, D- Crack opened half way through the plate thickness, E- Crack fully opened through the plate thickness)

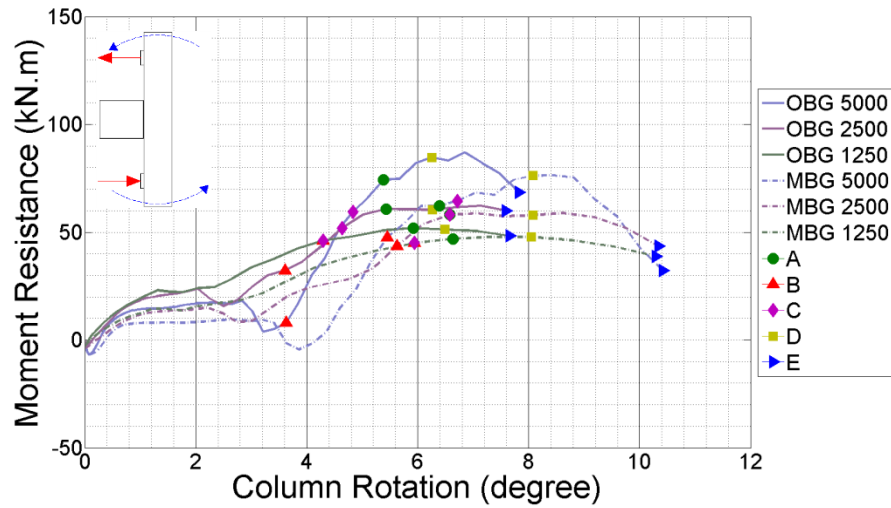


Figure 7-36 Moment and column rotation by BG more LT3 8mm, OBG is original bolt gauge and MBG is the maximum bolt gauge simulation.  
 (Coloured dots indicate the points at which: A- beam and column flanges made contact and prying action commenced, B- failure at the top of the welding, C- 1<sup>st</sup> element was eroded at crack opening, D- Crack opened half way through the plate thickness, E- Crack fully opened through the plate thickness)

## 7.6 Influence of bolt pitch on connection behaviour

The influence of bolt pitch was investigated by varying the original 70mm (OBP) from a minimum (LBP) of 60mm to a maximum (MBP) of 80mm. Two loading types (LT2 and LT3) with different loading rates and two plate thicknesses were used. Figure 7-37 shows the shear stress developed in the plate with a loading rate of 3500kN/s and pure tension loading type (LT2); (c) is the plate with original bolt pitch and the stress was reduced in the other two cases of bolt pitch (b,d). Figure 7-37 (a) shows the stress in the plate by increasing the loading rate up 7000kN/s for the 80mm bolt gauge (MBP) and shows how much rate can influence the plate behaviour.

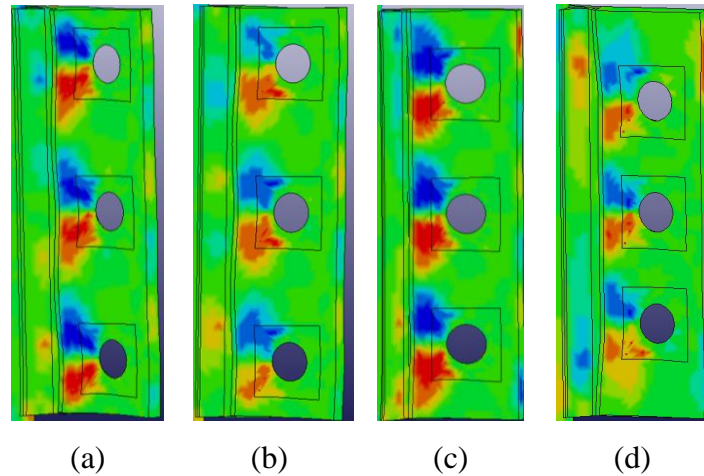


Figure 7-37 Shear stress generated in the connection  
 (a) MBP (7000kN/s) (b) MBP (3500kN/s) (c) OBP (3500kN/s) (d) LBP (3500kN/s)

Figure 7-38 shows the plate deformations under pure tension loading type (LT2) for different loading rates. The green colour shows the plastic area of the plate and blue is the non-affected location. Having the original bolt pitch (c) and highest loading rate case (a) resulted in the biggest area of plasticity compared to the other cases (b,d). The original bolt pitch in this condition was the optimum.

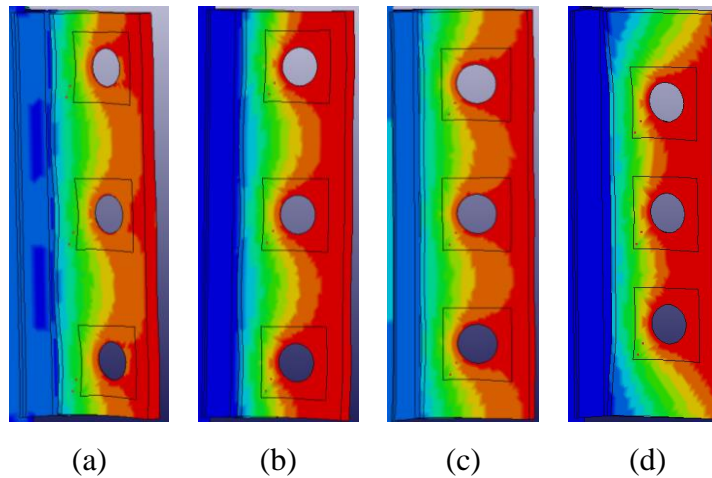


Figure 7-38 End plate deformation counter plot  
 (a) MBP (7000kN/s) (b) MBP (3500kN/s) (c) OBP (3500kN/s) (d) LBP (3500kN/s)

### 7.6.1 Column displacement in time

Figure 7-39 and Figure 7-40 compare the column displacement vs time for the original bolt pitch with the reduced and increased cases under pure tension loading type (LT2) across the loading rates for an 8mm thick end-plate connection. Loading rate had an effect on the connection behaviour and as the rate reduced the column displacement changed from the original column movement. Overall, reducing the bolt pitch made the connection less ductile and increasing the bolt pitch did the opposite.

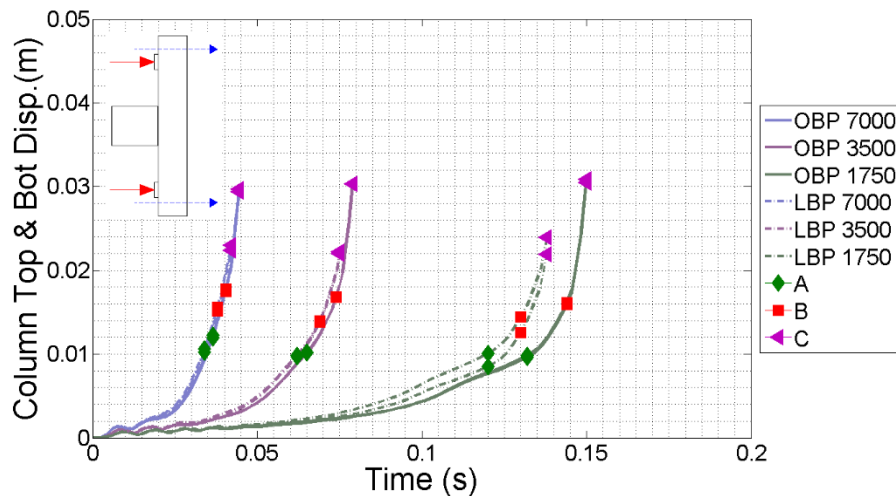


Figure 7-39 Column displacement time history by BD less LT2 8mm, OBP is original bolt pitch and LBP is the less bolt pitch simulations.

(Coloured dots indicate the points at which: A- 1st element was eroded at crack opening, B- Crack opened half way through the plate thickness, C- Cracked fully opened through the plate thickness)

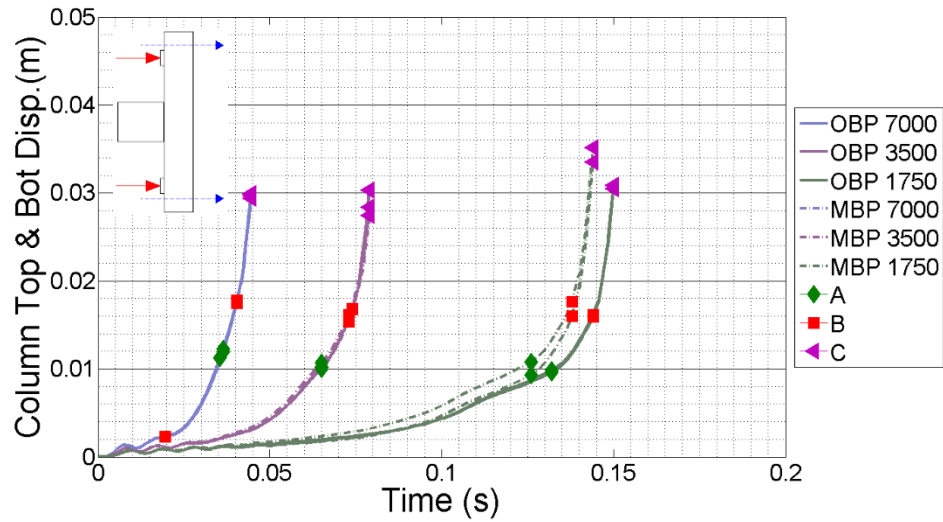


Figure 7-40 Column displacement time history by BD more LT2 8mm, OBP is original bolt pitch and MBP is the more bolt pitch simulations.  
 (Coloured dots indicate the points at which: A- 1st element was eroded at crack opening, B- Crack opened half way through the plate thickness, C- Cracked fully opened through the plate thickness)

### 7.6.2 Deformation of the End-plate

Figure 7-41 illustrates the results of plate deformation for more and less bolt pitch (MBP and LBP), under pure moment loading type, different loading rates and an 8mm thick end-plate. By reducing the bolt pitch, plate deformation was increased and gave more ductility to the connection as the crack opened with more plate deformation.

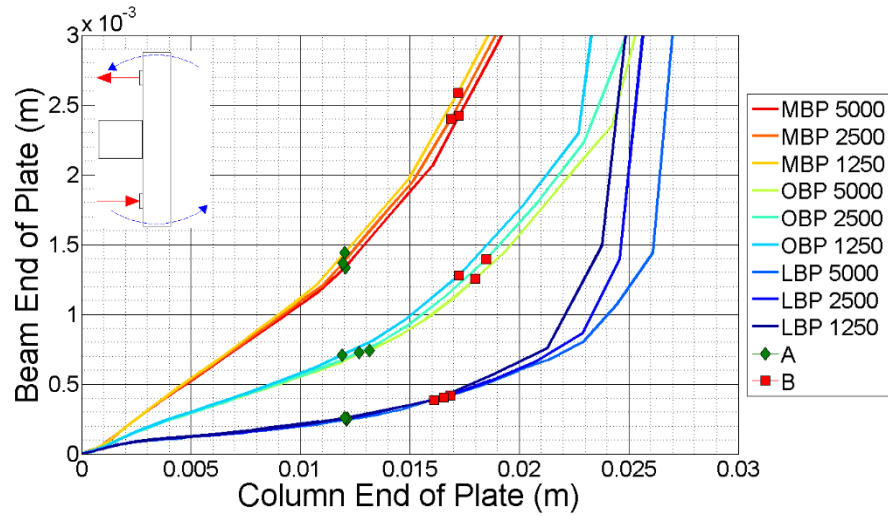


Figure 7-41 Displacement of the two corner by BD more and less LT3 8mm, OBP is original bolt pitch, MBP is the more bolt pitch simulations and LBP is the less bolt pitch simulations. (Coloured dots indicate the points at which: A- 1<sup>st</sup> element was eroded at crack opening, B- Crack opened half way through the plate thickness)

### 7.6.3 Connection force resistance

In both cases of changing the bolt pitch, the connection resistance did not change when the highest loading rate was applied, however the resistance dropped at the lower rates. The ductility was reduced in both cases (but reduced more in LBP). Results for force resistance of the connection vs column centre translation are provided in Figure 7-42 and Figure 7-43, for 10mm less bolt pitch (LBP) and more bolt pitch (MBP), under pure tension loading type (LT2), different loading rates and 8mm thick end-plate.

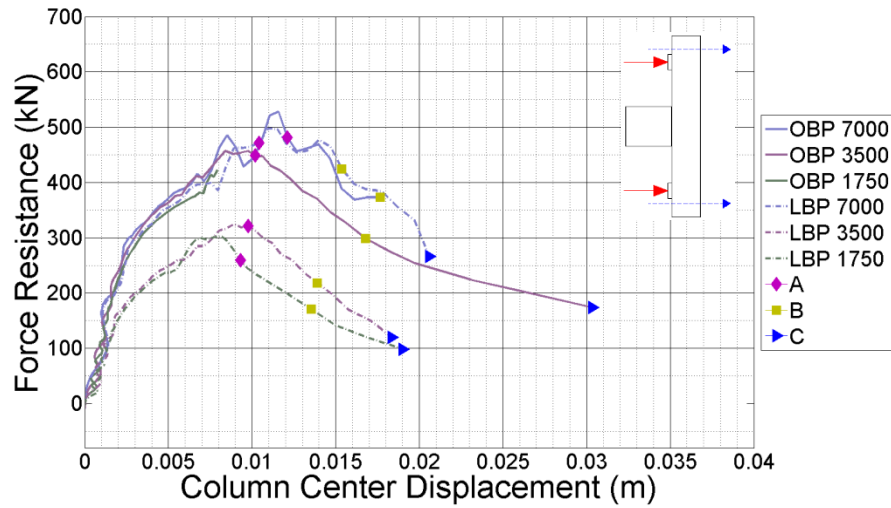


Figure 7-42 Force and column displacement by BD less LT2 8mm, OBP is original bolt pitch and LBP is the less bolt pitch simulations.  
 (Coloured dots indicate the points at which: A- 1<sup>st</sup> element was eroded at crack opening, B- Crack opened half way through the plate thickness, C- Crack fully opened through the plate thickness)

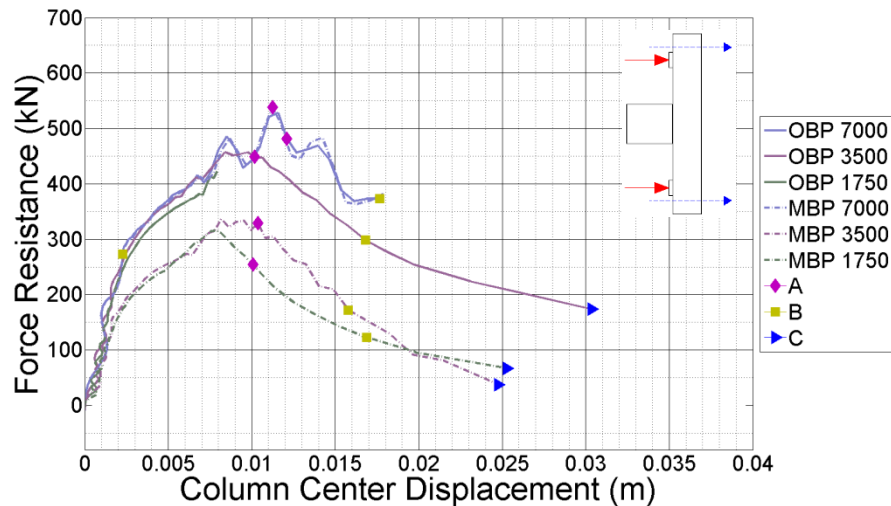


Figure 7-43 Force and column displacement by BD more LT2 8mm, OBP is original bolt pitch and MBP is the more bolt pitch simulations.  
 (Coloured dots indicate the points at which: A- 1<sup>st</sup> element was eroded at crack opening, B- Crack opened half way through the plate thickness, C- Crack fully opened through the plate thickness)

#### 7.6.4 Connection moment resistance

Figure 7-44 and Figure 7-45 plot moment resistance of the connection against column rotation under pure moment loading (type LT3) for different loading rates and an 8mm end-plate. Reducing the bolt pitch by 10mm gave the connection the ability to resist more

moment as the end-plate had the ability to deform more and the ductility of the connection increased, increasing the bolt pitch by 10mm was insignificant in moment resistance of the connection.

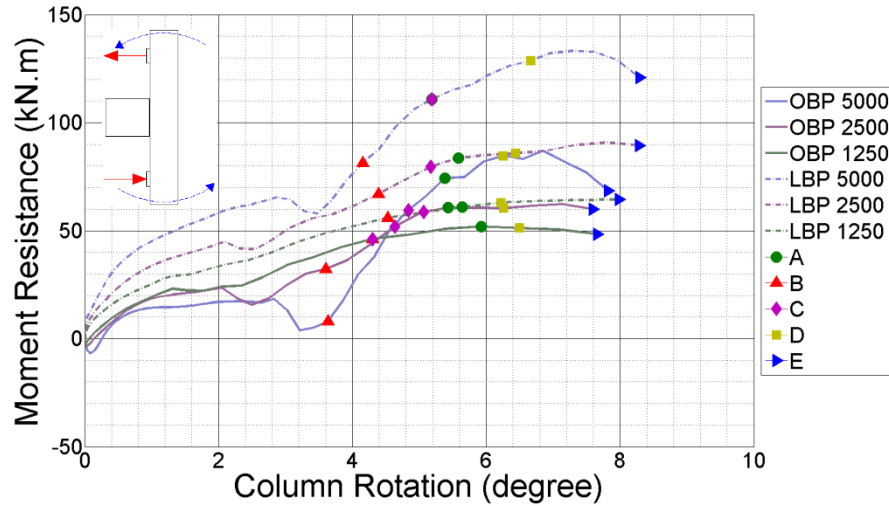


Figure 7-44 Moment and column rotation by BD less LT3 8mm, OBP is original bolt pitch and LBP is the less bolt pitch simulations.

(Coloured dots indicate the points at which: A- beam and column flanges made contact and prying action commenced, B- failure at the top of the welding, C- 1<sup>st</sup> element was eroded at crack opening, D- Crack opened half way through the plate thickness, E- Crack fully opened through the plate)

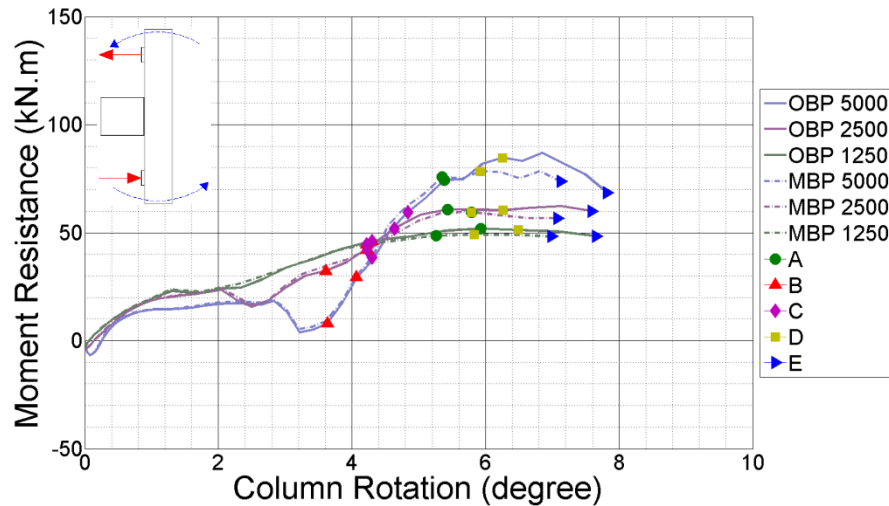


Figure 7-45 Moment and column rotation by BD more LT3 8mm, OBP is original bolt pitch and MBP is the more bolt pitch simulations.

(Coloured dots indicate the points at which: A- beam and column flanges made contact and prying action commenced, B- failure at the top of the welding, C- 1<sup>st</sup> element was eroded at crack opening, D- Crack opened half way through the plate thickness, E- Crack fully opened through the plate thickness)

## 7.7 Summary

Table 7-1 provides a summary of results from all parametric studies conducted on end-plate connections. This table demonstrates how different geometry or loading rates and types change different aspects of connection behaviour e.g. the column time histories, angle deformations, and force and moment resistance.

<i>End-plate Connection</i>	
	<b>Description</b>
Influence of Different Loading Types and Rates	<ul style="list-style-type: none"> <li>• <b>Column displacement in time</b> (Section 7.2.1): The connection behaviour changed at loading rates above around 700 kN/s as deformation in the connection were increased in quasi-static loading rates.</li> <li>• <b>Column response due to connection reaction</b> (Section 7.2.2): The column rotation and displacement was independent of loading rate for three loading types (LT1, LT2 and LT3), but in load type LT4 the rate had an effect on how much the column rotated or displaced.</li> <li>• <b>End-plate deformation</b> (Section 7.2.3): Plates deformed less in quasi-static loadings regardless of the thickness. 8mm thick plates had more deformation compared with a 10mm plate.</li> <li>• <b>Connection force resistance</b> (Section 7.2.4): Connection had more force resistance in the case of pure tension. The thickness of the plate changed the resistance i.e the 10mm had about twice the resistance of an 8mm thick plate. For both plate thicknesses the ductility remained similar and the loading rate had little effect.</li> <li>• <b>Connection moment resistance</b> (Section 7.2.5): The moment resistance of the connection reduced as the thickness of the plate changed from 10 to 8mm, also the magnitude of the resistance increased as the loading rate increased. In the pure tension loading the moment generated in the connection was close to zero as expected.</li> </ul>
Influence of Bolt Strength	<p>Similar to web-cleat connections, making the bolts stronger did not significantly change column displacement, angle deformation or force and moment resistance of the connection (Section 7.3).</p>
Effect of Washer Size	<p>There was no significant change in column displacement, angle deformation or force and moment resistance of the connection in this case (Section 7.4).</p>

Effect of Bolt Size	<ul style="list-style-type: none"> <li>• <b>Column displacement in time</b> (Section 7.5.1): Connection became stronger, there was a time delay and the failure happened with lower displacement. Connection behaved more rigidly.</li> <li>• <b>End-plate deformation</b> (Section 7.5.2): The plate deformed less which made the connection more brittle.</li> <li>• <b>Connection force resistance</b> (Section 7.5.3): Connection force resistance was increased irrespectively of the loading rate.</li> <li>• <b>Connection moment resistance</b> (Section 7.5.4): Connection moment resistance was also increased, and column rotation decreased.</li> </ul>
Influence of Bolt Gauge	<ul style="list-style-type: none"> <li>• <b>Column displacement in time</b> (Section 7.6.1): By having less bolt gauge, ductility reduced i.e. the column moved less in time and failed with less displacement. Adding to the bolt gauge had the opposite effect and the column moved more in time and the connection failed with more displacement; overall the connection was more ductile.</li> <li>• <b>End-plate deformation</b> (Section 7.6.2): Connection became more rigid by a small amount and the end plate deformed less as the bolt gauge reduced. On the other hand by increasing the bolt gauge the connection became more ductile and the effect was considerable.</li> <li>• <b>Connection force resistance</b> (Section 7.6.3): Connection force resistance did not change much but the ductility reduced when the bolt gauge was reduced, however adding to the bolt gauge allowed the column to move faster and the force resistance of the connection dropped.</li> <li>• <b>Connection moment resistance</b> (Section 7.6.4): By reducing the bolt gauge, moment resistance of the connection changed little much but the ductility reduced, and by increasing the bolt gauge the ductility increased and moment resistance dropped.</li> </ul>
Influence of Bolt Pitch	<ul style="list-style-type: none"> <li>• <b>Column displacement in time</b> (Section 7.7.1): Displacement pattern did not change but the ductility increased and the connection failed with more displacement when the bolt pitch was reduced, however by increasing the bolt pitch the ductility reduced.</li> <li>• <b>End-plate deformation</b> (Section 7.7.2): Plate deformation and ductility were increased as the bolt pitch reduced and they were reduced as the bolt pitch increased.</li> <li>• <b>Connection force resistance</b> (Section 7.7.3): For both more and less bolt pitch the force resistance was the same at the highest loading rate with the original bolt pitch; the force dropped at lower rates for both cases.</li> <li>• <b>Connection moment resistance</b> (Section 7.7.4): By reducing the bolt pitch moment resistance was increased as the lever arm between the beam flange and the lowest bolt was decreased and the connection could resist for longer, however by increasing the bolt pitch no change happened to the moment resistance of the connection.</li> </ul>

Table 7-1 Summary of parametric study results for end-plate

The final results of the parametric studies are provided in Table 6-2, which shows the translation and rotation of the column at the time of total failure of the connection. The force and moment resistance are the maximum resisted in the connection before the failure (two numbers separated by “/” shows the maximum and minimum for different range of loading rates).

End-plate Connection							
Thickness (mm) & Loading Type		Translation (mm)	Rotation (Degree)	Force (kN)	Moment (kN.m)		
Influence of Different Loading Types and Rates	10mm	1	3.5	5.5	120-170	60/70	
		2	12	0	500-580	0	
		3	5	5.5	-300-0	75-100	
		4	5	4.5	160-250	30-40	
	8mm	1	4	4	70-100	35-40	
		2	10	0	400-480	0	
		3	3	4	-300-0	50-75	
		4	4	3.5	120-180	15-30	
Influence of Bolt Strength	10mm	2	12	0	600	0	
		3	5	7	-300-0	80-110	
	8mm	2	10	0	550	0	
		3	2.5	5	-300-0	50-75	
Effect of Washer Size	10mm	2	12	0	600	0	
		3	5	7	-300-0	80-110	
	8mm	2	10	0	500	0	
		3	2.5	5	-300-0	50-75	
Effect of Bolt Size	10mm	2	-	0	-	0	
		4	4	5	250-300	30-40	
	8mm	2	-	0	-	0	
		4	5	3.5	150-250	20-30	
Influence of Bolt Gauge	More	8mm	2	15	0	350-450	0
			3	5	6	-300-0	50-80
	Less	8mm	2	10	0	150-550	0
			3	3	4.5	-300-0	60-100
Influence of Bolt Pitch	More	8mm	2	10	0	300-500	0
			3	3	4	-300-0	50-80
	Less	8mm	2	10	0	300-500	0
			3	3	5.5	-300-0	60-100

Table 7-2 End-plate connection results from parametric studies

## **7.8 Conclusion**

The effects of loading and geometry changes on an end-plate connection was discussed in this chapter. Similar to web-cleat connections, end-plate connections resisted the maximum tensile force when applied as pure tension. With moment and rotation the axial resistance dropped. In contrast to the web-cleat connection, end-plate connection resistance was dependent on the loading rate and plate thickness. Making the bolt and washer stronger did not change the ductility or resistance significantly.

The connection resistance was increased and ductility dropped as bolts were made stronger. Reducing the bolt gauge gave the connection more resistance at high rates and lower resistance at lower rates, increasing the bolt gauge reduced the connection resistance and improved the ductility. Connection force resistance did not change at the highest rate of loading but it dropped at the lower rates. The moment resistance increased when the bolt pitch changed. Also, by reducing the bolt pitch, connection moment resistance was increased.

## 8 Discussion

This chapter discusses the key findings of the modelling work described in the previous chapters and suggests how connection behaviour can be improved. Results from both the parametric and experimental studies showed the prying effect caused by the impact between the beam top flange and the column flange to be an important factor affecting connection behaviour, and this is discussed in detail in this chapter. A comparison is also provided between the two different type of connections studied in this work: web-cleat and end-plate. The discussion is based on the findings of the parametric studies for each connection presented in Chapters 6 and 7 respectively.

### 8.1 Overview of model results

The key finding of the numerical modelling results is that there is a significant difference in the rate-dependent behaviour of the web-cleat and flexible endplate connection types.

In the case of web-cleat connections, there is relatively little difference in the connection behaviour across a range of loading rates for the connection studied in this work. This appears to be due to the fact that the connections are able to deform in a relatively ductile fashion and hence, cushion the dynamic loading. The important factors here are plastic deformation of the cleat angles, and the fact that the ultimate failure mode is in the beam web. As a result, even at high rates of applied load, the strain rates developed in the different parts of the connection are not sufficiently high to result in significant differences in material behaviour, and the overall ductility and capacity of the connection are similar across the range of loading rates and load combinations considered. There are some variations in the detailed response and deformation of the web-cleat connections with increasing load rates, but these are of secondary significance.

Clearly, it would be possible to use cleat angles which were of such high strength and stiffness that they did not deform plastically, although this has not been considered in detail in this study. In such a case, it would be expected that the load would be transmitted through the cleat angles to the bolts and beam web in a much stiffer fashion, potentially leading to bolt shear or beam web failure with considerably less overall connection

ductility. This would also be more likely to impose high local strain rates in the failing parts of the connection, potentially leading to more brittle behaviour.

The important finding here is that, if the size of the cleat angles is carefully chosen to ensure plastic deformation, the small differences in response across the range of loading rates suggests that dynamic behaviour may be ignored, and the static response of the connection taken as indicative of the connection's performance in a dynamic frame response to column-loss scenarios.

Very different behaviour was observed in the case of the endplate connections. Here, the key issue is the behaviour once prying action commences after the contact of the beam and column flange. In the static loading cases, significant ductility of the connection occurred after prying commenced, before connection failure was finally initiated by local failure in the weld/HAZ in the region of the endplate/beam web connection closest to the most heavily loaded row of bolts.

In dynamic loading cases for the endplate connections, the onset of prying action resulted in a dynamic impact between the beam and column flange, due to the momentum generated in the connection whilst it was deforming with relatively little stiffness in the early stages of loading. This impact invariably led to spikes of strain in the key sections of the weld/HAZ, forcing localized regions to fail almost instantaneously, and initiating an unzipping of the weld/HAZ and the consequent overall failure of the connection at much lower overall connection ductility. This is discussed in detail in Section 8.3.4 below. The quantitative predictions of precise post-prying behaviour are inevitably tentative, due to the lack of authoritative data on the constitutive material model of the weld/HAZ, but the principle is clear. This secondary impact associated with prying action is clearly a detrimental feature, and results in significant loss of connection ductility. This effect is investigated in more detail in the rest of this chapter.

## 8.2 Web-cleat connection

To study the effect of the gap between the beam end and column face two new cases were introduced as shown in Figure 8-1. Case (a) (denoted “OG” in subsequent figures and text) is the normal situation in which there is a gap between the column and beam and prying can occur after some connection deformation. Case (b) (denoted “NG”) fills the gap between the column and beam by extending the beam flange to make initial contact with the column in the unloaded position and case, resulting in prying occurring from the offset, with no “impact” associated with prying in the dynamic loading cases. Case (c) (denoted “NC”) removes any possibility of contact between the beam and column flange (i.e. the beam flange is permitted to “pass through” the column). Case (c) is clearly not entirely physically realistic, but this approach was used in order to simulate the effect of chamfering the lower flange/web of the beam to eliminate prying without requiring detailed geometrical changes to the numerical model.

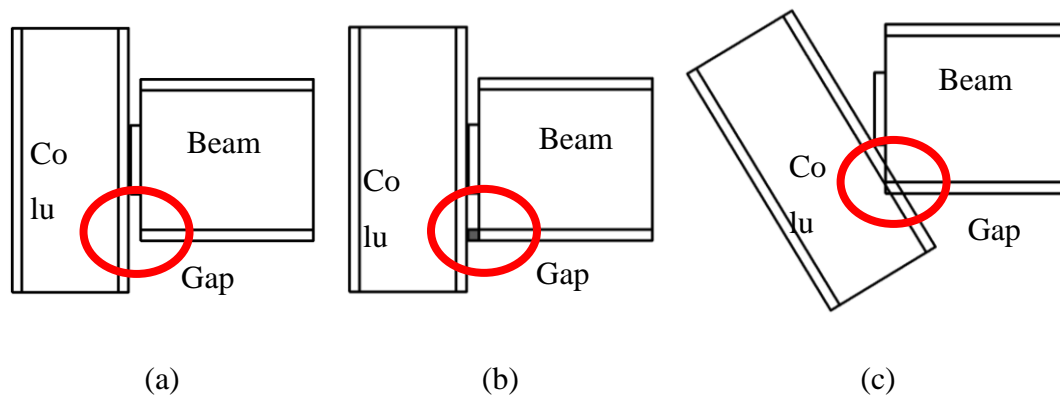


Figure 8-1 Different type of beam and column impact (a) the original gap (OG) (b) no gap (NG) (c) (NC) no contact

The response of the connection behaviour can be characterized by how the column responded to load and is illustrated in Figure 8-2 which plots the column rotation against displacement. As these results show, filling the gap between the beam and column flange reduced the ductility of the connection and column had less rotation and displacement compared to the original case; vice versa, having no contact increased the ductility as the connection became a pin after the failure of the second bolt.

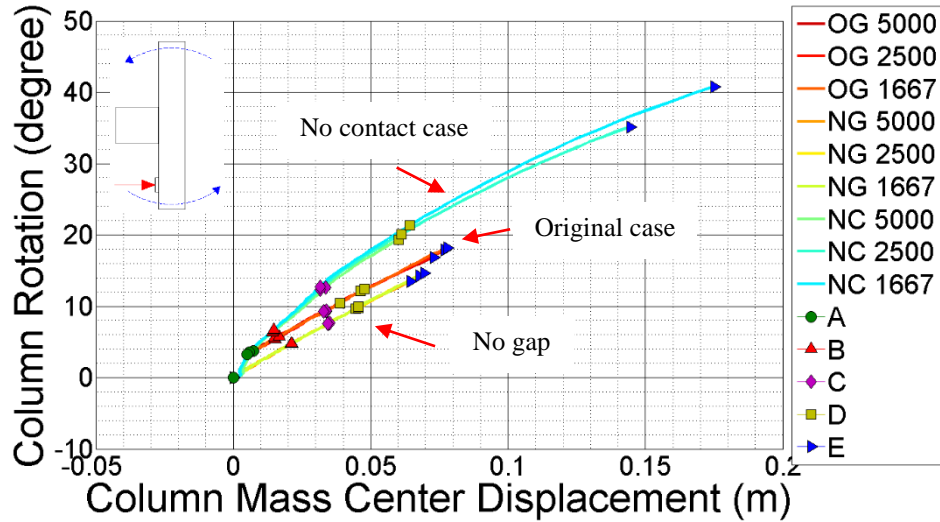


Figure 8-2 Column rotation and displacement LT1 10mm angle,  
(Coloured dots indicate the points at which: A- the beam and column flanges made contact and prying action commenced, B- 1<sup>st</sup> element in the model was eroded in vicinity of 1<sup>st</sup> bolt, C- Beam web totally failed in vicinity of 1<sup>st</sup> bolt, D- Beam web totally failed in vicinity of 2<sup>nd</sup> bolt, E- Beam web totally failed in vicinity of 3<sup>rd</sup> bolt)

### 8.2.1 Column displacement

Column displacement with time is a useful indicator of the effect of restricting rotational movement before contact is made between the column flange and beam lower flange. Figure 8-3 provides the results for three different loading rates and two configurations: (i) the connection in original gap with the contact (OG) and (ii) the connection with the gap filled (NG). Results show that as the loading rate increased the behaviour of these two were closer, and in general it took more time to reach the same displacement as the gap was filled. However the displacement at failure was very close in both cases.

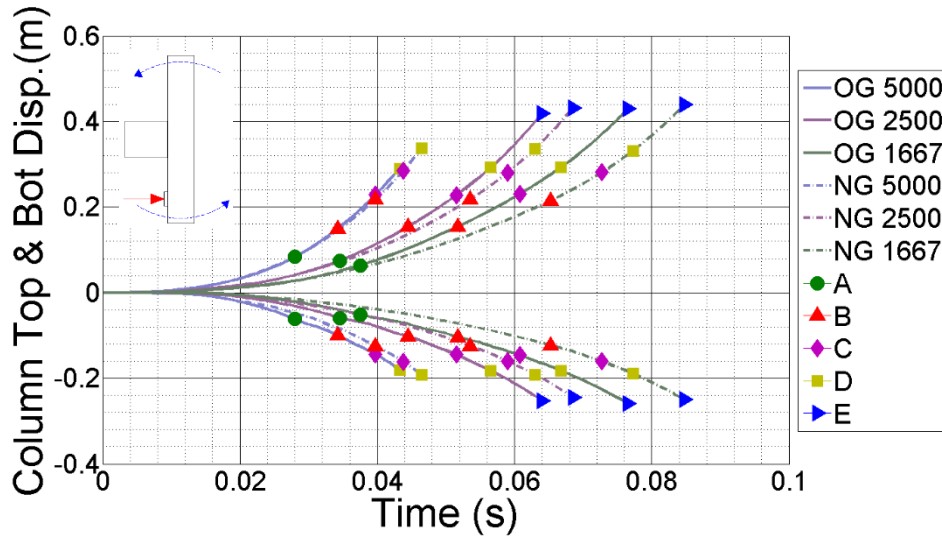


Figure 8-3 Column displacement time history LT1 8mm angle with and without a gap  
 (Coloured dots indicate the points at which: A- the beam and column flanges made contact and prying action commenced, B- 1<sup>st</sup> element in the model was eroded in vicinity of 1<sup>st</sup> bolt, C- Beam web totally failed in vicinity of 1<sup>st</sup> bolt, D- Beam web totally failed in vicinity of 2<sup>nd</sup> bolt, E- Beam web totally failed in vicinity of 3<sup>rd</sup> bolt)

Removing the contact between beam and column flange increased the ductility of the connection, as shown in Figure 8-4. This comparison is between two cases, one with the connection under the original condition (OC) and the other one in which the connection has no contact between the beam and column flange (NC). As expected, at the beginning both cases have similar behaviour until the gap was filled and then they separate. As the contact was removed the column had much more displacement before total failure of the connection which was caused by less lever arm generated in the connection to mobilise the prying effect.

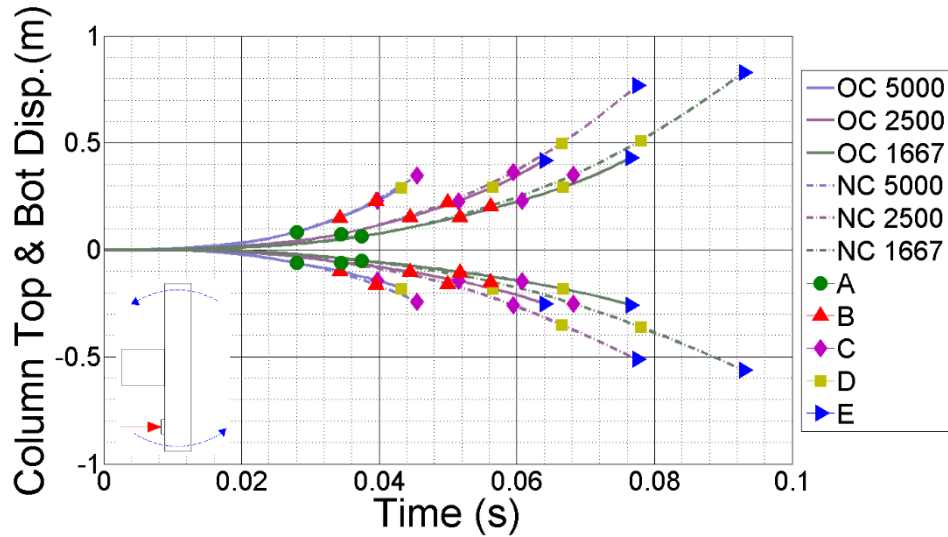


Figure 8-4 Column displacement time history LT1 8mm angle, no contact  
 (Coloured dots indicate the points at which: A- the beam and column flanges made contact and prying action commenced, B- 1<sup>st</sup> element in the model was eroded in vicinity of 1<sup>st</sup> bolt, C- Beam web totally failed in vicinity of 1<sup>st</sup> bolt, D- Beam web totally failed in vicinity of 2<sup>nd</sup> bolt, E- Beam web totally failed in vicinity of 3<sup>rd</sup> bolt)

### 8.2.2 Deformation of the Angle-cleat

It was important to know the angle behaviour and its deformation as it is the main component of web cleat connections and its behaviour changes the connection ductility, for this reason the displacement of the bolt at the centre of the angle was plotted against the column centre in Figure 8-5. These results show that by filling the gap and using a 10mm leg thickness angle the deformation was the same across all loading rates and with or without a gap between the beam and column. This shows that the 10mm thick angle is rigid enough to resist the force and deform less and the impact time had less effect on its deformation.

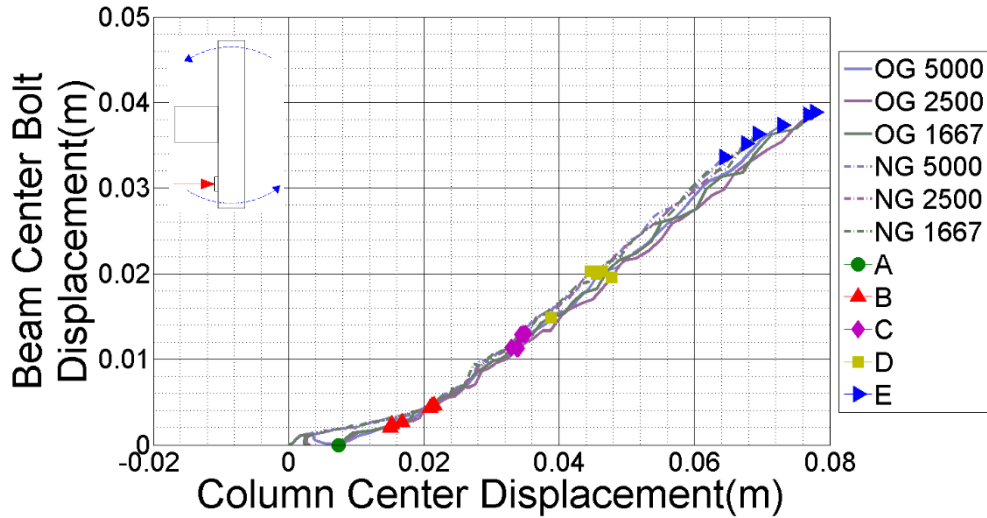


Figure 8-5 Mid bolt and column displacement LT1 10mm angle, no gap  
 (Coloured dots indicate the points at which: A- 1<sup>st</sup> element in the model was eroded in vicinity of 1<sup>st</sup> bolt, B- Beam web totally failed in vicinity of 1<sup>st</sup> bolt, C- Beam web totally failed in vicinity of 2<sup>nd</sup> bolt, D- Beam web totally failed in vicinity of 2<sup>nd</sup> bolt, E- Beam web totally failed in vicinity of 3<sup>rd</sup> bolt)

Although the presence or not of a gap had no effect on deformation with 10mm leg thickness angles it did change the behaviour on 8 and 6mm thick angles. Results are provided in Figure 8-6. Having different loading rates had no significant effect on angle deformation. Filling the gap also had no effect on a 10mm thick angle as this was strong enough to behave in a rigid manner and the time of impact had no significant effect, however as the 8 and 6mm thick angles were more flexible the time of impact became important and deformation increased.

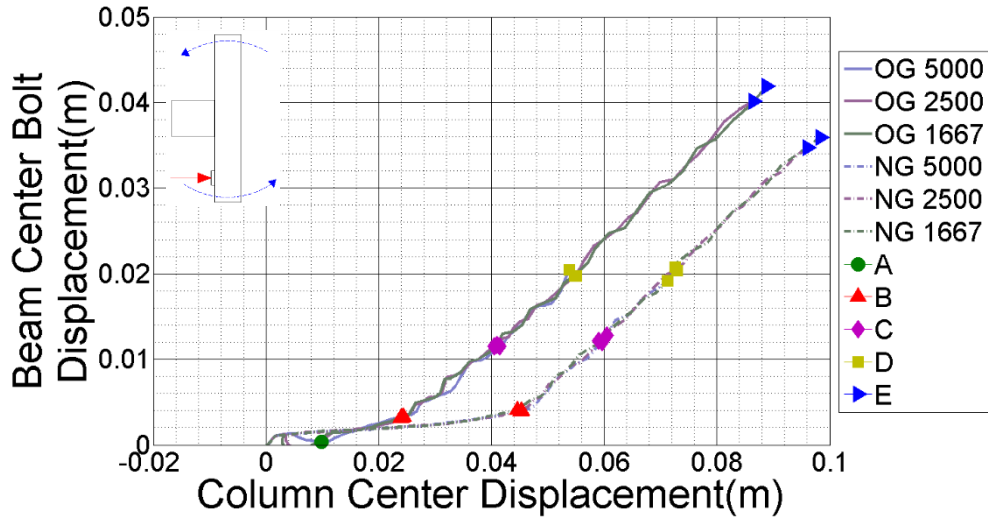


Figure 8-6 Mid bolt and column displacement LT1 8mm angle, no gap  
 (Coloured dots indicate the points at which: A- 1<sup>st</sup> element in the model was eroded in vicinity of 1<sup>st</sup> bolt, B- Beam web totally failed in vicinity of 1<sup>st</sup> bolt, C- Beam web totally failed in vicinity of 2<sup>nd</sup> bolt, D- Beam web totally failed in vicinity of 2<sup>nd</sup> bolt, E- Beam web totally failed in vicinity of 3<sup>rd</sup> bolt)

Removing the contact between the beam and column flange delayed the failure of the last bolt as explained before. This effect happened with all thicknesses of the angles; results for the 8mm angle are provided in Figure 8-7. As no contact was possible the connection began to rotate freely around the middle bolt until the lowest bolt hit the back of the hole and started to resist the movement; also the lever arm was reduced, and caused less prying effect in the angles. Overall, the angles were deformed less and the column moved more in this case for all thickness of the angles, and loading rate had no significant effect on connection behaviour.

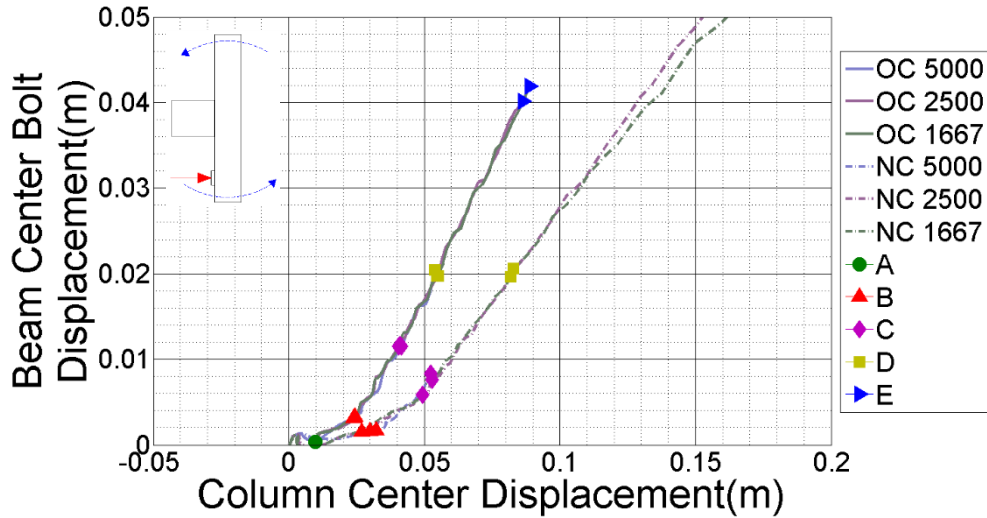


Figure 8-7 Mid bolt and column displacement LT1 8mm angle, no contact  
(Coloured dots indicate the points at which: A- 1<sup>st</sup> element in the model was eroded in vicinity of 1<sup>st</sup> bolt, B- Beam web totally failed in vicinity of 1<sup>st</sup> bolt, C- Beam web totally failed in vicinity of 2<sup>nd</sup> bolt, D- Beam web totally failed in vicinity of 2<sup>nd</sup> bolt, E- Beam web totally failed in vicinity of 3<sup>rd</sup> bolt)

### 8.2.3 Connection moment resistance

Moment resistance was improved when the gap was filled for all the angle thicknesses, however it increased the most when a 10mm thick angle was employed. Results of these studies are provided in Figure 8-8 and Figure 8-9 for both 10 and 8mm angles. As mentioned before angle deformation did not change with 10mm thickness and having earlier impact time caused the web to fail sooner, with less column rotation. In overall connection was stronger but less ductile. Tinier angles were more flexible so they could compensate and deformed more which resulted in similar column rotation and more resistance as in all cases filling the gap helped the force to be built up in the connection more gradually without an impact.

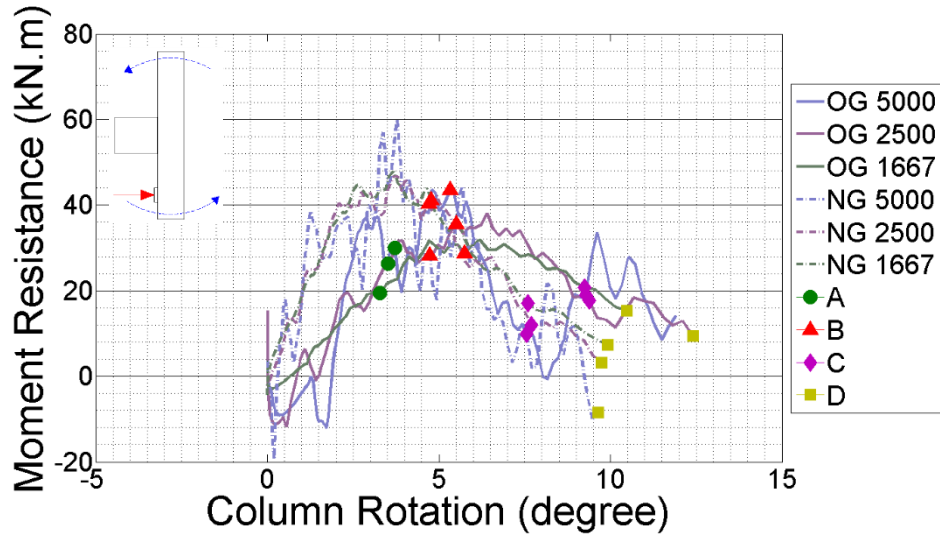


Figure 8-8 Moment and column rotation LT1 10mm angle, no gap  
 (Coloured dots indicate the points at which: A- the beam and column flanges made contact and prying action commenced, B- 1<sup>st</sup> element in the model was eroded in vicinity of 1<sup>st</sup> bolt, C- Beam web totally failed in vicinity of 1<sup>st</sup> bolt, D- Beam web totally failed in vicinity of 2<sup>nd</sup> bolt)

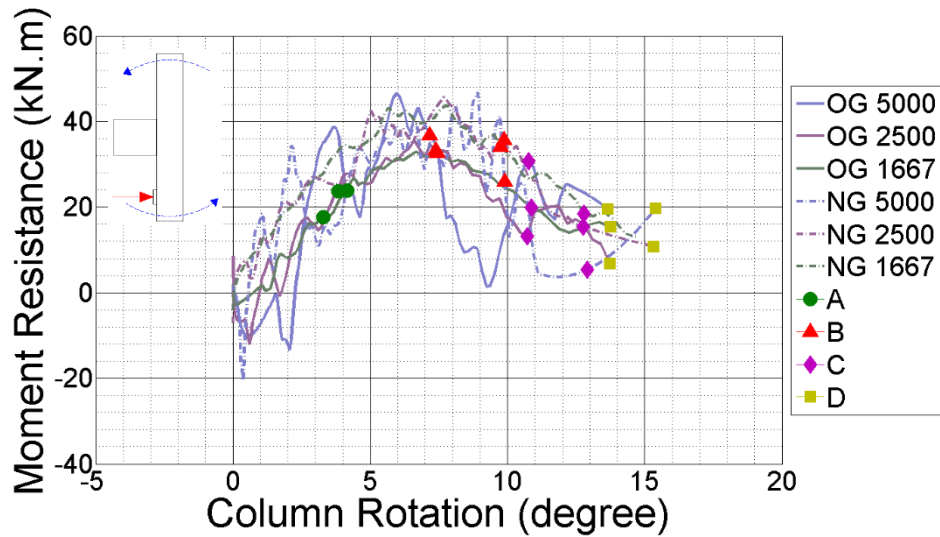


Figure 8-9 Moment and column rotation LT1 8mm angle, no gap  
 (Coloured dots indicate the points at which: A- the beam and column flanges made contact and prying action commenced, B- 1<sup>st</sup> element in the model was eroded in vicinity of 1<sup>st</sup> bolt, C- Beam web totally failed in vicinity of 1<sup>st</sup> bolt, D- Beam web totally failed in vicinity of 2<sup>nd</sup> bolt)

Removing the contact between the beam and column flanges changed the connection resistance and it behaved more like a pin with a much reduced moment resistance, especially after the failure of the second bolt (dot B on the graph). Figure 8-10 provides the results for an 8mm thick angle but this behaviour repeated for other thicknesses. Behaving less rigidly and more like a pin could be helpful in terms of ductility but on the

other hand lower resistance reduces load carrying capacity and the dissipation of energy in the connection.

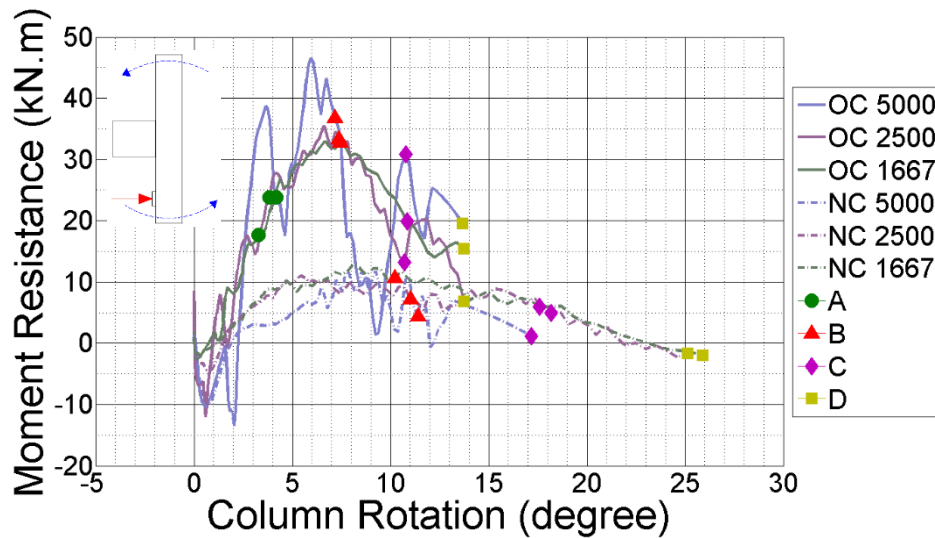


Figure 8-10 Moment and column rotation LT1 8mm angle, no contact  
 (Coloured dots indicate the points at which: A- the beam and column flanges made contact and prying action commenced, B- 1<sup>st</sup> element in the model was eroded in vicinity of 1<sup>st</sup> bolt, C- Beam web totally failed in vicinity of 1<sup>st</sup> bolt, D- Beam web totally failed in vicinity of 2<sup>nd</sup> bolt)

#### 8.2.4 Connection force resistance

Filling the gap in the connection did not change the force resistance of the connection compared with the original case, it did however increase the ductility (see Figure 8-11). Removing any possibility of contact in the connection reduced the resistance compared with the original case and delayed its failure as shown in Figure 8-12. In general filling the gap had no significant effect on connection force resistance but increased the ductility. As mentioned before having no gap allowed to the force to be built up by the time without sudden impact. Removing the contact caused the connection to behave more like a pin and have much lower force resistance. Filling the gap helped to increase the area under the Force-Displacement graph (Figure 8-11) which means more energy was dissipated however in the case with no contact, as the ductility increased the force resistance dropped and had significant effect on reduction of energy dissipation of the connection.

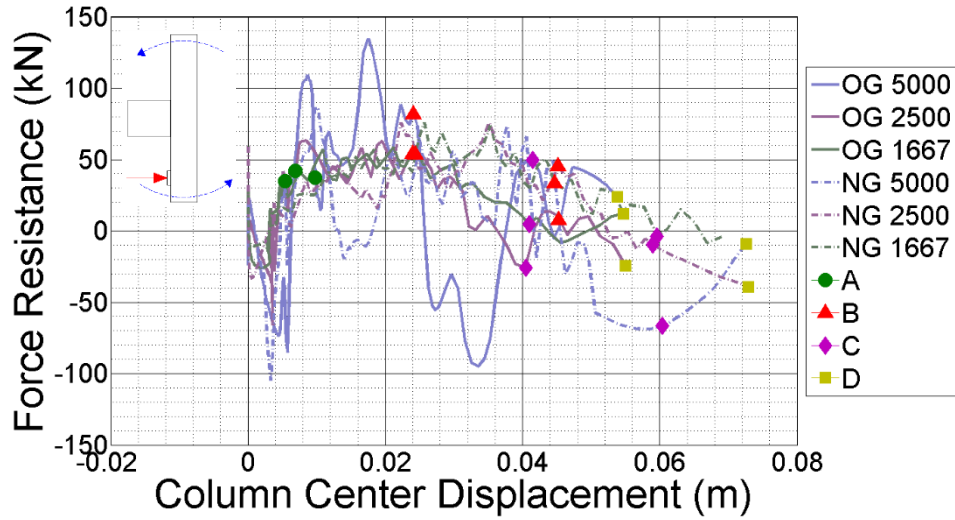


Figure 8-11 Force and column displacement LT1 8mm angle, no gap  
 (Coloured dots indicate the points at which: A- the beam and column flanges made contact and prying action commenced, B- 1<sup>st</sup> element in the model was eroded in vicinity of 1<sup>st</sup> bolt, C- Beam web totally failed in vicinity of 1<sup>st</sup> bolt, D- Beam web totally failed in vicinity of 2<sup>nd</sup> bolt)

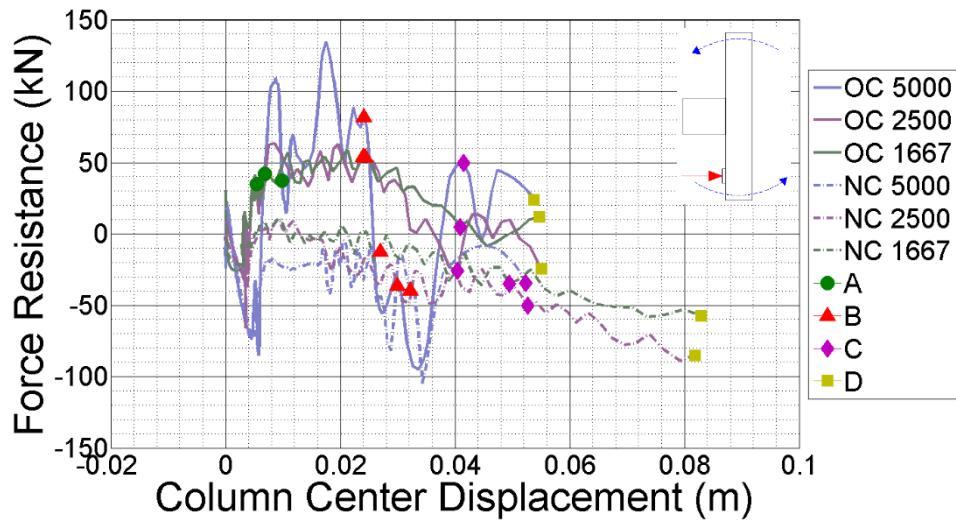


Figure 8-12 Force and column displacement LT1 8mm angle, no contact  
 (Coloured dots indicate the points at which: A- the beam and column flanges made contact and prying action commenced, B- 1<sup>st</sup> element in the model was eroded in vicinity of 1<sup>st</sup> bolt, C- Beam web totally failed in vicinity of 1<sup>st</sup> bolt, D- Beam web totally failed in vicinity of 2<sup>nd</sup> bolt)

### 8.3 End-plate connection

As mentioned before failure happened in the endplate connection as a crack opened at the top of the connection and propagated through the whole length of the plate as shown in Figure 8-13.

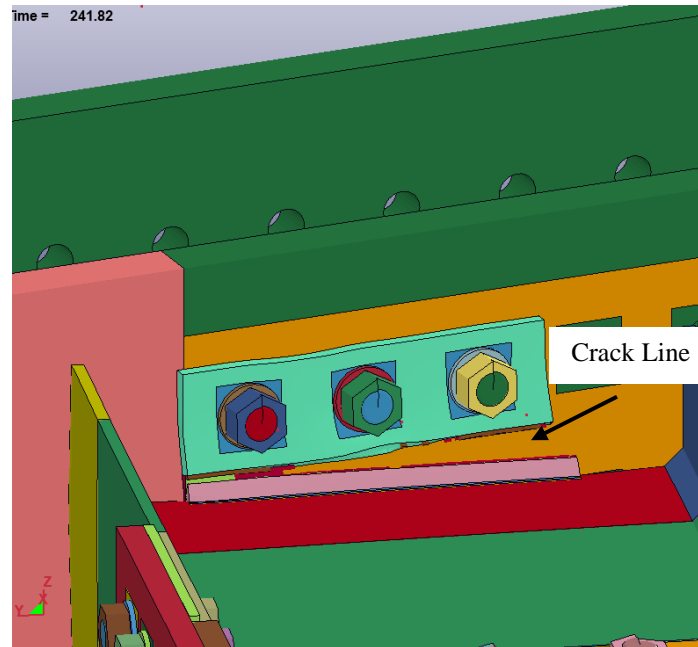


Figure 8-13 Example of end-plate connection failure

Figure 8-14 and Figure 8-15 show the column behaviour (rotation plotted against its displacement) for 10 and 8mm thick partial depth (flexible) endplates subjected to a range of loading rates and with the gap between the lower flange of the beam and column left open or filled. Filling the gap changed the relationship between column rotation and translation by filling the gap the force increased more gradually in the connection and had no impact on the connection this case the column reached a similar rotation in the 10mm thick plate and had more displacement which meant the ductility increased, but it had a different effect on the more flexible plate (8mm) which failed sooner with less rotation but the same displacement as the original case. Removing the contact had a similar effect on both the 10 and 8mm thick end-plate connections, both column rotation and displacement were increased. This extra ductility came from having less lever arm in this case.

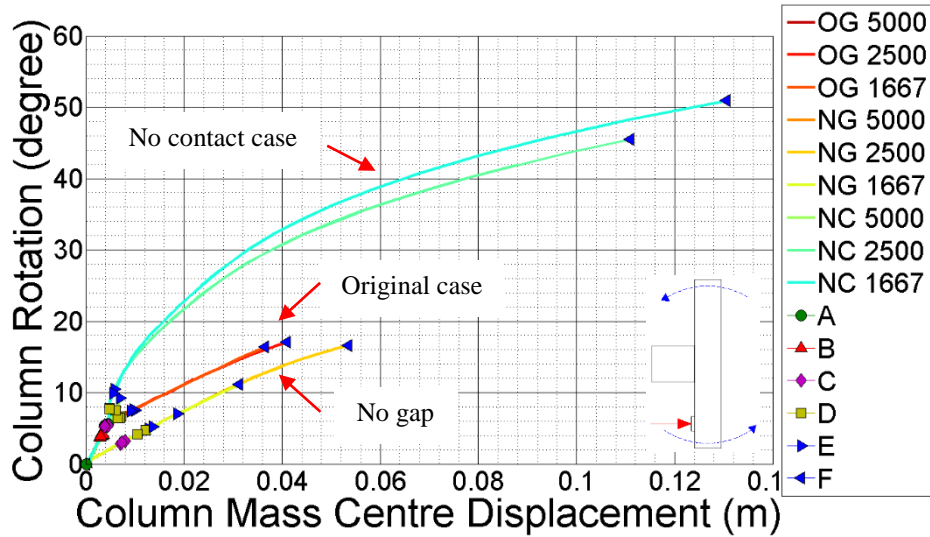


Figure 8-14 Column rotation against displacement LT1 10mm

(Coloured dots indicate the points at which: A- the beam and column flanges made contact and prying action commenced, B- Having failure at the top of the welding, C- 1<sup>st</sup> element in the model was eroded in the welding, D- Crack opened half way through the plate thickness, E- Cracked fully opened through the plate thickness, F- Crack went through whole length of the end plate)

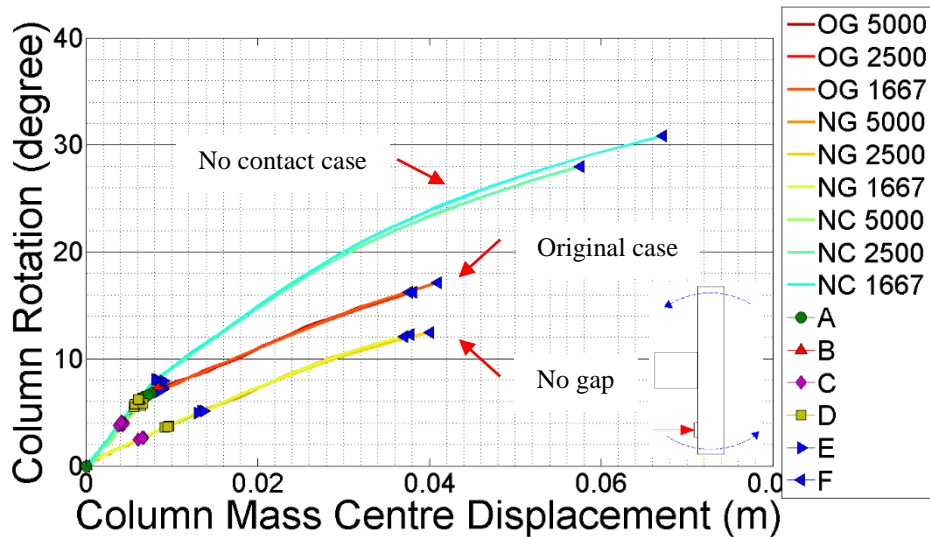


Figure 8-15 Column rotation against displacement LT1 8mm

(Coloured dots indicate the points at which: A- the beam and column flanges made contact and prying action commenced, B- Having failure at the top of the welding, C- 1<sup>st</sup> element in the model was eroded in the welding, D- Crack opened half way through the plate thickness, E- Cracked fully opened through the plate thickness, F- Crack went through whole length of the end plate)

### 8.3.1 Column displacement

Column displacement with time is a useful indicator of the effect of restricting rotational movement before contact is made between the column flange and beam lower flange. Figure 8-16 and Figure 8-17 both present the column displacement time history for 8mm thick plate, no gap and no contact in that order. In both cases there was a loading rate effect in the connection behaviour, higher loading rate results were closer to the original gap case. For 8mm thick plate the ductility reduced as the gap was filled and increased as the contacted was removed.

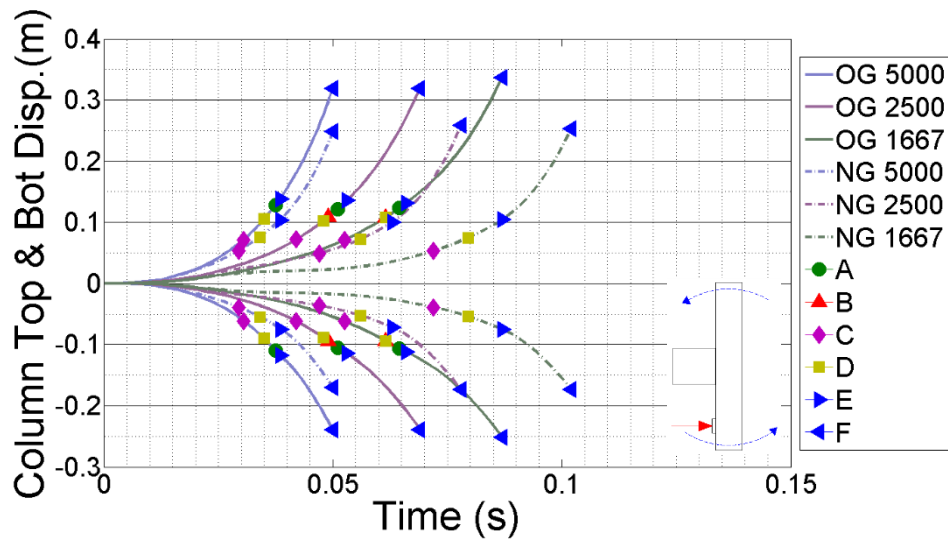


Figure 8-16 Column displacement time history LT1 8mm, no gap  
 (Coloured dots indicate the points at which: A- the beam and column flanges made contact and prying action commenced, B- Having failure at the top of the welding, C- 1<sup>st</sup> element in the model was eroded in the welding, D- Crack opened half way through the plate thickness, E- Cracked fully opened through the plate thickness, F- Crack went through whole length of the end plate)

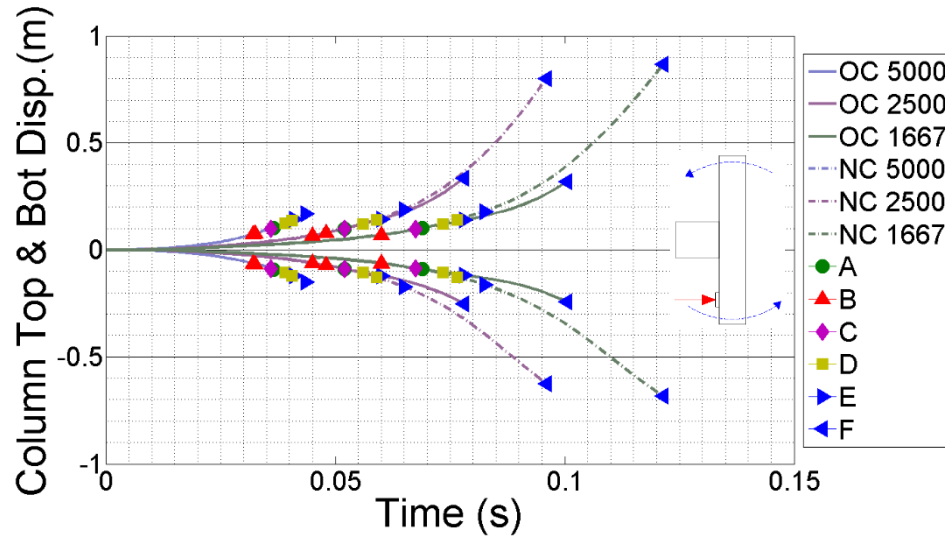


Figure 8-17 Column displacement time history LT1 10mm, no contact  
 (Coloured dots indicate the points at which: A- the beam and column flanges made contact and prying action commenced, B- Having failure at the top of the welding, C- 1<sup>st</sup> element in the model was eroded in the welding, D- Crack opened half way through the plate thickness, E- Cracked fully opened through the plate thickness, F- Crack went through whole length of the end plate)

### 8.3.2 Connection force resistance

There was no significant change in maximum value of force resistance of the connection as the gap was filled, however the force development was gradual and ductility was increased as there was no impact of flanges in this case. Figure 8-18 provides the results for 10mm thick plate under different loading rates; 8mm thick plate response was similar to 10mm. More column displacement with the same force resistance gave the connection the ability to dissipate more energy as the area under the Force-Displacement increased. On the opposite removing the contact reduced the resistance of the connection as the lever arm was reduced, overall dissipation of the energy was lower than the original case. Figure 8-19 provides the results for 8mm thick plate with no connection and different loading rates. Loading rate had no effect on force resistance in both cases.

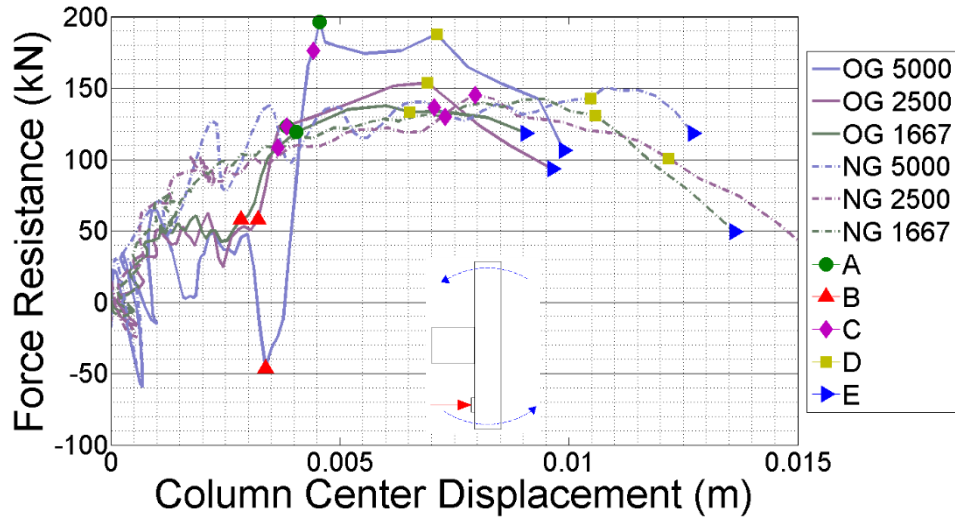


Figure 8-18 Force and column displacement LT1 10mm no gap  
 (Coloured dots indicate the points at which: A- the beam and column flanges made contact and prying action commenced, B- Having failure at the top of the welding, C- 1<sup>st</sup> element in the model was eroded in the welding, D- Crack opened half way through the plate thickness, E- Cracked fully opened through the plate thickness)

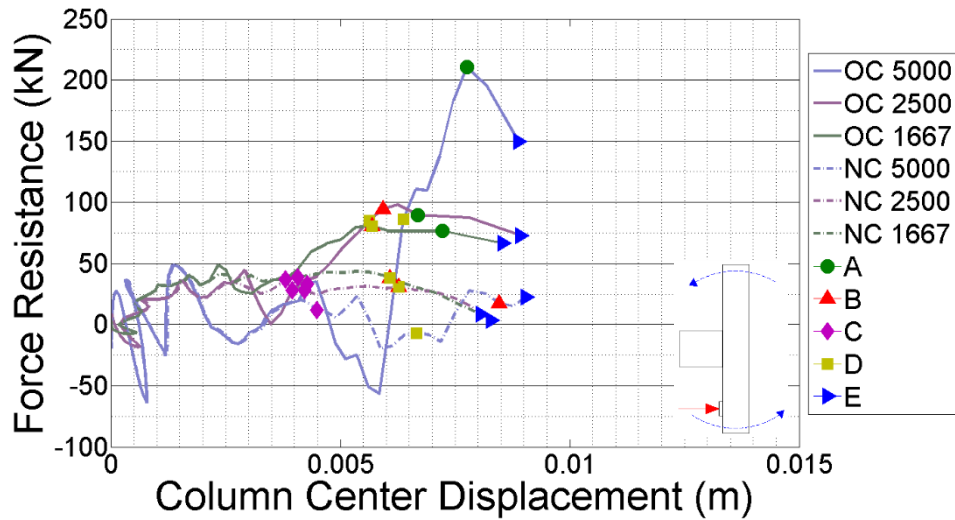


Figure 8-19 Force and column displacement LT1 8mm no contact  
 (Coloured dots indicate the points at which: A- the beam and column flanges made contact and prying action commenced, B- Having failure at the top of the welding, C- 1<sup>st</sup> element in the model was eroded in the welding, D- Crack opened half way through the plate thickness, E- Cracked fully opened through the plate thickness)

### 8.3.3 Connection moment resistance

Filling the gap caused the connection to mobilize the prying effect sooner and also increased the plate deformation and connection ductility. Consequently, the column rotated more slowly and the connection resisted more moment with both thicknesses and results for both plate thicknesses were similar, 8mm thick plate results are provided in Figure 8-20. Similar to force resistance, the area under the Moment-Rotation graph was increased which meant by filling the gap energy dissipation was increased.

Having no contact reduced the resistance and increased the column rotation at the point of failure. Comparing this behaviour to that of the web-cleat, the endplate connection never acted as a pin; even with no contact there was still a considerable amount of resistance compare to the original conditions. These results are provided in Figure 8-21.

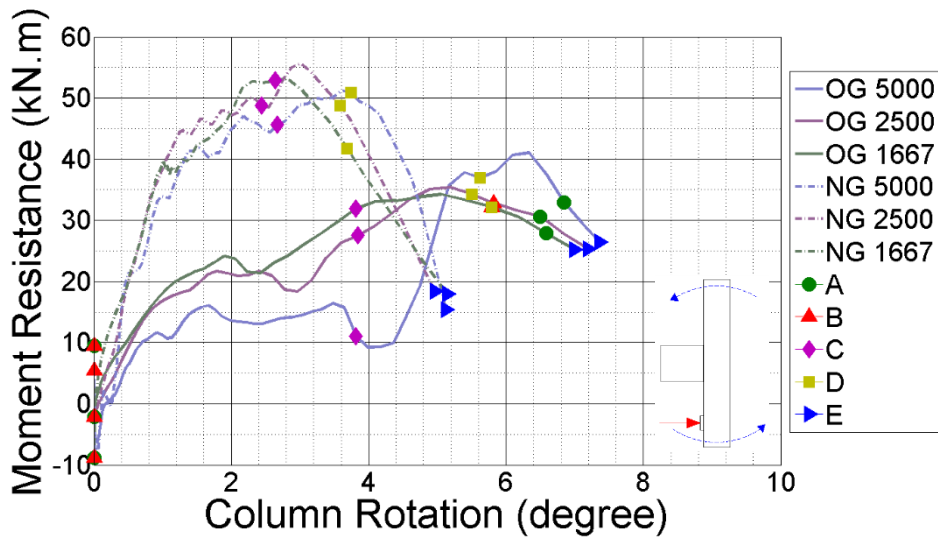


Figure 8-20 Moment and column rotation LT1 8mm no gap

(Coloured dots indicate the points at which: A- the beam and column flanges made contact and prying action commenced, B- Having failure at the top of the welding, C- 1<sup>st</sup> element in the model was eroded in the welding, D- Crack opened half way through the plate thickness, E- Cracked fully opened through the plate thickness)

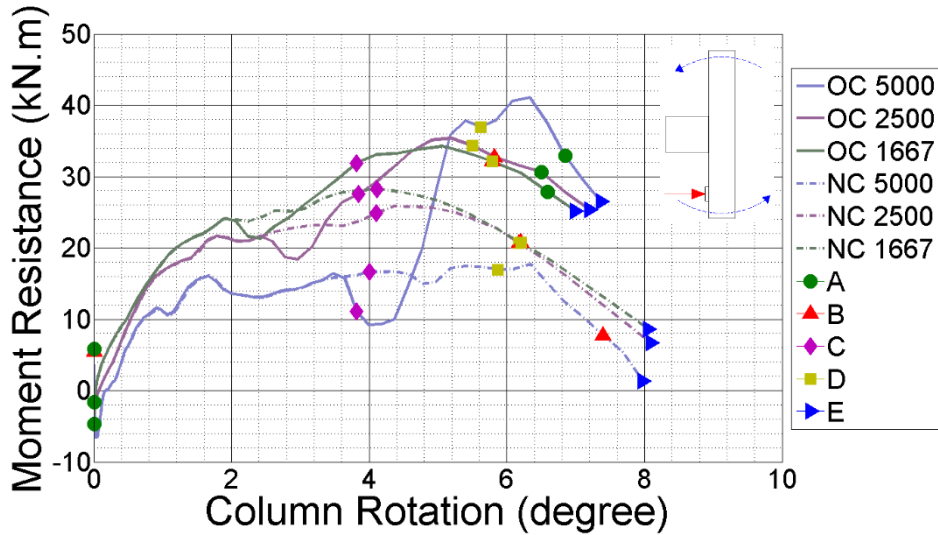


Figure 8-21 Moment and column rotation LT1 8mm no contact  
 (Coloured dots indicate the points at which: A- the beam and column flanges made contact and prying action commenced, B- Having failure at the top of the welding, C- 1<sup>st</sup> element in the model was eroded in the welding, D- Crack opened half way through the plate thickness, E- Cracked fully opened through the plate thickness)

### 8.3.4 Plate strain

In end-plate connections failure starts after the cracks begin to open. To understand how beam and column flange impact influence the failure, the strain of the element located in the area of crack initiation was measured. Figure 8-22 shows the location of the element as a single blue point and the red lines are the patterns of the cracks at two sides of the plate.

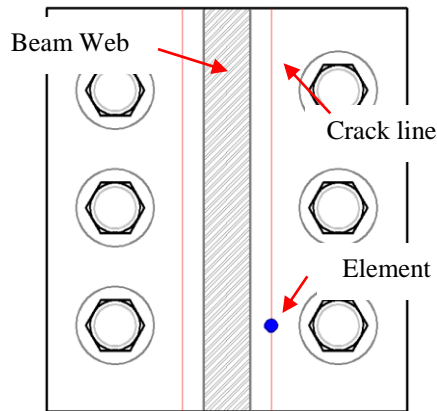


Figure 8-22 The location of the element on the plate which strain was measured

The amount and speed of deformation in the element could show the load distribution in the plate and how different loading rates and plate thicknesses can affect this distribution. Results from the strain measurements for this element are plotted against column rotation in Figure 8-23 under dynamic and static loading rates and having two different thicknesses.

To facilitate a more detailed comparison of the post-prying response and failure of the critical elements in the weld/HAZ at different loading rates, the strain in the first element to fail was plotted against normalised time, calculated as the ratio of actual time to the time at which prying commenced. As Figure 8-24 shows, the strain increased very rapidly in the dynamic models after the onset of prying whereas in the static analyses, the rate of increase was significantly less rapid; This appears to be a key feature, explaining the difference in the dynamic and static response of the endplate connections; a localized spike of strain in dynamic models, leading to premature failure of a section of the weld/HAZ, and consequently, to unzipping of the entire weld/HAZ at lower overall connection ductility than in the static loading.

As the strain started to increase dramatically it reached the maximum material strain resistance of 0.21 very rapidly. Unfortunately it was impossible to reduce the model output time step to a sufficiently low value to allow capture of the precise value of the peak strain resisted before element failure. It is clear, however, that the rapid rate at which the localized strain in the critical elements increases after the onset of prying in the dynamic models means that some elements will have exceeded their failure strain very quickly. Interestingly, whilst the precise quantitative predictions from these connection models must be treated with caution due to the lack of definitive rate-dependent material data for the weld/HAZ, it appears that the precise, rate-dependent value of the failure strain is of secondary importance, since the magnitude of strain in the critical elements will rapidly exceed this value in any case.

This suggests that the key feature of the dynamic behaviour of the endplate connections (the early failure with relatively little post-prying ductility) is due more to the impact loading associated with prying, than with inherent strain-rate dependent material

response. In other words, it is a structurally dynamic feature, rather than a material dynamic effect.

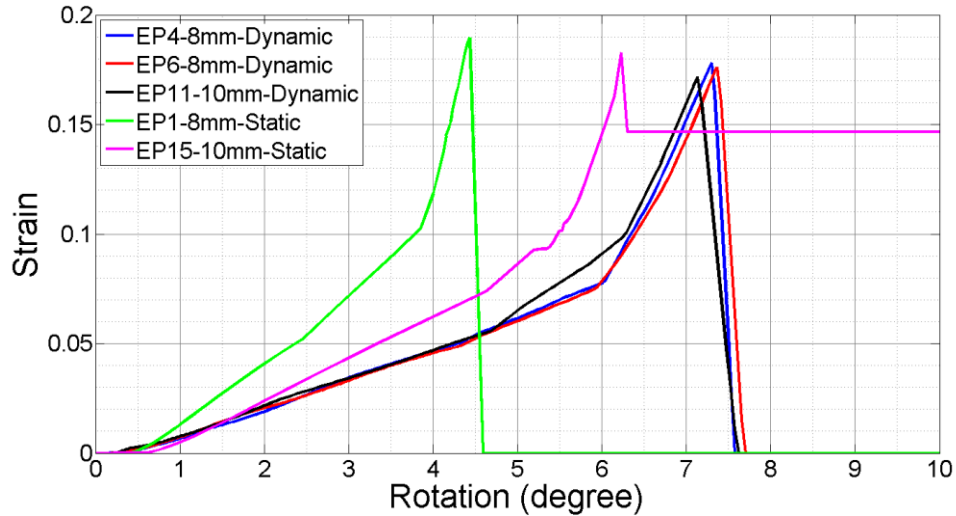


Figure 8-23 Strain against column rotation of the single element, with different loading rates

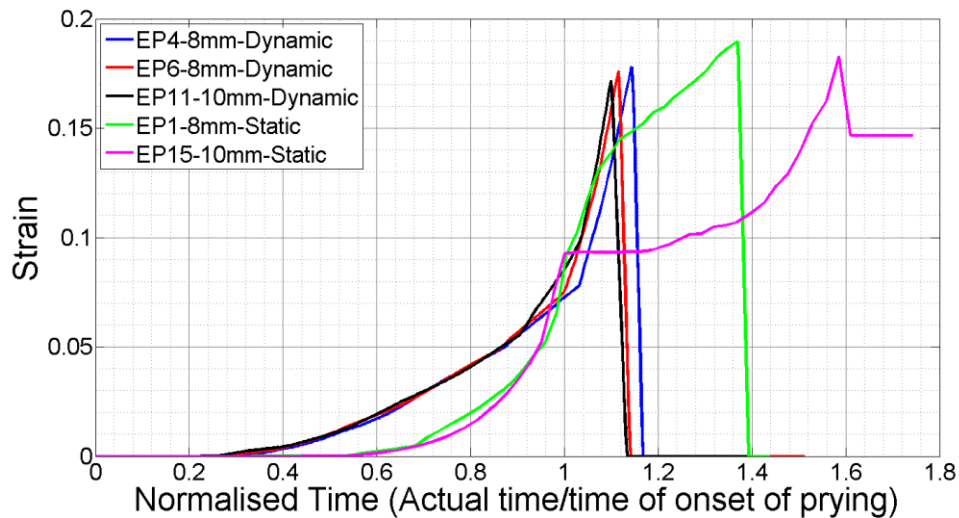


Figure 8-24 Strain against time unit of the single element, with different loading rates

As the impact associated with the onset of prying in the dynamic loading cases had a key role in inducing a rapid rise in the strain in the elements in the HAZ/weld region, this was investigated further with the modified (NG and NC) models. Three different elements located on the plate were measured to see the effects as the crack opens from point 3 and

goes up to the point 1, as shown in Figure 8-25. These studies were done based on two cases filling the gap and having no contact between the beam and column flange.

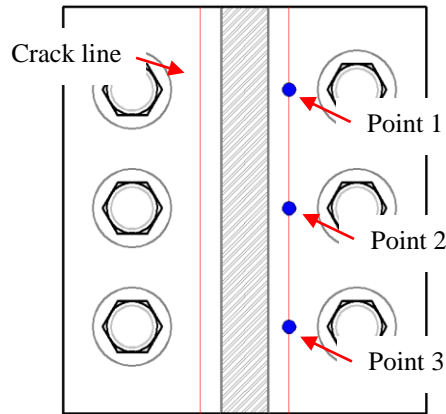


Figure 8-25 The location of three element on the plate which strain was measured

Figure 8-26 and Figure 8-27 provide the strain measurements of these three elements under different loading rates, and no gap and no contact cases in that order. In the case of no gap there was no significant difference in the highest dynamic rate, but the difference became more pronounced as the loading rate decreased and the element had more deformation. In general filling the gap helped the connection and as the deformation was more gradual ductility increased. Removing the contact made the connection more ductile, however compared to the original case there was no significant difference in strain at point3 and the other two points had more deformation. Having no contact helped the element deformation and introduced more ductility to the system, however compared to the case with the filled gap, ductility was less and not very gradual as there was some dramatic change of slope in strain (in all these plots strain did not reach to the maximum which was defined in the material properties, which was simply because it was impossible to capture all the results from analysis and some data can be missed between the time intervals of the output file).

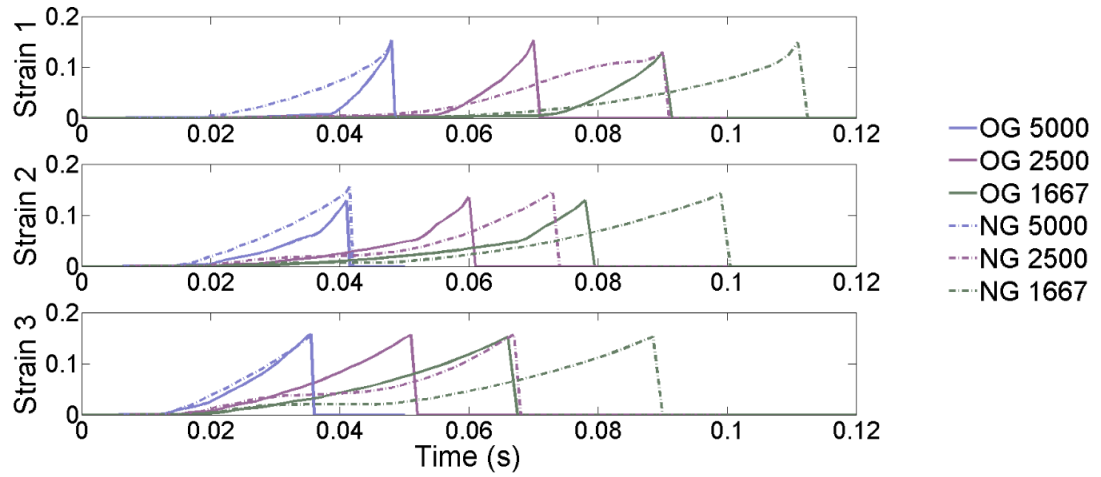


Figure 8-26 Strain against time of the three elements for 10mm thick plate, with different loading rates

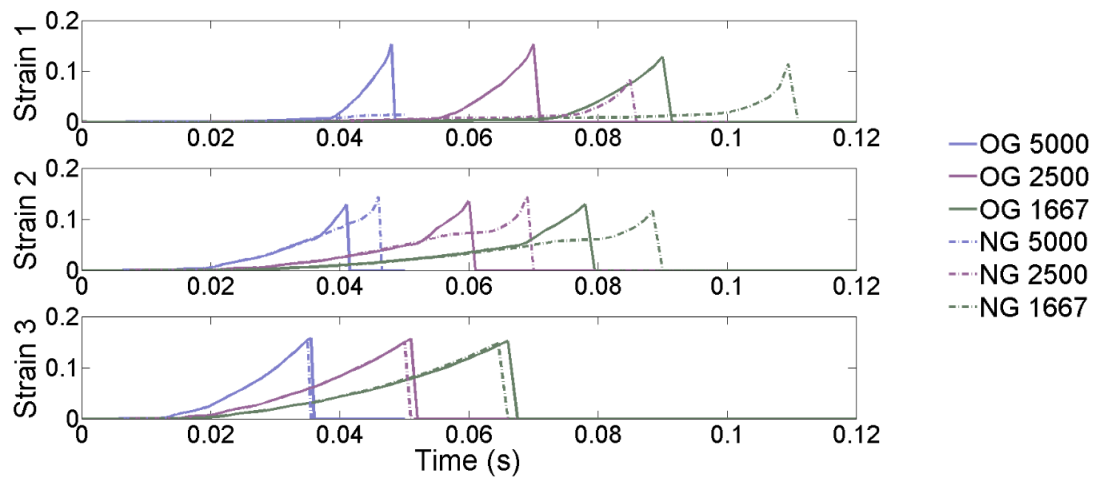


Figure 8-27 Strain against time of the three elements for 8mm thick plate, with different loading rates

## 8.4 Comparing two connections

To understand the difference between two different types of connections a comparison has been made based on the parametric studies (Section 6.8 and 7.8) and provided in Table 8-1.

<b>Comparison between two connections</b>	
	<b>Description</b>
Influence of Different Loading Types and Rates	<ul style="list-style-type: none"> <li>• Web-cleat: column displacement time history changed with different loading rates; angle deformed more in static than the dynamic loading; the connection can resist more force in pure tension; different loading rates did not change the resistance; lower angle thickness had lower ductility; the moment resistance did change by the type of the loading but not with the rate.</li> <li>• End-plate: displacement time history changed with different loading rates; the end plate had less deformation in static than dynamic loading; loading rate did not affect the ductility and resistance of the connection; pure tension loading caused more resistance in the connection; plate thickness had a major role in the connection force and moment resistance; the moment resistance of the connection did not change the loading rates.</li> </ul>
Influence of Bolt Strength	<ul style="list-style-type: none"> <li>• Web-cleat: connection became more rigid and brittle; angles deformed less; force and moment resistance of the connection did not change.</li> <li>• End-plate: connection behaviour did not change much; slightly more force resistance and no change in the moment resistance.</li> </ul>
Effect of Washer Size	<ul style="list-style-type: none"> <li>• Web-cleat: reduced the connection ductility and angle deformation; the force and moment resistance did not change.</li> <li>• End-plate: the connection ductility and plate deformation was reduced; the force and moment resistance increased by a small amount.</li> </ul>
Effect of Bolt Size	<ul style="list-style-type: none"> <li>• Web-cleat: column displacement and angle deformation were reduced; similar force resistance but increase in moment resistance.</li> <li>• End-plate: connection became stronger for both force and moment resistance and also it became more brittle with less plate deformation.</li> </ul>

Influence of Bolt Gauge	<ul style="list-style-type: none"> <li>• Web-cleat: (LBG) column displacement and angle deformation reduced but force and moment resistance of the connection unaffected; (MBG) column displacement and angle deformation were increased and the ductility improved but the force and moment resistance of the connection remained the same.</li> <li>• End-plate: (LBP) the ductility reduced but no change in the force and column resistance (MBG) the connection ductility and plate deformation increased, but the force and moment resistance were reduced.</li> </ul>
Influence of Bolt Pitch	<ul style="list-style-type: none"> <li>• Web-cleat: For both LBP and MBP the connection's ductility and resistance did not changed much.</li> <li>• End-plate: (LBP) increased the connection ductility and plate deformation; the force resistance was the same but the moment resistance of the connection increased (MBP) the column displacement, plate deformation, ductility, force and moment resistance were all reduced.</li> </ul>

Table 8-1 Comparison between two different connection types

## 8.5 Conclusion

In general filling the gap between the beam and column flange gave both types of connection (web-cleat and end-plate) more ductility. Doing so had no significant effect on web-cleat resistance but it could increase the resistance in end-plate connections. The overall consequence of this change was positive in terms of removing the sudden application of force from flange impacts and also increased the energy dissipation in the connection. Behaviour of both connections in this case was more smooth and gradual.

Removing the contact also increased the ductility, but reduced the resistance in both connections. This reduction was more in the web-cleat connection as this connection behaved more like a pin in this condition, however end-plates became more flexible but not close to a pin. Overall the amount of energy dissipated in the connection was reduced which is not a positive change.

Comparing these two connections shows that end-plate connection is more load rate dependent than the web-cleat. It is possible to have more ductility in end-plate connections and have more resistance in web-cleat connections. An end-plate connection is more sensitive to different changes compared to a web-cleat connection.

## 9 Conclusion

This research has examined the performance of web-cleat and end-plate connections under different ranging loading from quasi-static up to fast dynamic. Conducting experiments to understand connections response under rapidly applied loading is expensive which led to the main objective of this research, to investigate the possibility of developing a highly detailed dynamic FE model of these steel connections to behave similarly as the real connection.

These models were successfully developed and validated against repeatable controlled experimental data. Models are able to capture the key aspects of connections behaviour, including the failure modes, when loaded to failure in less than 100ms or more than 100s in combined axial extension and rotation. The validated models were used to generate data from parametric studies of load rate, connections geometry and material to examine the effect on both strength and ductility.

Numerical modelling and experimental results showed that there is a significant difference in the rate-dependent behaviour of the web-cleat and flexible endplate connection types. As rotation and moment were introduced to both connections, axial tension resistance of the connections dropped dramatically compared to pure axial tension loading.

The web-cleat connection was insensitive to the change of loading rate, the reason for this behaviour seems to be the highly ductile reaction of this type of connection under different rates of loading as plastic deformation of the angles dissipates the energy of the impact and the critical failure mode happens in the beam web. Plastic deformation of the angle helped to distribute the strain more evenly around the connection and damped the strain rate effects caused by the high loading rates, results showed insignificant effect in material behaviour. By these findings, if the size of different components in the connection are designed in a way to ensure plastic deformation, there is likely to be only a small difference in connection response across different loading range, and as result dynamic behaviour of the connection could be ignored and static response of the connection used in a dynamic frame response to column-loss scenarios analysis.

Parametric studies on web-cleat connection with different geometry revealed some important factors in this type of connection behaviour. Having stronger bolts or washers in the connection, ductility and resistance did not change, bigger bolt size did reduce the ductility but gave more resistance to the connection. Bolt gauge had a direct influence on ductility, however by increasing the bolt gauge connection resistance reduced. Changing the bolt pitch had an insignificant effect on overall connection behaviour, both on ductility and resistance.

End-plate connections behaved very differently to web-cleat, as by increasing the loading rates there was less time for the plate to deform and dissipate the energy caused by a dynamic impact between the beam and column flange, due to the momentum generated in the connection, this resulted in a localized concentration of high strain in the weld/HAZ in the region of the end-plate/beam web connection closest to the most heavily loaded row of bolts. This concentration of strain and not enough time for the plate to resist, resulted in an initiation of an unzipping of the weld/HAZ and consequently overall failure of the connection at much lower overall connection ductility.

Similar to web-cleat connections, parametric studies showed an insignificant effect on connection behaviour by having stronger bolts or washers. Bigger bolts gave more resistance and less ductility to the connection and reducing the bolt gauge increased the resistance and reduced the ductility. Moment resistance increased as the bolt pitch reduced, force resistance did not change at the highest loading rate for any change in bolt pitch and reduced at lower rates irrespective of bolt pitch.

Prying effect caused by the impact between the beam flange and the column flange was shown to be an essential factor in connection behaviour. Studies on filling the gap between the beam and column flange showed that both types of connection (web-cleat and end-plate) behaved in a more ductile manner. There was no significant change in web-cleat connection resistance and end-plate resistance. This change helped both connections to dissipate more energy which was a positive effect on the connection behaviour, by preventing a sudden application of force flange impact to have a more smooth and gradual development of the force in the connection.

On the other hand removing the contact between beam and column flanges increased the ductility but it also reduced the connection resistance, this reduction was more in web-clip connection as this connection behaved more like a pin without the contact., Dissipation of energy reduced in both types of connection and it was a negative point with respect to overall structural integrity.

There has been relatively little work conducted to understand the response of different types of connections to rapidly applied loads. This work has answered the important question of whether it is possible to develop finite element models capable of simulating the complex behaviour of connections under high rate loading. The validated tool is available to study the behaviour of these connections will assist researchers to develop component-based models of these connection and use them in frame analysis of structures for structural integrity analysis. Also there remains much work to be done for other connection types and failure mechanisms and the validated FE model is a valuable tool to conduct further studies.



## References

- [1] A. Tyas and J. B. Davison, “Response of Steel Beam-to-Column Connections to Dynamic Loading,” *EPSRC*, no. EP/F004338/1.
- [2] S. Paramasivam and M. Byfield, “Catenary Action in Steel-Framed Buildings,” *Proc. ICE - Struct. Build.*, vol. 160, no. 5, pp. 247–257, Jan. 2007.
- [3] P. Mlakar, Sr, and W. Corley, “The Oklahoma City bombing: Analysis of Blast Damage to The Murrah Building,” *J. Perform. Constr. Facil.*, no. August, pp. 113–119, 1998.
- [4] W. Corley, “Lessons learned on Improving Resistance of Buildings to Terrorist Attacks,” *J. Perform. Constr. Facil.*, no. May, pp. 68–78, 2004.
- [5] C. M. Yang and Y. M. Kim, “Cyclic Behavior of Bolted and Welded Beam-to-Column Joints,” *Int. J. Mech. Sci.*, vol. 49, no. 5, pp. 635–649, May 2007.
- [6] a. B. Izzuddin, a. Y. Elghazouli, a. D. Nethercot OBE, and a. G. Vlassis, “Assessment of Progressive Collapse in Multi-Storey Buildings,” *Proc. ICE - Struct. Build.*, vol. 160, no. 4, pp. 197–205, Jan. 2007.
- [7] G. Gudmundsson and B. Izzuddin, “The ‘Sudden Column Loss’ Idealisation for Disproportionate Collapse Assessment,” *Struct. Eng.*, vol. 88, no. March, pp. 22–26, 2010.
- [8] G. W. Owens and D. B. Moore, “The Robustness of Simple Connections,” *Struct. Eng.*, vol. 70, pp. 37–46, 1992.
- [9] E. P. Stoddart, M. P. Byfield, J. B. Davison, and A. Tyas, “Strain Rate Dependent Component Based Connection Modelling for Use in Non-Linear Dynamic Progressive Collapse Analysis,” *Eng. Struct.*, vol. 55, pp. 35–43, Oct. 2013.
- [10] R. Hamburger, “Alternative Methods of Evaluating and Achieving Progressive Collapse Resistance,” *Proc. North Am. Struct. Steel Conf., AISC*, pp. 1–10, 2006.
- [11] FEMA, “World Trade Center Building Performance Study,” 2002.
- [12] IStructE, “Safety in Tall Buildings and Other Buildings with Large Occupancy,” 2002.
- [13] C. Liu, K. H. Tan, and T. C. Fung, “Dynamic Behaviour of Web Cleat Connections Subjected to Sudden Column Removal Scenario,” *J. Constr. Steel Res.*, vol. 86, pp. 92–106, Jul. 2013.

- [14] A. Tyas, J. a. Warren, E. P. Stoddart, J. B. Davison, S. J. Tait, and Y. Huang, "A Methodology for Combined Rotation-Extension Testing of Simple Steel Beam to Column Joints at High Rates of Loading," *Exp. Mech.*, vol. 52, no. 8, pp. 1097–1109, Jan. 2012.
- [15] E. Stoddart, M. Byfield, and A. Tyas, "Blast Modeling of Steel Frames with Simple Connections," *J. Struct. Eng.*, no. 1, pp. 1–11, 2012.
- [16] T. Sabuwala, D. Linzell, and T. Krauthammer, "Finite element analysis of steel beam to column connections subjected to blast loads," *Int. J. Impact Eng.*, vol. 31, no. 7, pp. 861–876, Aug. 2005.
- [17] M. Engelhardt, T. Sabol, R. Aboutaha, and K. Frank, "Northridge Moment Connection Test Program." Eleventh World Conference on Earthquake Engineering, 1994.
- [18] J. Crawford, "Retrofit Methods to Mitigate Progressive Collapse," *Karagozian & Case*, 2002. [Online]. Available: [http://c.yimcdn.com/sites/www.nibs.org/resource/resmgr/mmc/wppc\\_crawfords\\_paper.pdf](http://c.yimcdn.com/sites/www.nibs.org/resource/resmgr/mmc/wppc_crawfords_paper.pdf).
- [19] K. Morrill, J. Crawford, J. Magallanes, and H. Choi, "Development of Simplified Tools to Predict Blast Response of Steel Beam-Column Connections," *Structures Congress*, 2007. [Online]. Available: [http://ascelibrary.org/doi/pdf/10.1061/40944\(249\)69](http://ascelibrary.org/doi/pdf/10.1061/40944(249)69). [Accessed: 12-Mar-2013].
- [20] H. Jahromi, B. Izzuddin, D. Nethercot, S. Donahue, M. Hadjioannou, E. Williamson, M. Engelhardt, D. Stevens, K. Marchand, and M. Waggoner, "Robustness Assessment of Building Structures under Explosion," *Buildings*, vol. 2, no. 4, pp. 497–518, Dec. 2012.
- [21] United States Office of the Chief Architect, "Progressive Collapse Analysis and Design Guidelines," 2003.
- [22] R. Nair, "Progressive Collapse Basics," in *Modern Steel Construction*, 2004, pp. 1–11.
- [23] K. Khandelwal and S. El-Tawil, "Collapse Behavior of Steel Special Moment Resisting Frame Connections," *J. Struct. Eng.*, vol. 133, no. 5, p. 646, 2007.
- [24] D. A. Taylor, "Progressive Collapse," *Can. J. Civ. Eng.*, vol. 2, no. 4, pp. 517–529, Dec. 1975.
- [25] B. R. Ellingwood and E. V. Leyendecker, "Approaches for Design against Progressive Collapse," *J. Struct. Div.*, vol. 104, no. 3, pp. 413–423, 1978.

- [26] B. Ellingwood and D. Dusenberry, "Building Design for Abnormal Loads and Progressive Collapse," *Comput. Civ. Infrastruct. Eng.*, vol. 20, pp. 194–205, 2005.
- [27] BS 8110, "Structural Use of Concrete–Part 1: Code of Practice for Design and Construction," 1997.
- [28] BS EN 1991-1-1, "Eurocode 1 : Actions on structures," *BSI*, 2002.
- [29] DoD, "DoD Research and Criteria for the Design of Buildings to Resist Progressive Collapse UFC 4-023-03," *Dep. Defense, USA.*, Sep. 2005.
- [30] B. Ellingwood and R. Smilowitz, "Best Practices for Reducing the Potential for Progressive Collapse in Buildings," National Institute of Standards and Technology, 2007.
- [31] Y. Li, X. Lu, H. Guan, and L. Ye, "An Improved Tie Force Method for Progressive Collapse Resistance Design of Reinforced Concrete Frame Structures," *Eng. Struct.*, vol. 33, no. 10, pp. 2931–2942, Oct. 2011.
- [32] K. L. Carper, "Mitigation the Risk for Progressive Disproportionate Structural Collapse," *J. Perform. Constr. Facil.*, vol. 20, no. 4, pp. 305–306, 2006.
- [33] O. A. Mohamed and M. Asce, "Progressive Collapse of Structures : Annotated Bibliography and Comparison of Codes and Standards," no. November, pp. 418–425, 2006.
- [34] K. Menchel and P. Bouillard, "Progressive Collapse: Comparison of Main Standards, Formulation and Validation of New Computational Procedures," 2008.
- [35] D. Cormie, G. Mays, and P. Smith, *Blast Effects on Buildings*, vol. 20, no. 9. Thomas Telford Ltd, 2009.
- [36] R. Martin, "L' Ambiance Plaza Collapse." [Online]. Available: [http://911research.wtc7.net/cache/wtc/analysis/compare/enguab\\_ambiance.htm](http://911research.wtc7.net/cache/wtc/analysis/compare/enguab_ambiance.htm).
- [37] Oklahoma Department of Civil Emergency Management, "After Action Report Alfred P . Murrah Federal Building Bombing 19 April 1995 in Oklahoma City , Oklahoma," *Dep. Cent. Serv. Cent. Print. Div.*, 1995.
- [38] K. Marchand and F. Alfawakhiri, "Facts for Steel Suildings: Blast and progressive collapse," *Am. Inst. Steel Constr. Inc.*, no. 2, 2004.
- [39] EPA, "EPA ' s Response to the World Trade Center Collapse : Challenges , Successes , and Areas for Improvement," *U.S. Environ. Prot. Agency.*, 2003.

- [40] R. Nair, “Progressive Collapse Basics,” *Mod. Steel Constr.*, pp. 1–11, 2004.
- [41] A. Society, “ASCE 7-05 Minimum Design Loads for Buildings and Other Structures.”
- [42] National Building Code of Canada (NBCC), “Part 4 and Commentary C,” 1995.
- [43] FEMA, “Reference Manual to Mitigate Potential Terrorist Attacks Against Buildings,” 2003.
- [44] K. Suita, K. Kaneta, and I. Khozu, “The Effect of Strain Rate in Steel Structural Joints Due to High Speed Cyclic Loading,” *Proc. 10th World Conf. Earthq. Eng.*, 1992.
- [45] BCSCA/SCI, “Joints in Steel Construction: Simple Connections,” 2002.
- [46] Arup, “Review of International Research on Structural Robustness and Disproportionate Collapse,” 2011.
- [47] U. Kuhlmann, L. Rolle, and J. Jaspart, “Robust Structure by Joint Ductility,” *IABSE Symp.*, pp. 1–10, Apr. 2009.
- [48] S. Engineering, “Unified Facilities Criteria ( UFC ) Structural Engineering,” 2011.
- [49] C. Harun, “3D Finite Element Analysis of Semi-Rigid Steel Cconnections,” Middle East Technical University, 2009.
- [50] E. Munoz-Garcia, B. Davison, and A. Tyas, “Structural Integrity of Steel Connections Subjected to Rapid Rates of Loading,” in *Structures Congress 2005*, 2005, pp. 1–12.
- [51] F. Sadek, J. Main, and H. Lew, “An Experimental and Computational Study of Steel Moment Connections Under a Column Removal Scenario,” *Natl. Institute Stand. Technol.*, 2010.
- [52] C. O. Rex and W. S. Easterling, “Behavior and Modeling of a Bolt Bearing on a Single Plate,” *J. Struct. Eng.*, vol. 129, no. 6, pp. 792–800, 2003.
- [53] P. Može and D. Beg, “A Complete Study of Bearing Stress in Single Bolt Connections,” *J. Constr. Steel Res.*, vol. 95, pp. 126–140, 2014.
- [54] G. W. Owens and B. Cheal, *Structural Steelwork Connections*. Butterworth-Heinemann, 1989.

- [55] P. Moe and D. Beg, "Investigation of High Strength Steel Connections With Several Bolts in Double Shear," *J. Constr. Steel Res.*, vol. 67, no. 3, pp. 333–347, 2011.
- [56] P. Može and D. Beg, "High Strength Steel Tension Splices With One or Two Bolts," *J. Constr. Steel Res.*, vol. 66, no. 8–9, pp. 1000–1010, 2010.
- [57] H. Draganić, T. Dokšanović, and D. Markulak, "Investigation of Bearing Failure in Steel Single Bolt Lap Connections," *J. Constr. Steel Res.*, vol. 98, pp. 59–72, 2014.
- [58] LSTC, "LS-DYNA keyword user's manual volume I," *Livermore Software Technology Corporation*, 2012. [Online]. Available: [http://ftp.lstc.com/anonymous/outgoing/trent001/manuals/LS-DYNA\\_manual\\_Vol\\_I\\_R6.1.0.pdf](http://ftp.lstc.com/anonymous/outgoing/trent001/manuals/LS-DYNA_manual_Vol_I_R6.1.0.pdf).
- [59] M. Jutras, "Improvement of The Characterisation Method of The Johnson-Cook Model," Université Laval, 2008.
- [60] N. Nsiampa, F. Coghe, and G. Dyckmans, "Numerical Investigation of The Bodywork Effect (K-Effect)," *DYMAT 2009 - 9th Int. Conf. Mech. Phys. Behav. Mater. under Dyn. Load.*, vol. 2, pp. 1561–1566, Sep. 2009.
- [61] G. Johnson and W. Cook, "Fracture Characteristics of Three Metals Subjected to Various Strains, Strain rates, Temperatures and Pressures," *Eng. Fract. Mech.*, vol. 21, no. 1, 1985.
- [62] G. Johnson and W. Cook, "A Constitutive Model and Data for Metals Subjected to Large Strains, High Strain Rates and High Temperatures," *Seventh Int. Symp. Ballist.*, 1983.
- [63] F. J. Zerilli and R. W. Armstrong, "Dislocation-Mechanics-Based Constitutive Relations for Material Dynamics Calculations," *J. Appl. Phys.*, vol. 61, no. 5, p. 1816, 1987.
- [64] V. Gyliene and V. Ostasevicius, "Cowper-Symonds Material Deformation Law Application in Material Cutting Process Using LS-DYNA FE Code," in *LS-DYNA® 8th European User's ...*, 2011.
- [65] A. Priyadarshini, S. K. Pal, and A. K. Samantaray, "Influence of The Johnson Cook Material Model Parameters and Friction Models on Simulation of Orthogonal Cutting Pprocess," Indian Institute of Technology Kharagpur.
- [66] T. Børvik, O. . Hopperstad, T. Berstad, and M. Langseth, "A Computational Model of Viscoplasticity and Ductile Damage for Impact and Penetration," *Eur. J. Mech. - A/Solids*, vol. 20, no. 5, pp. 685–712, Sep. 2001.

- [67] W.-Y. Li, T. Ma, and J. Li, “Numerical simulation of linear friction welding of titanium alloy: Effects of processing parameters,” *Mater. Des.*, vol. 31, no. 3, pp. 1497–1507, Mar. 2010.
- [68] P. Oscar and R. L. Eduardo, “Impact Performance of Advanced High Strength Steel Thin-Walled Columns,” vol. II, no. 0, pp. 2–7, 2008.
- [69] M. Mićunović and C. Albertini, “High Strain Rate Viscoplasticity of AISI316H Stainless Steel From Tension and Shear Experiments,” *Solid Mech.*, pp. 1–11, 1997.
- [70] M. Šlais, I. Dohnal, and M. Forejt, “Determination of Johnson-Cook Equation Parameters,” *Acta Metall. Slovaca*, vol. 18, no. 2, pp. 125–132, 2012.
- [71] NTIS, “Failure Modeling of Titanium-61-4V and 2024-T3 Aluminum with the Johnson-Cook Material Model,” 2002.
- [72] A. Dorogoy and D. Rittel, “Determination of the Johnson–Cook Material Parameters Using the SCS Specimen,” *Exp. Mech.*, vol. 0, 2009.
- [73] L. Schwer, “Optional Strain-rate forms for the Johnson Cook Constitutive Model and the Role of the parameter Epsilon\_0,” *LS-DYNA Anwenderforum, Frankenthal*, pp. 1–14, 2007.
- [74] G. Gray, S. Chen, W. Wright, and M. Lopez, “Constitutive Equations for Annealed Metals Under Compression at High Strain Rates and High Temperatures,” *New Mex. los Alamos Natl. Lab.*, 1994.
- [75] M. Dietenberger, M. Buyuk, and C. Kan, “Development of a High Strain-Rate Dependent Vehicle Model,” *LS-Dyna Anwenderforum, ...*, no. 1, pp. 1–10, 2005.
- [76] LSTC, “LS-DYNA Keyword User’s Manual Volume II,” 2012.
- [77] “Finite Element Analysis of Structures.” [Online]. Available: <http://www.varminal.com/aengr.htm>.
- [78] K. Vedantam, “Johnson - Cook Strength Models for Mild and DP 590 Steels,” in *AIP Conference Proceedings*, 2006, vol. 845, pp. 775–778.
- [79] P. Sreenivasan and S. Mannan, “Dynamic JR Curves and Tension-Impact Properties of AISI 308 Stainless Steel Weld,” *Int. J. Fract.*, pp. 229–249, 2000.
- [80] Q. Xue, D. Benson, M. a. Meyers, V. F. Nesterenko, and E. a. Olevsky, “Constitutive Response of Welded HSLA 100 Steel,” *Mater. Sci. Eng. A*, vol. 354, no. 1–2, pp. 166–179, Aug. 2003.

- [81] L.-E. Lindgren, "Numerical Modelling of Welding," *Comput. Methods Appl. Mech. Eng.*, vol. 195, no. 48–49, pp. 6710–6736, Oct. 2006.
- [82] T. Børvik, O. S. Hopperstad, S. Dey, E. V. Pizzinato, M. Langseth, and C. Albertini, "Strength and Ductility of Weldox 460 E Steel at High Strain Rates, Elevated Temperatures and Various Stress Triaxialities," *Eng. Fract. Mech.*, vol. 72, no. 7, pp. 1071–1087, May 2005.
- [83] B. Taylor and A. Guesnier, "Metallography of Welds," 2008.

## **Appendix A Model geometry and drawings**

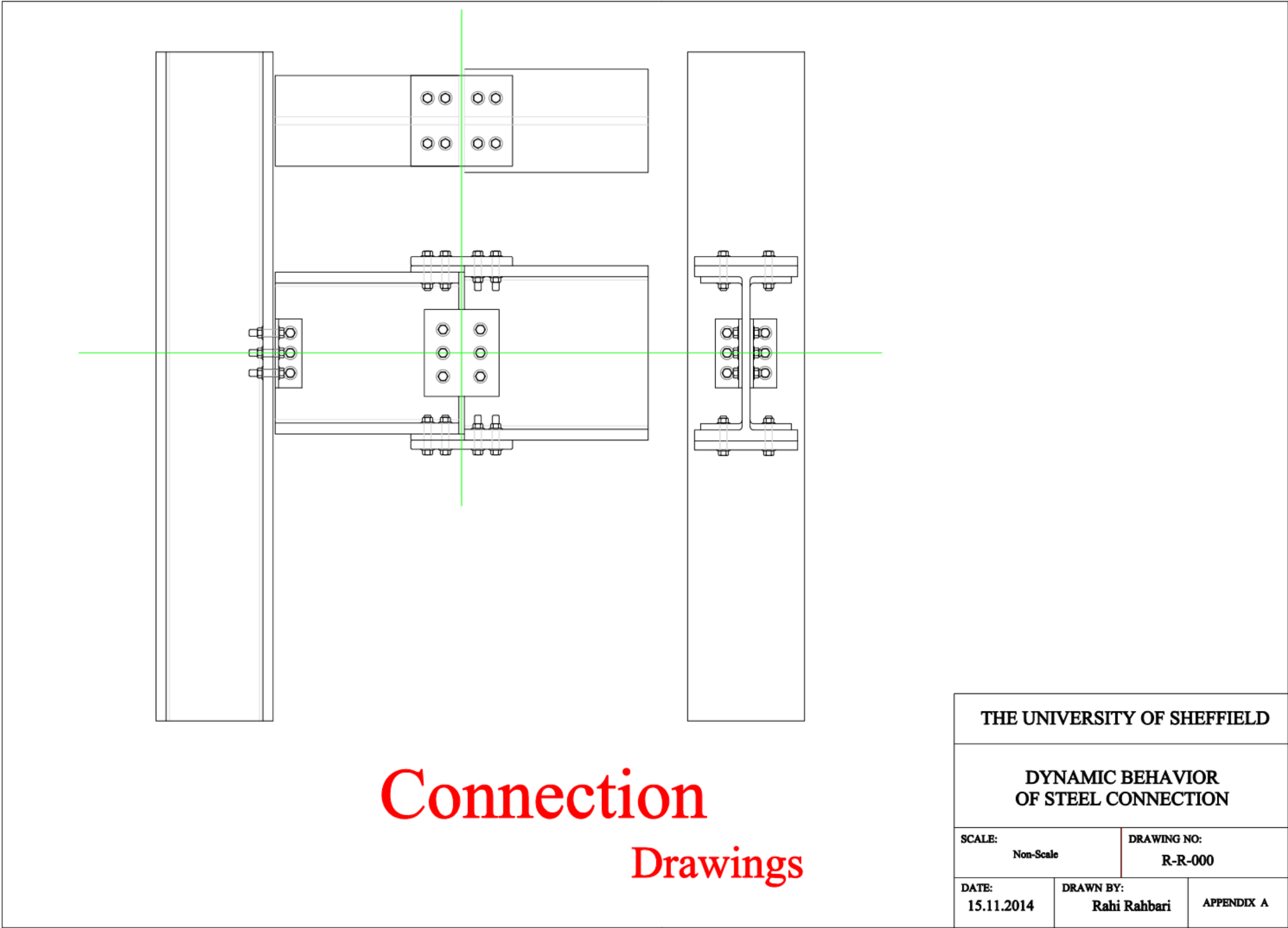


Figure A- 1, Main drawing of the model

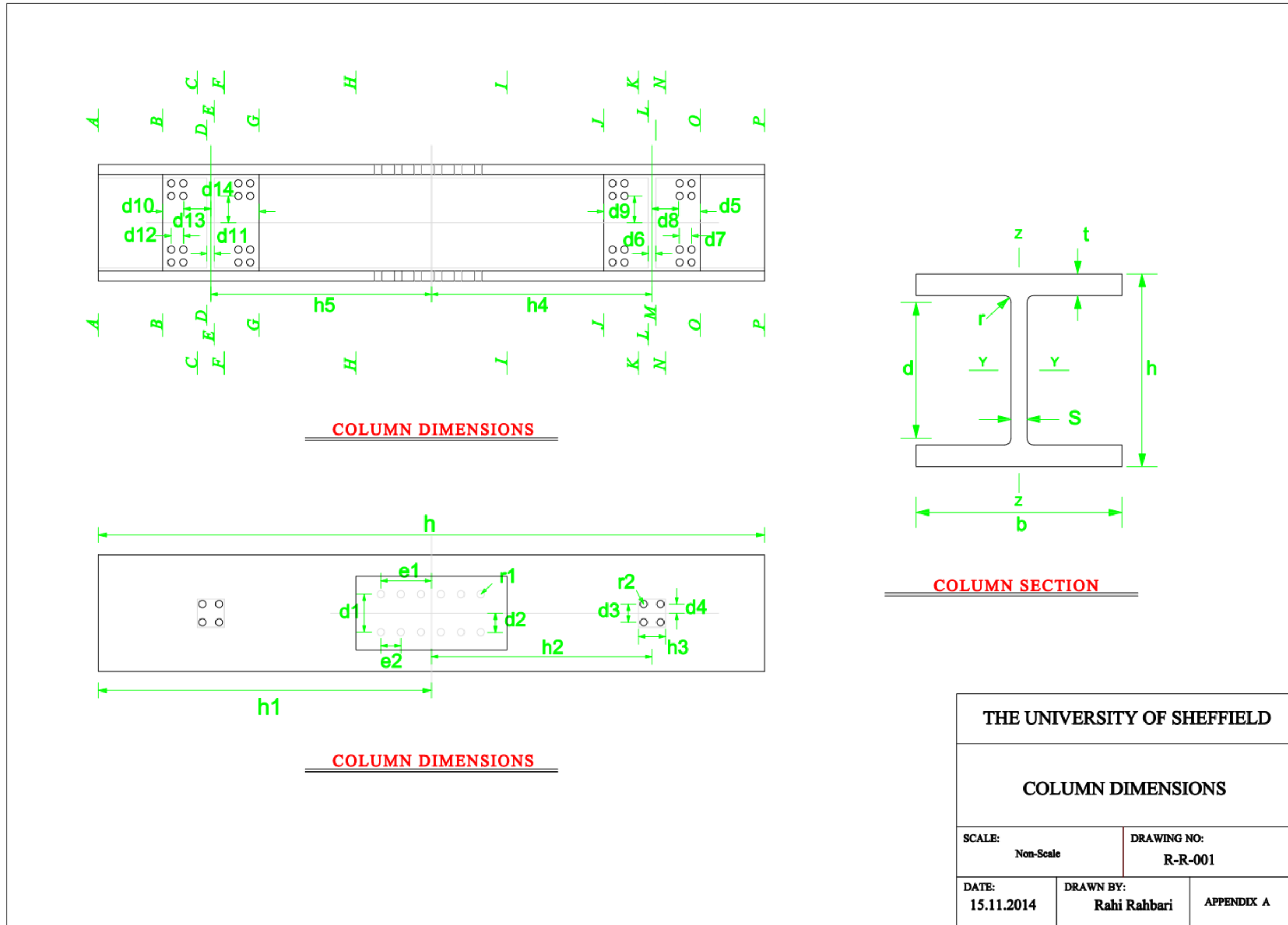


Figure A- 2, Column drawings

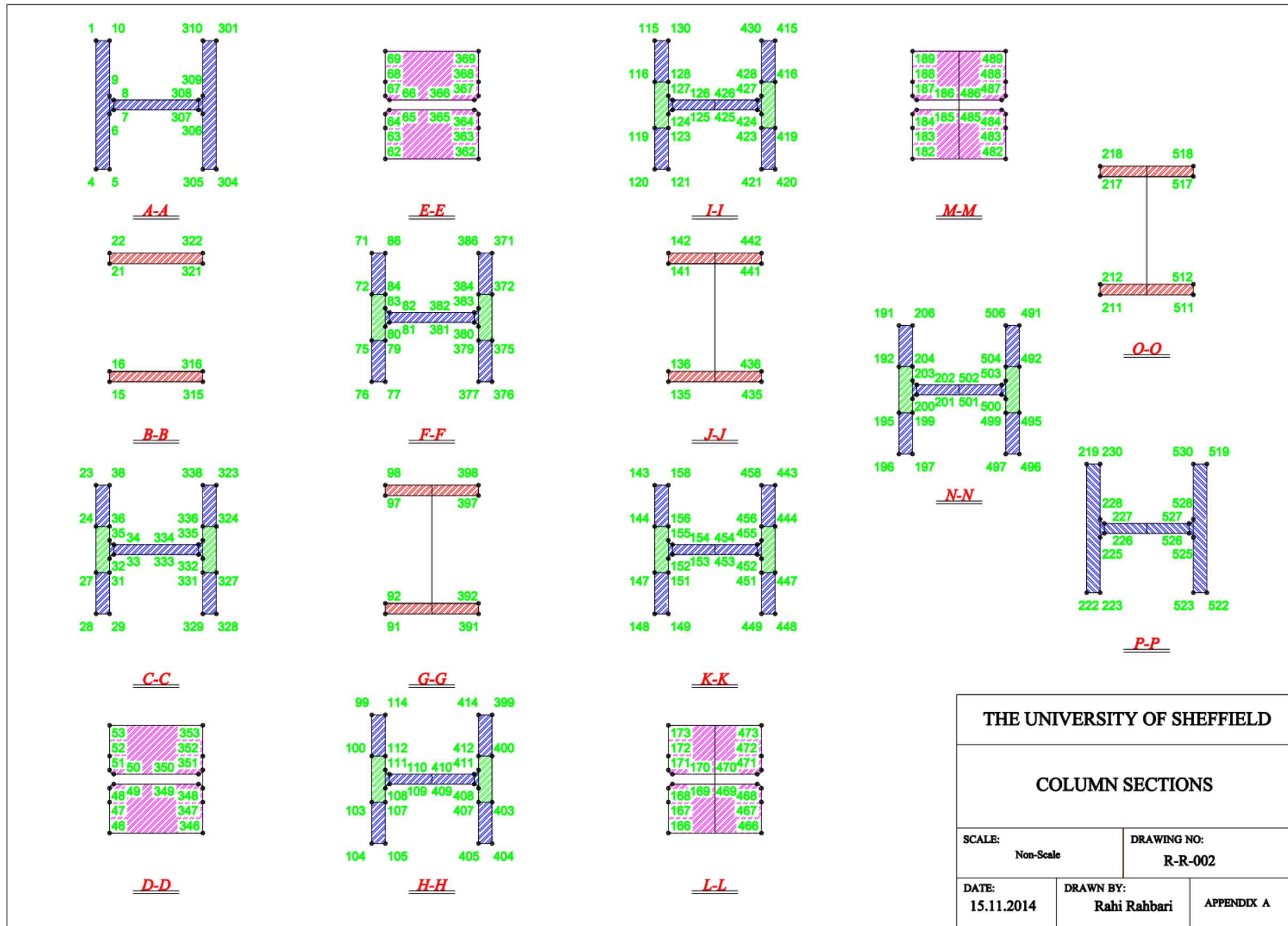
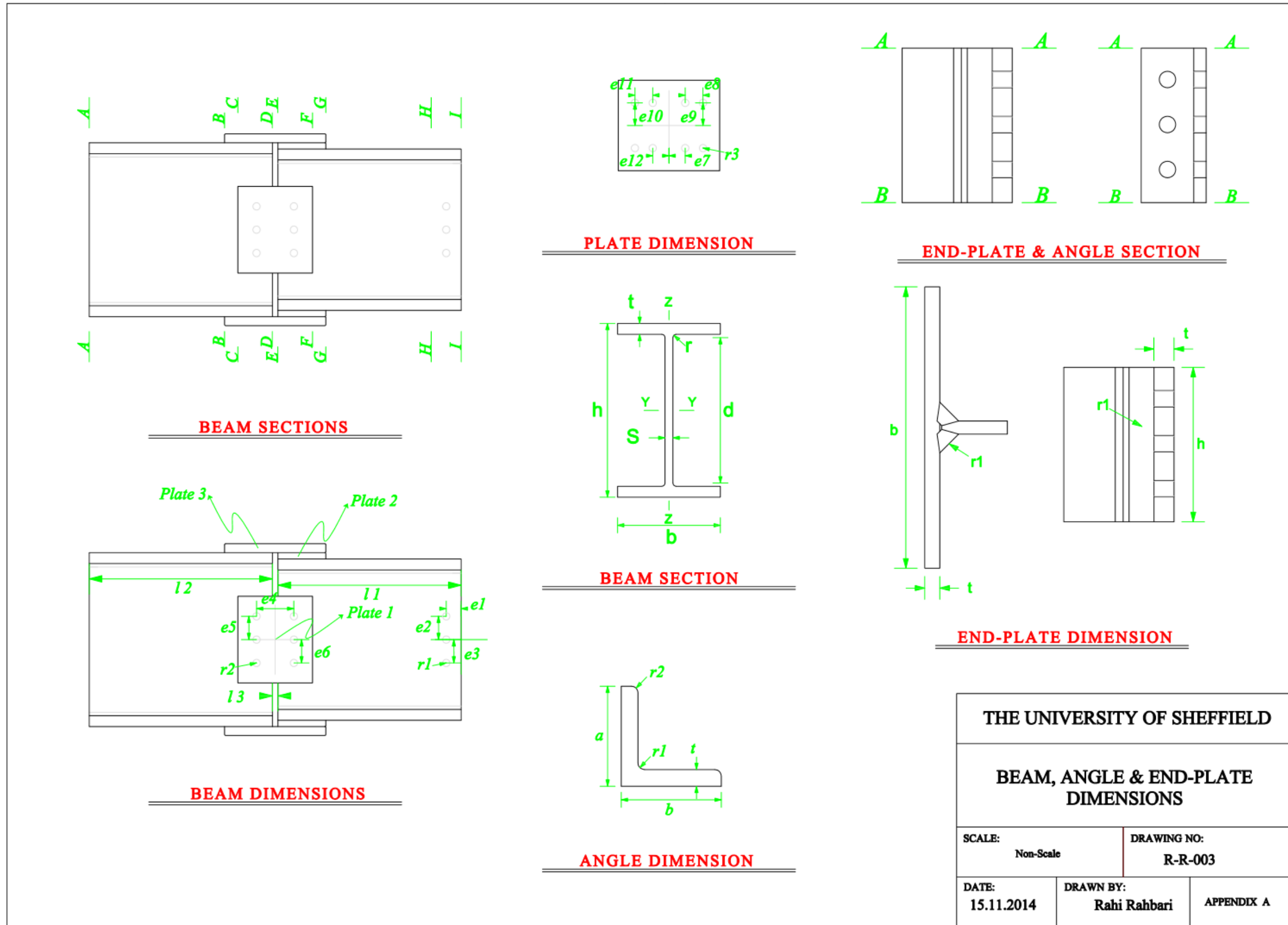


Figure A- 3, Column sections and key-points



<b>THE UNIVERSITY OF SHEFFIELD</b>		
<b>BEAM, ANGLE &amp; END-PLATE DIMENSIONS</b>		
SCALE: Non-Scale	DRAWING NO: R-R-003	
DATE: 15.11.2014	DRAWN BY: Rahi Rahbari	APPENDIX A

Figure A- 4, Beam drawings and dimensions

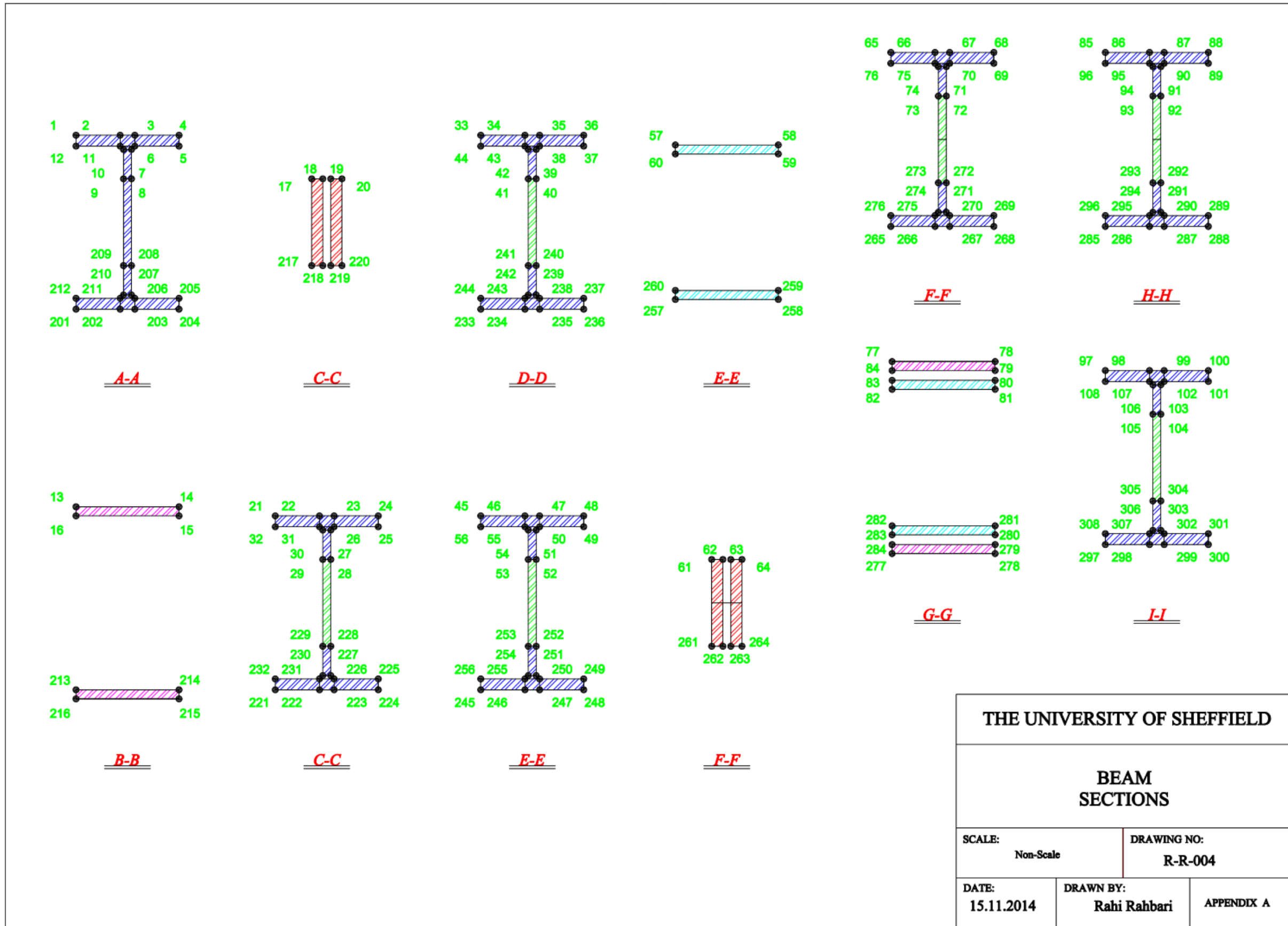
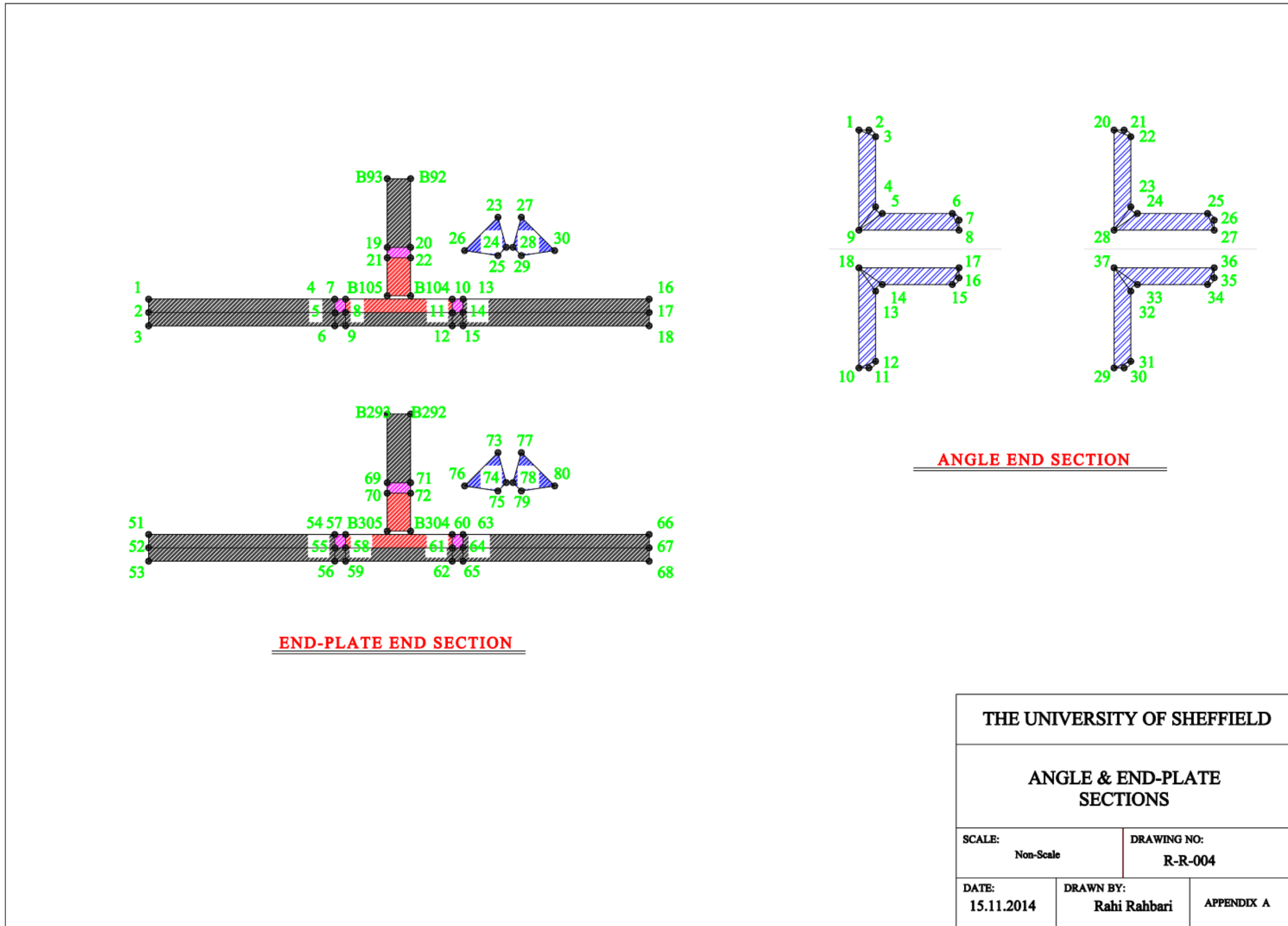


Figure A- 5, Beam sections and key-points



**END-PLATE END SECTION**

**ANGLE END SECTION**

THE UNIVERSITY OF SHEFFIELD		
ANGLE & END-PLATE SECTIONS		
SCALE: Non-Scale	DRAWING NO: R-R-004	
DATE: 15.11.2014	DRAWN BY: Rahi Rahbari	APPENDIX A

Figure A- 6, Angle and End-plate sections and key-points



## Appendix B Dimensions

This table provides the dimensions of different parts of the connections, the locations of each variable is provided in the drawings in Appendix A.

Column Dimensions					
	(m)		(m)		(m)
h	1.998	h1	1	e1	0.07
e2	0.07	d1	0.09	d2	0.045
r1	0.011	h2	0.555	h3	0.16
d3	0.1	d4	0.05	r2	0.011
r3	0.011	r4	0.015	hs	0.2891
b	0.2652	s	0.0192	t	0.0317
r	0.0127	d	200.3	d5	0.27
d6	0.05	d7	0.05	d8	0.03
d9	0.03	tp1	0.02	tp2	0.01

Beam Dimensions					
	(m)		(m)		(m)
h	0.364	t	0.0157	r	0.0102
s	0.007	b	0.1732	h2	0.352
t2	0.0069	rr2	0.0102	s2	0.007
b2	0.171	l1	0.425	l2	0.447
l3	0.0002	r1	0.011	e1	0.04
e2	0.07	e3	0.07	r2	0.0102
e4	0.101	e5	0.08	e6	0.08
r3	0.0102	e7	0.05	e8	0.05
e9	0.045	e10	0.045	e11	0.05
e12	0.05	Pl11	0.21	Plw1	0.26
Plt1	0.0151	Pl12	0.3	Plw2	0.2
Plt2	0.01	Pl13	0.3	Plw3	0.18
Plt3	0.0151				
Angle Dimension					
	(m)		(m)		(m)
a	0.09	b	0.09	t	0.01-0.006
l	0.22	r1	0.011	r2	0.0055
End- Plate Dimension					
	(m)		(m)		(m)
t	0.01	a	0.15	l	0.22
r1	0.011	r2	0.0055		

Weld Dimension					
	(m)		(m)		(m)
l	0.008	w	0.0025	hz1	0.002
hz2	0.002				
Bolt Dimension					
	(m)		(m)		(m)
r	0.008	d	0.002	t	0.002
gap	0.0009	Agap	0.0019	l	0.008
l1	0.001	d1	0.0002	wt	0.003
wr	0.0185	l2	0.01	l3	0.01

Table B- 1, Model dimensions